Université du Québec
à Rimouski

COMPORTEMENT ET DEVENIR DES NANOPARTICULES D'ARGENT DURANT UNE TRANSITION ESTUARIENNE

Thèse présentée

dans le cadre du programme de doctorat en Océanographie

en vue de l'obtention du grade de *Philosophiæ Doctor*

PAR

© MATHIEU MILLOUR

Mai 2018

Composition du jury :

Youssouf Djibril Soubaneh, Président du jury, Département de biologie, chimie et géographie, Université du Québec à Rimouski

Jean-Pierre Gagné, Directeur de recherche, Institut des sciences de la mer de Rimouski, Université du Québec à Rimouski

Émilien Pelletier, Codirecteur de recherche, Institut des sciences de la mer de Rimouski, Université du Québec à Rimouski

Viviane Yargeau, Examinatrice externe, Department of chemical engineering, McGill University

Richard Saint-Louis, Examinateur interne, Département de biologie, chimie et géographie, Université du Québec à Rimouski

Dépôt initial le 15 décembre 2017 Dépôt final le 15 mai 2018

« *L'eau de mer eft le réfultat du lavage de toute la furface du globe ; ce font en quelque façon les rinçures du grand laboratoire de la Nature, on doit donc s'attendre à trouver réunis dans cette eau, tous les fels qui peuvent fe rencontrer dans le règne minéral* » **Lavoisier 1772**

REMERCIEMENTS

Quand je suis arrivé à Rimouski, en 2008, mon intérêt scientifique portait essentiellement sur le comportement et le devenir des métaux traces dans le domaine marin. À ce moment-là, je ne connaissais pas encore le rôle majeur de la matière organique naturelle dans les systèmes aquatiques ainsi que dans mon devenir. Le Pr Jean-Pierre Gagné m'a alors proposé un projet de maîtrise sur les interactions entre la matière organique naturelle et les microalgues. Durant ce projet, nous nous sommes souvent posé des questions sur les interactions entre les métaux et la matière organique naturelle. Quelques années après, Jean-Pierre m'a proposé un sujet de doctorat portant sur les nanoparticules d'argent. Ayant découvert un nouveau sujet d'intérêt durant ma maîtrise, je lui ai indiqué que je voulais aussi travailler sur les interactions entre les nanoparticules d'argent et la matière organique. Ayant tout prévu, Jean-Pierre m'a indiqué que durant mon doctorat on allait extraire la matière organique de l'estuaire du Saint-Laurent. Cela m'a permis de battre un record du laboratoire ainsi qu'un record mondial. Durant l'été 2012, nous avons extrait environ 40 g de matière organique de 50 119 L d'eau estuarienne. Sans Jean-Pierre, je ne me serais jamais intéressé autant à la matière organique et à leurs interactions avec différents composés et organismes présents dans le domaine marin. Je le remercie pour cette nouvelle passion. Je le remercie aussi sincèrement de m'avoir offert l'opportunité de faire mes études universitaires (maîtrise et doctorat) au sein du LAEGO. Je le remercie pour son aide, ses conseils et les nombreuses discussions, qui ont fait évoluer mes centres d'intérêt ainsi que ma compréhension du sujet étudié, mais aussi pour l'autonomie et les responsabilités qu'il m'a données.

Je remercie aussi mon codirecteur le Pr Émilien Pelletier. En 2008, Émilien parlait déjà de prendre sa retraite, mais avec Émilien il y a toujours un « mais ». Il disait souvent, je vais prendre ma retraite, mais j'ai peut-être un projet pour toi. Ce fut mon cas en 2011, début de mon doctorat. Je te remercie sincèrement de ton rôle important dans mon cheminement scientifique ainsi que dans mon doctorat même durant ta « simili » retraite, débutée en

décembre 2015. Je te remercie aussi pour ta patience, ton appui et tes encouragements tout au long de cette grande expérience qu'est le doctorat.

Au Pr Youssouf Djibril Soubaneh, merci d'avoir accepté de juger ma thèse et de présider ce jury. Merci aux Pre Viviane Yargeau et Pr Richard Saint-Louis d'avoir accepté de juger ma thèse.

Je remercie aussi le Pr Peter GC. Campbell et le Dr Christian Gagnon, membres de mon comité de thèse, pour toutes les discussions tenues lors de différents colloques scientifiques et réunions qui ont fait évoluer mon projet de recherche.

Je remercie aussi la Pr Isabelle Marcotte de m'avoir accueilli au sein de son laboratoire de résonance magnétique nucléaire (RMN) des systèmes biologiques complexes de l'Université du Québec à Montréal. Un grand merci au Dr Alexandre Arnold pour m'avoir expliqué les subtilités de la RMN, mais aussi pour son aide dans la création des séquences d'analyses, de sa disponibilité, mais aussi de la confiance qu'il m'a accordée.

Merci à l'ISMER, à Québec-Océan et au CRSNG pour le soutien financier et logistique. Je remercie aussi l'ISMER et Québec-Océan de m'avoir permis de représenter les étudiants et d'exposer mes nombreux arguments au sein de nombreux comités (GCGLI, CA, CCDR, CPO…).

Je remercie aussi Dominique Lavallée, Mélanie Simard, Isabelle Desbiens, Nathalie Morin, Mathieu Babin, Sylvain Leblanc, Gilles Desmeules, Bruno Cayouette, Mickael Barthes et Pascal Rioux pour leurs conseils et leurs nombreuses aides techniques.

Merci aux stagiaires Kévin Raimondeau, Floriane Le Bihan, Clément Joly, Ophélie Achat, Thomas Conte--Chenuc, Audrey Tiercin et Manon Albor de m'avoir beaucoup appris sur l'encadrement et pour leurs aides. Merci à Kévin Osterheld, Alexandre Palardy et Gabriel Bardaxoglou pour leurs implications importantes dans ce projet en plus de leurs maîtrises.

Un grand merci au Dre Kim Doiron, ma coloc et amie, qui a bien voulu me conseiller tout au long de mon doctorat, et de relire cette thèse, malgré son emploi du temps chargé. Merci aussi d'avoir accepté de me former sur différents aspects de la microbiologie.

Merci à Béber, Berni, Max, Oli, Michèle, Enrique, Sam, les deux Pierre, Michel, Jory, Rachel, Cindy, Erwan, Cyréna, Pierre-Marc, Karine et bien d'autres, pour les nombreux bons moments passés au bureau ou au baro, les débats animés et les conseils. Je remercie aussi toutes les personnes que j'ai pu oublier et qui ont contribué de près ou de loin à ce projet.

Un grand merci pour le soutien psychologique et financier que ma famille m'a apporté malgré la grande distance, plus de 6 000 km, qui nous séparent. Merci plus particulièrement à mes parents qui m'ont poussé à continuer mes études et sans qui je ne serais pas là où je suis maintenant. Je vous dédie cette thèse.

Trugarez vras

RÉSUMÉ

Les nanoparticules d'argent (AgNPs) sont de plus en plus incorporées dans des matériaux d'emballage alimentaire, des tissus et équipements sportifs anti-odeurs, des cosmétiques, des peintures extérieures, des équipements électroniques et médicaux. De récents travaux suggèrent que ces matériaux peuvent se retrouver dans les environnements aquatiques à des concentrations comprises entre 1 ngAg.L^{-1} et quelques µgAg.L^{-1}. Actuellement, peu d'informations sont disponibles sur le devenir des AgNPs dans les environnements aquatiques et plus particulièrement en milieu estuarien. La majorité des études ont été réalisées à des concentrations élevées en AgNPs, plusieurs mgAg.L^{-1}. L'objectif général de cette recherche est de déterminer le comportement et le devenir des AgNPs, à très faible concentration (10 µgAg.L^{-1}), durant une transition estuarienne. Pour cela, un protocole pour mesurer l'agrégation des AgNPs à 10 µgAg.L^{-1} par diffusion dynamique de la lumière (DLS) a été développé. L'utilisation de ce protocole a permis d'observer deux populations de particules, une première ayant des particules de taille inférieure à 200 nm et la seconde, supérieure à 200 nm. Les effets de la concentration en AgNPs, en sels et en matière organique naturelle (NOM) ont aussi été étudiés, afin de mieux comprendre leurs rôles dans le comportement agrégatif des AgNPs.

Dans le chapitre 1, les effets de la concentration en sel ont été étudiés. En eau nanopure, la taille des AgNPs reste stable dans le temps. L'ajout de sel induit une augmentation rapide de leurs tailles, indiquant un phénomène d'agrégation. Cette étude montre que la vitesse d'agrégation augmente en fonction de la concentration en NaCl jusqu'à atteindre une valeur maximale. Ces expériences ont permis d'observer l'atteinte d'un état d'équilibre où la taille n'évolue plus dans le temps. L'agrégation a aussi été étudiée à différentes concentrations en AgNPs (10 mgAg.L^{-1} à 10 µgAg.L^{-1}). Les vitesses d'agrégation et la distribution de la taille des agrégats formés sont fortement influencées par la concentration initiale en AgNPs. À 10 et 1 mgAg.L^{-1}, moins de 30% des particules analysées ont une taille inférieure à 200 nm. À 100 et 10 µgAg.L^{-1}, cette population de petites particules représente 50 à 90% des particules analysées. Cette étude a permis de démontrer que la distribution de la taille des agrégats est modulée par la quantité initiale d'AgNPs et que l'état d'équilibre est atteint à 10^6 particules.mL^{-1}.

Dans le deuxième chapitre, le comportement agrégatif des AgNPs a été étudié dans des solutions d'exposition caractéristiques des eaux naturelles et des milieux utilisés dans les études écotoxicologiques. Cette étude montre que l'agrégation des AgNPs est modulée par la valence des cations. Les cations divalents favorisent une agrégation plus rapide que les cations monovalents. La présence d'anions comme du Cl^-, HCO_3^-, et du SO_4^{2-} et/ou de matière organique peut aussi moduler les vitesses d'agrégation en interagissant avec les surfaces des AgNPs.

Dans le chapitre 3, le rôle de la NOM dans l'agrégation des AgNPs (10 µgAg.L^{-1}) a été approfondi. Quatre fractions de NOM provenant de l'estuaire du Saint-Laurent ont été

extraites. Ces quatre fractions sont les acides fulviques, les acides humiques, une fraction hydrophile et une fraction hydrophobe. Dans cette étude, des cinétiques d'agrégation des AgNPs en présence de 2.5 et 25 mgNOM.L^{-1} ont été réalisées. En absence de sels, la présence de NOM induit une augmentation de la taille d'un facteur compris entre 1,4 et 2 fois, causée par la sorption de la NOM sur les surfaces des AgNPs. À 2.5 mgNOM.L^{-1} et en présence de sel, plus de 90% des particules analysées ont une taille inférieure à 200 nm, quelle que soit la NOM étudiée. À 25 mgNOM.L^{-1}, la distribution de la taille des agrégats est fortement modulée par la composition chimique de la NOM. Une NOM riche en carbones aromatiques et phénoliques comme les substances humiques favorise la formation d'agrégats ayant une taille supérieure à 200 nm. Une NOM ayant une teneur élevée en carbones aliphatiques non-polaires, induit la formation d'agrégats de moins de 200 nm. Cette étude montre que ces différences de taille sont essentiellement causées par la nature des groupements responsables des interactions hydrophobes ainsi que par le poids moléculaire de la NOM.

Dans le dernier chapitre, une expérience en mésocosme imitant un estuaire stratifié a été réalisée. Les données obtenues ont permis d'observer que les AgNPs s'agrègent dans chaque masse d'eau, mais la taille des agrégats formés diffère selon la masse d'eau. Dans les eaux douces, la distribution de la taille des particules présente des différences en présence ou en absence d'AgNPs. La présence d'AgNPs tend à faire augmenter la proportion des particules inférieures à 200 nm. Des échantillons analysés par ICP-MS ont permis de (1) valider les données de distribution de la taille obtenue par DLS ; (2) comprendre le devenir des AgNPs en milieu estuarien et (3) déterminer que l'halocline peut agir comme une frontière de forte densité limitant la sédimentation des AgNPs, mais favorisant leurs rétentions dans les eaux de surface et à l'halocline.

Cette étude présente de nombreuses données originales permettant de mieux comprendre le comportement et le devenir des AgNPs en milieu estuarien. Dans un environnement aquatique, et plus particulièrement dans un estuaire, les AgNPs s'agrégeront ensemble et avec les particules naturelles. Toutefois, la taille des agrégats est fortement influencée par la composition et la concentration en sel et par la concentration en particules comme les AgNPs, la NOM et la matière particulaire en suspension. Le devenir des AgNPs durant leurs transitions dans un estuaire est très dynamique et fortement influencé par la stratification du milieu. Les résultats obtenus dans cette thèse pourront aider à mieux orienter les futures études sur les nanomatériaux ainsi que permettre une meilleure régulation et législation de ces nouveaux composés d'intérêt.

Mots clés : Nanoparticules d'argent, agrégation, sels, matière organique naturelle, distribution de la taille, transition estuarienne

ABSTRACT

Silver nanoparticles (AgNPs) are incorporated into food packaging, anti-odor textiles, sports equipment, cosmetics, outdoor paints, electronic and medical equipments. Recent works suggest that these materials can be found in aquatic environments at concentrations ranging from 1 $ng.L^{-1}$ to a few $\mu g.L^{-1}$. Presently, limited information is available on the fate of AgNPs in aquatic environments, particularly in estuarine environments. The majority of recent studies were performed at high concentrations of AgNPs, several $mgAg.L^{-1}$, not representative of the possible levels in natural environment. The aim of this research was to determine the behavior and fate of AgNPs at low concentrations (10 $\mu gAg.L^{-1}$) during an estuarine transition. A protocol to measure the aggregation of AgNPs at 10 $\mu gAg.L^{-1}$ by dynamic light scattering (DLS) has been developed. With this protocol two particle populations are observed in aqueous sample. The first one with a size less than 200 nm and the second one higher than 200 nm. The effects of AgNPs, salts and natural organic matter (NOM) concentrations were also studied in order to increase the knowledge of their roles in AgNP aggregative behavior.

In chapter 1, the effects of salt concentration were studied. In nanopure water, the size of AgNPs remained stable over time. The addition of salt induced a rapid increase of the AgNP size, indicating an aggregation. This study showed that the aggregation rate increases according to the NaCl concentration until a maximum value. In these experiments, a steady state was reached when size did not evolve over time. Aggregation was also studied at different concentrations of AgNPs (10 $mgAg.L^{-1}$ to 10 $\mu gAg.L^{-1}$). The aggregation rate and the particle size distribution of the aggregates were strongly influenced by the AgNPs concentration. At 10 and 1 $mgAg.L^{-1}$, less than 30% of the analyzed particles had a size smaller than 200 nm. At 100 and 10 $\mu gAg.L^{-1}$, this small particles population accounts for 50 to 90% of the particles. This study demonstrated that size distribution of aggregates was modulated by the initial amount of AgNPs. When the quantity of particles reached 10^6 $particles.mL^{-1}$, the size of the aggregates did not evolve with time.

In the second chapter, the aggregative behavior of AgNPs was studied in exposure solutions being characteristic of natural waters and media used in ecotoxicologic studies. These four fractions are fulvic acids, humic acids, a hydrophilic fraction and a hydrophobic fraction. This study showed that aggregation of AgNPs was modulated by the valence of the cations. The divalent cations promoted a faster aggregation than the monovalent cations. The presence of anions such as Cl^-, HCO_3^-, and SO_4^{2-} and/or organic matter could also modulate aggregation rates by interacting with AgNPs surfaces.

In chapter 3, the role of the NOM in the AgNP aggregation (10 $\mu gAg.L^{-1}$) was studied. Four NOM fractions from the St.-Lawrence Estuary were extracted. In this study, aggregation kinetics of AgNPs were performed in presence of 2.5 and 25 $mgNOM.L^{-1}$. In absence of salts, the presence of NOM induced a size increase of 1.5 to 2 times, caused by sorption of NOM around AgNP surfaces. At 2.5 $mgNOM.L^{-1}$ and in the presence of salt, more than 90%

of the particles were smaller than 200 nm, whatever the NOM used. At 25 mgNOM.L^{-1}, the size distribution of aggregates was strongly modulated by the chemical composition of the NOM. NOM rich in aromatic and phenolic carbons such as humic substances favored the formation of aggregates with a size larger than 200 nm. NOM with a high non-polar aliphatic carbon content promoted the formation of aggregates less than 200 nm. This study showed that these size differences were mainly caused by the nature of the chemical groups implied in hydrophobic interactions as well as the molecular weight of the NOM.

In the last chapter, a mesocosm experiment mimicking a stratified estuary was performed. The obtained data showed that AgNPs aggregated in each water layer, but the size of the aggregates differed depending on the water mass. In freshwater, the particle size distribution differs in the presence or absence of AgNPs. The presence of AgNPs tends to increase the proportion of particles smaller than 200 nm. Samples, analyzed by ICP-MS, were used to (1) validate the size distribution data obtained by DLS; (2) understand the fate of AgNPs in the estuarine environment, and (3) determine the role of halocline, a density frontier limiting sedimentation of AgNPs, but favoring their retention in surface water and halocline.

This study presents original results which improve our understanding of the behavior and the fate of AgNPs in estuarine environment. In aquatic environments, and more particularly in estuaries, AgNPs will aggregate together and with natural particles. However, aggregates size is strongly influenced by salt composition and concentration; and particle concentration such as AgNPs, NOM and suspended particulate matter. The fate of AgNPs during their transition in an estuary is very dynamic and strongly influenced by the stratification. The results obtained in the present thesis provide much need knowledge to define future studies on nanomaterials and allow better regulation and legislation of these new compounds of interest.

Keywords: Silver nanoparticles, aggregation, salt, natural organic matter, particle size distribution, estuarine transition

TABLE DES MATIÈRES

REMERCIEMENTS ix

RÉSUMÉ xiii

ABSTRACT xv

TABLE DES MATIÈRES xvii

LISTE DES TABLEAUX xxiii

LISTE DES FIGURES xxv

LISTE DES ABRÉVIATIONS xxxi

INTRODUCTION GÉNÉRALE 1

LES NANOMATERIAUX 1

LES NANOPARTICULES D'ARGENT 4

COMPORTEMENT ET DEVENIR DES NANOPARTICULES D'ARGENT DANS L'ENVIRONNEMENT 6

Comportement individuel 9

Comportement de groupe 11

Taille des agrégats 20

DOSAGE ET CARACTERISATION DES NANOPARTICULES D'ARGENT 21

Caractérisation de la taille des nanoparticules 22

Caractérisation du potentiel zêta des nanoparticules 26

LA MATIERE ORGANIQUE EN MILIEU AQUATIQUE 28

Caractéristiques chimiques des substances humiques 29

Comportement des substances humiques selon le pH et la salinité 31

OBJECTIFS 32

CHAPITRE 1 EFFETS DE LA CONCENTRATION DES NANOPARTICULES D'ARGENT SUR LEURS COMPORTEMENTS AGRÉGATIFS ET SUR LA DISTRIBUTION DE LA TAILLE DES AGRÉGATS 35

1.1 RESUME 35
1.2 ABSTRACT 37
1.3 INTRODUCTION 38
1.4 MATERIALS AND METHODS 40
1.4.1 Synthesis and characterization of silver nanoparticles 40
1.4.2 Salt solutions 41
1.4.3 Aggregation kinetics 42
1.5 RESULTS AND DISCUSSION 44
1.5.1 Effects of silver nanoparticles concentrations on their properties in nanopure water 44
1.5.2 Effects of silver nanoparticles concentrations on their aggregative behavior in salty waters 46
1.5.3 Effects of silver nanoparticles concentration on critical coagulation concentration 48
1.5.4 Effects of silver nanoparticles concentration on the evolution of particle distribution 53
1.5.5 Effects of silver nanoparticles concentration on aggregates distribution 56
1.6 CONCLUSION 62
1.7 ACKNOWLEDGMENTS 63

CHAPITRE 2 LA CHIMIE D'UN MILIEU DE CULTURE BACTÉRIEN AFFECTE-T-ELLE LA STABILITÉ DES NANOPARTICULES DANS DES ESSAIS DE NANOTOXICITÉ ? 65

2.1 RESUME 65

2.2 ABSTRACT 67
2.3 INTRODUCTION 67
2.4 MATERIALS AND METHODS 69
2.5 RESULTS AND DISCUSSION 70
2.6 CONCLUSION 75
2.7 ACKNOWLEDGMENTS 75

CHAPITRE 3 EFFETS DE LA CONCENTRATION ET DE LA COMPOSITION CHIMIQUE DE LA MATIÈRE ORGANIQUE NATURELLE SUR LE COMPORTEMENT AGRÉGATIF DES NANOPARTICULES D'ARGENT 77

3.1 RESUME 77
3.2 ABSTRACT 79
3.3 INTRODUCTION 80
3.4 MATERIALS AND METHODS 82
3.4.1 Synthesis of silver nanoparticles 82
3.4.2 Natural organic matter extraction and chemical characterization 83
3.4.3 Zeta potential measurements 84
3.4.4 Silver nanoparticles aggregation kinetics 85
3.5 RESULTS AND DISCUSSION 87
3.5.1 Zeta potential 87
3.5.2 Effects of natural organic matter concentration and its nature on silver nanoparticles stability in nanopure water 88
3.5.3 Effects of natural organic matter concentration and its nature on silver nanoparticles stability in salty water 91
3.5.4 Effects of natural organic matter concentration and its nature on aggregate size distribution 93
3.5.5 Chemical composition of natural organic matter fractions and effects on silver nanoparticles aggregates 96

3.6 CONCLUSION 102
3.7 ACKNOWLEDGMENTS 103

CHAPITRE 4 COMPORTEMENT DES NANOPARTICULES D'ARGENT DANS DES MÉSOCOSMES ESTUARIENS STRATIFIÉS : DISTRIBUTION DE LA TAILLE DES PARTICULES ET RÔLE DE L'HALOCLINE 105

4.1 RESUME 105
4.2 ABSTRACT 107
4.3 INTRODUCTION 108
4.4 MATERIALS AND METHODS 110
4.4.1 Mesocosm design to mimic a stratified estuarine system 110
4.4.2 Freshwater and seawater inflows 112
4.4.3 Addition of silver nanoparticles 113
4.4.4 Analysis of dissolved and particulate silver 113
4.4.5 Measurement of hydrodynamic diameter and particle size distribution 114
4.4.6 Short-term aggregation kinetics of silver nanoparticles 115
4.5 RESULTS AND DISCUSSION 116
4.5.1 Estuarine mesocosms 116
4.5.2 Dissolved and particulate silver in water layers 118
4.5.3 Distribution of natural particles in water masses before adding AgNPs 121
4.5.4 Short-term aggregative behavior of silver particles in water masses 124
4.5.5 Long-term distribution of particles in water masses with addition of AgNPs 127
4.6 CONCLUSION 132
4.7 ACKNOWLEDGMENTS 133

CONCLUSION GÉNÉRALE 135

ANNEXE I SUPPORTING INFORMATION FOR EFFECTS OF SILVER NANOPARTICLES CONCENTRATION ON THEIR AGGREGATIVE BEHAVIOR AND SIZE DISTRIBUTION OF AGGREGATES 149

ANNEXE II SUPPORTING INFORMATION FOR EFFECTS OF CONCENTRATION AND CHEMICAL COMPOSITION OF NATURAL ORGANIC MATTER ON AGGREGATIVE BEHAVIOR OF SILVER NANOPARTICLES 155

ANNEXE III SUPPORTING INFORMATION FOR BEHAVIOR OF SILVER NANOPARTICLES IN STRATIFIED ESTUARINE MESOCOSMS: PARTICLE SIZE DISTRIBUTION AND THE ROLE OF THE HALOCLINE 161

RÉFÉRENCES BIBLIOGRAPHIQUES 177

LISTE DES TABLEAUX

Tableau 1 : Concentrations critiques de coagulation pour différentes nanoparticules d'argent (modifié de Baalousha *et al.* (2013)) 15

Table 2: Effects of silver nanoparticles concentration on the hydrodynamic diameter, zeta potential and peak of surface plasmon resonance absorbance 45

Table 3: Hydrodynamic diameter and proportion distribution of particle populations less than 200 nm ($P_{0\text{-}200}$) and higher than 200 nm ($P_{200\text{-}10\,000}$) observed between 36 000 and 43 200 s (last 2 h) for 12 h kinetics at four silver nanoparticles concentrations: 10 mgAg.L^{-1}, 1 mgAg.L^{-1}, 100 µgAg.L^{-1} and 10 µgAg.L^{-1} at 0, 9, 86 and 428 mM of NaCl 61

Table 4: Zeta potential (mV) of silver nanoparticles at 100 µgAg.L^{-1} with 0, 2.5 or 25 mgNOM.L^{-1} (n=3) of SLFA, SLHA, SL4ILE, or SL4OBE 88

Table 5: Slope ratio, elemental and functional groups (%, ^{13}C-NMR) composition of fulvic acids, humic acid, hydrophilic and hydrophobic fractions extracted with XAD-4 98

Table 6: Mean concentrations (n=12 by layer for each mesocosm) of dissolved and particulate silver in mesocosms over 35 days 119

Table 7: Effects of AgNPs concentration on distance (l), interaction surface (πl^2) and time taken for interactions between nanoparticles for AgNPs at 10 mgAg.L^{-1}, 1 mgAg.L^{-1}, 100 µgAg.L^{-1} and 10 µgAg.L^{-1} 152

Table 8: Hydrodynamic diameter of aggregates calculated between 5 400 and 7 200 s (last 30 min) for kinetics of 2 h at 10 mgAg.L^{-1}, 1 mgAg.L^{-1}, 100 µgAg.L^{-1} and 10 µgAg.L^{-1} at 0, 10, 20, 30, 40, 50, 100, 200, 400 and 500 mM of NaCl 153

Table 9: Hydrodynamic diameter and proportions distribution of particle population less than 200 nm ($P_{0\text{-}200}$) and higher than 200 nm ($P_{200\text{-}10\,000}$) observed between 5 400 and 7 200 s (last 30 min) for kinetics of 2 h at 10 mgAg.L^{-1}, 1 mgAg.L^{-1}, 100 µgAg.L^{-1} and 10 µgAg.L^{-1} at 0, 10, 20, 30, 40, 50, 100, 200, 400 and 500 mM of NaCl 154

Table 10: Hydrodynamic diameter and proportions distribution of particle populations less than 200 nm ($P_{0\text{-}200}$) and higher than 200 nm ($P_{200\text{-}10\,000}$) observed between 5 400 and 7 200 s (last 30 min) for kinetics of 2 h at 2.5 mgNOM.L^{-1}, of SLFA, SLHA, SL4ILE and SL4OBE at different NaCl concentration 0, 10, 20, 30, 40, 50, 100, 200, 400 and 500 mM 157

Table 11: Hydrodynamic diameter and proportions distribution of particle populations less than 200 nm ($P_{0\text{-}200}$) and higher than 200 nm ($P_{200\text{-}10\,000}$) observed between 5 400 and 7 200 s (last 30 min) for kinetics of 2 h at 25 mgNOM.L^{-1}, of SLFA, SLHA, SL4ILE and SL4OBE at different NaCl concentration 0, 10, 20, 30, 40, 50, 100, 200, 400 and 500 mM 158

Table 12: Correlation between the principal components 1 and 2 (PC1 and PC2) and the variables 159

Table 13: Flow rates and salinities of water masses in the mesocosms 161

Table 14: Size range, mean hydrodynamic diameter and proportion of particle populations $P_{0\text{-}200}$ and $P_{200\text{-}5\,000}$ in each mesocosm and water mass obtained over 35 days of experiment 162

LISTE DES FIGURES

Figure 1 : Gamme de tailles des principales particules et solutés se trouvant en milieu liquide 2

Figure 2 : Rejets des nanoparticules d'argent : de leurs sources aux différents compartiments environnementaux (traduit de Blaser *et al.,* 2008) 7

Figure 3 : Transformation et comportement général des nanoparticules d'argent dans un système aquatique 9

Figure 4 : Fluctuation de l'intensité lumineuse (a) et autocorrélogramme (b). Modifié de Malvern (2010) 24

Figure 5 : Relation entre la structure de la double couche électrique et le potentiel zêta (traduit de Xu, 2001a et Malvern, 2013b) 27

Figure 6 : Modèles des acides humiques (Stevenson, 1994) et des acides fulviques (Buffle, 1977) 30

Figure 7: Aggregation kinetics of AgNPs of 2 h a) at constant AgNPs concentration (1 $mgAg.L^{-1}$) and at NaCl concentration of 0 mM (blue circle), 10 mM (green square) and 500 mM (red diamond); and b): AgNPs decreasing concentrations: 10 $mgAg.L^{-1}$ (red diamond), 1 $mgAg.L^{-1}$ (yellow square), 100 $\mu gAg.L^{-1}$ (green triangle) and 10 $\mu gAg.L^{-1}$ (blue circle) in constant solution of NaCl 200 mM 47

Figure 8: Attachment efficiency of silver nanoparticles at a) 10 $mgAg.L^{-1}$ (red circle) and 1 $mgAg.L^{-1}$ (yellow circle) and at b) 100 $\mu gAg.L^{-1}$ (green circle) and 10 $\mu gAg.L^{-1}$ (blue circle) 49

Figure 9: Kinetics of particles distribution over 2 h at a) 10 $mgAg.L^{-1}$, b) 1 $mgAg.L^{-1}$, c) 100 $\mu gAg.L^{-1}$ and d) 10 $\mu gAg.L^{-1}$ of silver nanoparticles in a solution of NaCl at 200 mM 54

Figure 10: Hydrodynamic diameter and proportion distribution of particle populations less than 200 nm (red) and higher than 200 nm (black) observed between 5 400 and 7 200 s (last 30 min) for kinetics of 2 h at four silver nanoparticles concentrations: a

and b) 10 mgAg.L^{-1}, c and d) 1 mgAg.L^{-1}, e and f) 100 µgAg.L^{-1}; g and h) 10 µgAg.L^{-1} at different NaCl concentrations A 0 mM, B 10 mM, C 20 mM, D 30 mM, E 40 mM, F 50 mM, G 100 mM, H 200 mM, I 400 mM and J 500 mM 59

Figure 11: Aggregation kinetics of AgNPs at 93 µgAg.L^{-1} in A) nanopure water, B) in NaCl at 25 PSU, C) in $CaCl_2$ at 25 PSU and D) in $MgCl_2$ at 25 PSU 71

Figure 12: Aggregation kinetics of AgNPs at 93 µgAg.L^{-1} in A) artificial seawater, B) in F/2 media and C) in LB media 72

Figure 13: Aggregation kinetics over 2 h for AgNPs at 10 µgAg.L^{-1} with 0 mgNOM.L^{-1} (black) 2.5 mgNOM.L^{-1} (blue) and 25 mgNOM.L^{-1} (red), in nanopure water. a) SLFA, b) SLHA, c) SL4ILE, and d) SL4OBE. Continuous lines were obtained by averaging and smoothing for each time slot of 10 data 89

Figure 14: Aggregation kinetics over 2 h for AgNPs at 10 µgAg.L^{-1} with 0 mgNOM.L^{-1} (black) 2.5 mgNOM.L^{-1} (blue) and 25 mgNOM.L^{-1} (red), in 500 mM NaCl solution. a) SLFA, b) SLHA, c) SL4ILE, and d) SL4OBE. Continuous lines were obtained by averaging and smoothing for each time slot of 10 data 92

Figure 15: Hydrodynamic diameter and proportion of particle populations with size less than 200 nm (red) and larger than 200 nm (black) observed between 5 400 and 7 200 s (last 30 min) for AgNPs kinetics of 2 h with 2.5 mgNOM.L^{-1} of a and b) SLFA; c and d) SLHA; e and f) SL4ILE; g and h) SL4OBE at different NaCl concentration: A 0 mM ; B 10 mM ; C 20 mM ; D 30 mM ; E 40 mM ; F 50 mM ; G 100 mM ; H 200 mM ; I 400 mM and J 500 mM. The symbol * and ° represent the outside values 94

Figure 16: Hydrodynamic diameter and proportion of particle populations with size less than 200 nm (red) and larger than 200 nm (black) observed between 5 400 and 7 200 s (last 30 min) for AgNPs kinetics of 2 h with 25 mgNOM.L^{-1} of a and b) SLFA; c and d) SLHA; e and f) SL4ILE; g and h) SL4OBE at different NaCl concentration: A 0 mM ; B 10 mM ; C 20 mM ; D 30 mM ; E 40 mM ; F 50 mM ; G 100 mM ; H 200 mM ; I 400 mM and J 500 mM. The symbol * and ° represent the outside values 95

Figure 17: Linear regression between neperian logarithm of average hydrodynamic diameter of AgNPs and slope ratio (SR) a) in nanopure water and b) in salty water at 500 mM NaCl 96

Figure 18: Principal component analysis (PCA) of silver aggregate size distribution (hydrodynamic diameter $D_{h0\text{-}200}$ and $D_{h200\text{-}10\,000}$ in red and proportion $P_{0\text{-}200}$ and $P_{200\text{-}10\,000}$ called $P_{0\text{-}200}$ *(%)* and $P_{200\text{-}10\,000}$ *(%)* in brown) with elemental composition of NOM (black) and functional groups of NOM characterized by 13C NMR (blue), with 25 mgNOM.L^{-1}. a) in nanopure water and b) in salty water at 500 mM NaCl. For ^{13}C NMR results, the eight regions correspond to: (1) AliC: non-polar aliphatic carbons as CH_2 and CH_3 (0-45 ppm); (2) N-alkyl/OCH_3 (45-65 ppm); (3) HOCH from alcohols, non-anomerics carbohydrates and ethers (65-95 ppm); (4) O-C-O/O-CH-O from anomerics carbohydrates (95-110 ppm); (5) AromC: aromatic carbons (110-145 ppm); (6) PhenolC: phenolic carbons (145-160 ppm); (7) CAE: carboxylic, amides and esters (160-190 ppm) and (8) Ald/Ket: aldehydes and ketones (190-220 ppm) 100

Figure 19: Mesocosms (diameter: 1.45 m; height: 2.1 m; volume: 3.4 m^3) setup using a continuous flow system mimicking interactions between freshwater and seawater for mesocosms 1, 2 and 3 and between brackish water from mesocosm 3 and seawater for mesocosm 4. Mesocosm 1 was the control unit without silver nanoparticles added. Silver nanoparticles (20 nm) were continuously added to the surface of mesocosms 2 and 3, and in mesocosm 4 by the halocline transfer from mesocosm 3. Silver nanoparticles were added at a nominal concentration of 10 µgAg.L^{-1} 111

Figure 20: Salinity profile and natural particle size distributions in mesocosm 1. a) Salinity profile b) Particle size distributions obtained over 35 days between 0 and 5 000 nm (red) in freshwater, halocline and bottom seawater layers. The particle size distribution between 0 and 200 nm (black empty) have been magnified to show the presence of small particle populations 117

Figure 21: Aggregation kinetics over 12 h for AgNPs spiked at 10 µgAg.L^{-1}. a) surface water, b) halocline and c) bottom seawater layers in control mesocosm 1. Data in red correspond to hydrodynamic diameter before addition of AgNPs, and in black in presence of AgNPs..... 125

Figure 22: Average particle size distributions obtained over 35 days between 0 and 5 000 nm (red) in surface water, halocline and bottom seawater layers for a) mesocosm 2, b) mesocosm 3, and c) mesocosm 4. The particle size distribution between 0 and 200 nm (black empty) have been magnified to show the presence of small particle

populations. Particle size distributions were obtained by averaging the PSD measured each day during this 35 days experiment 129

Figure 23: Distribution of different particle populations added to the surface freshwater of mesocosms. a) clay at 10 mg.L^{-1} in dechlorinated water and filtered at 5 µm, b) natural organic matter at 6 mgDOC.L^{-1} of NOM in dechlorinated water and filtered at 5 µm, c) particle distribution calculate between 420 and 720 min from aggregation kinetics over 12 h of silver nanoparticles spiked in freshwater samples filtered at 5 µm and d) means of surface freshwater layer particle distribution in mesocosms 2 and 3 during the first week 131

Figure 24 : Mécanisme de formation des agrégats selon la concentration en nanoparticules d'argent 138

Figure 25 : Distribution de la taille des particules selon la concentration et la composition chimique de la NOM 140

Figure 26 : Devenir des nanoparticules d'argent dans un estuaire modèle 144

Figure 27: Transmission electron microscopy image of silver nanoparticles 150

Figure 28: Linear regression between slope ratio and zeta potential (mV) at a) 2.5 mgNOM.L^{-1} in nanopure water and b) 25 mgNOM.L^{-1} in nanopure water 156

Figure 29: Transmission electron microscopy image of silver nanoparticles 163

Figure 30: DLS signal (red triangle) and average hydrodynamic diameter (blue circle) at various AgNPs concentrations 165

Figure 31: Particle size distributions (black lines) and cumulative frequency plots (red curve) of 10 µAg.L^{-1} of AgNPs in a) 10 mM NaCl; b) 50 mM NaCl and c) 400 mM NaCl. These NaCl concentrations corresponded to salinity at 0.6, 2.9 and 23 PSU. Measurement of particle size distribution of AgNPs was performed directly after the addition of AgNPs 167

Figure 32: Particle size distributions observed in surface freshwater layer of mesocosm 1, during one week a) July 9, b) July 10, c) July 11, d) July 12, e) July 13, f) July 15, g) July 16 and h) the results averaged for the week 171

Figure 33: Cumulative frequency plots of particle size distributions observed in surface freshwater layer of mesocosm 1, during one week a) July 9, b) July 10, c) July 11, d) July 12, e) July 13, f) July 15, g) July 16 and h) the results averaged for the week. Some cumulative frequencies between 20 and 200 nm have been magnified to show the presence of small particles 172

Figure 34: Average cumulative frequency plots of particle size distributions, obtained over 35 days of experiment, observed in mesocosms 1, 2, 3 and 4 in surface water, halocline and bottom seawater. Some cumulative frequencies between 20 and 200 nm have been magnified to show the presence of small particles 173

Figure 35: Salinity profile in mesocosm 4 174

Figure 36: Particle size distributions of clay in absence (blue) and in presence (red) of 10 $\mu Ag.L^{-1}$ of AgNPs in dechlorinated water. Analysis of particle size distributions of clay with AgNPs was performed directly after the addition of AgNPs 176

xxx

LISTE DES ABRÉVIATIONS

Ald/Ket	Groupements aldéhydes et cétones
AliC	Carbones aliphatiques non-polaires
AFM	Microscopie à force atomique ; Atomic force microscopy
Ag	Argent
Ag_{dis}	Argent dissous
AgNPs	Nanoparticules d'argent ; Silver nanoparticles
Ag_{part}	Argent particulaire
AromC	Carbones aromatiques
ASW	Eau de mer artificielle ; Artificial seawater
LB	Luria Broth
CAE	Groupements carboxyliques, amides et esters
CCC	Concentration critique de coagulation
Da	Dalton
D_h	Diamètre hydrodynamique ; Hydrodynamic diameter
$D_{h0\text{-}200}$	Diamètre hydrodynamique moyen de la population de particules ayant une taille comprise entre 0 et 200 nm
$D_{h200\text{-}5\,000}$	Diamètre hydrodynamique moyen de la population de particules ayant une taille comprise entre 200 et 5 000 nm

$D_{h200\text{-}10\,000}$	Diamètre hydrodynamique moyen de la population de particules ayant une taille comprise entre 200 et 10 000 nm
DLA	Agrégation limitée par la diffusion ; Diffusion limited aggregation
DLS	Diffusion dynamique de la lumière ; Dynamic light scattering
DLVO	Théorie de Derjaguin, Landau, Verwey et Overbeek
DOC	Carbone organique dissous ; Dissolved organic carbon
ENMs	Nanomatériaux synthétisés
FA	Acides fulviques
HA	Acides humiques
HS	Substances humiques
HU	Humines
ICP-MS	Spectrométrie de masse par plasma à couplage inductif
IHSS	International humic substances society
ME	Microscopie électronique
nd	Non déterminé
NMR	Résonance magnétique nucléaire
NMs	Nanomatériaux
NOM	Matière organique naturelle ; Natural organic matter
$P_{0\text{-}200}$	Population de particules ayant une taille comprise entre 0 et 200 nm

$P_{200\text{-}5\,000}$	Population de particules ayant une taille comprise entre 200 et 5 000 nm
$P_{200\text{-}10\,000}$	Population de particules ayant une taille comprise entre 200 et 10 000 nm
PDI	Indice de polydispersité
PhenolC	Carbones phénoliques
PSD	Distribution de la taille des particules
Pξ	Potentiel zêta
RLA	Agrégation limitée réactionnellement ; Reaction limited aggregation
ROS	Espèces réactives de l'oxygène
SLFA	Acides fulviques du Saint-Laurent
SLHA	Acides humiques du Saint-Laurent
SL4ILE	Fraction hydrophile de la matière organique du Saint-Laurent
SL4OBE	Fraction hydrophobe de la matière organique du Saint-Laurent
TEM	Transmission electron microscopy
SPM	Matière particulaire en suspension ; Suspended particulate matter

INTRODUCTION GÉNÉRALE

LES NANOMATÉRIAUX

En chimie, une solution correspond à un mélange homogène (une seule phase) de composés dissous (solutés) dans un solvant (Chang and Goldsby, 2014; McNaught and Wilkinson, 2014). Dans une solution, une seule phase est observable et les solutés (ions et molécules) ont généralement une taille inférieure à 1 nm (Chang and Goldsby, 2014). Quand des particules sont dispersées dans un milieu dispersant, c'est une suspension (Chang and Goldsby, 2014; McNaught and Wilkinson, 2014). Plusieurs types de particules, de tailles et de compositions chimiques différentes peuvent former une suspension en milieu liquide (Figure 1). Dans une suspension, les particules peuvent être influencées par la gravité, ce qui peut favoriser leur sédimentation si leur densité est supérieure à celle du solvant (Graham and Cragg, 1956).

Une sous-famille des suspensions est nommée colloïde. Les colloïdes sont des particules dispersées uniformément (phase dispersée), ayant une taille comprise entre 1 nm et 1 µm (Figure 1), dans un milieu dispersant (phase dispersante) (Chang and Goldsby, 2014; Everett, 1992; Lead and Wilkinson, 2006; Zumdahl, 1998). Dans un système colloïdal, les particules dispersées sont suffisamment petites pour être influencées par le mouvement brownien, mais faiblement par la sédimentation (Buffle *et al.,* 1998; Everett, 1992; Graham and Cragg, 1956; Lead and Wilkinson, 2006). Ces particules présentent un fort ratio surface/volume (surface spécifique), leur conférant une énergie libre de surface et une forte réactivité (Everett, 1992). Les colloïdes représentent une vaste gamme de composés aussi

bien organiques qu'inorganiques. Lorsque des nanomatériaux (NMs) sont dispersés dans un solvant, ils forment des colloïdes.

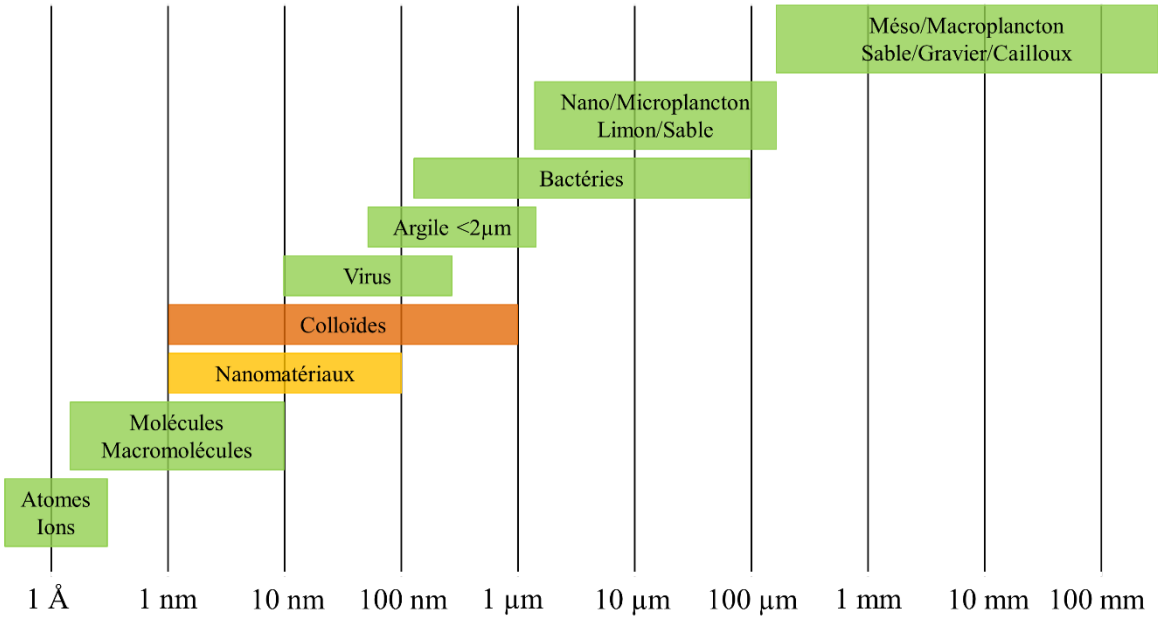

Figure 1 : Gamme de tailles des principales particules et solutés se trouvant en milieu liquide

Selon la norme ISO/TS27687:2008, 2008, les objets ayant leurs trois dimensions (longueur, largeur, hauteur) comprises entre 1 et 100 nm sont considérés comme nano-objets ou nanomatériaux(ISO/TS27687:2008, 2008). Toutefois, certains nano-objets, tels que les nanofibres, les nanotubes ou les nanoplaques peuvent avoir certaines de leurs dimensions supérieures à l'échelle nanométrique (ISO/TS80004-2:2015, 2015). Pour cela, la norme ISO/TS27687:2008 a été récemment remplacée par la norme ISO/TS80004-2:2015. Cette nouvelle norme définit les NMs comme étant tout matériau ayant au moins une dimension comprise entre 1 et 100 nm.

Les NMs sont des composés ubiquistes, présents dans l'ensemble des compartiments environnementaux : les sols, l'atmosphère et les systèmes aquatiques (Bhatt and Tripathi, 2011; Delay and Frimmel, 2012). Les NMs peuvent être d'origines naturelles, comme les

nanoargiles, les oxy/hydroxydes métalliques, les sulfures métalliques, les substances humiques... (Bhatt and Tripathi, 2011; Delay and Frimmel, 2012). D'autres NMs sont issus de l'activité humaine (Bhatt and Tripathi, 2011; Delay and Frimmel, 2012). Les NMs anthropiques peuvent être produits involontairement, comme durant la combustion d'énergie fossile, ou synthétisés par un procédé industriel (Bhatt and Tripathi, 2011). Les NMs présentent des propriétés physiques et chimiques différentes des matériaux massifs de même composition chimique (ISO/TS80004-2:2015, 2015; Labille and Brant, 2010; Tejamaya *et al.,* 2012). L'intérêt croissant envers les propriétés uniques des nanomatériaux a permis le développement de la nanotechnologie. Le but de la nanotechnologie est de créer de nouveaux produits ou matériaux à l'échelle nanométrique permettant, par exemple une amélioration de la conductivité, de la résistance, de la durabilité ou de la réactivité de certains matériaux (Powell *et al.,* 2008). Il est estimé qu'en 2018, la nanotechnologie aura un potentiel économique de trois mille milliards de dollars US (Nanotechproject, 2017). Actuellement, les nanomatériaux de synthèse (ENMs) peuvent être divisés en cinq grandes familles : (1) les ENMs à base de carbone ; (2) les oxydes métalliques comme les dioxydes de titane (TiO_2) ; (3) les points quantiques ; (4) les dendrimères ou polymères multifonctionnels complexes ; et (5) les métaux à valence zéro, tels que les nanoparticules de fer et d'argent (Bhatt and Tripathi, 2011). En 2014, la production globale d'ENMs a été estimée entre 360 et 450 $t.an^{-1}$ pour les ENMs à base d'argent, environ 3 000 $t.an^{-1}$ pour les nanotubes de carbone et de 10 000 $t.an^{-1}$ pour les oxydes de titane (Keller and Lazareva, 2014; Sun *et al.,* 2014). Les ENMs peuvent être utilisés en médecine, dans les composantes électroniques, les cosmétiques, les techniques de bioremédiation... (Nanotechproject, 2017; SCENIHR, 2014).

Actuellement, plus de 1800 produits contiennent des NMs, dont plus de 440 produits (plus de 24%) contiennent des nanoparticules d'argent (AgNPs) (Nanotechproject, 2017; Vance *et al.,* 2015). Les AgNPs sont couramment utilisées pour leurs propriétés antimicrobiennes, dans les textiles, les cosmétiques, les produits de soin personnel, la conservation d'aliments, les équipements médicaux, et les peintures extérieures (Kaegi *et al.,*

2010; Lem *et al.,* 2012; Nanotechproject, 2017; SCENIHR, 2014; Wijnhoven *et al.,* 2009; Yetisen *et al.,* 2016). Les AgNPs présentent aussi une conductivité, une stabilité chimique, une activité catalytique et un comportement optique unique (SCENIHR, 2014; Tolaymat *et al.,* 2010). Ces propriétés permettent des applications dans les secteurs de l'électronique, de la production d'énergie, dans les détecteurs ou capteurs (SCENIHR, 2014; Tolaymat *et al.,* 2010).

LES NANOPARTICULES D'ARGENT

L'argent est connu et utilisé depuis l'Antiquité comme monnaie d'échange, en bijouterie, en photographie argentique, dans la préservation d'aliment, mais aussi en médecine (Alexander, 2009; SCENIHR, 2014). L'utilisation de l'argent en médecine est due à sa forte toxicité sur les microorganismes (Alexander, 2009). L'argent inhibe l'activité de certaines enzymes comme la Na^+/K^+-ATPase, impacte l'activité mitochondriale, induit un stress oxydatif, réduit le taux de croissance et l'activité microbienne (Bone *et al.,* 2012; Navarro *et al.,* 2008a; Ratte, 1999; Wasmuth *et al.,* 2016).

Les AgNPs sont généralement obtenues par réduction d'un sel d'argent, par exemple du nitrate d'argent (Bhatt and Tripathi, 2011). Une des premières synthèses d'AgNPs, décrite en 1889, a été réalisée en ajoutant à une solution d'argent une solution réductrice de citrate ferreux (Lea, 1889; Nowack *et al.,* 2011). Actuellement, il existe un grand nombre de méthodes de synthèse pour obtenir des AgNPs ayant des propriétés physico-chimiques spécifiques. Ces propriétés sont : (1) la taille ; (2) la forme ; (3) le revêtement ou greffon ; (4) les charges de surface et le potentiel zêta ; (5) la surface spécifique ; (6) la topographie ou morphométrie de surface ; (7) la structure cristalline ou amorphe ; (8) la solubilité ; (9) la pureté ; (10) l'hydrophobicité de la surface ; (11) la dissolution ; et (12) l'état agrégé ou aggloméré (Delay and Frimmel, 2012; Nel *et al.,* 2009; SCENIHR, 2014).

Il est possible de diviser les AgNPs synthétisées en milieu aqueux en deux grandes familles : (1) les AgNPs nues (sans revêtement) ; et (2) les AgNPs avec un revêtement organique. Les AgNPs nues sont généralement obtenues en réduisant un sel d'argent avec un agent réducteur inorganique comme du $NaBH_4$ (El Badawy *et al.,* 2010; Lin *et al.,* 2012) ou en utilisant un sucre ayant une fonction aldéhyde (Huynh and Chen, 2011; Li *et al.,* 2012, 2010). La deuxième famille est obtenue, soit en ajoutant un composé organique à des AgNPs nues (Lin *et al.,* 2012) ou en utilisant un composé organique comme agent réducteur et agent de revêtement ou greffon (Al-Sid-Cheikh *et al.,* 2011; El Badawy *et al.,* 2010; Tejamaya *et al.,* 2012). L'ajout d'un revêtement organique aux AgNPs permet de modifier leurs propriétés physico-chimiques comme la taille, la forme, les charges de surface… (Tolaymat *et al.,* 2010; Wiley *et al.,* 2005; Yetisen *et al.,* 2016). Cela permet aussi d'augmenter la stabilité des dispersions colloïdales d'AgNPs et d'éviter leurs agrégations (Lin *et al.,* 2012). Les revêtements produisent des effets électrostatiques et/ou stériques (Levard *et al.,* 2012; Lin *et al.,* 2012). La stabilisation électrostatique, par exemple avec du citrate, est due à une modification des charges de surface, favorisant les répulsions électrostatiques entre les AgNPs (Lin *et al.,* 2012). La stabilisation stérique est due à l'arrangement spatial du revêtement autour des AgNPs. Cette stabilisation résulte d'une contribution osmotique et élastique (Lin *et al.,* 2012). En 2010, les AgNPs de taille inférieure à 40 nm et ayant un revêtement au citrate étaient les plus couramment utilisées (Tolaymat *et al.,* 2010).

Les nombreuses applications et la rapide augmentation du nombre de produits contenant des AgNPs soulèvent de fortes inquiétudes sur leurs effets dans l'environnement et sur la santé humaine (Nanotechproject, 2017; SCENIHR, 2014; Tolaymat *et al.,* 2010; US-EPA, 2014). De plus, l'utilisation journalière de produits de consommation contenant des AgNPs augmente la probabilité de les retrouver dans l'environnement (SCENIHR, 2014; US-EPA, 2014). Leurs comportements et devenirs en milieu naturel sont encore peu connus, et plus particulièrement dans les milieux de transition entre les eaux douces et les eaux salées, comme les milieux estuariens. Plusieurs agences gouvernementales indiquent que les

connaissances actuelles concernant les AgNPs dans les eaux naturelles ne fournissent pas de données suffisantes pour permettre une bonne législation de ces composés (OECD, 2011; SCENIHR, 2014; US-EPA, 2014). Une meilleure compréhension du comportement et du devenir des AgNPs dans les milieux aquatiques permettra une amélioration de la législation de ces composés.

COMPORTEMENT ET DEVENIR DES NANOPARTICULES D'ARGENT DANS L'ENVIRONNEMENT

Il est difficile d'estimer la quantité d'AgNPs rejetée dans l'environnement (Fabrega *et al.,* 2011; Holden *et al.,* 2014; Vance *et al.,* 2015). Toutefois, l'utilisation d'approche probabiliste de l'analyse des flux de matériaux permet d'évaluer les concentrations environnementales des ENMs, de leurs sources de production et d'utilisation jusqu'aux stations de traitement des eaux usées, eaux de surface, sédiments, sols et dans l'atmosphère (Coll *et al.,* 2016; Gottschalk *et al.,* 2013; Keller and Lazareva, 2014).

Les principales sources de rejets des AgNPs dans l'environnement (Figure 2) sont (1) les eaux usées provenant de la synthèse et de l'incorporation des AgNPs dans les produits de consommation (Bhatt and Tripathi, 2011; Fabrega *et al.,* 2011; Sayes and Aquino, 2017) ; (2) les eaux usées provenant du lavage de produits de consommation contenant des AgNPs (Benn and Westerhoff, 2008; Geranio *et al.,* 2009; Sayes and Aquino, 2017; Yetisen *et al.,* 2016) ; et (3) les déchets solides provenant des usines synthétisant ou incorporant des AgNPs, ainsi que la dégradation de ces produits en milieu naturel (Blaser *et al.,* 2008; Sayes and Aquino, 2017). Une partie des eaux usées est directement rejetée dans l'environnement aquatique, dont les estuaires. Une autre partie passe par des stations de traitement des eaux usées (Blaser *et al.,* 2008; Sayes and Aquino, 2017). Ces stations peuvent retenir jusqu'à 95% des AgNPs dans les boues (Kaegi *et al.,* 2011; Sayes and Aquino, 2017). Les boues peuvent être incinérées avec les déchets solides ou être directement utilisées sur les terres agricoles

pour les fertiliser (Markus *et al.,* 2017; Sayes and Aquino, 2017). Les cendres produites par l'incinération des boues et des déchets peuvent être placées dans des sites d'enfouissement (Blaser *et al.,* 2008; Sayes and Aquino, 2017; Sun *et al.,* 2014). Lors d'évènements pluvieux, le lessivage des sites d'enfouissement, des sols et des surfaces peut exporter les AgNPs dans les systèmes aquatiques (Blaser *et al.,* 2008; Brar *et al.,* 2010; Kaegi *et al.,* 2010; Sayes and Aquino, 2017).

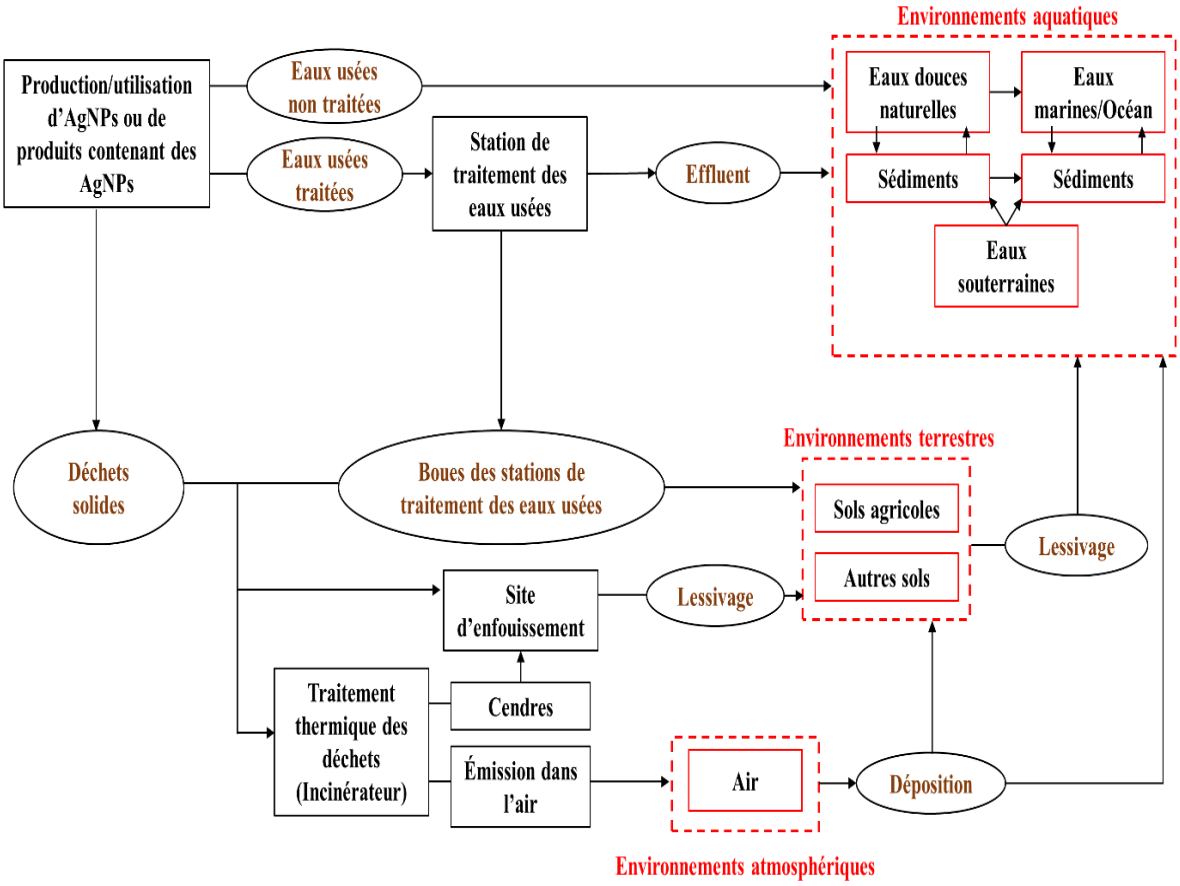

Figure 2 : Rejets des nanoparticules d'argent : de leurs sources aux différents compartiments environnementaux (traduit de Blaser *et al.,* 2008)

Les utilisations multiples des AgNPs rendent inévitables les rejets vers les rivières et les eaux côtières. Les concentrations estimées, par différents modèles, sont comprises entre : 10 ngAg.L^{-1} et quelques µgAg.L^{-1} dans les eaux de surface, entre 30 ngAg.L^{-1} et 70 µgAg.L^{-1} dans les effluents des stations de traitement des eaux usées et entre 1 et 5 mgAg.kg^{-1} dans les boues des stations de traitement des eaux usées (Gottschalk *et al.,* 2013; Keller and Lazareva, 2014; McGillicuddy *et al.,* 2017). À cause de ces risques de rejets, elles sont répertoriées comme contaminants aquatiques d'intérêt (SCENIHR, 2014; US-EPA, 2014). Comme plus de 60% de la population mondiale vit proche des côtes (Bianchi, 2007), les risques de libération accidentelle ou chronique des AgNPs dans les zones côtières, et plus particulièrement les systèmes estuariens, sont importants. Un estuaire est une zone à l'interface entre les continents et les océans (Bianchi, 2007). Les estuaires présentent de fortes variabilités spatio-temporelles des conditions redox (milieu oxique, hypoxique ou anoxique), de la salinité, du pH, de la concentration en matière organique naturelle (NOM) et en matière particulaire en suspension (SPM) (Bianchi, 2007; D'Anglejan and Ingram, 1976; Hélie and Hillaire-Marcel, 2006; Simons *et al.,* 2010; Tremblay and Gagné, 2009). Cette forte variabilité peut induire des transformations complexes des AgNPs (Figure 3).

Ces transformations sont contrôlées par les propriétés spécifiques aux AgNPs (taille, revêtement, charges de surface...) ainsi que par les propriétés physico-chimiques du milieu récepteur (Lowry *et al.,* 2012b; SCENIHR, 2014). Les transformations des AgNPs peuvent être divisées en deux types de processus : (1) un comportement individuel impliquant des particules uniques subissant une oxydation ou une sulfidation ; et (2) un comportement de groupe impliquant plusieurs particules, conduisant à l'autoagrégation ou l'hétéroagrégation. De plus, certaines transformations, par exemple la sorption ou les interactions entre les AgNPs, les sels ou la NOM, peuvent fortement moduler les comportements individuels et les comportements de groupe.

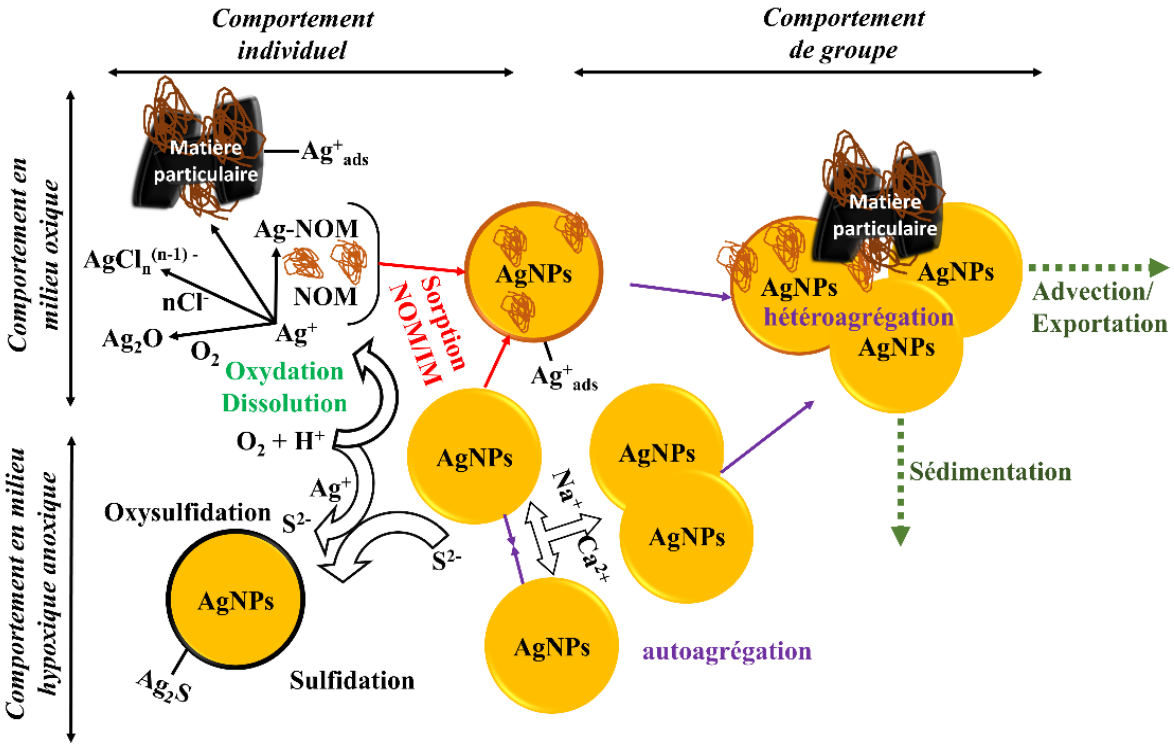

Figure 3 : Transformation et comportement général des nanoparticules d'argent dans un système aquatique

COMPORTEMENT INDIVIDUEL

- Oxydation-dissolution

En milieu oxique, la présence d'oxygène dissous peut induire une oxydation de la surface des AgNPs (Liu and Hurt, 2010; Zhang *et al.,* 2016), selon l'équation 1.

$$AgNPs + ¼\ O_{2\,(aq)} + H^{+} = Ag^{+}_{(aq)} + ½\ H_2O \qquad (1)$$

Le processus d'oxydation-dissolution est directement influencé par le pH du milieu (Peretyazhko, 2014; Zhang *et al.,* 2016). Il est aussi influencé par la taille des AgNPs, plus important pour des AgNPs de petite taille (Dobias and Bernier-Latmani, 2013; Peretyazhko, 2014; Zhang *et al.,* 2016). La composition du milieu, comme la présence de chlorure et de

NOM, peut diminuer la dissolution des AgNPs (Gunsolus *et al.,* 2015; Ho *et al.,* 2010; Labille and Brant, 2010; Liu and Hurt, 2010; Philippe and Schaumann, 2014; Wang *et al.,* 2016), ainsi que la présence d'un revêtement organique (Ho *et al.,* 2010; Liu and Hurt, 2010). L'argent libéré dans le milieu par dissolution peut atteindre entre 2 et 3% de l'argent total après 14 jours, et jusqu'à 30% après 4 mois (Dobias and Bernier-Latmani, 2013; Li *et al.,* 2012; Zhang *et al.,* 2016). Les ions Ag^+ relargués peuvent interagir avec les composés présents dans le milieu récepteur, dont les chlorures, les carbonates, et les sulfates (Levard *et al.,* 2012). La présence de chlorure dans les eaux estuariennes favorise thermodynamiquement la formation de chlorocomplexes d'argent ($AgCl_n^{(n-1)-}$). La spéciation de ces complexes est influencée par le ratio Cl/Ag du milieu (Levard *et al.,* 2013). Un faible ratio favorise la formation d'AgCl alors qu'un fort ratio induit la formation $AgCl_2^-$, $AgCl_3^{2-}$ et $AgCl_4^{3-}$. Ces sels peuvent interagir avec les surfaces des AgNPs par sorption. Ils peuvent aussi précipiter dans le milieu et former de nouveaux nanomatériaux d'argent (K_{spAgCl} = 1.77 x 10^{-10} (Levard *et al.,* 2012)). Les ions Ag^+ peuvent aussi former des sels plus ou moins solubles avec les oxydes (K_{spAgO} = 4.00 x 10^{-11}), les carbonates ($K_{spAg_2CO_3}$ = 8.46 x 10^{-12}) et les sulfates ($K_{spAg_2SO_4}$ = 1.20 x 10^{-5}) (Levard *et al.,* 2012). Selon leurs solubilités, ils peuvent précipiter et interagir avec les surfaces des AgNPs par sorption. Les ions Ag^+ peuvent aussi interagir avec la NOM et former de nouvelles AgNPs (Adegboyegs *et al.,* 2013; Akaighe *et al.,* 2012, 2011; Wang *et al.,* 2016) ainsi qu'interagir avec la SPM, par exemple les argiles (Zhou *et al.,* 2012).

- Sulfidation

La sulfidation est un processus se développant principalement en milieu hypoxique et anoxique, en présence d'ions sulfures S^{2-} (Levard *et al.,* 2012). Cette transformation peut se produire dans les stations de traitement des eaux usées (Kaegi *et al.,* 2011; Levard *et al.,* 2012, 2011), dans les sols et les sédiments (Colman *et al.,* 2013; Dale *et al.,* 2013; Lowry *et al.,* 2012a), et dans certaines zones estuariennes présentant de faibles concentrations

d'oxygène dissous. Les ions S^{2-} peuvent interagir avec les AgNPs soit par oxysulfidation ou par sulfidation directe. L'oxysulfidation est un processus où les ions Ag^{+} formés par oxydation-dissolution interagissent avec les ions S^{2-} (Liu *et al.,* 2011). Le sulfure d'argent (Ag_2S) étant très peu soluble (K_{sp} = 5.92 x 10^{-51} (Levard *et al.,* 2012)), il peut précipiter et former de nouveaux nanomatériaux d'argent ou sorber autour des AgNPs (Liu *et al.,* 2011). Ce processus est moins important que la sulfidation directe (Baalousha *et al.,* 2015). La sulfidation directe des AgNPs résulte d'une interaction entre les ions S^{2-} et les surfaces des AgNPs, induisant la formation d'une couche Ag_2S (Baalousha *et al.,* 2015; Liu *et al.,* 2011). La sulfidation est influencée par le revêtement des AgNPs (Baalousha *et al.,* 2015; Levard *et al.,* 2011; Liu *et al.,* 2011). De plus, c'est un processus limité permettant la conservation de certaines propriétés des AgNPs d'origine (avant sulfidation) (Baalousha *et al.,* 2015).

COMPORTEMENT DE GROUPE

- Sorption

La sorption est un processus complexe où une substance interagit avec un solide, ou sorbant, impliquant de l'adsorption ou de l'absorption (McNaught and Wilkinson, 2014). L'adsorption se produit lorsque les composés dissous interagissent avec la surface du solide et y sont retenus. L'absorption est un phénomène tridimensionnel où le composé dissous interagit avec le solide par incorporation. Si le composé ad/absorbé se sépare du sorbant, c'est le phénomène de désorption (McNaught and Wilkinson, 2014). La sorption de composés inorganiques ou organiques sur les AgNPs peut modifier les surfaces des AgNPs et moduler leurs comportements individuels ou l'agrégation.

Les charges de surface des particules montrent des valeurs très différentes lorsque les particules sont dans de l'eau de mer contenant ou non de la NOM (Neihof and Loeb, 1974, 1972). Dans une eau de mer sans NOM, les charges de surface des particules peuvent être positives ou négatives. Ces surfaces présentent toutes des charges de surface négatives en

présence de NOM en milieu estuarien (Neihof and Loeb, 1974, 1972). Comme la sorption est un phénomène exothermique et spontané (Somorjai, 1994), cela signifie qu'en milieu estuarien la NOM peut interagir avec des particules comme les AgNPs (Delay *et al.,* 2011; Nason *et al.,* 2012) et moduler les charges de surface. Les interactions entre la NOM et les ENMs, dont les AgNPs, peuvent se produire par divers mécanismes : des interactions de van der Waals, des interactions hydrophobes, des interactions électrostatiques, des échanges de ligands, des ligands pontants, et des liaisons hydrogène (Louie *et al.,* 2016; Philippe and Schaumann, 2014; Wang *et al.,* 2016). Des études indiquent que l'adsorption de la NOM sur les AgNPs et d'autres ENMs s'effectue par des interactions avec les groupements carboxyliques, aliphatiques, aromatiques et phénoliques ainsi que par des groupements fonctionnels contenant de l'azote et du soufre (Gunsolus *et al.,* 2015; Louie *et al.,* 2016; Philippe and Schaumann, 2014; Sánchez-Cortés *et al.,* 1998; Wang *et al.,* 2016). De plus, la NOM ayant un poids moléculaire élevé tend à interagir avec les surfaces par formation de liaison hydrogène (Philippe and Schaumann, 2014; Sánchez-Cortés *et al.,* 1998). La NOM ayant un poids moléculaire plus faible s'adsorbe par la formation d'interactions électrostatiques et hydrophobes (Philippe and Schaumann, 2014; Sánchez-Cortés *et al.,* 1998). Le revêtement de NOM peut prendre différentes conformations et tailles selon la quantité de NOM adsorbée (Louie *et al.,* 2016), ce qui peut influencer le comportement et le devenir des AgNPs dans les systèmes estuariens.

- Agrégation

L'agrégation est définie comme un processus où des particules dispersées tendent à interagir ensemble, formant un assemblage de particules nommé agrégat (McNaught and Wilkinson, 2014). Dans un système colloïdal, les AgNPs se déplacent aléatoirement, un phénomène attribuable au mouvement brownien causé par l'agitation thermique (Elimelech *et al.,* 1998; Petosa *et al.,* 2010). Durant ce déplacement, les AgNPs peuvent entrer en collision et interagir pour former des associations de particules plus larges, des agrégats.

Selon les conditions physico-chimiques du milieu, les collisions peuvent être efficaces, induisant la formation d'agrégats, ou inefficaces et ne produisant aucun assemblage (Elimelech *et al.,* 1998; Petosa *et al.,* 2010). Ces interactions peuvent être modélisées par la théorie Derjaguin, Landau, Verwey et Overbeek (DLVO) ou la DLVO-étendue (Derjaguin and Landau, 1941; Grasso *et al.,* 2002; Verwey and Overbeek, 1948).

La DLVO indique que l'agrégation est un processus contrôlé par des forces attractives et par des forces répulsives (Derjaguin and Landau, 1941; Verwey and Overbeek, 1948). Les forces attractives correspondent aux forces de van der Waals. Les forces répulsives sont des répulsions électrostatiques causées par le chevauchement de la double couche électrique des AgNPs en interaction. Ces forces sont additives et permettent de déterminer l'énergie totale d'interaction entre les particules en fonction de la distance qui les sépare (Elimelech *et al.,* 1998). La stabilité des AgNPs en suspension est observée quand les forces répulsives sont plus importantes que les forces attractives (Elimelech *et al.,* 1998; Petosa *et al.,* 2010). La présence de sels dans une suspension d'AgNPs déstabilise l'état d'équilibre de cette suspension par différents processus complémentaires. L'augmentation de la force ionique, due à l'ajout de sel, induit une diminution de l'épaisseur de la double couche électrique (Elimelech *et al.,* 1998; Petosa *et al.,* 2010). De plus, les contre-ions provenant des sels peuvent aussi moduler les charges de surface (Levard *et al.,* 2012). Les cations interagissent avec les surfaces chargées négativement, alors que les anions sont attirés par les surfaces chargées positivement. Les forces répulsives diminuent. Si les forces répulsives demeurent plus fortes que les forces attractives, les collisions entre les AgNPs ne sont pas toutes efficaces. L'agrégation est considérée comme limitée réactionnellement (Labille and Brant, 2010; Petosa *et al.,* 2010). Dans ces conditions, la vitesse d'agrégation augmente avec une augmentation de la concentration en sel. Par ailleurs, si les forces attractives sont égales ou plus importantes que les forces répulsives, les collisions entre AgNPs sont toutes efficaces. L'agrégation est considérée comme limitée par la diffusion (Labille and Brant, 2010; Petosa *et al.,* 2010). La vitesse d'agrégation reste constante même avec une augmentation de la

concentration en sel. La zone de transition des concentrations en sels entre des conditions non favorables et des conditions favorables est appelée la concentration critique de coagulation (CCC) (Petosa *et al.,* 2010). La CCC dépend de la valence des ions, des charges de surface (Petosa *et al.,* 2010) et de la nature du revêtement (Huynh and Chen, 2011), comme présenté dans le Tableau 1. Plus la valence des ions augmente, plus la CCC diminue, signifiant un effet déstabilisateur plus important de ces ions. Cet effet est défini par la règle de Schulze-Hardy qui indique que la concentration critique de coagulation est proportionnelle à la valence des contre-ions (z^{-6}) (Elimelech *et al.,* 1998; McNaught and Wilkinson, 2014). En solution aqueuse, les CCC des AgNPs sont supérieures à 30 mM de sels monovalents (Tableau 1). En présence de sels multivalents, les CCC sont généralement inférieures à 10 mM, sauf pour certains polymères. Comme les estuaires présentent une forte variation de la salinité, les vitesses d'agrégation des AgNPs différeront selon la concentration en sel, inférieure ou supérieure à la CCC. Des études menées sur des ENMs à base d'oxydes métalliques (CeO_2 et ZnO) ont démontré que la température du milieu peut aussi fortement moduler les CCC et les tailles des agrégats (Chen *et al.,* 2012; Yung *et al.,* 2017). Une augmentation de la température induit une diminution de la viscosité du milieu et une augmentation du coefficient de diffusion des particules, leurs permettant de se déplacer plus rapidement. De plus, les forces répulsives semblent diminuer lors d'une augmentation de la température (Chen *et al.,* 2012).

La nature chimique du revêtement organique modifie aussi le comportement des AgNPs (Tableau 1). Des AgNPs possédant un revêtement citrate ont une CCC plus faible (Baalousha *et al.,* 2013; El Badawy *et al.,* 2012) que des AgNPs possédant des revêtements polymériques comme le polyvinylpyrrolidone (Chen and Zhang, 2012; Huynh and Chen, 2011) ou la gomme arabique (Lin *et al.,* 2012). Avec certains revêtements, comme le Tween 80 (monooléate de polyoxyéthylène sorbitane), la CCC des AgNPs est supérieure à 1 M (Li *et al.,* 2012).

Tableau 1 : Concentrations critiques de coagulation pour différentes nanoparticules d'argent (modifié de Baalousha *et al.* (2013))

revêtement	Taille (nm)	CCC NaCl (mM)	CCC $NaNO_3$ (mM)	CCC $CaCl_2$ (mM)	CCC $Ca(NO_3)_2$ (mM)	Référence
Nue (aucun revêtement)	67	25	30	nd	3	(El Badawy *et al.,* 2012)
	82	40	30	2	nd	(Li *et al.,* 2012, 2010)
	22	nd	200	nd	nd	(Lin *et al.,* 2012)
Citrate	30	122	117	2.2	1.7	(Baalousha *et al.,* 2013)
	58	70	70	nd	5	(El Badawy *et al.,* 2012)
	72	47.6	nd	2.1	nd	(Huynh and Chen, 2011)
	82	40	30	2	nd	(Li *et al.,* 2012, 2010)
	170	40	30	2	nd	(Li *et al.,* 2012, 2010)
Caséine	58	138	nd	3.3	nd	(Zhang *et al.,* 2012)
Dextrine	28	589	nd	4.7	nd	(Zhang *et al.,* 2012)
Gomme arabique	174	nd	>1 000	nd	nd	(Lin *et al.,* 2012)

revêtement	Taille (nm)	CCC NaCl (mM)	CCC $NaNO_3$ (mM)	CCC $CaCl_2$ (mM)	CCC $Ca(NO_3)_2$ (mM)	Référence
Polyethyleneimine	95	Pas observé	Pas observé	nd	Pas observé	(El Badawy *et al.,* 2012)
Polyvinylpyrrolidone	nd	2 322	nd	57.2	nd	(Chen and Zhang, 2012)
	72	Pas observé	Pas observé	nd	Pas observé	(El Badawy *et al.,* 2012)
	67	111.5	nd	4.9	nd	(Huynh and Chen, 2011)
	69	nd	530	nd	nd	(Lin *et al.,* 2012)
	30	1 011	nd	18.8	nd	(Zhang *et al.,* 2012)
SDS (1 mM)	82	40	30	2	nd	(Li *et al.,* 2012, 2010)
SDS (10 mM)	82	50	40	4	nd	(Li *et al.,* 2012, 2010)
Tween 80	88	500	>1 000	700	nd	(Li *et al.,* 2012, 2010)

nd : non déterminé

Selon la DLVO, la CCC est directement corrélée aux charges de surface, reliées au potentiel zêta (Pξ) (El Badawy *et al.,* 2010; Philippe and Schaumann, 2014). Elles proviennent du type d'ENMs, du revêtement, des composés sorbés, ou de l'état d'oxydation de la surface (Doane *et al.,* 2012; Labille and Brant, 2010; Xu, 2001a). C'est le cas pour des AgNPs stabilisées par du citrate (El Badawy *et al.,* 2010; Philippe and Schaumann, 2014). Toutefois, cette corrélation ne fonctionne pas pour des AgNPs ayant un revêtement polymérique comme le polyvinylpyrrolidone. Avec ce type de revêtement, les AgNPs ont un Pξ relativement faible, mais une CCC importante (Chen and Zhang, 2012; El Badawy *et al.,* 2012; Huynh and Chen, 2011). Dans ce cas, il est important d'utiliser la DLVO-étendue pour décrire le comportement agrégatif. La DLVO-étendue prend en compte : les liaisons hydrogène, les interactions hydrophobes, les interactions stériques, la pression d'hydratation, la polarisabilité des surfaces comme les interactions entre donneur et accepteur d'électrons, les interactions acide-base de Lewis (Grasso *et al.,* 2002; Labille and Brant, 2010). Les interactions peuvent provenir du revêtement organique ou de la sorption de la NOM.

Comme décrits dans l'approche « à trois composants colloïdaux » par Buffle *et al.* (1998), la stabilité des colloïdes inorganiques naturels varie selon la nature de la NOM. Les substances humiques ont tendance à stabiliser les colloïdes, alors que les polysaccharides rigides peuvent les ponter, favorisant l'agrégation et la sédimentation (Buffle *et al.,* 1998). La présence de NOM sur les surfaces des AgNPs, due à l'adsorption, contrôle aussi la dispersion ou l'agrégation des AgNPs (Philippe and Schaumann, 2014; Wang *et al.,* 2016). La présence de substances humiques tend à faire augmenter la CCC des AgNPs et leur stabilité. En présence d'acides fulviques provenant de la rivière Suwannee (États-Unis), la CCC d'AgNPs avec un revêtement au citrate passe de 122 à 152 mM de NaCl (Baalousha *et al.,* 2013). Avec des acides humiques de la rivière Suwannee, elle augmente de 48 à 72 mM de NaCl (Huynh and Chen, 2011). La NOM étant un polyélectrolyte chargé négativement, son adsorption sur les AgNPs tend à ajouter des charges négatives aux surfaces, favorisant les répulsions électrostatiques (Huynh and Chen, 2011; Louie *et al.,* 2016; Philippe and

Schaumann, 2014; Wang *et al.,* 2016). Ce revêtement favorise aussi la formation d'effets stériques (Chen and Zhang, 2012; Louie *et al.,* 2016; Philippe and Schaumann, 2014). En présence de NOM, les ions divalents induisent une évolution de la CCC plus faible que les ions monovalents et tendent à déstabiliser les AgNPs. Pour des AgNPs-citrate, la CCC passe de 2.2 mM à 3 mM de $CaCl_2$ en présence d'acides fulviques de la rivière Suwannee (Baalousha *et al.,* 2013). Une étude indique qu'en présence de Ca^{2+} et d'acides humiques de la rivière Suwannee, aucune distinction entre l'agrégation limitée réactionnellement et l'agrégation limitée par la diffusion n'est observable (Huynh and Chen, 2011). Ces différences peuvent être causées par la formation de complexes entre les substances humiques adsorbées sur les AgNPs et les ions Ca^{2+} (Baalousha *et al.,* 2013; Chen and Zhang, 2012; Philippe and Schaumann, 2014).

La nature de la matière organique modifie aussi la stabilité des nanoparticules (Furman *et al.,* 2013; Nason *et al.,* 2012; Philippe and Schaumann, 2014). Les AgNPs sont plus stables en présence d'acides humiques qu'en présence d'acides fulviques (Furman *et al.,* 2013). Pour des nanoparticules d'or, il faut une concentration plus importante en acides fulviques qu'en acides humiques pour les stabiliser (Nason *et al.,* 2012). Toutefois, une étude indique que la présence d'acides fulviques provenant du réservoir Vallsjøen (Norvège) ne modifie pas la CCC d'AgNPs sans revêtement organique (Li *et al.,* 2010). De plus, la composition élémentaire, et plus particulièrement la teneur en azote et en soufre de la NOM, module les vitesses d'agrégations des AgNPs et d'autres ENMs (Deonarine *et al.,* 2011; Gunsolus *et al.,* 2015; Louie *et al.,* 2015; Nason *et al.,* 2012). La concentration en matière organique a aussi un impact sur la stabilité des AgNPs. Gao *et al.* (2012) ont observé qu'en dessous de 10 $mgC.L^{-1}$ d'acides humiques, les AgNPs restent dispersées dans le milieu. À une concentration supérieure à 10 $mgC.L^{-1}$, les AgNPs sédimentent. Ceci est essentiellement attribuable à l'agrégation (Gao *et al.,* 2012). Cet effet peut être expliqué par l'approche « à trois composants colloïdaux » de Buffle *et al.* (1998). Les auteurs indiquent qu'entre 0.5 et 10 $mgNOM.L^{-1}$, les acides fulviques et humiques stabilisent les colloïdes inorganiques par

des effets électrostatiques (Buffle *et al.,* 1998). À plus forte concentration, ils tendent à former une structure de type gel (Buffle *et al.,* 1998). Ces données indiquent que la stabilité des AgNPs diffère selon l'origine (géographique…), la nature (acides humiques, acides fulviques…), la concentration et la composition chimique de la NOM. Actuellement, il n'y a pas de données sur le comportement agrégatif des AgNPs en présence de NOM estuarienne. Il est important de mieux comprendre le rôle de la NOM estuarienne sur la stabilité des AgNPs en milieu estuarien.

Dans un milieu aquatique complexe comme les estuaires, les colloïdes naturels sont connus pour interagir avec les métaux, les nutriments et des composés organiques (Buffle *et al.,* 1998; Lead and Wilkinson, 2006). Dans ces milieux, des interactions multiples peuvent se produire entre les AgNPs, et entre les AgNPs et les particules naturelles, comme les substances humiques, les argiles, les substances polymériques extracellulaires ou les exopolysaccharides et d'autres composés d'origine biologique (Nel *et al.,* 2009; Philippe and Schaumann, 2014; Wang *et al.,* 2015, 2016; Zhou *et al.,* 2012). Selon les particules en interactions, deux types d'agrégations peuvent être observés. L'autoagrégation se produit entre des particules identiques interagissant ensemble et l'hétéroagrégation pour des particules de nature différente (Wang *et al.,* 2015; Yu and Borkovec, 2002). En milieu aquatique naturel, l'hétéroagrégation des AgNPs avec d'autres particules ou colloïdes est le processus principal (Wang *et al.,* 2015), car la concentration en AgNPs est comprise entre 10 ngAg.L^{-1} et quelques µgAg.L^{-1}, alors que les concentrations des particules en suspension, des colloïdes et de la NOM sont de l'ordre du mg.L^{-1} (Hélie and Hillaire-Marcel, 2006; Klaine *et al.,* 2008; Tremblay and Gagné, 2009; Wang *et al.,* 2015). Les interactions entre les AgNPs et les colloïdes naturels, qui peuvent aussi s'agréger (voir section Comportement des substances humiques selon le pH et la salinité) (Baalousha *et al.,* 2006; Buffle *et al.,* 1998; Tombácz and Szekeres, 2004) peuvent influencer le comportement et le devenir des AgNPs dans ces milieux. Dans les eaux naturelles, comme les estuaires, avec une composition complexe en ions, l'agrégation des AgNPs (Baalousha *et al.,* 2013) ou des

colloïdes naturels est contrôlée par des effets additifs ou synergiques de chaque ion et est fortement influencée par l'ion dominant. Les cations divalents influencent l'agrégation en eau douce (Ca^{2+} à 0.33 mM, Mg^{2+} à 0.15 mM et Na^{+} à 0.23 mM, (Bianchi, 2007)) alors qu'en eau de mer, ce sont les cations monovalents (Na^{+} : 468 mM, Ca^{2+} : 10.2 mM, et Mg^{2+} : 53.2 mM (Bianchi, 2007)). Dans les milieux estuariens, il y a une forte évolution de la composition en ions et plus particulièrement des ions dominants, ce qui peut moduler l'agrégation des AgNPs. Plusieurs études ont permis de mieux comprendre le rôle de la NOM dans l'autoagrégation, toutefois il existe très peu d'études qui traitent du rôle de la NOM dans l'hétéroagrégation (Wang *et al.,* 2015).

TAILLE DES AGRÉGATS

Selon Baalousha *et al.* (2016) le comportement agrégatif des AgNPs est influencé par leurs concentrations. Actuellement, un grand nombre d'études menées sur l'agrégation des AgNPs ont été réalisées à des concentrations élevées, plusieurs centaines de $\mu gAg.L^{-1}$ à plusieurs $mgAg.L^{-1}$ d'AgNPs (Baalousha *et al.,* 2016, 2013; Chen and Zhang, 2012; El Badawy *et al.,* 2012; Huynh and Chen, 2011; Li *et al.,* 2012, 2010; Lin *et al.,* 2015). Toutefois, l'ensemble de ces études décrivent les vitesses d'agrégation ainsi que les CCC, mais ne fournissent aucune information sur la taille des agrégats. Des études utilisant différentes techniques analytiques comme la microscopie électronique, la diffusion dynamique de la lumière, des dosages par ICP-MS ou des analyses du suivi individuel des nanoparticules montrent une évolution de la distribution de la taille des agrégats formés (Baalousha *et al.,* 2016; Lawler *et al.,* 2015; Milne *et al.,* 2017; Wasmuth *et al.,* 2016; Zhang *et al.,* 2017). Toutefois, à ma connaissance seulement deux études ont été réalisées entre 1 et 500 $\mu Ag.L^{-1}$. Une faible concentration en AgNPs dans un milieu salé induit la formation de petits agrégats composés d'une à cinq nanoparticules (Baalousha *et al.,* 2016). Plus la concentration en AgNPs augmente, plus la taille des agrégats augmente. Selon Lawler *et al.* (2015), deux populations de particules sont observables. La première a un diamètre

hydrodynamique inférieur à 100 nm et la deuxième population a une taille supérieure à 100 nm. Cette étude montre aussi que les proportions de ces deux populations évoluent selon la concentration en AgNPs. À 500 $\mu Ag.L^{-1}$, environ 50% des particules ont un diamètre inférieur à 100 nm. La proportion des petites particules augmente avec une diminution de la concentration en AgNPs. Toutefois, ces distributions ont été peu étudiées en fonction de la force ionique du milieu et selon la concentration et le type de NOM. Si l'agrégation et la taille des agrégats sont réduites à de faibles concentrations en AgNPs, les agrégats seront relativement plus mobiles et resteront dans la colonne d'eau (Baalousha *et al.,* 2016). Avec les conditions couramment utilisées dans la littérature, les agrégats auront tendance à sédimenter. Comme les concentrations environnementales, estimées entre quelques $ngAg.L^{-1}$ au $\mu gAg.L^{-1}$ (Gottschalk *et al.,* 2013; Keller and Lazareva, 2014), il est important de travailler dans des conditions réalistes en AgNPs. Selon la tailles des agrégats d'argent, le comportement (autoagrégation et hétéroagrégation), le devenir et la toxicité des AgNPs pourront être différents (Osterheld *et al.,* 2018). Actuellement, il y a peu de données sur la distribution de taille des agrégats selon la concentration en AgNPs, et aucune selon la concentration en sel ou en NOM. Ces effets de concentrations doivent d'être approfondies et plus particulièrement pour les systèmes estuariens.

DOSAGE ET CARACTÉRISATION DES NANOPARTICULES D'ARGENT

Le dosage et la caractérisation des AgNPs dans l'environnement, dont les estuaires, sont très complexes à cause de leurs faibles concentrations et des transformations décrites précédemment. Plusieurs techniques analytiques permettent d'étudier leurs propriétés physiques (taille et forme) et leurs propriétés chimiques (les charges de surface, la structure cristalline…). Ces techniques permettent aussi de caractériser les transformations.

La détermination des propriétés physiques des AgNPs peut être effectuée par des méthodes microscopiques et spectroscopiques. La taille des AgNPs étant nanométrique, la

microscopie optique traditionnelle ne peut être utilisée (Liu *et al.,* 2012). Cependant, la microscopie électronique (ME) et la microscopie à force atomique (AFM) permettent de caractériser la taille, la forme et la topographie des AgNPs (Liu *et al.,* 2012). La préparation des échantillons peut entraîner une mauvaise interprétation des données, car les échantillons doivent généralement être séchés, ce qui peut induire de nombreux artefacts comme un fort rapprochement des AgNPs donnant une impression d'agrégats (Liu *et al.,* 2012). De plus, il peut y avoir l'effet de l'observateur. Pour cela, il faut analyser plusieurs centaines à milliers de nanoparticules, ce qui peut être laborieux, fastidieux et demander beaucoup de temps (Liu *et al.,* 2012).

Les propriétés et mécanismes chimiques les plus importants pour les AgNPs sont la structure cristalline, la dissolution et les charges de surface. Pour caractériser la structure cristalline ou amorphe des AgNPs, les techniques les plus utilisées reposent sur la spectroscopie à rayons X. Elles permettent aussi de connaître la composition élémentaire, la spéciation de l'argent et la forme du réseau cristallin (Levard *et al.,* 2011; Liu *et al.,* 2012). Il existe plusieurs techniques pour étudier la dissolution des AgNPs. Le plus souvent, une partie de la solution est digérée puis analysée en ICP-MS afin d'obtenir la concentration totale en Ag (Liu *et al.,* 2012). L'autre partie de la solution subit une étape de séparation par ultrafiltration ou ultracentrifugation, permettant d'obtenir d'une part les AgNPs et d'autre part les ions Ag^+ issus de la dissolution (Liu *et al.,* 2012).

CARACTÉRISATION DE LA TAILLE DES NANOPARTICULES

Il existe plusieurs méthodes spectroscopiques pour caractériser la taille des AgNPs. Deux techniques sont couramment utilisées : (1) l'étude de l'absorbance des plasmons de surface ; et (2) la spectroscopie de corrélation de photons ou diffusion dynamique de la lumière (Baalousha *et al.,* 2013; Delay *et al.,* 2011; Lin *et al.,* 2012; Xu, 2001b). Un spectre UV-Visible d'AgNPs colloïdal présente un maximum d'absorbance, entre 390 et 420 nm, caractéristique des plasmons de surface (Delay *et al.,* 2011). Les plasmons de surface

résultent d'une interaction entre une onde électromagnétique, comme la lumière, et les électrons libres à l'interface entre un métal et un milieu diélectrique (Barnes *et al.,* 2003). Les électrons libres oscillent en résonance avec l'onde électromagnétique (Barnes *et al.,* 2003), conduisant à une bande d'absorption caractéristique (Montano *et al.,* 2014). Ce maximum d'absorbance est relié à la taille des AgNPs (Liu *et al.,* 2012; Montano *et al.,* 2014). Toutefois, le maximum d'absorbance est influencé par le revêtement et la présence de NOM en solution (Delay *et al.,* 2011) et par l'agrégation des AgNPs qui cause une forte diminution de l'absorbance (Pillai, 2004).

La diffusion dynamique de la lumière (DLS) aussi connue sous le nom de spectroscopie de corrélation des photons est une technique qui étudie la fluctuation de la lumière diffusée par les particules dans le temps (Hassan *et al.,* 2015; Malvern, 2013a; Xu, 2001b). Pour cela, une onde électromagnétique monochromatique produite par un laser est dirigée vers une cellule contenant des particules en suspension. Une partie de cette lumière est absorbée alors qu'une autre partie est diffusée dans toutes les directions (théorie de Rayleigh et de Mie) (Hassan *et al.,* 2015; Malvern, 2013a; Xu, 2001b). Comme les particules se déplacent aléatoirement dans la solution (mouvement brownien), l'intensité lumineuse diffusée fluctue dans le temps et induit la formation d'interférences constructives et destructives (Hassan *et al.,* 2015; Malvern, 2013a; Xu, 2001b). La mesure de cette fluctuation dans le temps permet alors, par traitement du signal, d'obtenir une fonction d'autocorrélation. Pour cela, des intervalles de temps (Δt) à des instants différents τ (τ en ns ou µs) sont sélectionnés (Figure 4). En comparant Δt et $\Delta t+\tau$, il est possible de déterminer la corrélation du signal (Malvern, 2010a), comme le montre la Figure 4. Une corrélation parfaite tend vers 1 alors qu'une corrélation nulle tend vers 0.

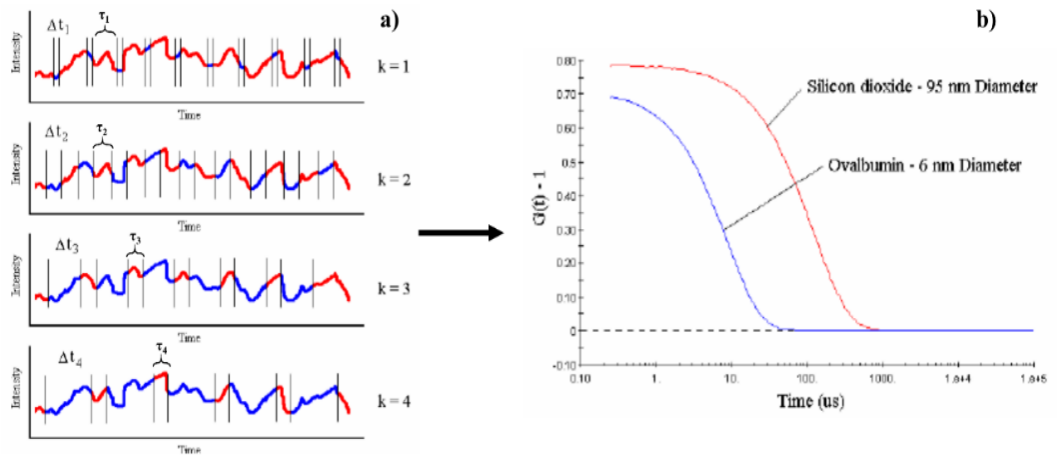

Figure 4 : Fluctuation de l'intensité lumineuse (a) et autocorrélogramme (b). Modifié de Malvern (2010)

Comme cette technique permet de mesurer le mouvement brownien dans le temps, il est possible de déterminer le coefficient de diffusion (Xu, 2001b). Selon l'équation 2 de Stokes-Einstein, le coefficient de diffusion (D) est lié au diamètre hydrodynamique des particules (D_h) (Xu, 2001b). Cette équation prend en compte la constante de Boltzmann (k), la température absolue (T) et la viscosité (η).

$$D_h = \frac{kT}{3\pi\eta D} \qquad (2)$$

Plusieurs algorithmes permettant de traiter la fonction d'autocorrélation peuvent être utilisés pour obtenir la taille des particules. Lorsque la solution contient des particules monodispersées, cas simple, la méthode des cumulants peut être utilisée. Elle permet d'obtenir le diamètre moyen Z (Z-Average) et un indice de polydispersité (PDI, compris entre 0 et 1) (Bhattacharjee, 2016; Hassan *et al.,* 2015; Malvern, 2013a; Xu, 2001b). Selon la norme ISO13321:1996(E), le Z-Average est une valeur de taille unique pour chaque échantillon et le PDI est une estimation de la largeur de la distribution de la taille des particules dans les échantillons (Bhattacharjee, 2016; Hassan *et al.,* 2015;

ISO13321:1996(E), 1996; Malvern, 2013a; Xu, 2001b). Toutefois, pour des échantillons polydispersés, le PDI tend vers 1. Quand le PDI est supérieur à 0.1, l'utilisation de la méthode des cumulants n'est pas conseillée (Hassan *et al.,* 2015; Malvern, 2013a; Xu, 2001b). D'autres algorithmes doivent alors être utilisés tels que la méthode des moindres carrés non négatifs (NNLS), l'échantillonnage exponentiel et la méthode CONTIN (Hassan *et al.,* 2015; Xu, 2001b), pour obtenir une distribution de la taille des particules (PSD).

Ces algorithmes transforment les signaux d'intensité en PSD pondérées en fonction de l'intensité diffusée (Anderson *et al.,* 2013; Hassan *et al.,* 2015). Cette distribution de la taille des particules en fonction de l'intensité décrit la quantité de lumière diffusée par des particules de différentes classes de tailles (Anderson *et al.,* 2013; Hassan *et al.,* 2015). La PSD en intensité peut aussi être convertie en distribution estimant le volume des particules ou le nombre de particules dans les différentes classes de tailles (Anderson *et al.,* 2013; Hassan *et al.,* 2015). La PSD en intensité peut être utilisée pour les échantillons monodispersés. Toutefois, pour les échantillons polydispersés, les PSD en intensité sont biaisés par la présence de grosses particules (Anderson *et al.,* 2013). Un petit nombre de grosses particules peut masquer la présence de nombreuses petites particules, car l'intensité diffusée est fonction de la taille à la puissance six (Anderson *et al.,* 2013; Xu, 2001b). Afin de diminuer la dépendance des PSD à la présence de grosses particules, les PSD sont exprimées en distribution en fonction du volume, car cette distribution est moins influencée par les grosses particules (puissance trois) (Malvern, 2009).

Contrairement à la ME et à l'AFM, la DLS permet de travailler en milieu liquide et à différentes températures. Toutefois, cette technique est souvent critiquée dans la littérature (Amini *et al.,* 2016; Anderson *et al.,* 2013; Baalousha and Lead, 2012; Cascio *et al.,* 2014), car (1) elle considère que toutes les particules sont sphériques ; (2) elle ne permet pas de différencier des particules ayant une différence de taille inférieure à un facteur 3 ; et (3) elle est considérée comme peu sensible. Dans le cadre de cette thèse, les AgNPs synthétisées ont

une forme sphérique, ce qui permet l'utilisation de l'équation de Stokes-Einstein (2). Cette technique peut être utilisée pour différencier les AgNPs (20 nm) des autres particules si la différence de taille est supérieure à un ratio de 3. Si l'intensité diffusée par les particules est trop faible par rapport à l'intensité diffusée par le solvant, cette technique ne peut être utilisée (Hassan *et al.,* 2015; Xu, 2015). Hassan *et al.* (2015) suggèrent d'effectuer des mesures, quand l'intensité diffusée par les particules est au minimum dix fois plus importante que l'intensité diffusée par le solvant. C'est un paramètre important dans la réalisation d'études sur les AgNPs par DLS. En plus de mesurer la distribution de la taille des particules à un instant donné, cette technique permet aussi de suivre l'évolution de la taille en fonction du temps (TR-DLS). Ce mode d'analyse permet d'étudier l'agrégation, si la taille augmente dans le temps, ou d'étudier la dissolution ou rupture quand la taille diminue.

CARACTÉRISATION DU POTENTIEL ZÊTA DES NANOPARTICULES

Selon la théorie de Gouy-Chapman ou théorie de la double couche électrique, les charges de surface peuvent être reliées au potentiel zêta (Pξ) (El Badawy *et al.,* 2010; Xu, 2001a). En milieu liquide, il y a formation de la couche de Stern autour des particules, où les ions présents sont de charges opposées aux charges de surface (Xu, 2001a). Plus on s'éloigne de la couche de Stern, moins la composition du milieu environnant est influencée par les charges de surface (Xu, 2001a), comme présentée dans la Figure 5. Le Pξ est défini comme étant le potentiel électrique au niveau du plan de glissement (Xu, 2001a).

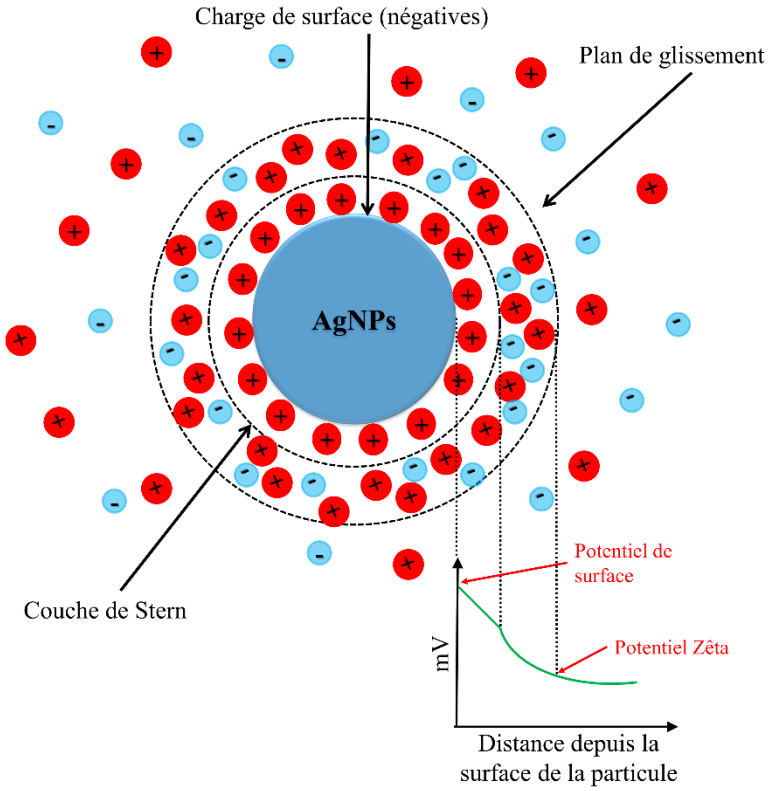

Figure 5 : Relation entre la structure de la double couche électrique et le potentiel zêta (traduit de Xu, 2001a et Malvern, 2013b)

Lorsque des particules chargées sont soumises à un champ électrique, elles se déplacent avec une vélocité permettant de déterminer la mobilité électrophorétique (μ) (Xu, 2001a). Il est alors possible de calculer le Pξ selon l'équation 3 (Xu, 2001a). Cette équation prend en compte la constante diélectrique du milieu (ε), la viscosité (η) et la fonction de Henry (f(kr)). La fonction de Henry dépend de l'épaisseur de la double couche électrique, ou longueur de Debye, et de la force ionique du milieu (Doane *et al.,* 2012; Malvern, 2013b).

$$\mu = \left(\frac{2\,P\xi\ \varepsilon}{3\eta}\right) f(kr) \qquad (3)$$

L'étude du Pξ permet aussi de déterminer la stabilité d'une suspension colloïdale (Xu, 2001a). Pour des particules ayant une stabilisation électrostatique, si le Pξ est compris entre -20 mV et +20 mV, les particules sont considérées comme peu stables et auront tendance à s'agréger (Everett, 1992; Xu, 2001a). De plus, le Pξ est directement influencé par la concentration et la valence des ions (Cl^-, Na^+, Ca^{2+}) (El Badawy *et al.,* 2010; Xu, 2001a), le pH (El Badawy *et al.,* 2010), mais aussi par la nature du revêtement (Lourenco *et al.,* 1996) et la présence de NOM (Gao *et al.,* 2012; Piccapietra *et al.,* 2012).

LA MATIÈRE ORGANIQUE EN MILIEU AQUATIQUE

Chaque année, 2.5 x 10^{14} g de carbone organique dissous (DOC) sont exportés des continents vers les zones estuariennes et côtières (Cauwet, 2002; Emerson and Hedges, 2008). Dans ces systèmes, 50 à 80% du DOC n'est pas caractérisé au niveau moléculaire (Eglinton and Repeta, 2003; Perdue and Ritchie, 2005; Wakeham *et al.,* 1997). Pour permettre une meilleure caractérisation du DOC, l'extraction sur des résines de type XAD/DAX ou d'autres résines de type échangeuses d'ions permet de le fractionner (Aiken *et al.,* 1979; Thurman *et al.,* 1978). À un pH inférieur à 2, la résine DAX-8 permet de séparer le DOC en trois fractions : (1) une fraction non retenue par la résine (Malcolm and MacCarthy, 1992; Martin-Mousset *et al.,* 1997; Thurman *et al.,* 1978) ; (2) une fraction, les substances humiques (HS), sorbant sur la résine à pH acide et désorbant à pH basique (Malcolm and MacCarthy, 1992; Thurman *et al.,* 1978) ; et (3) une fraction hydrophobe retenue par la résine et récupérée par extraction avec du méthanol ou de l'acétonitrile, après extraction des HS (Malcolm and MacCarthy, 1992). Une autre famille de composés, les acides hydrophiles, est extraite avec la résine XAD-4 (Malcolm and MacCarthy, 1992; Martin-Mousset *et al.,* 1997; Thurman *et al.,* 1978).

Les HS constituent l'une des principales composantes du DOC. Elles représentent 50 à 80% du DOC des eaux douces, 15 à 50% du DOC des estuaires et 10 à 30% du DOC des

eaux marines (Thurman, 1985; Tremblay and Gagné, 2009). Ces substances proviennent de la diagenèse primaire de la matière organique détritique. Durant cette diagenèse, plusieurs types de composés, tels que des lipides, des lignines, des polysaccharides et des protéines sont fractionnés et/ou condensés par de nombreux processus chimiques et biochimiques (MacCarthy, 2001). Ces processus plus ou moins complexes conduisent à une humification de la matière organique (Gjessing, 1976; Stevenson, 1994). L'utilisation en tandem des résines DAX-8 et XAD-4 permet d'extraire plus de 85% du DOC des lacs, dont 25% du DOC avec la résine XAD-4 (Malcolm and MacCarthy, 1992; Martin-Mousset *et al.,* 1997; Thurman *et al.,* 1978). Aucune donnée, utilisant ces résines en tandem, n'existe pour le domaine marin. Les fractions obtenues avec ces résines présentent des différences chimiques (Boerschke *et al.,* 1996). Les fractions humiques (DAX-8) présentent un plus haut degré d'aromaticité, mais moins de groupements carboxyliques et de groupements aliphatiques non-polaires que les fractions obtenues avec la résine XAD-4.

Les études menées sur les interactions entre les AgNPs et la NOM en milieu aqueux sont généralement effectuées avec des acides humiques (Chen and Zhang, 2012; Gao *et al.,* 2012; Huynh and Chen, 2011; Kühn *et al.,* 2015; Philippe and Schaumann, 2014). Dans les systèmes aquatiques, dont les estuaires, la concentration en acides fulviques est plus importante que celle des acides humiques (fulviques/humiques : 2 à 10) (Buffle *et al.,* 1998; Tremblay and Gagné, 2009). Il est important de mieux comprendre les interactions entre les acides fulviques et les AgNPs. De plus, il n'y a pas d'information sur les interactions entre les nanoparticules et les fractions obtenues avec la résine XAD-4.

CARACTÉRISTIQUES CHIMIQUES DES SUBSTANCES HUMIQUES

Les HS sont composées de carbone, d'hydrogène, d'oxygène et d'azote et contiennent de faibles proportions de soufre et de phosphore (Gjessing, 1976; IHSS, 2017; Stevenson, 1994; Thurman and Malcolm, 1981). Elles sont divisées en trois fractions, selon leurs solubilités : (1) les humines (HU) insolubles à tous les pH ; (2) les acides humiques (HA)

insolubles à pH<2 ; et (3) les acides fulviques (FA) solubles à tous les pH (MacCarthy, 2001; Thurman and Malcolm, 1981).

La proportion de carbone tend à augmenter entre les FA, les HA et les HU, alors que la quantité d'oxygène tend à diminuer. Le poids moléculaire des FA est généralement entre 1 000 et 2 000 Da (Davies *et al.,* 2014; Perdue and Ritchie, 2005; Senesi *et al.,* 2009). Le poids moléculaire des HA est aux environs de 2 000 Da dans les milieux aquatiques et peut atteindre 1 x 10^6 Da dans les sols (MacCarthy, 2001). Pour les HU, leur poids moléculaire fluctue moins que celui des HA. Les HS sont des composés complexes ayant des structures chimiques mal connues. Des études suggèrent que les HS sont des agrégats moléculaires formés par des associations de molécules organiques de faible poids moléculaire (Conte and Piccolo, 1999; Senesi, 1999; Sutton and Sposito, 2005). La Figure 6 présente des modèles structuraux théoriques des HA et des FA. Les HS sont des assemblages hétérogènes de molécules complexes possédant des caractères amphiphiles et des propriétés acides (Leenheer, 2009; Senesi *et al.,* 2009). Les propriétés acides et hydrophiles proviennent majoritairement des groupements carboxyliques et phénoliques et minoritairement des groupements quinones et amines (Davies *et al.,* 2014; Gjessing, 1976; Stevenson, 1994). Les HS possèdent aussi des composantes hydrophobes provenant des groupements aliphatiques non-polaires et des groupements aromatiques (Davies *et al.,* 2014; IHSS, 2017; Mao *et al.,* 2007).

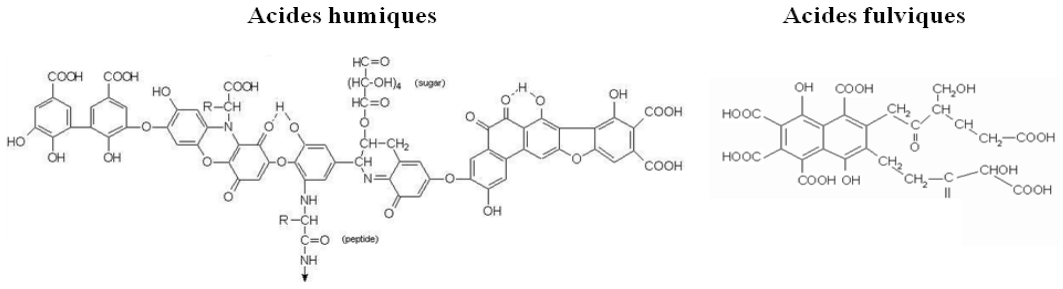

Figure 6 : Modèles des acides humiques (Stevenson, 1994) et des acides fulviques (Buffle, 1977)

COMPORTEMENT DES SUBSTANCES HUMIQUES SELON LE pH ET LA SALINITÉ

Les HS peuvent aussi s'agréger selon les conditions physico-chimiques du milieu récepteur. Les HS possèdent des groupements carboxyliques qui sont protonés (─COOH) à un pH acide et sont ionisés (─COO^-) à pH basique. Les groupements phénoliques des HS se comportent de façon similaire. Les parties hydrophobes sont aussi influencées par le pH (Sutton and Sposito, 2006, 2005) modifiant la conformation spatiale des agrégats en solution (Alvarez-Puebla *et al.,* 2006). À pH acide, les HS sont peu chargées, ce qui entraîne de faibles répulsions électrostatiques (Alvarez-Puebla *et al.,* 2006). Les HS ont tendance à se replier, afin de permettre la formation de liaisons hydrogène, de liaisons électrostatiques et des interactions de van der Waals (Alvarez-Puebla *et al.,* 2006). Cela conduit à une forte agrégation des HS. Au point isoélectrique, les HS possèdent des groupements chargés positivement et d'autres négativement, alors que la charge totale est neutre. Elles sont dans un état zwittérion. Lorsque le pH augmente (milieu basique), la charge totale des HS devient négative, car les groupements carboxyliques (─COOH) et hydroxyles (–OH) perdent leur proton, ce qui augmente les répulsions électrostatiques (Alvarez-Puebla *et al.,* 2006), diminuant l'agrégation. Dans un environnement aquatique naturel comme les estuaires, à un pH compris entre 5 et 8, les groupements carboxyliques sont généralement anioniques et quelques groupements phénoliques peuvent aussi être ionisés (Sutton *et al.,* 2005). Ces groupements interagissent avec les cations présents dans le milieu. Le pontage des cations sur les groupements carboxyliques et phénoliques ionisés diminue les charges négatives des HS. Cela entraîne une diminution des répulsions électrostatiques (Brigante *et al.,* 2007) et augmente l'agrégation des HS (Baalousha *et al.,* 2006; Sholkovitz, 1976). À des forces ioniques élevées, comme les estuaires, les HS peuvent s'agréger, précipiter et sorber sur des surfaces naturelles. Ces paramètres jouent un rôle important dans la réactivité des HS dans l'environnement, et peuvent influencer le comportement et le devenir des AgNPs en milieu estuarien.

OBJECTIFS

Le développement rapide de la nanotechnologie et l'incorporation des AgNPs dans de nombreux biens de consommation, augmente le risque de les retrouver dans l'environnement. Les connaissances sur le comportement et le devenir des AgNPs dans les systèmes estuariens font actuellement défaut. De plus, beaucoup d'études sur l'agrégation des AgNPs ont été menées à fortes concentrations en AgNPs, il devient donc important de travailler dans des conditions réalistes en AgNPs, à de faibles concentrations, afin d'améliorer les connaissances actuelles concernant les AgNPs dans les eaux naturelles. De plus, un estuaire étant une zone de transition terre/océan présentant une très grande variabilité temporelle et spatiale des paramètres physico-chimiques (Bianchi, 2007), l'évolution de ces propriétés, et plus particulièrement la salinité et la teneur en NOM, peut moduler les différentes transformations des AgNPs, et tout particulièrement l'agrégation.

L'objectif général de cette recherche est de déterminer par une approche expérimentale le comportement et le devenir des nanoparticules d'argent, à faible concentration, durant une transition estuarienne.

Afin de répondre à l'objectif principal, les travaux présentés dans cette thèse sont rassemblés en quatre chapitres sous la forme d'articles scientifiques, présentant plusieurs sous-objectifs.

Chapitre 1 : Effets de la concentration des nanoparticules d'argent sur leur comportement agrégatif et la distribution de la taille des agrégats

Le chapitre 1 expose le rôle de la concentration, en AgNPs et en sel, sur l'agrégation. L'objectif principal est de caractériser l'influence de la concentration en AgNPs sur l'agrégation ainsi que sur la distribution de la taille des agrégats formés. De plus, il faut développer un protocole afin de suivre le comportement agrégatif des AgNPs à faible

concentration. Pour cela, quatre concentrations en AgNPs ont été utilisées : 10 mgAg.L^{-1}, 1 mgAg.L^{-1}, 100 µgAg.L^{-1} et 10 µgAg.L^{-1}. Ce chapitre propose des mécanismes qui peuvent influencer la distribution de la taille des agrégats formés en fonction du temps, de la concentration en AgNPs et de la force ionique. Ce chapitre démontre aussi l'importance de considérer la concentration en particules en plus de la concentration massique.

Chapitre 2 : La chimie d'un milieu de culture bactérien, affecte-t-elle la stabilité des nanoparticules d'argent dans les essais de nanotoxicité ?

Le chapitre 2 expose le rôle de différents constituants de milieu de culture utilisé dans les études de nanotoxicité. L'objectif principal est d'évaluer la stabilité des suspensions d'AgNPs, dans le temps, dans des solutions de différents sels, des solutions d'exposition caractéristiques, soit des eaux naturelles, soit des milieux de culture. De plus, ce chapitre montre l'importance de contrôler le vieillissement des suspensions colloïdales d'AgNPs au cours des essais de toxicité afin de mieux comprendre les effets toxiques des AgNPs sur divers microorganismes.

Chapitre 3 : Effets de la concentration et de la composition chimique de la matière organique naturelle sur le comportement agrégatif des nanoparticules d'argent

Le chapitre 3 expose le rôle de la matière organique naturelle sur l'agrégation des AgNPs. L'objectif principal est de déterminer l'influence de la concentration et de la composition chimique de différentes fractions de NOM, provenant du Saint-Laurent, sur l'évolution temporelle du diamètre hydrodynamique et sur la distribution de la taille des agrégats d'argent. Ce chapitre montre que selon la concentration en NOM l'agrégation diffère. Ce chapitre démontre aussi le rôle de certains groupements chimiques dans la distribution de la taille des agrégats.

Chapitre 4 : Comportement des nanoparticules d'argent dans des mésocosmes estuariens stratifiés : distribution de la taille des particules et rôle de l'halocline

L'objectif principal du chapitre 4 est de suivre le comportement des AgNPs lors d'une addition chronique d'AgNPs dans un système stratifié estuarien. Pour cela, des mésocosmes ont été utilisés avec des entrées continues en eau douce et en eau de mer. Cela nous a permis d'obtenir une masse d'eau douce séparée d'une masse d'eau salée par une halocline. Ce chapitre montre que les AgNPs s'agrègent, quelle que soit la masse d'eau étudiée. En analysant la distribution de la taille des particules par DLS et par ICP-MS, nous observons que l'ajout d'AgNPs modifie cette distribution. De plus, ce chapitre démontre que le comportement et le devenir des AgNPs sont des processus très dynamiques influencés par les conditions physico-chimiques et par la stratification estuarienne.

CHAPITRE 1
EFFETS DE LA CONCENTRATION DES NANOPARTICULES D'ARGENT SUR LEURS COMPORTEMENTS AGRÉGATIFS ET SUR LA DISTRIBUTION DE LA TAILLE DES AGRÉGATS

1.1 RÉSUMÉ

Cette étude caractérise l'agrégation des nanoparticules d'argent (AgNPs) et la distribution de la taille des agrégats d'argent à des concentrations comprises entre 10 mgAg.L^{-1} et 10 µgAg.L^{-1}, par diffusion dynamique de la lumière (DLS). Des cinétiques d'agrégation des AgNPs ont été effectuées à 10 concentrations de NaCl pendant 2 h afin de déterminer la concentration critique de coagulation (CCC) et la distribution de la taille des particules. Des cinétiques d'agrégation ont également été réalisées à quatre concentrations de NaCl pendant 12 h afin de caractériser l'évolution de la distribution de la taille des particules. À 10 et 1 mgAg.L^{-1}, la CCC est observée vers 70 mM de NaCl, mais augmente à environ 150 mM de NaCl à 100 et à 10 µgAg.L^{-1}. La taille des agrégats est fortement influencée par la concentration en AgNPs. À 10 et 1 mgAg.L^{-1}, plus de 80% des agrégats ont un diamètre hydrodynamique (D_h) supérieur à 200 nm après 2 h, et augmentent à 95% après 12 h. Une distribution très différente est observée à 100 et 10 µgAg.L^{-1}, entre 60 à 90% des agrégats ont un D_h compris entre 40 et 100 nm. L'évolution de la distribution de la taille des agrégats est expliquée par la concentration en particule. À 10 et 1 mgAg.L^{-1}, la concentration en particule reste suffisamment élevée pour favoriser les interactions entre les AgNPs et les agrégats, favorisant la formation de gros agrégats, mais ce n'est pas le cas à 100 et 10 µgAg.L^{-1}. Quand la quantité de particules est proche de 10^6 particules.mL^{-1}, l'agrégation des AgNPs

est fortement réduite et peut expliquer la présence d'un plateau dans les cinétiques d'agrégation.

Ce premier article, intitulé « *Effects of silver nanoparticles concentration on their aggregative behavior and size distribution of aggregates* », fut corédigé par moi-même ainsi que par le professeur Émilien Pelletier, par la docteure Kim Doiron, par la professeure Karine Lemarchand et par le professeur Jean-Pierre Gagné. En tant que premier auteur, ma contribution à ce travail fut d'effectuer une recherche bibliographique poussée, les analyses de laboratoire, le traitement des données et la rédaction de l'article. Les professeurs Émilien Pelletier et Jean-Pierre Gagné ont fourni l'idée originale et ont participé au traitement des données et à la rédaction de l'article. La docteure Kim Doiron et la professeure Karine Lemarchand ont aidé dans le traitement statistique des données et dans la révision de l'article. Une version abrégée de cet article a été présentée à la conférence *Écobim* au Havre (France) au printemps 2016.

EFFECTS OF SILVER NANOPARTICLES CONCENTRATION ON THEIR AGGREGATIVE BEHAVIOR AND SIZE DISTRIBUTION OF AGGREGATES

1.2 ABSTRACT

This study describes the aggregation kinetics of silver nanoparticles (AgNPs) and the size distribution of silver aggregates at concentrations ranging from 10 mgAg.L^{-1} to 10 µgAg.L^{-1}, with dynamic light scattering (DLS). Aggregation kinetics of AgNPs were conducted at 10 different NaCl concentrations for 2 h to determine the critical coagulation concentration (CCC) and the particle size distribution. Aggregation kinetics of AgNPs were also conducted at four NaCl concentrations for 12 h to characterize the evolution of their size distribution. At 10 and 1 mgAg.L^{-1}, the CCC was observed near 70 mM of NaCl, and increased to near 150 mM at 100 and at 10 µgAg.L^{-1}. Furthermore, the size of aggregates was strongly affected by AgNPs concentration. At 10 and 1 mgAg.L^{-1} more than 80% of aggregates had a hydrodynamic diameter (D_h) higher than 200 nm after 2 h, and still increasing to more than 95% after 12 h. A very different distribution was observed at 100 and 10 µgAg.L^{-1}, where 60 to 90% of the aggregates had a D_h between 40 and 100 nm. Changes in aggregate size distribution is explained by the particle concentration. At 10 and 1 mgAg.L^{-1}, the particle concentration remained high enough to promote interactions between AgNPs and aggregates, favoring the formation of large aggregates, but it was not the case at 100 and 10 µgAg.L^{-1}. Moreover, when the particle concentration was at 10^6 particles.mL^{-1}, the aggregation of AgNPs was strongly reduced and could explain the presence of a plateau in aggregation kinetics.

Keywords: Citrate-coated silver nanoparticles, aggregation, salt effects, silver nanoparticles concentration effects, particle distribution, aggregates.

1.3 INTRODUCTION

In the last two decades, the nanotechnology developed as a new division of material sciences showing a high potential for applications in medicine, electronic, energy production and consumption, alimentary safety, remediation, water treatment, and many others (Nanotechproject, 2017; OECD, 2011). Among nanomaterials currently available on the market, silver nanoparticles (AgNPs) are used in many applications as food packaging materials, odor-resistant textiles, goods for children, electronics and household appliances, cosmetics and medical devices (Nanotechproject, 2017; Wijnhoven *et al.,* 2009). AgNPs are generally used in these products to limit the growth of harmful bacteria to humans. In 2016, more than 440 consumer products containing AgNPs were inventoried (Nanotechproject, 2017). Some studies (Benn and Westerhoff, 2008; Geranio *et al.,* 2009; Kaegi *et al.,* 2010; Yetisen *et al.,* 2016) have shown that AgNPs incorporated in nanoproducts as nanotextiles or outdoor paint are released during washing cycles or rain runoff events and could be exported to aquatic environments. In 2009, US-EPA and the European Commission have included AgNPs as an emerging aquatic contaminant (SCENIHR, 2014; US-EPA, 2009).

When AgNPs are released in aquatic environment, some physical and chemical transformations occur: (1) aggregation influenced by ionic strength (salt composition and concentration) and natural organic matter (Baalousha *et al.,* 2013; Millour *et al.,* 2015, 2013); (2) dissolution by oxidation in oxic systems (Liu and Hurt, 2010); (3) oxysulfidation in oxic systems in presence of sulfur ions (Levard *et al.,* 2011; Liu *et al.,* 2011); or (4) sulfidation in anoxic systems (Kaegi *et al.,* 2011; Levard *et al.,* 2011). The main process affecting AgNPs in the aquatic system is aggregation. The aggregation of AgNPs can be described by the Derjaguin, Landau, Verwey and Overbeek (DLVO) theory (Derjaguin and Landau, 1941; Petosa *et al.,* 2010; Verwey and Overbeek, 1948). This theoretical model shows that the aggregative behavior is controlled by attractive and repulsive forces, and is generally applied to determine the critical coagulation concentration (CCC) of nanomaterials and colloids in

salty water (Baalousha *et al.,* 2013; Chen and Elimelech, 2006; Huynh and Chen, 2011; Petosa *et al.,* 2010). The CCC determined for AgNPs in water are generally higher than 50 mM in presence of monovalent salts and smaller than 60 mM for divalent salts depending on the coating added to AgNPs (Baalousha *et al.,* 2013; Hu *et al.,* 2011; Huynh and Chen, 2011). The CCC is particularly useful to investigate early steps of AgNPs aggregation when the size evolves rapidly with time.

However, the CCC provides little information about the size of aggregates, particularly when the size is evolving slowly. The toxicity mechanisms of AgNPs and the environmental fate could be different depending on the size of aggregates (Millour *et al.,* 2015; Osterheld *et al.,* 2018). Small aggregates could interact directly with cell surface and could be internalized while large aggregates could not penetrate the cells, but just interact with cell membrane (Millour *et al.,* 2015). Large aggregates have a small specific area and can settle rapidly. Small aggregates are settling slowly, but have a high specific area which could mean a higher reactivity with biological surface. To our knowledge, only one study has shown a change in the particle size distribution of AgNPs during the first minutes of aggregation process (Baalousha *et al.,* 2013). It is important to determine the size and the distribution of aggregates produced for risk assessment of AgNPs.

Many studies on AgNPs stability were conducted at silver concentration between 1 and 100 $mgAg.L^{-1}$ (Chen and Zhang, 2012; Delay *et al.,* 2011; El Badawy *et al.,* 2012; Huynh and Chen, 2011; Li *et al.,* 2012, 2010; Lin *et al.,* 2015; Zhang *et al.,* 2012). According to Gottschalk studies (Gottschalk *et al.,* 2013; Gottschalk and Sonderer, 2009), who have modeled environmental concentrations of nanomaterials from their sources to different compartments such as wastewater treatment effluent, surface water, sediment, soil and atmosphere, those concentrations are unrealistic. The model predicted concentrations of AgNPs (Gottschalk *et al.,* 2013) between 1 and 10 $ngAg.L^{-1}$ in surface waters, and in certain cases it could reach 1 $\mu gAg.L^{-1}$. Actually, few information is available about aggregative behavior and the size distribution of aggregates at low AgNP concentrations. Some studies

indicate that at low AgNPs concentration, the aggregates could have a multimodal distribution, with a presence of aggregates smaller than 100 nm and were composed of 1 to 5 nanoparticles (Baalousha *et al.,* 2016; Lawler *et al.,* 2015). However the effects of an increase of salt concentration were not studied.

The aim of this study was to determine the influence of AgNPs concentrations on the hydrodynamic diameter evolution, and the particle size distribution of silver aggregates formed during aggregation process. Specific objectives were to study effects of AgNPs concentrations: (1) on their properties such as hydrodynamic diameter, zeta potential and wavelength of the peak of surface plasmon resonance absorbance in nanopure water; (2) on the evolution of aggregate hydrodynamic diameters with time; and (3) on the size distribution of aggregates. To reach these specific objectives, aggregation kinetics of AgNPs were studied at 10 mgAg.L^{-1}, 1 mgAg.L^{-1}, 100 µgAg.L^{-1} and 10 µgAg.L^{-1} and at different NaCl concentrations during 2 and 12 h.

1.4 MATERIALS AND METHODS

1.4.1 SYNTHESIS AND CHARACTERIZATION OF SILVER NANOPARTICLES

AgNPs were prepared in nanopure water (18.2 MΩ·cm resistivity, NANOpure Infinity, Barnstead) by the reduction of silver nitrate with trisodium citrate during 3 h under reflux. The AgNPs colloidal solution was filtered on 0.2 µm polycarbonate filter (Whatman) and centrifuged to remove impurities and reagents. After the clean-up process, concentrations of AgNPs and silver ions were determined by inductively coupled plasma mass spectrometry (ICP-MS). Synthesis and purification of stock AgNPs solution are fully described in supporting information (Annexe I p149).

AgNPs properties such as hydrodynamic diameter (D_h), zeta potential (Pζ) and the wavelength of the peak of surface plasmon resonance absorbance (SPR) were determined at 10 mgAg.L^{-1}, 1 mgAg.L^{-1}, 100 µgAg.L^{-1} and 10 µgAg.L^{-1} in nanopure water. The D_h and Pζ

were measured with a Zetasizer Nano ZS (ZEN 3600, Malvern). For the D_h, analysis was conducted with 3 mL of AgNPs solution at 25 °C with 180 s for temperature equilibration time. Analysis was performed with 6 successive measures, with a 5 s delay between each measure. One measure corresponded to 6 scans of 15 s each, measured in backscattering mode with an angle of 173°. The Pζ was measured using a folded capillary cells (DTS 1060, Malvern). Analysis was conducted at 25 °C with 180 s for temperature equilibration time. Analysis was performed at 150 V with 3 measures with a delay of 45 s between each measure for limiting Joule heating. One measurement corresponds to 100 scans. No electrode blackening and sample degradation were observed with these parameters. The SPR was measured with UV/Visible spectrophotometer (Lambda 35, Perkin Elmer). Spectra were recorded between 700 and 200 nm with a 10 mm quartz cell, slit of 2 nm and one measure each nanometer.

1.4.2 SALT SOLUTIONS

Aggregation kinetics of AgNPs were conducted in NaCl solutions. NaCl was chosen because it is one of the major salts in aquatic systems and is dominant in seawater systems (Bianchi, 2007). Salt solution was prepared by dissolving 14.61 g of NaCl (ACS grade, LabMat) in 500 mL of nanopure water. The pH of the solution was adjusted to pH 7.00±0.05. Solution was shaken overnight and filtered on 0.2 µm polycarbonate filter (Whatman) to remove impurities. After filtration, this stock solution was diluted with nanopure water to get NaCl solutions at 0, 9, 10, 20, 30, 40, 50, 86, 100, 200, 400, 428 and 500 mM. For monovalent salt, the ionic strength of the medium is equal to the molar concentration of salts. In this study, ionic strength was comprised between 0 and 500 mM. Furthermore, these NaCl concentrations correspond to a salinity range of 0 to 29 PSU which is characteristic of estuarine salinity gradients.

1.4.3 AGGREGATION KINETICS

Aggregation kinetics of silver nanoparticles were determined in time resolved dynamics light scattering with Zetasizer Nano ZS. Firstly, a background level was determined with 3 mL of salt solutions at 25 °C with a temperature equilibration time of 180 s. The background value was used to detect a possible contamination of salt solutions with particles and to determine the effect of salt on the count rate. During the background determination, the count rate (kilo counts per second: kcps) did not exceed 40 kcps. This value was near the detection limit in nanopure water (≈ 20 kcps). After the background recording, AgNPs suspension was rapidly injected with a microsyringe into the sample holder. Four AgNPs concentrations were studied: 10 $mgAg.L^{-1}$, 1 $mgAg.L^{-1}$, 100 $\mu gAg.L^{-1}$ and 10 $\mu gAg.L^{-1}$, and correspond to solutions between 92.7 to 0.093 µM of silver. In absence of AgNPs, the aqueous media produced a "blank" count rate of 20 kcps. The addition of AgNPs increased the signal to 280 kcps at 10 $\mu gAg.L^{-1}$ and 170 000 kcps at 10 $mgAg.L^{-1}$. At 10 $\mu gAg.L^{-1}$, the signal/noise ratio was 14/1. This ratio is higher than the ratio of 10 suggested by Hassan *et al.* (2015) for DLS and much more than the usual ratio 3/1 used to determine the limit of detection in analytical chemistry.

Two different kinetics were performed. Kinetics over 2 h was conducted for NaCl concentrations: 0, 10, 20, 30, 40, 50, 100, 200, 400 and 500 mM. The parameters used for 2 h kinetics were 480 measures, each measure corresponding to one run of 15 s. Kinetics over 12 h were performed at 0, 9, 86 and 428 mM of NaCl. The parameters were 720 measures (one measure: 4 run of 15 s). For the 12 h kinetics these concentrations correspond to salinities of 0.5, 5 and 25 PSU.

D_h evolution and particle size distribution were determined by using the volume distribution instead of the Z-Average value. The Z-Average diameter corresponds to the intensity weighted mean hydrodynamic size (Malvern, 2010b). This value is strongly affected by the presence of a small proportion of large particles, because the intensity

scattering by particles was proportional to the particle radius (R^6) (Malvern, 2010c). With a mixture of nanoparticles with different sizes, the D_h obtained with Z-Average was different from the real proportion of each population, but this bias is not observed with the volume distribution (Malvern, 2010c). In this study, D_h of the AgNPs determined with the Z-Average was near 70 nm, but only 20 nm using the volume distribution which was similar to the diameter of AgNPs estimated by transmission electron microscopy (TEM) shown in supporting information (Figure 27, Annexe I p149). Effects of refractive index and absorbance on D_h and PSD was investigated with values of AgNPs (0.135), silver oxides (1.02 and 2.07 (Nwanya *et al.,* 2013)), silver chloride (2.048 (Tilton *et al.,* 1950)) and default value in Malvern software (1.59). These different refractive indexes were tested because the presence of oxygen and chloride in the medium could transform the AgNPs surfaces. According to value of refractive index used, no differences were observed at 10 $mgAg.L^{-1}$ and 10 $\mu gAg.L^{-1}$ (Tukey test, $p>0.05$). For these reasons, D_h and PSD measured in this study were in volume distribution, using the default value of refractive index in Malvern software.

The early step of aggregation kinetics was investigated with the DLVO theory (Petosa *et al.,* 2010), when two regimes of aggregation can occur. Reaction-limited (RLA) and diffusion-limited (DLA) were determined with aggregation rate constants. The transition between these two regimes was observed at the critical coagulation concentration (CCC) (Petosa *et al.,* 2010). CCC was determined by calculating the attachment efficiency (α) at different salt concentrations. The α was obtained with equation 4 (Petosa *et al.,* 2010):

$$\alpha = \frac{1}{W} = \frac{K_{RLA}}{K_{DLA}} \quad (4)$$

where K was determined for each condition or concentration of NaCl, with equation 5 and W the stability ratio (Petosa *et al.,* 2010):

$$K = \frac{1}{N_0}\frac{\Delta_{Dh}}{\Delta_t} \quad (5)$$

where N_0 is the initial particle concentration (particle.mL^{-1}) and Δ_{Dh}/Δ_t was obtained with a linear regression (slope) applied during the early step, rapid D_h increase. In this study, Δ_{Dh}/Δ_t was calculated between 0 and 120 s for the kinetics at 10 and 1 mgAg.L^{-1} and between 0 and 2 h for the 100 and 10 µgAg.L^{-1} concentrations.

Particles distribution kinetics were computed using MATLAB software version 8.3.0.532 (MathWorks Inc., Novi, USA). Presence of outliers was investigated with the Modified Thompson Tau test (Cimbala, 2011), fully described in supporting information (Annexe I p149). Box plots were created with SYSTAT software version 12.0 (Systat Software Inc., Chicago, USA). Box plots were made with the data obtained between 5 400 and 7 200 s (last 30 min) for kinetics of 2 h and between 36 000 and 43 200 s (last 2 h) for 12 h kinetics.

1.5 RESULTS AND DISCUSSION

1.5.1 EFFECTS OF SILVER NANOPARTICLES CONCENTRATIONS ON THEIR PROPERTIES IN NANOPURE WATER

The first important step in this study was to determine the potential effects that the concentration of AgNPs could have on parameters D_h, Pζ, and SPR to evaluate the stability of colloidal suspension. In addition, these results would help to choose the appropriate technique for studying the AgNPs aggregation at different concentrations. Two techniques have been generally used for aggregation studies: the dynamic light scattering (DLS) and the UV/Visible spectrophotometry (Baalousha *et al.,* 2013; Chen and Elimelech, 2006; Huynh and Chen, 2011).

Table 2 shows D_h, Pζ and SPR values at 10 mgAg.L^{-1}, 1 mgAg.L^{-1}, 100 µgAg.L^{-1} and 10 µgAg.L^{-1} in nanopure water. D_h values did not change with different concentrations of AgNPs, and shown an average value of 20±2 nm. This result indicates the absence of aggregation between AgNPs and a great stability of colloidal suspension. The Pζ values were

very stable between -34 and -35 mV for each concentration with an average value of -34.4±0.5 mV, except at 10 µgAg.L^{-1} where the concentration was too low to allow determination of this property. The negative values of Pζ were caused by the negative charges of citrate moieties at pH 7.00 (pKa_1 3.13; pKa_2 4.76; pKa_3 6.40 (Goldberg *et al.,* 2002)). This suggests that stability of AgNPs in nanopure water was controlled by electrostatic repulsive forces (Xu, 2001a), reflected by the highly negative Pζ values. The stability of colloidal suspension was also confirmed by SPR observed at 420 nm. SPR did not change with decreasing concentration of AgNPs, with the exception at 10 µgAg.L^{-1}, where the concentration was too low to allow measurement. Steady SPR values indicate that the AgNPs in suspension were stable. These results show that the properties of AgNPs were not affected by a change of 1 000 folds in concentration of AgNPs in nanopure water. To our knowledge, this is the first study using the DLS to determine the aggregation of AgNPs at low AgNPs concentrations of 100 and 10 µgAg.L^{-1}.

Table 2: Effects of silver nanoparticles concentration on the hydrodynamic diameter, zeta potential and peak of surface plasmon resonance absorbance

AgNPs concentration	**Hydrodynamic diameter (nm)**	**Zeta potential (mV)**	**Wavelength peak of surface plasmon resonance absorbance (nm)**
10 mgAg.L^{-1}	19±2	-35.1±0.2	420
1 mgAg.L^{-1}	20±1	-34.0±0.2	420
100 µgAg.L^{-1}	18±4	-34.1±1.0	420
10 µgAg.L^{-1}	24±4	<DL	<DL
Average	20±2	-34.4±0.5	420

<DL: below the detection limit

1.5.2 EFFECTS OF SILVER NANOPARTICLES CONCENTRATIONS ON THEIR AGGREGATIVE BEHAVIOR IN SALTY WATERS

The effects of increasing salt concentrations on aggregation kinetics at constant AgNPs concentration (1 mgAg.L^{-1} or 9.3 µM) are shown in Figure 7a. In nanopure water (0 mM NaCl), the D_h was stable with time, with a size near 20 nm. The aggregate size distribution at 10 mM NaCl induced a D_h increase between 0 and 3 000 s, and the rise was even more important, between 0 and 1 000 s, at 500 mM NaCl. The increase in D_h with time in NaCl solution was consistent with DLVO and Gouy-Chapman theory (Derjaguin and Landau, 1941; Petosa *et al.,* 2010; Verwey and Overbeek, 1948). AgNPs have an electrical double layer perturbed by the variation of ionic strength. The ionic strength was 0, 10 and 500 mM for 0, 10 and 500 mM NaCl, respectively. In presence of salt at these concentrations, the ionic strength of the medium increases and the thickness of AgNPs double layer decreases (Elimelech *et al.,* 1998). In addition, the citrate moieties are negatively charged and interact strongly with sodium cations as counterions. This interaction reduced the negative charges of AgNPs and decreased Pζ as reported in previous studies (Baalousha *et al.,* 2006; Huynh and Chen, 2011). A decrease in the electrostatic repulsion between each nanoparticle favors the close encounter of AgNPs and their aggregations (Xu, 2001a), as shown in Figure 7a.

Modification in AgNPs concentrations also affects the aggregation kinetics. Figure 7b shows variations in hydrodynamic diameter of AgNPs in saline solution at 200 mM NaCl and at four AgNPs concentrations. For each concentration, D_h was 20 nm just after the addition of AgNPs, the same D_h as the AgNPs suspended in nanopure water (Table 2). The D_h of AgNPs increased rapidly with time at 10 and 1 mgAg.L^{-1}. This rapid change was observed in less than 1 000 s at 10 mgAg.L^{-1} and in less than 3 000 s at 1 mgAg.L^{-1}. In contrast, low concentrations of 100 and 10 µgAg.L^{-1} did not induce any fast increase of size, the D_h increased slowly with time.

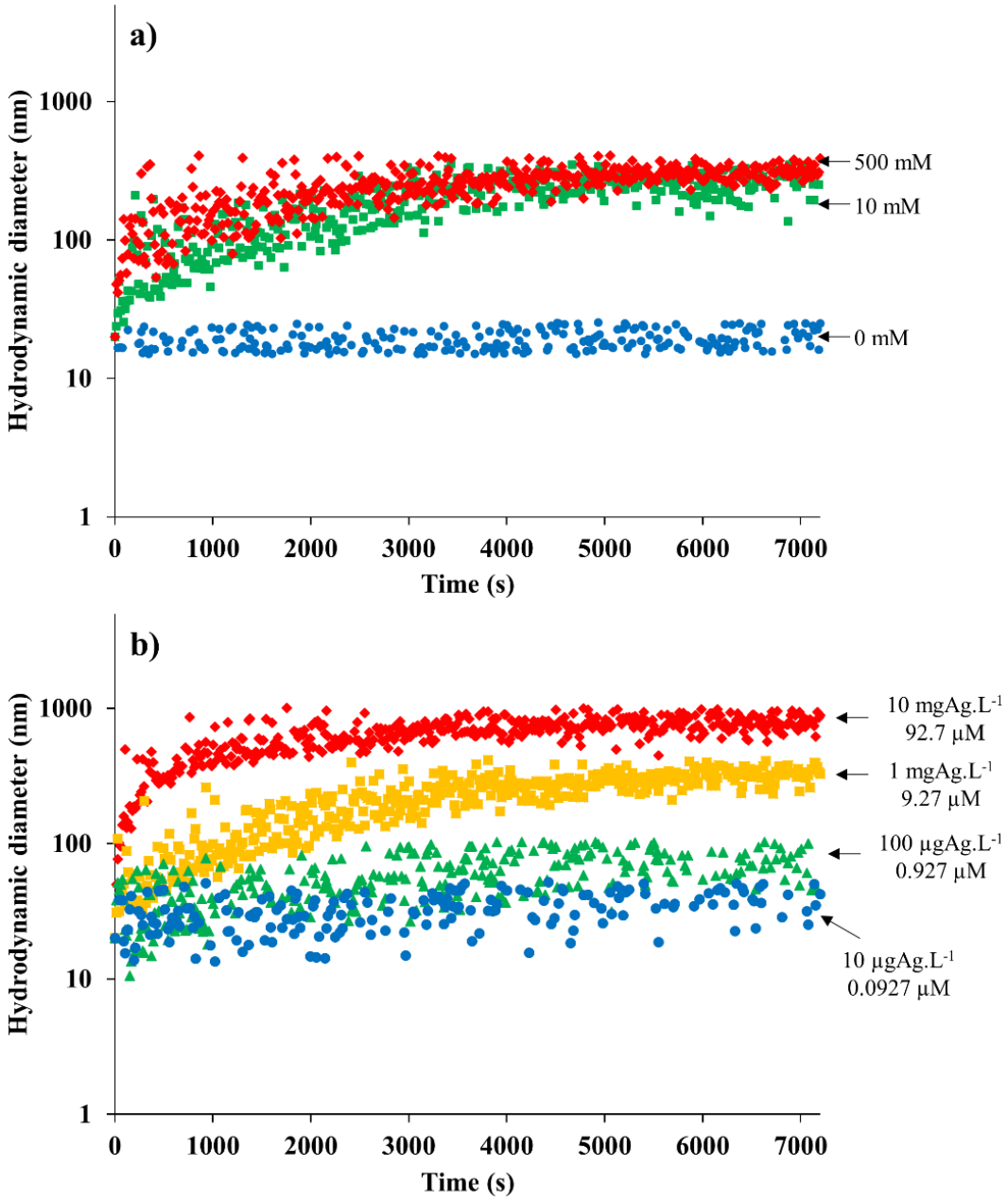

Figure 7: Aggregation kinetics of AgNPs of 2 h a) at constant AgNPs concentration (1 mgAg.L^{-1}) and at NaCl concentration of 0 mM (blue circle), 10 mM (green square) and 500 mM (red diamond); and b): AgNPs decreasing concentrations: 10 mgAg.L^{-1} (red diamond), 1 mgAg.L^{-1} (yellow square), 100 µgAg.L^{-1} (green triangle) and 10 µgAg.L^{-1} (blue circle) in constant solution of NaCl 200 mM

As observed in Figure 7, D_h values showed a plateau with time (5 400-7 200 s) and was steady whatever the concentration of salt and AgNPs. For the same AgNPs concentration, the D_h of aggregates formed in salty solutions appeared to be very close (Figure 7 and Table 8 (Annexe I p149)). The D_h of aggregates differed according to the AgNPs concentration. At 200 mM NaCl, D_h was at 783±106 nm at 10 mgAg.L^{-1}, at 318±39 nm at 1 mgAg.L^{-1} and between 60 and 250 nm with a D_h at 101±34 nm and 46±11 nm at 100 and 10 µgAg.L^{-1}, respectively. In salty water, the aggregation rate seems to be controlled by the salt concentration and by the AgNPs concentration, but the size of aggregates was essentially related to the AgNPs concentration.

1.5.3 EFFECTS OF SILVER NANOPARTICLES CONCENTRATION ON CRITICAL COAGULATION CONCENTRATION

The attachment efficiency (α) was determined following the equation 4 at different NaCl concentrations and for each AgNPs concentration. In Figure 8a, α value was determined at 10 and 1 mgAg.L^{-1} and at different NaCl concentrations. α values increased between 0 and 100 mM, but at salt concentrations higher than 100 mM, α values reached a plateau. The CCC was graphically fitted at 72 mM NaCl for 10 mgAg.L^{-1} and at 79 mM NaCl for 1 mgAg.L^{-1}. According to the DLVO theory (Derjaguin and Landau, 1941; Petosa *et al.,* 2010; Verwey and Overbeek, 1948), the aggregation of AgNPs was in RLA regime between 0 and near 70 mM. In this regime, the repulsive forces were higher than the attractive ones (Petosa *et al.,* 2010), but the increase of salt concentration induced a decrease of repulsive forces as described earlier. At salt concentration higher than 70 mM, the repulsive forces were equal or lower than attractive forces (Petosa *et al.,* 2010). The aggregation regime changed from RLA to DLA. Aggregation rate of AgNPs differs depending on the regime of aggregation: slow rate corresponds to RLA whereas a fast rate is associated to DLA (Petosa *et al.,* 2010).

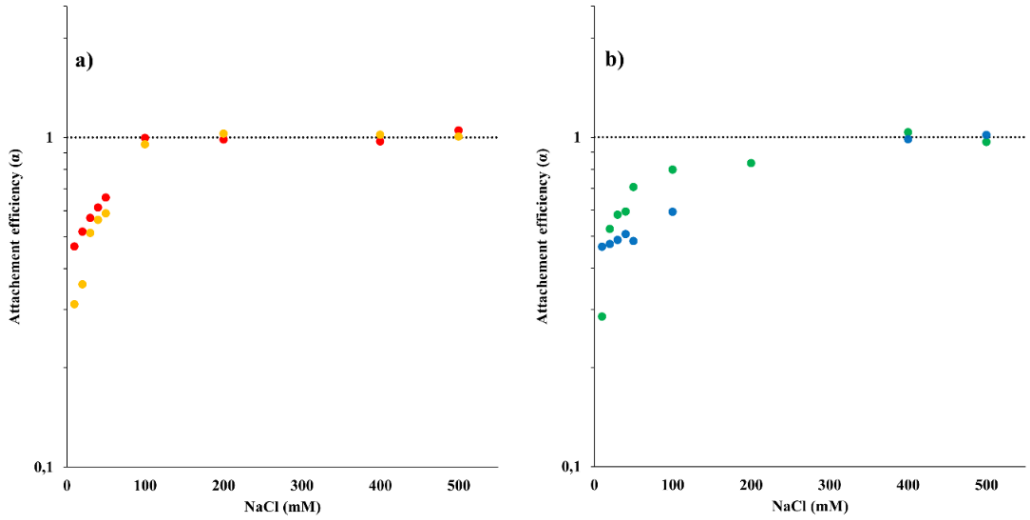

Figure 8: Attachment efficiency of silver nanoparticles at a) 10 mgAg.L^{-1} (red circle) and 1 mgAg.L^{-1} (yellow circle) and at b) 100 µgAg.L^{-1} (green circle) and 10 µgAg.L^{-1} (blue circle)

These CCC values are similar to values obtained by El Badawy *et al.* (2012) but differ from other studies (Baalousha *et al.,* 2013; Chen and Zhang, 2012; Huynh and Chen, 2011; Li *et al.,* 2012, 2010; Lin *et al.,* 2015; Zhang *et al.,* 2012). Some of the differences observed can be explained by the coating agent used to stabilize AgNPs. For citrate-coated AgNPs three ranges of values were observed: near 40 mM (Huynh and Chen, 2011; Li *et al.,* 2012, 2010), near 70 mM for this study and the study of El Badawy *et al.* (2012) and between 86 and 122 mM for Baalousha *et al.* (2013). Some studies explained the difference of CCC, between 40 and 70 mM, by the proportion of citrate covering the AgNPs surface (Baalousha *et al.,* 2013; El Badawy *et al.,* 2012; Huynh and Chen, 2011). At 40 mM, AgNPs appeared incompletely coated by citrate, but completely at 70 mM (El Badawy *et al.,* 2012; Huynh and Chen, 2011). Another explanation could be related to the synthesis method used to obtain AgNPs. With the Tollen's synthesis CCC value was near 40 mM, although with the Turkevich's synthesis values were near 70 mM and near 100 mM when AgNPs were synthesized with $AgNO_3$, citrate and $NaBH_4$. During the Tollen's synthesis, AgNPs were first obtained by reducing action of the aldehyde groups (Beaudoin *et al.,* 1987) of sugars, as

D-maltose, and the citrate was added after the purification process. With this synthesis, the citrate was in interaction with the surface of AgNPs, citrate was used as an overlay agent (El Badawy *et al.,* 2012). In contrast, when citrate was used as a reducing agent, the citrate could be incorporated into the AgNPs and was a coating agent. Pillai (2004) has hypothesized that during silver reduction with citrate, a silver-citrate complex was formed, promoting the formation of AgNPs. These differences in synthesis could explain variations of CCC values.

The α values obtained at 100 and 10 µgAg.L^{-1} depending on NaCl concentrations are shown in Figure 8b. At these concentrations, the CCC value was very different compared to the one obtained at 10 and 1 mgAg.L^{-1}. At these low AgNPs concentrations, the CCC was graphically fitted at 148 mM NaCl for 100 µgAg.L^{-1} and at 161 mM NaCl for 10 µgAg.L^{-1}. To our knowledge, it is the first study that reports a CCC value at these low AgNPs concentrations and effects of AgNPs concentration on CCC. The repulsive (V_{EDL}) and attractive forces (V_{vdW}) described by the DLVO theory could be estimated with equations 6 and 7 (Elimelech *et al.,* 1998; Petosa *et al.,* 2010):

$$V_{EDL} = 32\pi\varepsilon_0\varepsilon_r a\left(\frac{K_bT}{ze}\right)^2 \Gamma^2 \exp(-\kappa h) \quad (6)$$

$$V_{vdW} = -\frac{A_{121}a}{12h\left(1+{}^{14h}/_{\lambda}\right)} \quad (7)$$

In these equations, many of the variables are specific to the AgNPs properties, as radius (a), dimensionless surface potential ($\Gamma=\tanh[(ze\psi)/(4K_bT)]$ with ψ the surface potential), inverse Debye length ($\kappa=\sqrt{((\varepsilon_0\varepsilon_r K_bT)/(e^2\sum n_i z_i^2))}$) and Hamaker constant (A_{121}) or to the medium properties as dielectric permittivity of the solution (ε_r), temperature (T) and counterion valence (z). Four parameter are constants as dielectric permittivity in the vacuum (ε_0), Boltzmann constant (K_b), electron charge (e) and characteristic wavelength (λ, e.g. =100 nm) (Petosa *et al.,* 2010; Song *et al.,* 2011). In equations 6 and 7, the surface-to-surface separation distance (h) indicates that the repulsive and attractive forces increase when

h tends to zero. When h becomes higher than 10% of the radius, these forces are too low to promote interactions between particles (Elimelech *et al.,* 1998). However, concentrations of AgNPs can affect aggregation as discussed below.

According to the Smoluchowski equation (8), the aggregation rate, $t_{1/2}$ corresponds to the half-time of the aggregations, is controlled by the diffusion coefficient (D), by the initial particle concentration (N_0) and the hydrodynamic diameter (D_h) (Everett, 1992; Holthoff *et al.,* 1997; Petosa *et al.,* 2010):

$$t_{1/2} = \frac{1}{4\pi D_h D N_0} \quad (8)$$

The diffusion coefficient is obtained with the Stokes-Einstein equation (9), where K_b is the Boltzmann constant, T is the temperature in Kelvin, η is the viscosity (Pa.s) of the medium and D_h stands for the hydrodynamic diameter of particles.

$$D = \frac{K_b T}{3\pi\eta D_h} \quad (9)$$

With the equation 9, the equation 8 can be simplified to the equation 10.

$$t_{1/2} = \frac{3\eta}{4K_b T N_0} \quad (10)$$

According to the equation 10, aggregation of AgNPs is directly affected by the initial particle concentration (N_0). Differences observed in aggregation rates (Figure 7b) are related to the initial particle concentration. The diffusion coefficient of initial AgNPs or the other physicochemical parameters such as SPR, Pζ, shape, coating, etc., cannot explain the differences observed in the CCC because the AgNPs are the same for all concentrations (Table 2).

If we assume that the AgNPs were equidistant from one another, the distance between each particle (*l*) according to the sample volume (V) and the initial particle concentration (N_0) could be calculated by equation 11:

$$l = \left(\frac{V}{N_0}\right)^{\frac{1}{3}} \quad (11)$$

Initial particle concentrations (N_0) were at 2.3×10^{11}, 2.3×10^{10}, 2.3×10^{9} and 2.3×10^{8} particles.mL^{-1} for 10 mgAg.L^{-1}, 1 mgAg.L^{-1}, 100 µgAg.L^{-1} and 10 µgAg.L^{-1}, respectively. Calculated distances in our solutions increased from 1.6 to 16.3 µm when AgNPs concentration decreases, and corresponded to the interaction surface (πl^2) 8.4 to 837 µm^2 (Table 7, Annexe I p149). Using equation 9, the diffusion coefficient of 20 nm AgNPs, at 25 °C, was estimated to 24.5 and 23.2 µm^2.s^{-1} for 0 and 500 mM NaCl, respectively. With the diffusion coefficient and the interaction surface, the time taken by particles to travel these surfaces was estimated between 0.34 and 34.2 s at 0 mM of NaCl and between 0.36 and 36.1 s at 500 mM of NaCl (Table 7). At high AgNPs concentration (mgAg.L^{-1}), the time taken by particles to encounter and interact together is short (0.36 s) and the aggregation rate is increased, but at lower concentrations (µgAg.L^{-1}), the time was in the order of many seconds (36.1 s), explaining why the aggregation rate decreased. Furthermore, during these times taken by particles to travel these distances, some chemical transformations of AgNPs could have occurred. These transformations could be: 1) sorption of silver salt as AgCl on AgNPs (Baalousha *et al.,* 2013; Levard *et al.,* 2012), 2) formation of AgCl nanoparticles (Baalousha *et al.,* 2013; Levard *et al.,* 2012) and/or 3) oxidation of AgNPs surfaces (Li *et al.,* 2012, 2010). These transformations modify the coating of AgNPs. With this new coating, the value of the variables Γ and A_{121} described in the equations 6 and 7 can evolve, resulting in a modification of the attractive and repulsive forces between AgNPs. As these forces were altered, the CCC was changed (Elimelech *et al.,* 1998) and this could explain the increase of CCC observed in this study.

1.5.4 EFFECTS OF SILVER NANOPARTICLES CONCENTRATION ON THE EVOLUTION OF PARTICLE DISTRIBUTION

The distribution of particle sizes was also measured by DLS (Figure 9). Particle distributions during 2 h in a NaCl 200 mM solution and AgNPs concentrations of 10 mgAg.L^{-1}, 1 mgAg.L^{-1}, 100 µgAg.L^{-1} and 10 µgAg.L^{-1} are shown with conditions already described in Figure 7b.

At 10 mgAg.L^{-1} (92.7 µM), two particle populations were observed during the first 1 000 s (Figure 9a). The first population shown particles in the range 0 and 190 nm and the second one was in the size range 220 and 10 000 nm. During this period of time, the relative proportion of the first population (0-200 nm) was much higher than the second one (200-10 000 nm). With time the proportion of the first population decreased and proportion of the second one increased proportionally. The presence of these two particle populations and the rapid change of proportion correspond to the phase of rapid D_h evolution shown in Figure 7b. After 1 000 s, the dominant population was observed in the range 300-1 000 nm with a higher proportion of particles between 800 and 900 nm. This distribution appears to be stable during the last hour. For the other AgNPs concentrations, the presence of both particle populations persisted for a much longer time compared to 10 mgAg.L^{-1}. They were present throughout the experiment. However, a change in the proportion was observed according to the concentration of AgNPs. At 1 mgAg.L^{-1} (9.27 µM), the particles with a D_h between 0 and 190 nm, were more abundant during the first 3 000 s (Figure 9b). This phase corresponds to the rapid increase of D_h observed in Figure 7b. After 3 000 s, the particles with a D_h between 220 and 550 nm were in majority and their distribution was stable.

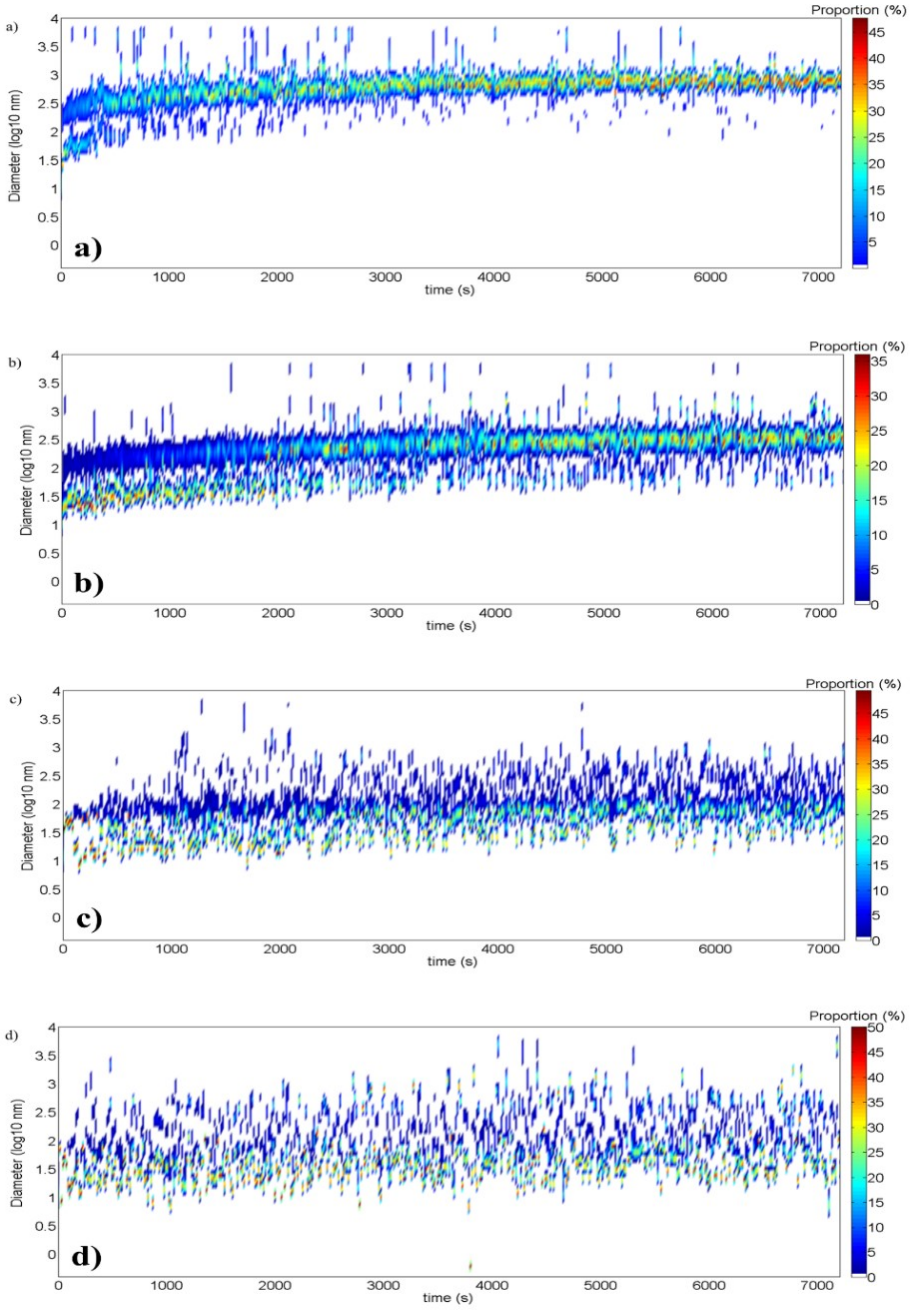

Figure 9: Kinetics of particles distribution over 2 h at a) 10 mgAg.L^{-1}, b) 1 mgAg.L^{-1}, c) 100 µgAg.L^{-1} and d) 10 µgAg.L^{-1} of silver nanoparticles in a solution of NaCl at 200 mM

At 100 and 10 µgAg.L^{-1} (0.927 and 0.0927 µM), the proportion of particle population between 0 and 190 nm remained higher than at high AgNPs concentrations (92.7 and 9.27 µM). Moreover, their D_h changed during the first few seconds to minutes (Figure 9c and Figure 9d).

In this initial period, the D_h increased rapidly. After, the D_h decreases near 10 nm, half of the initial D_h and then increased again rapidly. This fast change was more pronounced at 100 µgAg.L^{-1} than at 10 µgAg.L^{-1}. This phenomenon has been observed in other studies (Baalousha *et al.,* 2013; Li *et al.,* 2012, 2010) with AgNPs concentrations between 300 µgAg.L^{-1} and 2 mgAg.L^{-1}. Li *et al.* (2012, 2010) have suggested this decrease of D_h could be related to the dissolution of Ag_2O layers around AgNPs and/or by a rapid change of silver ions sorbed into the surface of AgNPs by other ions, sodium ions in this study. Baalousha *et al.* (2013) suggested other phenomena such as the shrinkage of diffuse layer caused by the increase of ionic strength, oxidative dissolution of AgNPs, and formation of AgCl nanoparticles. When particles are in liquid medium, a double layer structure appears: Stern layer and diffuse layer (Xu, 2001a). The diameter of AgNPs measured with TEM (Figure 27) was near 20 nm. TEM measurement was done under high vacuum and with a dry sample. With this technique, the double layer cannot be observed. In this study, as the size obtained with TEM and DLS were very close, the double layer was not observed. This observation is consistent with the conclusion of Baalousha *et al.* (2013) that the shrinkage of diffuse layer cannot explain a decrease of 50% of the D_h. They have also estimated a decrease of D_h between 39 and 45% corresponded to a dissolution of AgNPs between 77 and 84% (Baalousha *et al.,* 2013). In the present study the decrease of D_h would represent a dissolution of 87%. Some authors (Dobias and Bernier-Latmani, 2013; Li *et al.,* 2010; Liu and Hurt, 2010) have studied the dissolution of AgNPs during several days in different water solutions. They have estimated a dissolution of 2% after 14 days to 30% after four months (Dobias and Bernier-Latmani, 2013; Li *et al.,* 2012). Dissolution of AgNPs is a slow process and could not explain the rapid change of D_h observed in this study. The last phenomenon to explain

the decrease of D_h is the formation of AgCl nanoparticles/colloids (Baalousha *et al.,* 2013; Li *et al.,* 2012, 2010). The formation of AgCl nanoparticles could change the particle distribution by increasing the number of small particles (Baalousha *et al.,* 2013) and inducing a D_h decrease as observed at 100 and 10 µgAg.L^{-1} during the first minutes of aggregation. The two possible silver sources were 1) the presence of silver ions in the AgNPs stock solution and 2) silver oxide (Ag_2O) sorbed (Dobias and Bernier-Latmani, 2013; Li *et al.,* 2010; Lok *et al.,* 2007; Sotiriou *et al.,* 2012) at AgNPs surface. According to the low concentration of silver ions (below detection limit of ICP-MS: 0.015 µgAg.L^{-1}) in the stock AgNPs solution (at 585 mgAg.L^{-1}) and after a dilution factor between 58.5 and 58 500 to obtain AgNPs from 10 mgAg.L^{-1} to 10 µgAg.L^{-1}, this source of silver cannot explain the formation of AgCl nanoparticles in this study. Some studies (Dobias and Bernier-Latmani, 2013; Li *et al.,* 2010) on AgNPs dissolution has observed a high release of silver followed by a decrease of dissolved silver content in the medium during the first minutes of experiments. Sotiriou *et al.* (2012) have hypothesized that this source of silver comes from the desorption or dissolution of Ag_2O layers from AgNPs surface. Desorption of sorbed silver at AgNPs surfaces (Dobias and Bernier-Latmani, 2013; Li *et al.,* 2012; Sotiriou *et al.,* 2012) into the medium and an interaction with chloride could explain the formation of AgCl nanoparticles. Furthermore, the formation of AgCl nanoparticles could explain the increase of the CCC observed in this study at low concentrations (Figure 8). However, this decrease of D_h was not observed at high concentrations of AgNPs. It was consistent with other studies where high AgNPs concentrations were used (Chen and Zhang, 2012; El Badawy *et al.,* 2012). As aggregation was fast, formation of AgCl nanoparticles could be limited or occulted by excess of citrate-coated AgNPs.

1.5.5 EFFECTS OF SILVER NANOPARTICLES CONCENTRATION ON AGGREGATES DISTRIBUTION

The aggregation of AgNPs produced two particle populations. The first population included particles with a D_h less than 200 nm called as $P_{0\text{-}200}$. The second population contains

all aggregates with sizes larger than 200 nm and is identified as $P_{200\text{-}10\,000}$. These two particle populations can be characterized by determining their averaged hydrodynamic diameters, identified as $D_{h0\text{-}200}$ for $P_{0\text{-}200}$ and as $D_{h200\text{-}10\,000}$ for $P_{200\text{-}10\,000}$, and their relative proportions. To our knowledge, this is the first study describing the distribution of aggregates at several AgNPs concentrations with an increasing salt concentration.

Figure 10 and Table 9 (Annexe I p149) present the averaged particle diameters and the particles distributions (% composition of total particles) observed during the last thirty minutes for the 2 h kinetic study, when the sizes were constant. As shown in Figure 10 in nanopure water and for all AgNPs concentrations, more than 99% of particles had a $D_{h0\text{-}200}$ at 20±3 nm (Table 9). This high proportion of small particles changed according to AgNPs concentration and salt concentration. At 10 mgAg.L^{-1}, the proportion of small particles was very low (≤0.2%) with $D_{h0\text{-}200}$ near 156 nm (Figure 10a and b and Table 9) and more than 99% of particles formed the population $P_{200\text{-}10\,000}$ with $D_{h200\text{-}10\,000}$ near 820 nm. At this high AgNPs concentration, the presence of salt, did not change the final size distribution of aggregates. However, this is not the case for lower AgNPs concentrations. At 1 mgAg.L^{-1}, large aggregates ($P_{200\text{-}10\,000}$, Figure 10c and d) were always present in higher proportion (between 68 and 89%) than small particles ($P_{0\text{-}200}$). Moreover, the proportion of $P_{200\text{-}10\,000}$ was stable around 85% at high salt level, but decrease at salt concentration lower than 30 mM NaCl. At 100 and 10 µgAg.L^{-1} (Figure 10e, f, g and h), the proportion of $P_{200\text{-}10\,000}$ was lower than proportion of $P_{0\text{-}200}$, contrary to PSD observed at high AgNPs concentrations. At these low concentrations $P_{0\text{-}200}$ were dominant, more than 90% of particles. Moreover, the size of $P_{0\text{-}200}$ and $P_{200\text{-}10\,000}$ was smaller. At 10 µgAg.L^{-1}, the size distribution of the aggregates was more dispersed than for the other AgNPs concentrations as observed by the height of box plots. Lawler *et al.* (2015) observed similar results at 125 µAg.L^{-1}, with more than 85% of particles with a D_h comprised between 30 and 100 nm.

Differences observed in the D_h and proportions of aggregates could be explained by the initial particle concentration. At t_0, when the particles are small (20 nm), the diffusion

coefficient is high according to the Stoke-Einstein equation (9). In the first few seconds, the D_h increases due to the efficient collision between two initial AgNPs. These small aggregates can interact and aggregate together or with initial AgNPs, explaining the polymodal distribution observed at each AgNPs concentration. During aggregation, as the D_h of particles increases, the diffusion coefficient and the particle concentration decrease. The decrease of both resulted in increasing the distance between each particle (equation 11) inducing an increase in the elapse time between collisions (equation 10). At high particles concentration (10 or 1 mgAg.L^{-1}), even if the diffusion coefficient decreases during the aggregation, the particle concentration could remain sufficiently important to promote collisions for a longer period of time. This could favor interactions and aggregation of small aggregates themselves and promote the formation of larger aggregates, and could explain the high proportion (70 to 100%) of large aggregates ($P_{200\text{-}10\,000}$) observed at 10 and 1 mgAg.L^{-1}. At low concentrations (100 and 10 µgAg.L^{-1}), the particle concentration would be too low to promote aggregation for a long period of time and favors only the interactions between AgNPs themselves, and between AgNPs and small aggregates. This process can explain the change in proportion observed, where 50 to 90% of particles formed the population $P_{0\text{-}200}$. In the last 30 min (5 400-7 200 s) of kinetics, the particle concentrations in salty solutions were estimated at 2.7 x 10^6, 3.7 x 10^6, 6.2 x 10^6 and 1.0 x 10^6 particles.mL^{-1} for 10 mgAg.L^{-1}, 1 mgAg.L^{-1}, 100 µgAg.L^{-1} and 10 µgAg.L^{-1}, respectively.

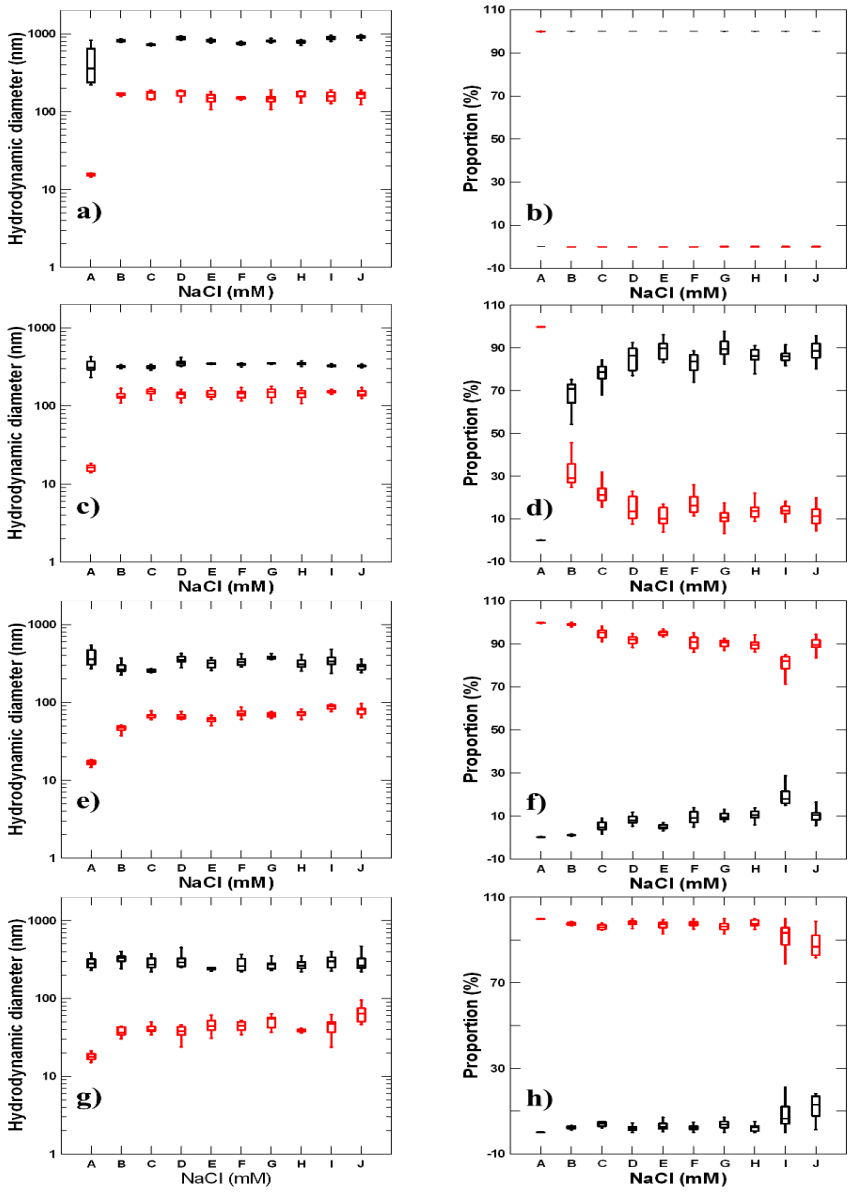

Figure 10: Hydrodynamic diameter and proportion distribution of particle populations less than 200 nm (red) and higher than 200 nm (black) observed between 5 400 and 7 200 s (last 30 min) for kinetics of 2 h at four silver nanoparticles concentrations: a and b) 10 mgAg.L^{-1}, c and d) 1 mgAg.L^{-1}, e and f) 100 µgAg.L^{-1}; g and h) 10 µgAg.L^{-1} at different NaCl concentrations A 0 mM, B 10 mM, C 20 mM, D 30 mM, E 40 mM, F 50 mM, G 100 mM, H 200 mM, I 400 mM and J 500 mM

Kinetics over 12 h were also performed at four salt concentrations: 0, 9, 86 and 428 mM of NaCl for each AgNPs concentration. Table 3 shows D_h and proportions of particle populations $P_{0\text{-}200}$ and $P_{200\text{-}10\,000}$ observed between 36 000 and 43 200 s (last 2 h). In nanopure water, distribution of AgNPs was not influenced by time and particle concentration as previously observed for 2 h. At 10 mgAg.L^{-1}, in presence of NaCl, the proportion appeared very close to those observed for 2 h kinetics, more than 99% of particles formed the population $P_{200\text{-}10\,000}$. However, average D_h of $P_{200\text{-}10\,000}$ decreased from 820 to 660 nm. This decrease could be explained by a transformation of aggregates as: 1) dissolution, 2) breakage of aggregates (Tourbin and Frances, 2008) , and 3) evolution of the morphology of aggregates (Eggersdorfer *et al.,* 2011). However, the same pattern was not observed for the other AgNPs concentrations. At 1 mgAg.L^{-1} and 100 µgAg.L^{-1}, the D_h and the proportion of the two particle populations changed with time. At 1 mgAg.L^{-1}, after 12 h, between 94 and 99% of particles composed population $P_{200\text{-}10\,000}$ and had $D_{h200\text{-}10\,000}$ at 445±35 nm. The population $P_{0\text{-}200}$ had a mean $D_{h0\text{-}200}$ at 138±17 nm. At 100 µgAg.L^{-1}, this change was more pronounced. The proportion of particles of $P_{0\text{-}200}$ decreased to 68% of particles with $D_{h0\text{-}200}$ at 88±8 nm. For the population $P_{200\text{-}10\,000}$, $D_{h200\text{-}10\,000}$ was at 424±48 nm. The evolution of particle size distribution (proportions, $D_{h0\text{-}200}$, $D_{h200\text{-}10\,000}$) between 2 and 12 h could be related to a slow aggregation of the small aggregates ($P_{0\text{-}200}$) inducing formation of larger aggregates ($P_{200\text{-}10\,000}$). At 10 µgAg.L^{-1}, neither evolution in D_h and proportion of populations was observed between 2 and 12 h. After 12 h, the particle concentrations were at the same level as observed after 2 h: 10^6 particles.mL^{-1} (6.4×10^6, 1.6×10^6, 1.3×10^6 and 1.8×10^6 particles.mL^{-1}), and suggested: (1) when particle concentration was at 10^6 particles.mL^{-1}, the number of particles in the medium was too low, or a limiting factor; and (2) distance between each particle was too high to promote aggregation and could explain the presence of a plateau in D_h evolution at each AgNPs concentration.

Table 3: Hydrodynamic diameter and proportion distribution of particle populations less than 200 nm ($P_{0\text{-}200}$) and higher than 200 nm ($P_{200\text{-}10\,000}$) observed between 36 000 and 43 200 s (last 2 h) for 12 h kinetics at four silver nanoparticles concentrations: 10 mgAg.L^{-1}, 1 mgAg.L^{-1}, 100 µgAg.L^{-1} and 10 µgAg.L^{-1} at 0, 9, 86 and 428 mM of NaCl

		10 mgAg.L^{-1} (92.7 µM)		1 mgAg.L^{-1} (9.27 µM)		100 µgAg.L^{-1} (0.927 µM)		10 µgAg.L^{-1} (0.0927 µM)	
		$P_{0\text{-}200}$	$P_{200\text{-}10\,000}$	$P_{0\text{-}200}$	$P_{200\text{-}10\,000}$	$P_{0\text{-}200}$	$P_{200\text{-}10\,000}$	$P_{0\text{-}200}$	$P_{200\text{-}10\,000}$
0 mM	**D_h (nm)**	**15±1**	**229±9**	**15±1**	**245±36**	**17±1**	**359±40**	**20±2**	**315±51**
	Proportion (%)	99.9±0.1	0.03±0.03	99.8±0.1	0.1±0.05	99.7±0.1	0.2±0.1	99.7±0.2	0.3±0.2
9 mM	**D_h (nm)**	**nd**	**684±37**	**140±15**	**458±13**	**86±7**	**436±47**	**37±5**	**240±17**
	Proportion (%)	0±0.01	100±0.01	1.0±0.8	99.0±0.8	72.0±4.3	28.0±4.3	98.8±0.5	1.2±0.5
86 mM	**D_h (nm)**	**nd**	**645±30**	**141±21**	**471±22**	**84±5**	**383±32**	**58±12**	**285±26**
	Proportion (%)	0±0.01	100±0.01	4.7±2.5	95.3±2.5	72.6±2.6	27.4±2.6	95.0±1.9	5.0±1.9
428 mM	**D_h (nm)**	**nd**	**659±45**	**132±10**	**406±25**	**94±6**	**451±36**	**82±14**	**383±78**
	Proportion (%)	0±0.01	100±0.01	5.7±1.7	94.3±1.7	60.0±3.5	40.0±3.5	76.1±10.6	23.9±10.6
Average 9-428 mM	**D_h (nm)**	**nd**	**662±41**	**138±17**	**445±35**	**88±8**	**424±48**	**59±22**	**303±77**
	Proportion (%)	0±0.01	100±0.01	3.8±2.7	96.2±2.7	68.2±6.8	31.8±6.8	90.0±11.7	10±11.7

nd: no data

1.6 CONCLUSION

We reported, here, the first experimental study of AgNPs aggregation at different AgNPs concentrations during 2 h and 12 h. This study showed effects of salts and AgNPs concentrations on the aggregation rate as follows: (1) at a constant AgNPs concentration, the rate increased with an increase of NaCl concentration to a maximal value; (2) at a constant NaCl concentration, the rate decreased with a reduction of AgNPs concentration. In addition, the influence of AgNPs concentration on critical coagulation concentration could be related to a chemical transformation of AgNPs surface. Furthermore, this study showed the strong influence of AgNPs concentration on size distribution of aggregates. At a high AgNPs concentration, less than 20% of the aggregates formed after 2 h tends to have a D_h smaller than 200 nm. Proportion of this population decreases to 0-5% after 12 h. At low concentration, the distribution was very different, between 60 and 90% of the aggregates have a D_h less than 200 nm.

This study provides important information for ecotoxicology and environmental studies at low AgNPs concentrations. It is important to follow the evolution of the size distribution of aggregates during the nanotoxicity assay and more particularly for studies with microorganisms. Kinetics of 2 h, show that it is important to use aged AgNPs, after 1 h of aggregation, for toxicological assay, as some studies did (Doiron *et al.,* 2014), because whatever the AgNPs concentration, the organisms can be exposed to the same particle concentration, 10^6 particles.mL^{-1}, but the D_h and particle size distribution of aggregates are different.

Kinetics of 12 h, give important information for risk assessment of AgNPs in aquatic environment, because: 1) AgNPs concentration used can help to predict the behavior and fate of AgNPs during accidental release (10 and 1 mgAg.L^{-1}) and chronic release (10 µgAg.L^{-1}); and 2) NaCl concentration used correspond to a salinity of 0.5, 5 and 25 PSU, characteristic of estuarine transition between fresh and marine waters. However, the salinity seems to have

little effects on the aggregates size. At high AgNPs concentration, 95% of particles had D_h higher than 200 nm, AgNPs aggregates could correspond to natural suspended particulate matter fraction and could settle depending on the stratification of aquatic environment. At low AgNPs concentrations, more than 60% of the aggregates have a D_h less than 200 nm, the aggregates could be less affected by the settling, increasing their residence time in the water column and promoting their exportation from rivers to the ocean.

1.7 ACKNOWLEDGMENTS

This work was supported by Strategic Project Grants of the National Sciences Engineering Research Council of Canada (Émilien Pelletier and Jean-Pierre Gagné), Discovery Project Grants of the National Sciences Engineering Research Council of Canada (Jean-Pierre Gagné) and Québec-Océan for its financial support. The authors are grateful to Daniel Bourgault and Dany Dumont for the MATLAB programming and Clément Joly and Audrey Tiercin for their technical support.

CHAPITRE 2
LA CHIMIE D'UN MILIEU DE CULTURE BACTÉRIEN AFFECTE-T-ELLE LA STABILITÉ DES NANOPARTICULES DANS DES ESSAIS DE NANOTOXICITÉ ?

2.1 RÉSUMÉ

Le but de cette étude est d'évaluer la stabilité de suspensions d'AgNPs dans différentes solutions d'exposition caractéristiques des eaux naturelles ou des milieux utilisés dans les études d'écotoxicologie microbienne. Dans l'eau nanopure, la taille des AgNPs est stable dans le temps. Lorsque la force ionique des solutions est augmentée, par ajout de NaCl, $CaCl_2$ ou $MgCl_2$ à 25 PSU, cela favorise une augmentation importante de la taille des AgNPs, correspondant à une agrégation des nanoparticules. Cette agrégation est modulée par la valence des cations. Les cations divalents favorisent une agrégation plus rapide que les cations monovalents. La présence d'un mélange complexe d'anions dans les eaux de mer artificielles ou dans le milieu de culture F/2 (Cl^-, HCO_3^-, SO_4^{2-}), diminue la vitesse d'agrégation en interagissant avec les surfaces des AgNPs. En milieu de force ionique importante, la présence de matière organique comme du tryptone et des extraits de levure dans les milieux de culture (Luria Broth, LB) ralentit l'agrégation des AgNPs. Le ralentissement des vitesses d'agrégation, causé par la sorption de la matière organique, est temporaire et ne semble pas durer plus de quelques heures. Cette étude montre l'importance de contrôler le vieillissement des suspensions colloïdales d'AgNPs pour des essais de nanotoxicité.

Ce deuxième article, intitulé « *Does the bacterial media culture chemistry affect the stability of nanoparticles in nanotoxicity assays?* », fut corédigé par moi-même ainsi que par la docteure Kim Doiron, la professeure Karine Lemarchand et par le professeur Jean-Pierre Gagné. En tant que premier auteur, ma contribution à ce travail fut d'effectuer une recherche bibliographique poussée, les analyses de laboratoire, le traitement des données et la rédaction de l'article. La docteure Kim Doiron a fourni l'idée originale, a participé aux analyses de laboratoire et à la rédaction de l'article. Les professeurs Karine Lemarchand et Jean-Pierre Gagné ont fourni l'idée originale et ont participé à la rédaction de l'article. Cet article a été accepté pour publication dans sa version finale dans le journal : *Journal of Xenobiotics* en décembre 2015, et accessible en ligne en janvier 2016. Une version abrégée de cet article a été présentée aux conférences : *Forum québécois des sciences de la mer* à Mont-Joli (Québec) et *Gagilau* à Québec (Québec) en automne 2012, *Journée annuelle de la recherche environnementale* à Montréal (Québec) et *FODAR-Rimouski* à Rimouski (Québec) au printemps 2013, *Canadian Society for Chemistry* à Québec (Québec) en été 2013.

DOES THE BACTERIAL MEDIA CULTURE CHEMISTRY AFFECT THE STABILITY OF NANOPARTICLES IN NANOTOXICITY ASSAYS?

2.2 ABSTRACT

The aim of this study was to evaluate the stability of AgNPs suspensions in different exposure solutions characteristic of natural waters or culture medium used in microbial ecotoxicology studies. In nanopure water, the size of AgNPs was stable over time. When the ionic strength of the solution was enhanced, by adding NaCl, $CaCl_2$ or $MgCl_2$ at 25 PSU, the size of AgNPs increased rapidly and corresponded to an aggregation of the nanoparticles. This aggregation was modulated by the valence of the cations. The divalent cations favored a faster aggregation than monovalent cations. The presence of a complex mixture of anions as in artificial seawater or as in the F/2 medium (Cl^-, HCO_3^-, SO_4^{2-}) decreased the aggregation rate by interacting with AgNP surfaces. At high ionic strength, the presence of organic matter such as tryptone and yeast extract in culture media (Luria Broth, LB) decreased the aggregation rate of AgNPs. The lower aggregation rate, caused by the sorption of organic matter, was temporary and did not exceed a few hours. This study shows the importance to control the aging of colloidal AgNPs suspensions for nanotoxicity assays.

Keywords: Citrate-coated silver nanoparticles, aggregation, salt effects, culture media effects.

2.3 INTRODUCTION

New classes of silver nanoparticles (AgNPs) with antimicrobial activities are under rapid development for incorporation into consumer products. Important applications are in food packaging materials, odor-resistant textiles, paints, cosmetics, medical devices, water disinfectants… (SCENIHR, 2014). This increasing use of AgNPs raised the issue of the release of nanosilver from a variety of sources, under different forms, into aquatic

environments. Recent studies have confirmed the release of AgNPs from socks and nanotextiles during washing (Benn and Westerhoff, 2008; Geranio *et al.,* 2009) or from surfaces coated by nanosilver paints during rainwater runoff events (Kaegi *et al.,* 2010). The environmental effects of the AgNPs discharged into aquatic environments are largely unknown (ENRHES, 2009; SCENIHR, 2014). However, laboratory ecotoxicological studies on fishes, crustaceans, algae and bacteria have shown toxic effects on test organisms exposed to AgNPs (Doiron *et al.,* 2014, 2012; ENRHES, 2009; SCENIHR, 2014). Due to the antimicrobial properties of AgNPs, it is important to understand which factors control their toxicity toward environmental microorganisms since they play important roles in major biogeochemical cycles, in the production of natural organic matter and in the recycling of nutrients.

Bacterial sensitivity to silver nanoparticles and ionic silver have been demonstrated on reference bacterial strains of the genera *Bacillus*, *Escherichia, Pseudomonas* and *Vibrio* (Chambers *et al.,* 2014; Doiron *et al.,* 2014; Jin *et al.,* 2010; Marambio-Jones and Hoek, 2010) as well as on bacterial communities (Das *et al.,* 2012b, 2012a; Doiron *et al.,* 2012). Today, there is no consensus on the mechanisms of antimicrobial action of AgNPs. Proposed processes (Chambers *et al.,* 2014; Jin *et al.,* 2010; Lapresta-Fernández *et al.,* 2011; Marambio-Jones and Hoek, 2010; SCENIHR, 2014) include: (1) free silver ion dissolution from AgNPs followed by cellular uptake and disturbance of intracellular reactions; (2) cellular uptake of AgNPs followed by reactive oxygen species (ROS) generation and release of silver ions impacting DNA replication and ATP production; and (3) direct interaction of AgNPs with cell surface altering protein function and membrane permeability. These processes were demonstrated to be dependent on nanoparticle's size and specific properties (shape, chemical composition, surface charge, coating…). Moreover, the chemical composition of exposure media (pH, ionic strength, ionic composition, quality and quantity of natural organic matter) is also a relevant factor that would affect the toxicity of AgNPs. The solution chemistry could play an important role in the aggregation and in the fate of

AgNPs. If aggregation occurs, the size of AgNPs in solution will change, modifying the sedimentation and the ability of AgNPs to interact with proteins at the cellular surface or to cross cellular membranes. Thus, aggregation can modulate the toxicity of nanoparticles. Considering that the size of AgNPs can be a significant factor controlling the toxicity of silver nanoparticles, it is important to understand how the exposition media (*e.g.*, culture broths) modify the size of the nanoparticles used in toxicity assays. The purpose of this study is to assess the stability of AgNPs suspensions with time in different exposure solutions characteristic of natural waters or of media currently used in microbial ecotoxicology studies. We aim to show the importance to control the aging of AgNPs colloidal suspensions during toxicity assays.

2.4 MATERIALS AND METHODS

All experiments were conducted with citrate coated silver nanoparticles obtained by the reduction of $AgNO_3$ with sodium citrate. Suspension of AgNPs was purified to remove excess of $AgNO_3$ and citrate and to concentrate AgNPs. AgNPs synthetized had a hydrodynamic diameter of 9±2 nm. Salt solutions were at 428 mM of NaCl and 214 mM of $CaCl_2$ and $MgCl_2$ (ACS grade, LabMat), and corresponded to solutions with isomolar concentration of chloride. Ionic strengths were at 0.43, 0.64 and 0.64 M for NaCl, $CaCl_2$ and $MgCl_2$ respectively. Artificial seawater (ASW) was made by mixing 400 mM of NaCl, 41.4 mM of $MgSO_4$. 7 H_2O and 1.8 mM of $NaHCO_3$, corresponding to ionic strength at 0.57 M. Salt solutions and ASW were prepared and regulated at pH 7 and at 25 PSU, based on the conductivity of the solution. This salinity is characteristic of estuarine environments. These solutions were filtered on 0.2 µm pore-sized polycarbonate membrane. Culture media tested were Guillard's F/2, generally used for marine microalgae culture, and Luria Broth (LB), commonly used for bacterial growth. F/2 media was prepared by diluting trace elements (nitrate, phosphate, metal and vitamins) in ASW. LB media was composed of 10 g of tryptone, 5 g of yeast extract and 10 g of NaCl for 1 L of nanopure water at pH 7.2. The

evolution of hydrodynamic diameters of the AgNPs suspensions at concentrations of 93 µgAg.L^{-1} was measured by time resolved dynamic light scattering (TR-DLS) using Zetasizer Nano ZS (ZEN 3600, Malvern) instrument during 17 h at 25 °C. Parameters used for the TR-DLS was one measure each 10 min with an angle of 173°. One measure was obtained with 10 scans of 15 s each. The concentration used (93 µgAg.L^{-1}) in the experiments was in the lower range of concentrations used to test the toxicity of AgNPs to microorganisms.

2.5 RESULTS AND DISCUSSION

Figure 11 shows the evolution in hydrodynamic diameter (D_h) for AgNPs over 17 h in nanopure water, NaCl, $CaCl_2$ or $MgCl_2$ solution. In nanopure water, the D_h of AgNPs remained stable at 9±2 nm during 17 h (Figure 11A). In presence of NaCl at 25 SPU, the D_h of AgNPs (9 nm) evolved rapidly (Figure 11B) to reach 550±280 nm after 100 min. When $CaCl_2$ was added to nanopure water at 25 PSU, the D_h of AgNPs increased rapidly during the first 50 min (Figure 11C) suggesting that the rate of AgNPs aggregation is modulated by the nature of cations in solution. After 50 min, the D_h did not evolve anymore and stabilized at 424±69 nm. In presence of $MgCl_2$ added to nanopure water at 25 PSU, the behavior of AgNPs was the same as in the $CaCl_2$ solution (Figure 11D). After the rapid increase (50 min), the D_h remained at 548±105 nm. The rapid, but different, increases of D_h observed in NaCl, $CaCl_2$ and $MgCl_2$ solutions reflected the aggregation of AgNPs in presence of various cations and showed that divalent cations were more effective in accelerating aggregation than monovalent cations.

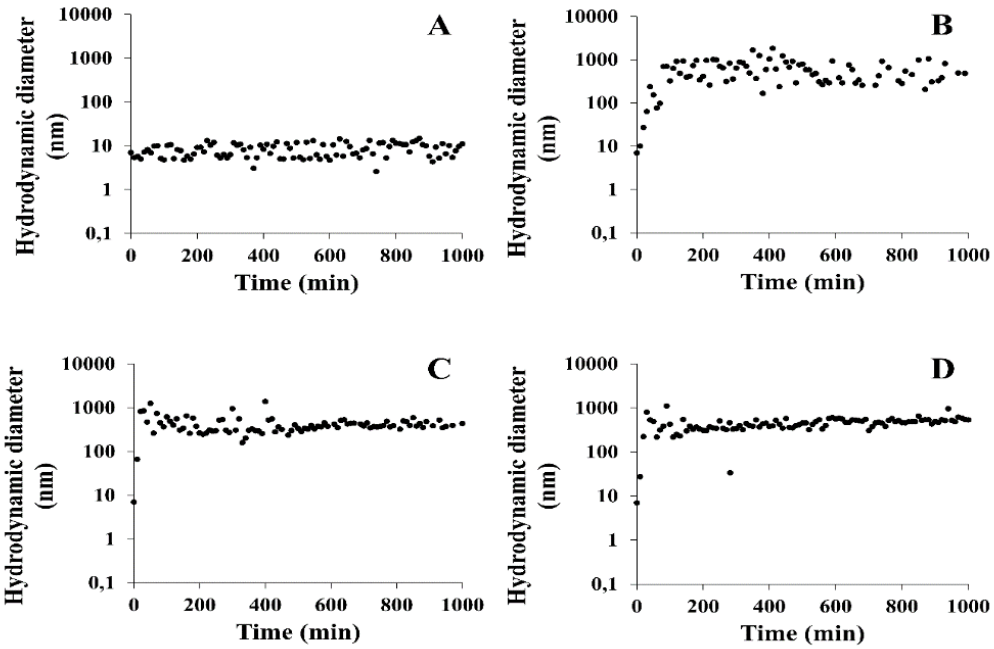

Figure 11: Aggregation kinetics of AgNPs at 93 µgAg.L^{-1} in A) nanopure water, B) in NaCl at 25 PSU, C) in $CaCl_2$ at 25 PSU and D) in $MgCl_2$ at 25 PSU

Figure 12 presents the time evolution of AgNPs diameter in ASW, F/2 and LB media. In ASW, from 0 min to 200 min, the D_h increased rapidly from 9 nm to near 400 nm as shown in Figure 12A. After 200 min the D_h reached 422±255 nm. In F/2 medium (Figure 12B), the behavior of AgNPs was similar to that observed in ASW. A rapid increase in D_h was observed during the first 200 min afterward the D_h remained at 635±253 nm. In LB broth, the D_h of AgNPs increased rapidly during the first 250 min. Later on, the diameter stabilized around 511±365 nm. In complex solutions (Figure 12) slower changes in aggregation rates were observed compared to those observed in simple solutions (Figure 11) during the first 100 min. This involves that for a complex aqueous solution, the rate of aggregation is modified by the presence of cations but also by other components, such as organic matter (vitamins in F/2 medium and tryptone and yeast extract in LB medium) present in the culture media.

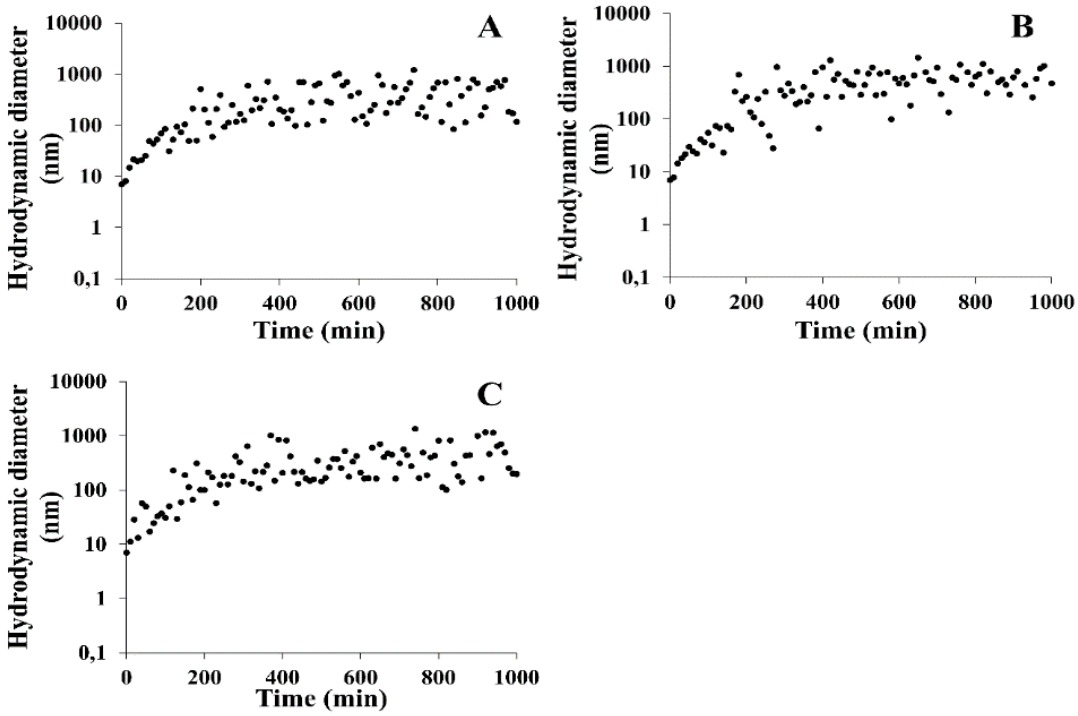

Figure 12: Aggregation kinetics of AgNPs at 93 µgAg.L^{-1} in A) artificial seawater, B) in F/2 media and C) in LB media

Stability or aggregation of AgNPs could be rationalized, in first approximation, by the Derjaguin, Landau, Verwey and Overbeek (DLVO) theory (Petosa *et al.,* 2010). Stability is controlled by attractive and repulsive interactions. Attractive interactions are van der Waals forces and repulsive interactions are governed by the electrical double layer (Petosa *et al.,* 2010). When repulsive interactions are greater than attractive interactions, the conditions are unfavorable for aggregation, but when repulsive interactions are equal or lower than attractive forces, the aggregation is promoted. The transition between these two steps is characterized by the critical coagulation concentration (CCC). For AgNPs coated with citrate, the CCC was generally close to 50 mM for NaCl and near 2 mM for divalent cations (Huynh and Chen, 2011) present in $CaCl_2$ or $MgCl_2$ solution. In this study, the pH solution was near 7 and the salt concentrations were greater than the CCC, thus aggregation occurs.

In nanopure water, the citrate moieties of AgNPs were negatively charged. This promotes the electrostatic repulsions between AgNPs, thus avoiding the aggregation of AgNPs (El Badawy *et al.,* 2010; Petosa *et al.,* 2010). Moreover, the aggregate size distribution has increased the ionic strength of the solution decreasing the thickness of the electrical double layer around the silver nanoparticles. This has enhanced the close encounter of AgNPs and therefore the aggregation. However, the aggregate size distribution also affected the charges at the surface of AgNPs. Citrate moieties were negatively charged and can interact with cations. Interactions between citrate and cations decreased the negative charges of AgNPs and lowered the electrostatic repulsion between particles (El Badawy *et al.,* 2010; Petosa *et al.,* 2010). These phenomena enhanced the aggregation of AgNPs (Zhang *et al.,* 2009) and can explain the behavior of AgNPs in nanopure water and salt solutions. Another process that could contribute to the aggregation was the presence of multivalent cations. Those cations could form a bridge between two adjacent AgNPs facilitating the aggregation of nanoparticles (El Badawy *et al.,* 2010). The difference observed in the rapid increase in D_h of AgNPs in presence of NaCl and $CaCl_2$ or $MgCl_2$ could be explained by this process.

In complex media such as ASW, F/2 or LB, the aggregation rate was lower than in salt solutions. Jin *et al.* (2010) have discussed the effects of synthetic freshwater composition on aggregation and dissolution of AgNPs. When freshwater contained the same salts as those in ASW, the aggregation of AgNPs was modified. This modification was caused by the reaction of Ag^+, released from AgNPs, with anions like Cl^- or HCO_3^-. The salts formed during the reaction were insoluble and could interact with the surface of AgNPs to create a new coating (Levard *et al.,* 2012). With this new coating, the toxicity of nanoparticles could be different than the toxicity of the native nanoparticles.

In F/2 medium, the trace element concentration could be too low to affect AgNPs aggregation. The behavior of AgNPs in F/2 medium was controlled by the most important cation, Na^+, in this culture broth. The anions, such as Cl^- and HCO_3^-, can precipitate with

silver ions around the AgNPs as described for ASW. The LB medium has a concentration in NaCl near 171 mM, higher than the CCC. However, the presence of organic matter (NOM), like tryptone and yeast extract, could affect the aggregation of AgNPs by increasing the CCC. The addition of NOM could create a new coating on AgNPs (Huynh and Chen, 2011). This new coating would modify the interactions between AgNPs, NOM and ions in solution thereby producing a new equilibrium characterized by a decrease of AgNPs aggregation rate. This hypothesis could explain the difference in the time evolution of AgNPs size observed in this study.

As shown in Figure 11 and Figure 12, aggregation of nanoparticles is a common phenomenon in complex aqueous environments. The rapid changes in size observed during the first hours of our experiments are related to the charge of the cations, the presence of NOM in the culture media, the nature of nanoparticles and the contact time between nanoparticles and the surrounding solution. A steady state in the size of the aggregates has been observed after different time periods, from 50 min in solution of divalent cations to about 200-250 min in culture broth F/2 or LB. In the steady state, for ASW, LB and F/2 respectively, the D_h of the aggregates increased by 46, 57 and 70 folds compared to the nominal D_h of AgNPs. This can have a strong incidence on the toxicity. For instance, the increase in D_h in F/2 medium decreased the number of nanoparticles by about 10 000 between the beginning and the end of the experiment. Such variations in particle numbers, in size and in the time period where aggregation occurs can lead to misrepresentative results or interpretations if toxicological assays are discussed without an in-depth description of conditions used in experiments. The time between the addition of nanoparticles to culture media and the duration of the toxicological assay should be clearly mentioned in the materials and methods of any nanotoxicological study.

2.6 CONCLUSION

Aggregation of AgNPs could have effects on microalgae and bacterial growth and as a consequence modulates the AgNPs toxicity. The growth of these organisms was characterized by four steps: lag phase, exponential phase, stationary phase and decline or death phase. Aggregation of AgNPs could extend the lag phase or decrease growth rate of cultured microorganisms since they need to adapt to the evolution of AgNPs size and particle numbers in solution. During the rapid increase of D_h of AgNPs, the culture media are in constant evolution. This could increase the lag phase as observed in some studies (Doiron *et al.,* 2014, 2012). During aggregation, the toxicity mechanism could change. The small aggregates of AgNPs could penetrate in the cell and produce ROS inside the cell. When the aggregates become larger, they cannot penetrate the cell but can interact with their surfaces and alter membrane permeability and protein functions. The decrease of particle concentration can also modify the response of organisms exposed to AgNPs. Depending on the aggregation state of the AgNPs suspension, toxicity of AgNPs could be different. This study demonstrates that characterizing the behavior of AgNPs in the toxicity assay media is essential to better understand the real effects of AgNPs toward microorganisms.

2.7 ACKNOWLEDGMENTS

This work was supported by Strategic Project Grants of the National Sciences Engineering Research Council of Canada (Émilien Pelletier and Jean-Pierre Gagné), Discovery Project Grants of the National Sciences Engineering Research Council of Canada (Jean-Pierre Gagné) and Québec-Océan for its financial support.

CHAPITRE 3
EFFETS DE LA CONCENTRATION ET DE LA COMPOSITION CHIMIQUE DE LA MATIÈRE ORGANIQUE NATURELLE SUR LE COMPORTEMENT AGRÉGATIF DES NANOPARTICULES D'ARGENT

3.1 RÉSUMÉ

Le but de cette étude est de caractériser le comportement agrégatif des nanoparticules d'argent (AgNPs) en situation proche des conditions environnementales en présence de différentes fractions de matière organique naturelle (NOM). Des cinétiques d'agrégation des AgNPs à 10 µgAg.L^{-1} ont été effectuées à dix concentrations de NaCl pendant 2 h avec 2.5 ou 25 mgNOM.L^{-1}. Quatre fractions de la NOM, les acides fulviques (SLFA), les acides humiques (SLHA), des extraits hydrophiles (SL4ILE) et des extraits hydrophobes (SL4OBE), ont été étudiées suite à leurs extractions de 50 m^3 d'eau de l'estuaire du Saint-Laurent. Dans l'eau nanopure sans NOM, le diamètre hydrodynamique (D_h) des AgNPs est stable dans le temps. L'addition de NOM produit une légère augmentation de la taille des AgNPs selon la concentration en NOM et selon la fraction étudiée. Cette augmentation de taille est attribuée à la sorption de NOM autour des AgNPs. Cela induit une évolution des forces impliquées dans l'agrégation, par addition d'effets stériques et d'interactions hydrophobes. La présence simultanée de sel et de NOM génère une agrégation qui altère significativement la taille des AgNPs. À 2.5 mgNOM.L^{-1}, plus de 90% des particules analysées ont une taille inférieure à 200 nm, quelle que soit la fraction de NOM utilisée. À 25 mgNOM.L^{-1}, la distribution de la taille des particules est fortement influencée par la nature de la NOM (fraction). En présence de SLFA et SLHA, plus de 99% des particules ont une taille supérieure à 200 nm. En présence de SL4ILE et SL4OBE, la population de particules inférieure à 200 nm est plus importante, elle représente près de 80% des particules. Cette étude a mis en évidence l'importance de la teneur en carbones aliphatiques non-polaires et aromatiques, qui sont impliqués dans les effets hydrophobes, sur la

distribution de la taille des agrégats. La NOM avec une forte teneur en carbones aromatiques comme SLFA et SLHA favorise les agrégats supérieurs à 200 nm. Une teneur élevée en carbones aliphatiques non-polaires, comme observée dans SL4ILE et SL4OBE, a un effet stabilisant favorisant la présence d'agrégats de petite taille. Le soufre, présent en faible proportion dans la NOM, semble aussi intervenir dans l'agrégation des nanoparticules d'argent dans l'eau salée.

Ce troisième article, intitulé « *Effects of concentration and chemical composition of natural organic matter on aggregative behavior of silver nanoparticles* », fut corédigé par moi-même ainsi que par la docteure Kim Doiron, par le professeur Émilien Pelletier et par le professeur Jean-Pierre Gagné. En tant que premier auteur, ma contribution à ce travail fut d'effectuer une recherche bibliographique poussée, les analyses de laboratoire, le traitement des données, à la rédaction et à la correction de l'article. Les professeurs Émilien Pelletier et Jean-Pierre Gagné ont fourni l'idée originale et ont participé au traitement des données et à la rédaction de l'article. La docteure Kim Doiron a aidé au traitement statistique des données et à la révision de l'article. Une version abrégée de cet article a été présentée aux conférences *International Humic Substances Society* à Kanazawa (Japon) et à *Québec-Océan* à Rimouski (Québec) en automne 2016.

EFFECTS OF CONCENTRATION AND CHEMICAL COMPOSITION OF NATURAL ORGANIC MATTER ON AGGREGATIVE BEHAVIOR OF SILVER NANOPARTICLES

3.2 ABSTRACT

The aim of this study was to characterize the aggregative behavior of silver nanoparticles (AgNPs) at level near environmental concentration and their interactions in presence of different fractions of natural organic matter (NOM). Aggregation kinetics of AgNPs at 10 µgAg.L^{-1} were conducted at ten NaCl concentrations during 2 h with 2.5 or 25 mgNOM.L^{-1}. Four NOM fractions: fulvic acids (SLFA), humic acids (SLHA), hydrophilic (SL4ILE) and hydrophobic (SL4OBE), were extracted from 50 m^3 of estuarine water sampled in St.-Lawrence Estuary. In nanopure water without NOM, the hydrodynamic diameter (D_h) of AgNPs remained stable with time at an average size of 20 nm. Addition of NOM to aqueous AgNPs dispersion produced only a small increase in AgNPs size depending on NOM concentration and fraction used. These rises are explained by the sorption of NOM around AgNPs, inducing an evolution of forces involved in aggregation by adding steric effects and hydrophobic interactions. The simultaneous presence of salt and NOM altered significantly the size of AgNPs with time. With 2.5 mgNOM.L^{-1}, more than 90% of particles analyzed have a size smaller than 200 nm whatever the NOM fraction used. At 25 mgNOM.L^{-1}, the particle size distribution was strongly affected by the nature of the NOM fraction. With SLFA and SLHA more than 99% of particles were higher than 200 nm. In presence of SL4ILE and SL4OBE, the particle population being less than 200 nm was more important, and accounted near 80% of particles. This study highlighted the importance of the nature of NOM and the content in non-polar aliphatic and aromatic carbons, involved in hydrophobic effects, on the aggregate size distribution. NOM with highly aromatic carbons content as SLFA and SLHA promoted the formation of largest aggregates. A high content in non-polar aliphatic carbon as observed in SL4ILE and SL4OBE, stabilized aggregates at smaller size. Sulfur, present in a small proportion in the NOM, also appears to be involved in the aggregation of silver nanoparticles in salty water.

Keywords: Citrate-coated silver nanoparticles, aggregation, natural organic matter, chemical composition and concentration effects, particle size distribution of aggregates, estuaries.

3.3 INTRODUCTION

The development of nanotechnology is a dynamic sector in expansion with an economic potential of several billion dollars (Nanotechproject, 2017; OECD, 2011). Silver nanoparticles (AgNPs) are found in more than 440 consumer products as food packaging materials, toothpaste, cosmetics and medical devices, air and water purification, outdoor paints, nanotextiles and goods for children (Nanotechproject, 2017; Wijnhoven *et al.,* 2009; Yetisen *et al.,* 2016). Many studies (Benn and Westerhoff, 2008; Geranio *et al.,* 2009; Kaegi *et al.,* 2010; Yetisen *et al.,* 2016) have shown the high potential of AgNPs release in aquatic environments during washing cycles or rain runoff events. Leached nanomaterials could be exported from rivers to oceans with a passage in dynamic estuarine systems where transient physicochemical conditions of water masses evolved quickly in salt and organic matter contents.

In natural aquatic environment, engineered nanoparticles fate and AgNPs behavior are complex (Dwivedi *et al.,* 2015; Osterheld *et al.,* 2018). Processes affecting AgNPs are (1) aggregation influenced by salts composition and concentration (Huynh and Chen, 2011; Millour *et al.,* 2015, 2013); (2) dissolution governed by oxidation (Liu and Hurt, 2010); and/or (3) oxysulfidation or sulfidation which is depending on the dioxygen and sulfur levels (Levard *et al.,* 2011; Liu *et al.,* 2011). However, these transformations are influenced by the presence of inorganic salts and organic compounds. Natural organic matter (NOM) is a complex assemblage of ill-defined molecules that can sorb on AgNPs surface to create a new overlay. The presence of NOM overlay could modify the aggregation behavior and stability of AgNPs. Moreover, this process can limit the transformations of AgNPs (Gunsolus *et al.,* 2015; Liu and Hurt, 2010). Furthermore, NOM in solution can interact directly with silver ions released from native nanomaterials to form new AgNPs (Akaighe *et al.,* 2011). In presence of NOM, autoaggregation of AgNPs decreases (Baalousha *et al.,* 2013; Chen and Zhang, 2012; Gunsolus *et al.,* 2015; Huynh and Chen, 2011), but promotes

heteroaggregation in presence of multivalent cations (Huynh and Chen, 2011; Quik *et al.,* 2014). The toxicity of AgNPs is also modulated in presence of NOM as observed for bacteria (Doiron *et al.,* 2014; Fabrega *et al.,* 2009), microalgae (Navarro *et al.,* 2008b) and zooplankton (Gao *et al.,* 2012; Seitz *et al.,* 2015).

In pristine natural waters, wastewaters, industrial waters or inside biological cells, NOM is ubiquitous. Humic substances represent 50 to 80% of dissolved organic carbon in freshwater, 15 to 50% in estuarine waters and 10 to 30% in seawater (Thurman, 1985; Tremblay and Gagné, 2009). Interactions between NOM and AgNPs, in aqueous environment, are mostly studied with humic substances and more specifically with humic acids (Chen and Zhang, 2012; Doiron *et al.,* 2014; Huynh and Chen, 2011; Kim and Ryu, 2013; Philippe and Schaumann, 2014; Sani-Kast *et al.,* 2017; Wang *et al.,* 2016). However, humic acids are not the dominant substances in natural waters. Fulvic acids are often 2 to 5 folds more concentrated than humic acids in freshwater (Thurman, 1985) and 2 to 10 times in estuaries (Tremblay and Gagné, 2009). The effects of other NOM types on the behavior of nanoparticles are still limited and suffered from a lack of knowledge.

NOM presents a large molecular weight distribution and a wide range of polarity. Different approaches are used to recover different types of NOM from fresh and marine waters. NOM can be isolated and concentrated by membrane filtration (ultrafiltration or reverse osmosis/electrically assisted dialysis) or by continuous liquid-solid extraction (chromatography). Each technique has their own advantages and drawbacks. Membrane filtration separates molecules by size/molecular weight while chromatography can extract compounds or families of compounds with specific chemical moieties and polarities. To study the interactions between NOM and nanomaterials it is better to use NOM extracts obtained by chromatographic methods because chromatographic separations limit the molecular weight distribution and allow to recover different families of compounds in discrete fractions. The use of chromatographic resins in tandem, DAX-8 and XAD-4, allows to extract more than 80% of dissolved organic carbon from lakes (Boerschke *et al.,* 1996; Malcolm and MacCarthy, 1992).

Studies on effects of NOM on AgNPs aggregation were often conducted at high and unrealistic environmental AgNPs concentrations, between 1 and 100 $mgAg.L^{-1}$ (Chen and

Zhang, 2012; Delay *et al.,* 2011; Gunsolus *et al.,* 2015; Huynh and Chen, 2011; Li *et al.,* 2012). Estimations of environmental concentrations of AgNPs were between hundred ngAg.L^{-1} to few µgAg.L^{-1} in waters (Coll *et al.,* 2016; Gottschalk *et al.,* 2013; Keller and Lazareva, 2014; McGillicuddy *et al.,* 2017). Our previous work has shown strong effects of AgNPs concentrations on aggregate size distribution (Chapter 1 p35). At low 10 and 100 µgAg.L^{-1} content, particles smaller than 200 nm are dominant, but not at mgAg.L^{-1} levels. To our knowledge no study yet has described the effects of estuarine NOM concentration and chemical composition on AgNPs aggregation and aggregate size distribution.

The aim of this study was to determine the influence of concentration and chemical composition of estuarine NOM fractions on the size distribution of silver aggregates at low AgNPs concentration, 10 µgAg.L^{-1}. Specific objectives were to study effects of NOM concentration and chemical composition on: (1) AgNPs properties such as zeta potential and hydrodynamic diameter in nanopure water; (2) on the AgNPs aggregative behavior; and (3) on the size distribution of silver aggregates. To reach these specific objectives, NOM from St.-Lawrence Estuary was extracted and aggregation kinetics of AgNPs were studied at 10 µgAg.L^{-1} during 2 h with 2.5 and 25 mgNOM.L^{-1} of four NOM fractions at different NaCl concentrations.

3.4 MATERIALS AND METHODS

3.4.1 SYNTHESIS OF SILVER NANOPARTICLES

AgNPs were prepared in nanopure water (18.2 MΩ·cm resistivity, NANOpure Infinity, Barnstead) by reduction of silver nitrate (>99%, Sigma-Aldrich) with trisodium citrate (>99%, Sigma-Aldrich) during 3 h under reflux. After the synthesis, AgNPs colloidal solution was purified by filtration on 0.2 µm polycarbonate filter (Whatman), followed by centrifugation to remove impurities and reagents. Concentrations of AgNPs and silver ions were determined by inductively coupled plasma mass spectrometry (ICP-MS). Synthesis and purification of the stock AgNPs solution is fully described in chapter 1 (Annexe I p149). Silver ion concentration in stock solution was below the detection limit of ICP-MS (0.015 µgAg.L^{-1}). The average hydrodynamic diameter (D_h) of AgNPs,

measured by dynamic light scattering (Zetasizer Nano ZS, Malvern) in volume size distribution, was at 20±2 nm.

3.4.2 NATURAL ORGANIC MATTER EXTRACTION AND CHEMICAL CHARACTERIZATION

Natural organic matter was extracted on DAX-8 and XAD-4 resins in tandem from 50 m^3 (50 119 L) of St.-Lawrence Estuary water (Canada) according to Malcolm and MacCarthy (1992) protocol. Extraction was performed from June 4 to August 6, 2012, at Station aquicole de Pointe-au-Père, Rimouski, Canada. This station was continuously supplied with salty water from St.-Lawrence Estuary, pumped at 12 m depth at 1 km of the coast. This estuarine water was passed through a strainer and sandfiltered to remove particles greater than 50 µm. Estuarine water was prefiltered at 3.1 µm (A/D Glass fiber Filter, Pall), then filtered at 0.5 µm (Glass fiber Filter, PreSen, General Electric) and acidified at pH 2 with hydrochloric acid (37.2%, Fisher). All glass filters were burned during 8 h at 450 °C before use. Acidified water was passed through a DAX-8 resin (8 L in 140 mm column diameter) at 1.7 $L.min^{-1}$. A portion of the eluent from DAX-8 resin was transferred to the XAD-4 resin at 200 $mL.min^{-1}$ for more intensive extraction. Humic substances were desorbed from the DAX-8 resin with a 0.1 M NaOH solution. This solution was re-acidified at pH 2 to separate fulvic acids (SLFA, soluble at any pH) from humic acids (SLHA, insoluble at pH 2) by centrifugation. With the XAD-4 resin, two NOM fractions were desorbed. A hydrophilic fraction (SL4ILE) was firstly desorbed from XAD-4 with a 0.1 M NaOH solution. Then, a hydrophobic fraction (SL4OBE) was extracted from dry resin with methanol in soxhlet extractor. SLFA, SLHA and SL4ILE were protonated prior freeze-drying. Fraction SL4OBE was concentrated to obtain a powder with a rotary evaporator under vacuum. A stock solution at 200 $mgNOM.L^{-1}$ of each fraction was prepared in nanopure water, adjusted to pH 7 and was shaken 24 h before use.

The elemental composition of each NOM fraction was determined on an EAS1108 analyzer (Fisons Instruments S.p.A). 2 mg of dry sample was introduced in a tin cup and combusted at 1021 °C under He/O_2 flow, and gazes CO_2, H_2O, N_2 and SO_2 were separated by a chromatographic column and detected by a thermal conductivity detector. With this

system proportions of carbon (C%), hydrogen (H%), nitrogen (N%) and sulfur (S%) were analyzed and oxygen (O%) was estimated according to equation 12:

$$O\% = 100 - (C\% + H\% + N\% + S\%) \quad (12)$$

Samples at 2.5 mgNOM.L^{-1} were prepared in nanopure water for UV-Visible spectroscopy. Analysis was performed with a 1 cm path length quartz cell, scanning wavelength between 700 and 200 nm with a slit at 2 nm and measurements each nanometer. Slope ratio (SR) was calculated from the spectral slope coefficient estimated between 275 and 295 nm divided by the spectral slope coefficient between 350 and 400 nm (Helms *et al.,* 2008). Spectral slopes at 275-295 nm and 350-400 nm were obtained by a linear regression of the neperian logarithm transformed spectra as described by Helms *et al.* (2008).

Nuclear magnetic resonance (NMR) analyzes of NOM were performed in a solid state 400 MHz NMR (Bruker, Avance III HD), in quantitative ^{13}C direct polarization magic angle spinning (DP/MAS). Samples were filed in 4 mm rotor and spinning at 15 kHz to minimize the spinning sideband. The 90° ^{13}C pulse length was 3.3 µs and with a recycle delays of 30 s. Hahn echo, obtained by a pulse at 180°, was used before detection and 2048 scans were performed. Quantitative NMR data were obtained from chemical shifts and peak areas identified for eight regions in the spectrum: non-polar aliphatic carbons as CH_2 and CH_3 (AliC, 0-45 ppm); N-alkyl/OCH_3 (45-65 ppm); HOCH from alcohols, non-anomeric carbohydrates and ethers (65-95 ppm); O-C-O and O-CH-O from anomeric carbohydrates (95-110 ppm); aromatic carbons (AromC, 110-145 ppm); phenolic carbons (PhenolC, 145-160 ppm); carboxylic, amides and esters (CAE, 160-190 ppm) and ketones and aldehydes (Ald/Ket, 190-220 ppm).

3.4.3 ZETA POTENTIAL MEASUREMENTS

Assays have been done to measure Zeta potential (Pζ) for aqueous suspension of bulk silver citrate nanoparticles at 10 µgAg.L^{-1} and for solutions of individual NOM fractions at 2.5 and 25 mgNOM.L^{-1}. At these concentrations signals were unstable and no reproducible results were obtained. Following preliminary tests, Pζ of AgNPs was determined in triplicate at 100 µgAg.L^{-1} in nanopure water in absence and presence of 2.5 and

25 mgNOM.L^{-1}, with a Zetasizer Nano ZS (ZEN 3600, Malvern). The Pζ was measured using a folded capillary cell (DTS 1060, Malvern), with a temperature equilibration time of 180 s at 25 °C. Measurements were performed at 150 V. One measure was obtained by averaging 100 scans, with a delay of 45 s between each measure to limit the Joule heating. No electrode blackening and sample degradation were observed.

3.4.4 SILVER NANOPARTICLES AGGREGATION KINETICS

Aggregation kinetics of AgNPs were conducted in NaCl solutions with 2.5 and 25 mgNOM.L^{-1}, corresponding to carbon concentration ranges of 1.02-1.37 and 10.2-13.7 mgC.L^{-1} depending on the extract of NOM used. Salt solution was prepared by dissolving 17.53 g of NaCl (ACS grade, LabMat) in 500 mL of nanopure water. The pH of the solution was adjusted at pH 7.00±0.05, with NaOH at 0.1 M. Solution was shaken overnight and filtered on 0.2 µm polycarbonate filter (Whatman) to remove impurities. After filtration, this stock solution was diluted with nanopure water and with NOM stock solution to get solutions at 0, 10, 20, 30, 40, 50, 100, 200, 400 and 500 mM NaCl with 2.5 or 25 mgNOM.L^{-1}. These solutions were prepared 24 h before use, to allow NOM's conformation to stabilize. In this study, ionic strength was comprised between 0 and 500 mM and these NaCl concentrations correspond to a salinity range of 0 to 29 PSU which is characteristic of estuarine salinity gradients.

Aggregation kinetics were performed by time resolved dynamics light scattering with Zetasizer Nano ZS. The procedure was to measure the background level with 3 mL of solutions with a temperature equilibration time of 180 s at 25 °C, following by 12 measures of 15 s each. Background was used to determine the particle size distribution of NOM fractions depending on their concentration and salt concentration. After the background recording, AgNPs suspension was rapidly added, with a microsyringe, into the sample cell, to obtain a solution at 10 µgAg.L^{-1}. Then, two hours kinetic studies were performed corresponding to 480 measurements. Each measurement corresponded to particle size data acquisition of 15 s. Under the conditions used, the correlation function intercept was between 0.6 and 1, the range of values recommended by Malvern (Malvern, 2013a, 2010d, 2010a). These data indicate that the light scattered by AgNPs at 10 µgAg.L^{-1} or 0.0927 µM of silver with NOM gave a sufficient signal to allow D_h measurements.

Each measurement included particle sizes distributed in 70 size classes covering 0.3 nm to 10 000 nm (Zetasizer software, version 7.12). This allowed to observe the particle size distribution (PSD) for 15 s at a specific time to see if particles are present in mono or multimodal distribution mode. They also allowed to calculate an averaged hydrodynamic diameter (D_h) for a snapshot time of 15 s. D_h evolution and PSD were determined using the volume size distribution. Volume size distribution can be affected by the refractive index of particles. Then, effects of refractive index on D_h and PSD was investigated with values of AgNPs (0.135), silver oxide (1.02 (Nwanya *et al.,* 2013)), natural organic matter (1.363 (Esfahani *et al.,* 2015)) and default value in Malvern software (1.59). No statistical differences in D_h and PSD were observed at 2.5 mgNOM.L^{-1} and 25 mgNOM.L^{-1} of SLHA using the different refractive indices (Tukey test, $p>0.05$). Statistics were performed with SLHA, because this fraction induced a strong modification of D_h and PSD according to NOM concentration. For these reasons, D_h and PSD were measured in volume distribution, with default value of refractive index proposed in Malvern software.

After addition of AgNPs, kinetic studies shown variations in hydrodynamic diameters (D_h) and are characterized by two time zones in presence of salt and NOM. The first zone showed a rapid change in particle sizes while a second region was characterized by a plateau having steady particle diameters. DLS analysis was used to produce three data sets, a short term averaged hydrodynamic diameter (D_h) for a period of 15 s, a particle size distribution (PSD) and an averaged hydrodynamic diameter ($\bar{D_h}$) observed for a long time period (5 400 and 7 200 s), corresponding to the plateau. From the PSD of 15 s, the software calculates an averaged hydrodynamic diameter, D_h. Because kinetic experiments showed an equilibrium and reached a plateau in sizes after a while, a long-term hydrodynamic diameter average ($\bar{D_h}$) was calculated, and was used to compare sizes of aggregate under different experimental conditions. Examination of PSD showed multimodal distributions of particles. For this reason and to help in data comparison, two other average hydrodynamic diameters were calculated for particle populations observed between 0-200 nm and between 200 and 10 000 nm, for the long time period 5 400 and 7 200 s, named $P_{0\text{-}200}$ and $P_{200\text{-}10\,000}$. The hydrodynamic diameters calculated for these two populations were called $D_{h0\text{-}200}$ and $D_{h200\text{-}10\,000}$, respectively.

All statistics tests used SYSTAT software version 12.0 (Systat Software Inc., Chicago, USA) with α=0.05, and with XLSTAT software (statistical packaging for Microsoft Excel) for the principal component analysis (PCA). The D_h^- and Pζ were done by a two-way ANOVA for testing effects of concentration and fractions of NOM. One-way ANOVA or Kruskal-Wallis were also used for particle size distribution ($P_{0\text{-}200}$, $P_{200\text{-}10\,000}$, $D_{h0\text{-}200}$ and $D_{h200\text{-}10\,000}$). Data normality and distribution were verified by Kolmogorov-Smirnov and Levene test, respectively. The Tukey test was chosen to compare NOM concentration and fraction effects when the probability was significant. For D_h^-, a neperian logarithm transformation was performed to obtain normality. Box plots were made with the data collected between 5 400 and 7 200 s (last 30 min), when the particle size was stable. PCA and linear regression were used to describe the effects of NOM chemical composition on aggregate size distribution.

3.5 RESULTS AND DISCUSSION

3.5.1 ZETA POTENTIAL

In the absence of NOM, the Zeta potential (Pζ) of AgNPs was at -34.4 mV. In presence of NOM, the Pζ decreased between -42.8 mV and -47.6 mV at 2.5 mgNOM.L^{-1} and between -55.6 mV and -62.5 mV at 25 mgNOM.L^{-1} depending on the nature of the organic matter (Table 4). Pζ were significantly different according to NOM concentration ($p<0.001$). Under circumneutral pH, the negative charge of AgNPs results from the presence of citrate anions (pKa_1 3.13; pKa_2 4.76; pKa_3 6.40 (Goldberg *et al.,* 2002)) bound to silver core of AgNPs. Considering the classical Derjaguin–Landau–Verwey–Overbeek (DLVO) theory of colloidal suspension, which is based on equilibrium between repulsive interactions from electric double layer and van der Waals attractive interactions (Derjaguin and Landau, 1941; Elimelech *et al.,* 1998; Petosa *et al.,* 2010; Verwey and Overbeek, 1948), the Pζ of AgNPs at -34.4 mV in nanopure water insures strong electrostatic repulsions between nanoparticles resulting in stable aqueous suspension, where aggregation should be very limited. Colloidal particles with Pζ more negatively than -30 mV are generally considered highly stable (Bhattacharjee, 2016; Malvern, 2013a; Xu, 2001a). However, the addition of NOM to AgNPs changed the Pζ to more negative values.

This indicates that NOM, a polyelectrolyte substrate negatively charged in natural waters (Philippe and Schaumann, 2014; Thurman, 1985), instead to be repulsed by the negative environment surrounding AgNPs, interact with these particles to produce a more negative potential. Interactions are stronger if more NOM was added to water, Pζ reached more negative values at higher NOM concentration. The negative charges can result from 1) more carboxylic citrate groups ionized in presence of NOM; 2) by the substitution of citrate moieties by NOM ligands rich in negative charges; 3) by selective chemical interactions between chemical moieties of NOM with the surface of the AgNPs causing adsorption and the presence of more negative charges; and 4) by a combination of these processes. If NOM replaces citrate or sorbs on AgNPs surface, the size of the nanoparticles will increase, but Pζ does not allow measuring this process. As discussed in supporting information Figure 28 (Annexe II p155), the higher negative Pζ is well correlated with higher molecular weight at high NOM contents whereas the correlation is weaker at low NOM levels. This suggests that behavior of AgNPs is influenced by electrostatic and van der Waals interactions but also by chemical composition, conformation and molecular weight of NOM in aqueous media.

Table 4: Zeta potential (mV) of silver nanoparticles at 100 µgAg.L^{-1} with 0, 2.5 or 25 mgNOM.L^{-1} (n=3) of SLFA, SLHA, SL4ILE, or SL4OBE

NOM concentration	SLFA mV	SLHA mV	SL4ILE mV	SL4OBE mV
0 mgNOM.L^{-1}	-34.4±0.5	-34.4±0.5	-34.4±0.5	-34.4±0.5
2.5 mgNOM.L^{-1}	-42.8±1.6	-45.8±0.3	-47.6±0.9	-42.8±1.0
25 mgNOM.L^{-1}	-61.4±0.9	-62.5±1.4	-58.7±1. 9	-55.6±0.7

3.5.2 EFFECTS OF NATURAL ORGANIC MATTER CONCENTRATION AND ITS NATURE ON SILVER NANOPARTICLES STABILITY IN NANOPURE WATER

Figure 13 shows the evolution of hydrodynamic diameter (D_h) of AgNPs at 10 µgAg.L^{-1} during 2 h in nanopure water at different concentrations (0, 2.5 and 25 mgNOM.L^{-1}) of SLFA, SLHA, SL4ILE or SL4OBE. In absence of NOM, the D_h of AgNPs remained stable over time (Figure 13), with an average diameter $\bar{D_h}$ at 20±1 nm. In presence of SLFA and SLHA (Figure 13a and Figure 13b), D_h increased in the first 250-

500 s depending on the NOM concentration. After the rise, D_h remained stable with time at 37 nm and 59 nm at 2.5 and 25 mgNOM.L^{-1}, respectively. For SL4ILE and SL4OBE a fast but smaller increase in D_h was observed (Figure 13c and Figure 13d). With 2.5 mgNOM.L^{-1} of SL4ILE and SL4OBE, D_h^- was near 27 nm. At 25 mgNOM.L^{-1}, D_h^- were close to 38 nm. The presence of humic substances extracted by the DAX-8 resin increased the hydrodynamic diameter of AgNPs by 2 to 3 folds depending on the concentration. NOM isolated by XAD-4 resin induced a 1.4 to 2 folds rise in the hydrodynamic diameter of nanoparticles. With SLFA, SLHA and SL4ILE D_h^- were significantly different independently of the NOM concentration used ($p<0.001$). For SL4OBE, D_h^- differenced between 0 and 2.5 mgNOM.L^{-1} ($p<0.001$), but not between 2.5 and 25 mgNOM.L^{-1}.

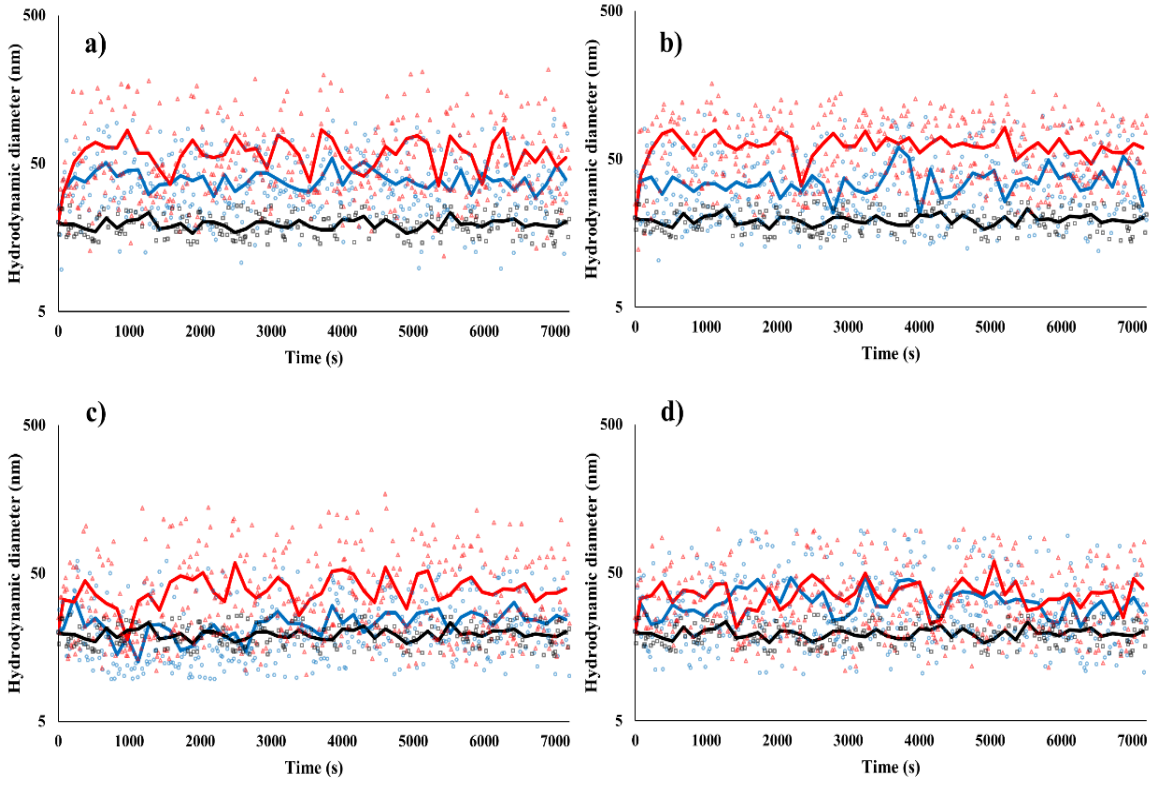

Figure 13: Aggregation kinetics over 2 h for AgNPs at 10 µgAg.L^{-1} with 0 mgNOM.L^{-1} (black) 2.5 mgNOM.L^{-1} (blue) and 25 mgNOM.L^{-1} (red), in nanopure water. a) SLFA, b) SLHA, c) SL4ILE, and d) SL4OBE. Continuous lines were obtained by averaging and smoothing for each time slot of 10 data

Assuming that Pζ measured at 100 µgAg.L^{-1} of AgNPs is representative of Pζ at 10 µgAg.L^{-1}, the highly negative potential measured for nanoparticles, between -34.4 mV and -62.5 mV, should prevent aggregation as predicted by DLVO. However, a measurable increase in size was observed (Figure 13) and depends on the concentration and the nature of NOM. Classical DLVO theory assumes that colloidal particles in interaction are spherical. However, in this study, AgNPs are assumed spherical but this is not the case for the NOM. These compounds bearing different chemical moieties (Mao *et al.,* 2011, 2007) could have irregular shape affecting interactions described in DLVO. For instance, models of humic substances described these compounds as polyelectrolytes of variable molecular weight (Chen and Schnitzer, 1976; Colombo *et al.,* 2015; Hayes and Clapp, 2001); as coiled long-chain molecules which may be slightly cross-linked (Stevenson, 1994) that behave like flexible linear polymers at neutral pH, low ionic strength and low concentration (Conte and Piccolo, 1999); as soft spheroid (Colombo *et al.,* 2015; Duval *et al.,* 2005; Swift, 1989); as micellar association steadied by forces such as hydrogen bonding, π-bonding and charge transfer complexes (Colombo *et al.,* 2015; Wershaw, 1986). Also, Piccolo (2001) suggested that HS are supramolecular aggregates of molecules with low molecular weight, stabilized by weak dispersive forces. The apparent HS supramolecular structure was caused by van der Waals, π- π and CH– π interactions and hydrogen bonds and was modulated by the pH and ionic strength of the medium (Colombo *et al.,* 2015; Piccolo, 2001). Moreover, depending on humic acids or NOM concentration and pH, sponge-like structures, small spheroid disks, aggregates of globular units, chain-like assemblies, perforated sheets, and sponge-like structures have been observed (Balnois *et al.,* 1999; Colombo *et al.,* 2015; Gorham *et al.,* 2007). All these structural characteristics can modulate the aggregation of AgNPs. Recently, researchers have begun to recognize the importance of elongated shape of particles in the colloidal aggregation of humic acids and other substrates (Colombo *et al.,* 2015; Wu *et al.,* 2017).

The change in size of AgNPs in presence of NOM (Figure 13) of different composition and conformation could result from: 1) replacement of citrate ligands by more voluminous NOM ligands at the surface of nanoparticles (Diegoli *et al.,* 2008; Ju-Nam and Lead, 2008; Metreveli *et al.,* 2015); 2) intercalation of NOM between citrate moieties; 3) interactions between NOM and AgNPs surface creating a new overlay with steric

constrain; 4) bridging between AgNPs particles and NOM (NOM is a sorbant); 5) heteroaggregation between AgNPs and NOM colloids; or 6) by a combination of previous processes. We cannot specify which process is responsible for increasing nanoparticle sizes from DLS measurements. However, composition, conformation and molecular weight or dimensions of NOM in interaction with AgNPs are involved.

3.5.3 EFFECTS OF NATURAL ORGANIC MATTER CONCENTRATION AND ITS NATURE ON SILVER NANOPARTICLES STABILITY IN SALTY WATER

Figure 14 present aggregation kinetics of AgNPs in presence of 500 mM NaCl with 0, 2.5 and 25 mgNOM.L^{-1}. Just after the addition of AgNPs and in absence of NOM, D_h was near 20 nm, and increased steadily to stabilize near 100 nm after 3 000 s. The presence of organic matter at 2.5 mgNOM.L^{-1} in salty water induced a small increase in D_h (between 110 and 147 nm) in 3 000 s whatever the NOM fraction used. However, at higher NOM content, AgNPs aggregation with compounds extracted by DAX-8 and XAD-4 resins shown differences. At 25 mgNOM.L^{-1} of SLFA and SLHA, D_h reached steady close to 790 nm and 1500 nm, respectively. At the same concentration of SL4ILE and SL4OBE, D_h attained 110 nm and 215 nm. Statistical analysis indicates that whatever the NOM fraction used, no differences in sizes (D_h^-) were observed between 0 and 2.5 mgNOM.L^{-1} ($p>0.05$). However, for SLFA, SLHA and SL4OBE, D_h^- was significantly different between 2.5 and 25 mgNOM.L^{-1} ($p<0.05$) while for SL4ILE, D_h^- was not different between 2.5 and 25 mgNOM.L^{-1} ($p>0.05$).

In salty water without NOM (Figure 14), AgNPs autoaggregated. According to DLVO theory, this is due to shrinkage of AgNPs double layer thickness at high ionic strength favoring a closer encounter and aggregation of particles. Moreover, interactions of sodium ions with negative charges of citrate moieties of AgNPs also decrease the electrostatic repulsions (Derjaguin and Landau, 1941; Petosa *et al.,* 2010; Verwey and Overbeek, 1948).

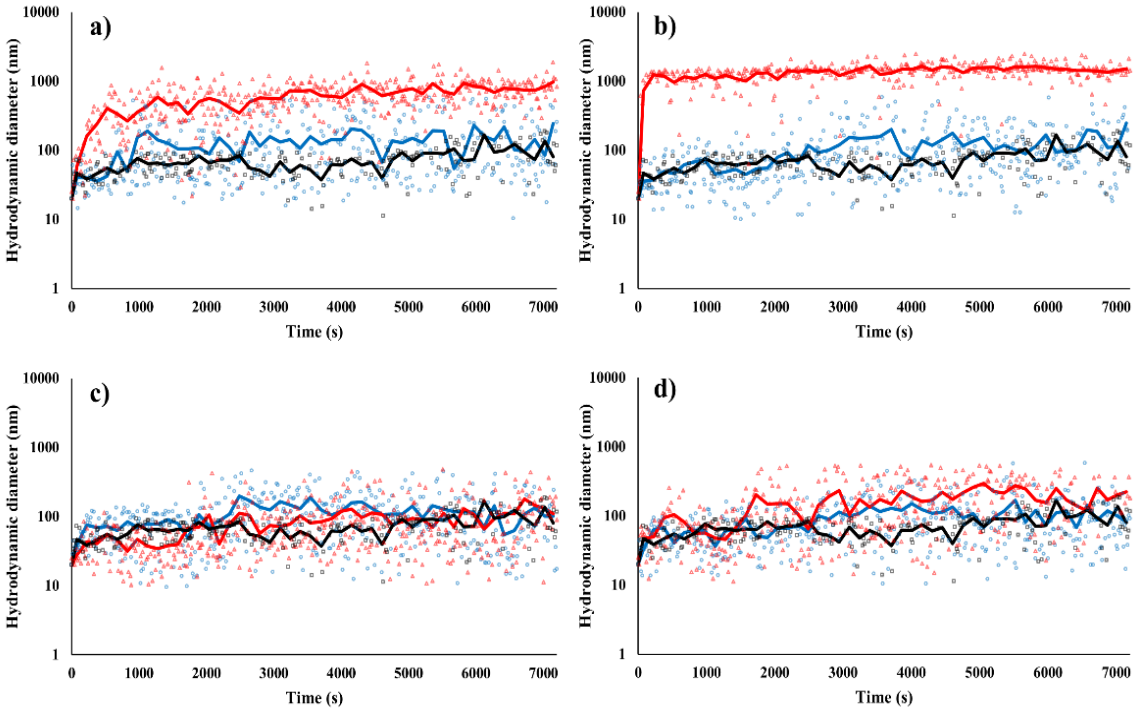

Figure 14: Aggregation kinetics over 2 h for AgNPs at 10 µgAg.L^{-1} with 0 mgNOM.L^{-1} (black) 2.5 mgNOM.L^{-1} (blue) and 25 mgNOM.L^{-1} (red), in 500 mM NaCl solution. a) SLFA, b) SLHA, c) SL4ILE, and d) SL4OBE. Continuous lines were obtained by averaging and smoothing for each time slot of 10 data

Even if salt had strong effects on the stability of AgNPs, the addition of NOM induced a new equilibrium where the stability of AgNPs was altered and the final size of the aggregates are refitted depending on the concentration and nature of NOM. Studies suggest that NOM sorbed or bounded to the surface of nanoparticles can adopt a "mushroom" configuration when NOM interacts at low concentration and extends into a denser "brush" structure at high NOM content (Doane *et al.,* 2012; Louie *et al.,* 2016; Wang *et al.,* 2016). Brush structures could favor steric repulsion. Moreover, at high salt concentration, colloidal humic acids aggregate and produce particles larger than 200 nm in brackish waters (Baalousha *et al.,* 2006). Heteroaggregation of AgNPs with large particles of SLFA or SLHA could explain the larger particle size observed. With SL4ILE and SL4OBE, aggregate sizes were similar or slightly higher compared to lower concentrations. This suggests that SL4ILE and SL4OBE have different chemical composition and conformation that behave differently from humic or fulvic acids in presence of AgNPs. The resulting effect is the formation of small aggregates.

3.5.4 EFFECTS OF NATURAL ORGANIC MATTER CONCENTRATION AND ITS NATURE ON AGGREGATE SIZE DISTRIBUTION

Figure 15 and Figure 16 present hydrodynamic diameters ($D_{h0\text{-}200}$ and $D_{h200\text{-}10\,000}$) and proportions of particle populations ($P_{0\text{-}200}$ and $P_{200\text{-}10\,000}$) of AgNPs in presence of 2.5 or 25 mgNOM.L^{-1} at ten NaCl concentrations observed during the last 30 min (5 400 and 7 200 s) of the 2 h kinetic experiments (data in Table 10 and Table 11, supporting information Annexe II p155). Clear trends were observed for colloidal suspension at 2.5 mgNOM.L^{-1}. A coexistence of two particle populations occurred (Figure 15) whatever the salt concentration or the type of organic matter. In presence of salt, small AgNPs aggregates ($D_{h0\text{-}200}$) were around 45-65 nm while larger particles ($D_{h200\text{-}10\,000}$) were mostly between 400 and 800 nm according to the nature of organic matter (Table 10). The smaller sizes were generally observed at low salt contents for SL4ILE and SL4OBE. But SLHA and SLFA generated the largest aggregates. It is very interesting to note that small particles ($P_{0\text{-}200}$) always form the most important population of particles in suspension. These particles accounted for 78 to 86% of all particles when 2.5 mgNOM.L^{-1} was added in brackish water, while large particles ($P_{200\text{-}10\,000}$) represented less than 22% of particles.

PSD measured at 25 mgNOM.L^{-1} (Figure 16 and Table 11) appeared different from PSD obtained at 2.5 mgNOM.L^{-1} ($p<0.05$). In all cases two particle populations were also observed. However, compounds isolated with DAX-8 and XAD-4 resins showed distinctive behaviors related to the nature or chemical composition of organic matter. For SLFA and SLHA, small aggregates ($D_{h0\text{-}200}$) were mostly present at 133 nm and 171 nm while larger particles ($D_{h200\text{-}10\,000}$) were at 885 nm and 1614 nm (Table 11). At high humic substances content, it is the largest aggregates ($P_{200\text{-}10\,000}$) that control the particle size distribution (Figure 16) with more than 97% of all colloids. With SL4ILE and SL4OBE, the size distribution was significantly different ($p<0.001$). In presence of these NOM fractions, small aggregates $P_{0\text{-}200}$ corresponded to more than 80% of particles with $D_{h0\text{-}200}$ at 54 nm. The remaining particles formed the population $P_{200\text{-}10\,000}$, with size between 400 and 500 nm.

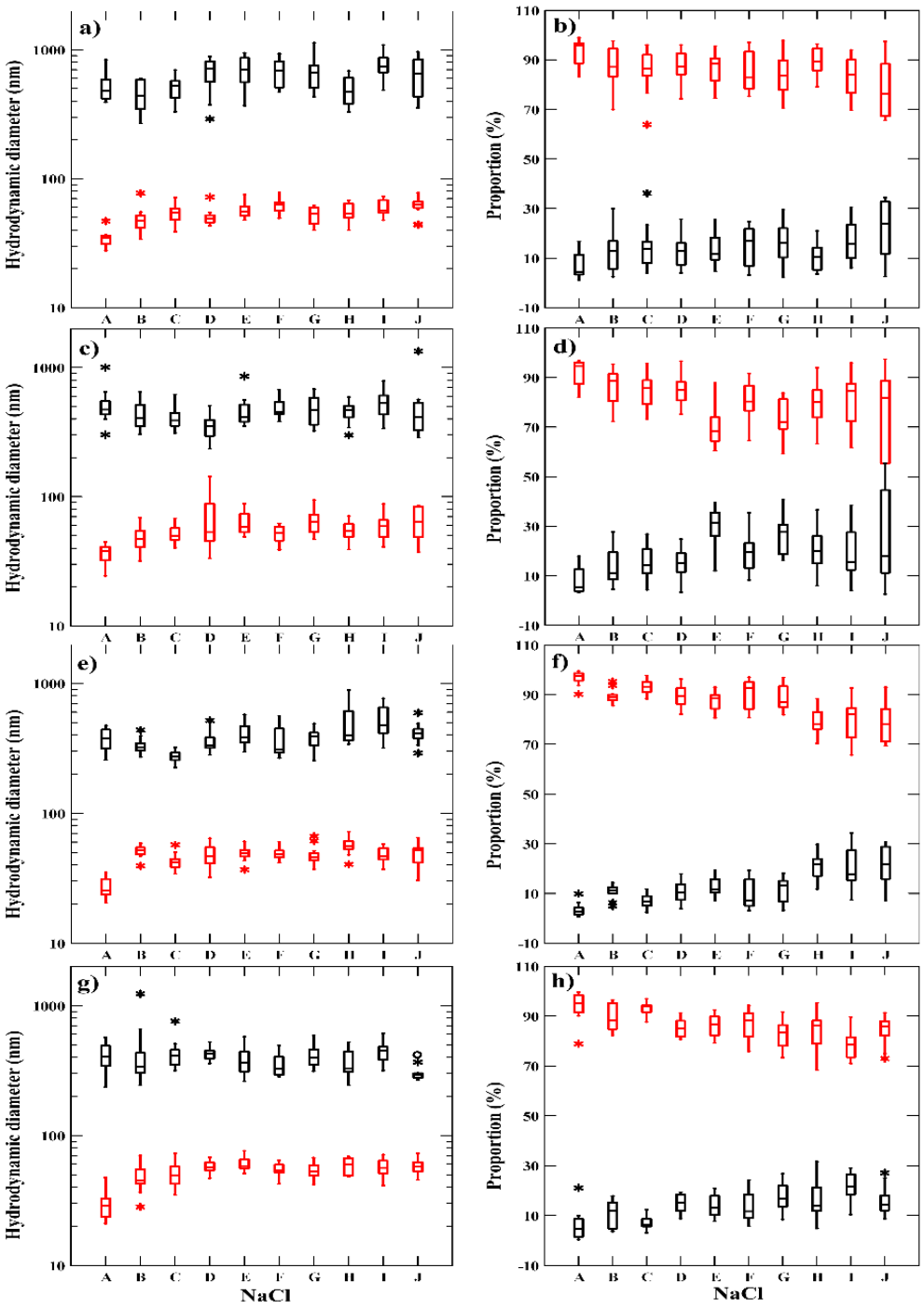

Figure 15: Hydrodynamic diameter and proportion of particle populations with size less than 200 nm (red) and larger than 200 nm (black) observed between 5 400 and 7 200 s (last 30 min) for AgNPs kinetics of 2 h with 2.5 mgNOM.L^{-1} of a and b) SLFA; c and d) SLHA; e and f) SL4ILE; g and h) SL4OBE at different NaCl concentration: A 0 mM ; B 10 mM ; C 20 mM ; D 30 mM ; E 40 mM ; F 50 mM ; G 100 mM ; H 200 mM ; I 400 mM and J 500 mM. The symbol * and ° represent the outside values

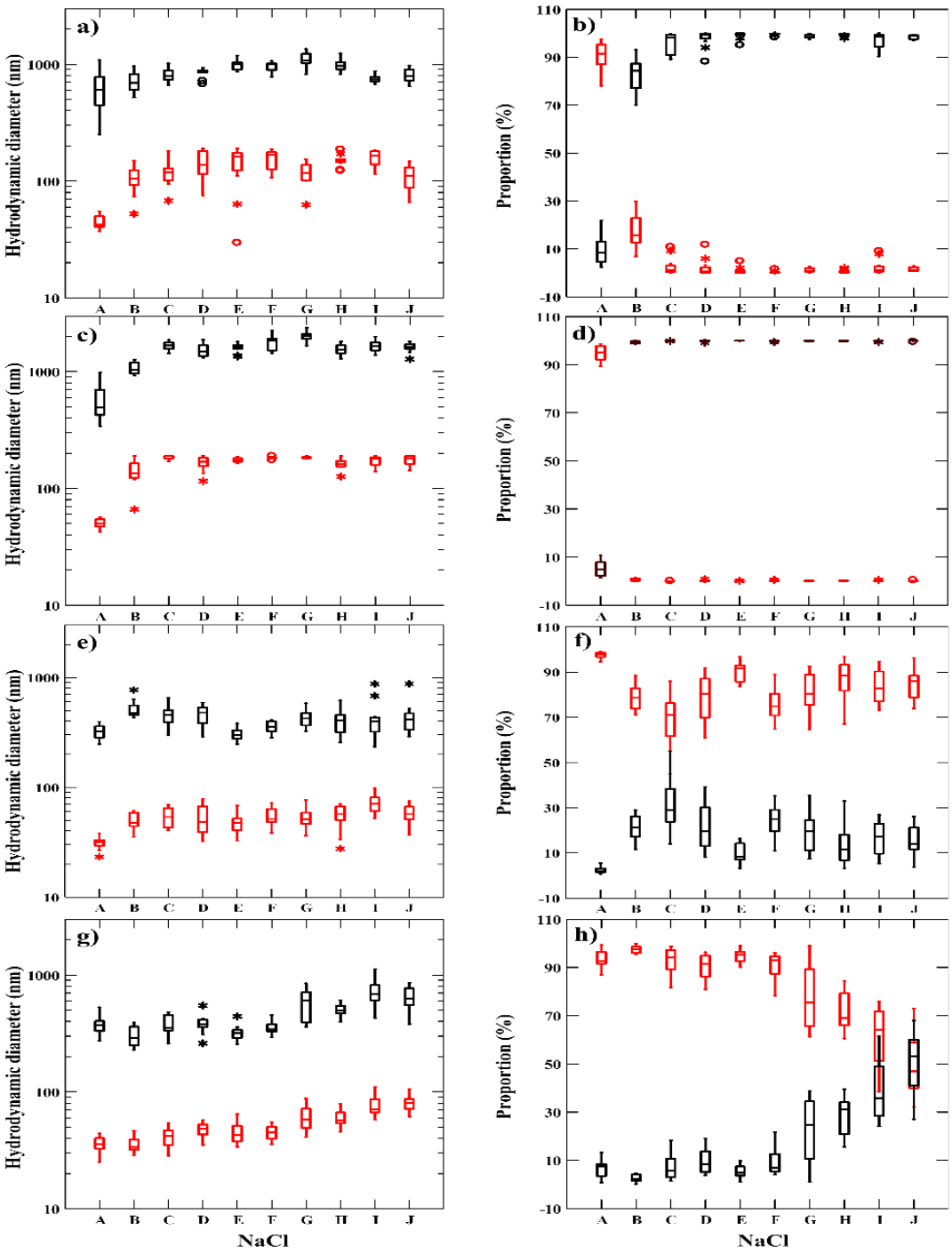

Figure 16: Hydrodynamic diameter and proportion of particle populations with size less than 200 nm (red) and larger than 200 nm (black) observed between 5 400 and 7 200 s (last 30 min) for AgNPs kinetics of 2 h with 25 mgNOM.L^{-1} of a and b) SLFA; c and d) SLHA; e and f) SL4ILE; g and h) SL4OBE at different NaCl concentration: A 0 mM ; B 10 mM ; C 20 mM ; D 30 mM ; E 40 mM ; F 50 mM ; G 100 mM ; H 200 mM ; I 400 mM and J 500 mM. The symbol * and ° represent the outside values

3.5.5 CHEMICAL COMPOSITION OF NATURAL ORGANIC MATTER FRACTIONS AND EFFECTS ON SILVER NANOPARTICLES AGGREGATES

In absence of salt (Figure 13), the size of AgNPs aggregates at 10 µgAg.L^{-1} has increased by 1.2 to 3 folds (from 20 to 60 nm) in presence of different types of NOM and at levels between 2.5 and 25 mgNOM.L^{-1}. In salty solutions (Figure 14), the size increases even more to reach 5-8 folds at 2.5 mgNOM.L^{-1} and can reach near 6, 11, 40 and 75 folds for SL4ILE, SL4OBE, SLFA, SLHA at 25 mgNOM.L^{-1}. These data show that NOM composition and concentration influence more strongly the size evolution of nanoparticles in aqueous media than salt content. However, as shown in Figure 14, the time needed to arrive to final steady size varied with the NOM added. This indicates that the nature of NOM interfere in the aggregation process and play a key role by determining the time required to achieve colloidal stability. Some studies had already reported effects of NOM chemical composition and molecular weight on aggregative behavior of nanoparticles (Deonarine *et al.,* 2011; Gunsolus *et al.,* 2015; Louie *et al.,* 2015; Nason *et al.,* 2012). Moreover, NOM also contributes significantly to fixing the final size of AgNPs-NOM aggregates depending on the nature of NOM.

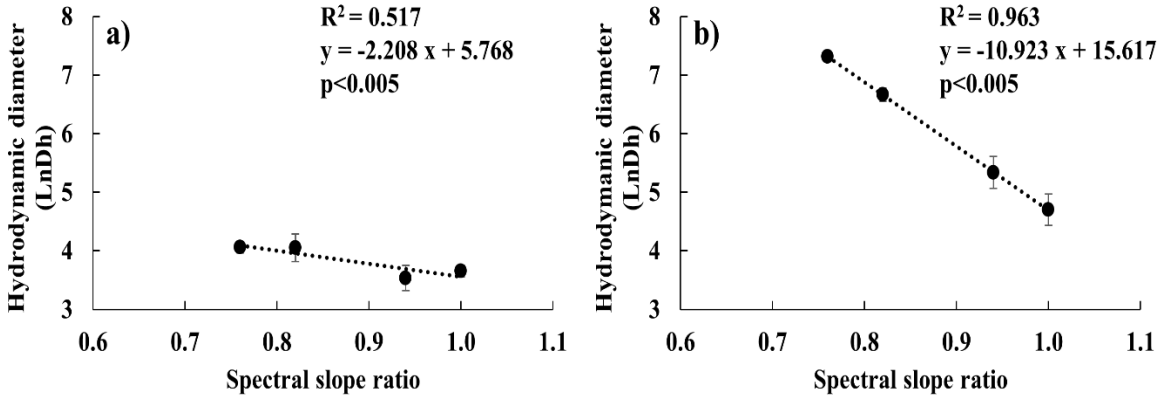

Figure 17: Linear regression between neperian logarithm of average hydrodynamic diameter of AgNPs and slope ratio (SR) a) in nanopure water and b) in salty water at 500 mM NaCl

Slope ratio (SR) calculated from UV-Visible spectra varied from 0.76 for SLHA to 1.00 for SL4ILE (Table 5). Following Helms *et al.* (2008), SR is a proxy inversely

correlated to molecular weight of NOM. In this study, SLHA have the highest molecular weight and SL4ILE the lowest. As shown in Figure 17, an increase in hydrodynamic diameters is linearly correlated to a decrease of SR, manifesting the influence of higher molecular weights. The relationship is lower in nanopure water ($R^2 = 0.517$, $p<0.005$) than in the presence of salt ($R^2 = 0.963$, $p<0.005$). Some studies shown that an increase of molecular weight of NOM tended to decrease the aggregation rate of nanoparticles and in certain cases raise their own stability (Deonarine *et al.,* 2011; Gunsolus *et al.,* 2015; Louie *et al.,* 2015), but the effects of molecular weight on aggregates size are lacking. SR and molecular weights of NOM are generic descriptors of NOM. Evolution of AgNPs size with NOM slope ratio could be explained by (1) formation of NOM layers around AgNPs, adding steric effects, in nanopure water and (2) NOM with higher molecular weight tended to produce larger NOM aggregates in salty water. They do not allow finding the factors responsible for increasing size of aggregates. Differences in chemical composition of NOM could explain the variations observed on PSD. To better understand the NOM properties with the greatest influence the AgNPs-NOM aggregates, the elemental composition was determined and chemical composition of NOM was estimated by NMR.

Elemental composition of NOM extracts differed as observed in Table 5. Carbon content was generally high, more than 50%, but SLFA (41%) differs from other compounds. Oxygen was between 36-41% for SLHA, SL4ILE and SL4OBE, but it reached a high level of 54% in SLFA. Fulvic acids are known to contain high oxygen content as carboxylic moieties (Stevenson, 1994). Hydrogen was between 3.9-4.4% for SLFA, SLHA and SL4ILE, but it reached 6.6% in SL4OBE. This is indicative of a high proportion of non-polar moieties in this extract compared to other NOM. Nitrogen was less than 2% in most of extracts, but SL4OBE was enriched in nitrogen with 5.2%. Sulfur was detected in all fractions at level lower than 1%. SLHA showed the highest content at 0.9%. Sulfur and nitrogen have a high affinity for silver (Gunsolus *et al.,* 2015) and could influence the behavior of nanoparticles in aqueous media if these elements are close enough to interact with AgNPs. Elemental composition of NOM extracts suggests that SLFA, SLHA and SL4OBE have distinctive chemical composition.

Table 5: Slope ratio, elemental and functional groups (%, ^{13}C-NMR) composition of fulvic acids, humic acid, hydrophilic and hydrophobic fractions extracted with XAD-4

		SLFA	SLHA	SL4ILE	SL4OBE
UV-Vis	SR	0.82	0.76	1.00	0.94
Elemental composition	%C	41	55	52	52
	%O	54	38	41	36
	%H	3.9	4.4	4.8	6.6
	%N	0.4	2.1	1.3	5.2
	%S	0.3	0.9	0.5	0.3
NMR (%)	0-45 ppm: CH_2 and CH_3 non-polar aliphatic carbon	32	21	34	40
	45-65 ppm: N-alkyl/OCH_3	8	6	8	12
	65-95 ppm: HOCH alcohols, non-anomerics carbohydrate, ethers	16	15	16	12
	95-110 ppm: O-C-O/O-CH-O anomerics carbohydrate	5	9	8	14
	110-145 ppm: aromatic carbon	14	23	7	6
	145-160 ppm: phenolic carbon	4	8	5	4
	160-190 ppm: carboxylic, amide, ester	17	14	18	10
	190-220 ppm: Ketones, aldehydes	4	4	4	2

Solid-state NMR spectroscopy is very useful to discover the complex chemical composition of NOM (Mao *et al.,* 2017, 2011, 2007) by providing a molecular level description. Table 5 shows quantitative structural variations in NOM extracts used in this study. Important similarities and differences were observed between NOM extracts. Non-polar aliphatic carbon (AliC, 0-45 ppm) was the preeminent chemical group in NOM with more than 30%. One exception was SLHA where aromatic carbon (AromC, 110-145ppm) was slightly more abundant than non-polar aliphatic carbon, but AliC was the second most important moiety. Aromatic carbon was not very important in NOM except for humic substances and especially for SLHA. The non-polar aliphatic structures and the aromatic groups could develop van der Waals interactions if they are close enough together or very close to the AgNPs surfaces. Generally, the second families of structure in importance in NMR spectra were the HOCH group associated to alcohols, non-anomeric carbohydrates and ethers (65-95 ppm) and the carboxylic amide and ester functional groups (CAE, 160-190 ppm) present in the four extracts (10-18%). Carbohydrates are common in NOM (Aluwihare *et al.,* 2002) and have been shown to react with nanoparticles (Sánchez-Cortés *et al.,* 1998). Third important moieties observed in NMR analysis were O-C-O/O-CH-O anomerics carbohydrate (95-110 ppm) and N-alkyl/OCH_3 (45-65 ppm) at 5-9% except for SL4OBE at 12-14%. The OCH_3 groups suggest the presence of lignin residues in NOM. The chemical functionalities observed in the lowest levels were phenolic carbon (PhenolC, 145-160 ppm) at 4-8% and ketones and aldehydes (Ald/Ket, 190-220 ppm) at 2-4%.

In this study, various variables were used (size of aggregates, proportion of small and large aggregates, salt content, NOM content, elemental composition and NMR chemical moieties in NOM types) to understand which properties control the reactivity of AgNPs in presence of NOM and salt. To help the understanding of data sets, non-parametric method was applied to extract relevant information. Principal component analysis (PCA) is a standard tool to reduce a complex data set to reveal hidden, simplified structure that often underlies it

(Shlens, 2014). PCA analyzes were performed on data collected when 25 mgNOM.L^{-1} was present in nanopure water or in brackish water at 500 mM of NaCl as shown in Figure 18.

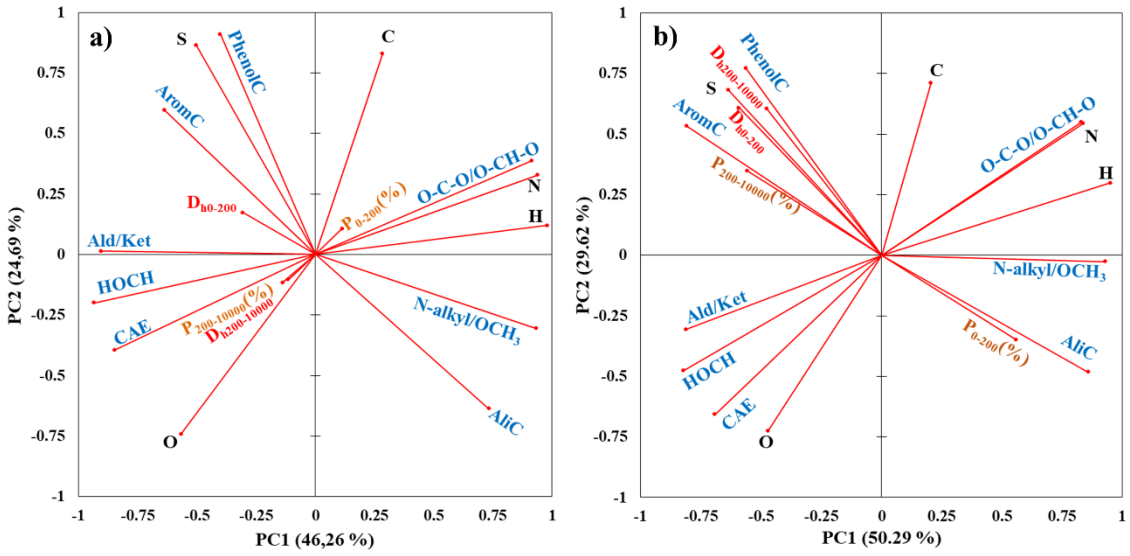

Figure 18: Principal component analysis (PCA) of silver aggregate size distribution (hydrodynamic diameter $D_{h0\text{-}200}$ and $D_{h200\text{-}10\,000}$ in red and proportion $P_{0\text{-}200}$ and $P_{200\text{-}10\,000}$ called $P_{0\text{-}200}$ *(%)* and $P_{200\text{-}10\,000}$ *(%)* in brown) with elemental composition of NOM (black) and functional groups of NOM characterized by 13C NMR (blue), with 25 mgNOM.L^{-1}. a) in nanopure water and b) in salty water at 500 mM NaCl. For ^{13}C NMR results, the eight regions correspond to: (1) AliC: non-polar aliphatic carbons as CH_2 and CH_3 (0-45 ppm); (2) N-alkyl/OCH_3 (45-65 ppm); (3) HOCH from alcohols, non-anomerics carbohydrates and ethers (65-95 ppm); (4) O-C-O/O-CH-O from anomerics carbohydrates (95-110 ppm); (5) AromC: aromatic carbons (110-145 ppm); (6) PhenolC: phenolic carbons (145-160 ppm); (7) CAE: carboxylic, amides and esters (160-190 ppm) and (8) Ald/Ket: aldehydes and ketones (190-220 ppm)

In nanopure water containing 25 mgNOM.L^{-1} and AgNPs, the cumulative explained variance with the first two principal components was near 70.9% of the total variance. The first component contained 46.3% of the variance, whereas the second component explained 24.7% of the variance. As shown in Figure 18a, the first principal component (PC1) is strongly positively correlated with five variables H>N>N-alkyl/OCH_3>O-C-O/O-CH-

O>AliC (Table 12 in supporting information, Annexe II p155) and negatively correlated with three variables HOCH>Ket/Ald>CAE. Sánchez-Cortés *et al.* (1998) has reported interactions of silver nanoparticles with aliphatic, aromatic and phenolic carbons and in a less extend with polysaccharides. The second component (PC2) is positively correlated to PhenolC>S>C and negatively correlated with O>AliC. As shown in Figure 18a, aggregate size and population did not show strong correlation with PC1 or PC2. However, populations have a correlation with a third component, PC3, contributing ~13.5% of the total variance of the system.

When AgNPs was added to salty water (500 mM NaCl), the aggregation behavior changed as discussed previously. Under this condition, the cumulative variance with the first two principal components goes up to 79.9%. The correlation with chemical composition is changed with PC1 (50.3%) strongly correlated with H>N-alkyl/OCH_3> AliC>N>O-C-O/O-CH-O anomeric carbohydrates (Table 12) and negatively correlated with HOCH>Ket/Ald>AromC>CAE. For PC2 (29.6%), the positive correlation is in the order PhenolC>C>S and negatively correlated with O>CAE. Similarly to nanopure water, population has a correlation with a third component, PC3, contributing ~15.5% of the total variance of the system. Figure 18b is very interesting because few vectors were very close to each other indicating a relationship between the variables (Shlens, 2014). Hence, the size $D_{h0\text{-}200}$ is related to the presence of S and $D_{h200\text{-}10\,000}$ is related to PhenolC moieties. Effects of sulfur on AgNPs or other nanomaterials behavior have been recently reported (Gunsolus *et al.,* 2015; Louie *et al.,* 2015). This effect was generally associated with the high affinity of silver for electrons donating groups containing sulfur as thiols (Gunsolus *et al.,* 2015). If S has an effect on aggregate sizes, it seems that other factors control the particle population. The proportion of small aggregate $P_{0\text{-}200}$ is directly related to the presence of AliC and the proportion of large aggregates $P_{200\text{-}10\,000}$ is correlated to the presence of AromC (Figure 18b).

In summary, in salt water, the size of aggregate, see linked to sulfur for small aggregates and to phenolic content of NOM for large assemblies. On the other hand, the

proportion of small aggregates is clearly associated with the presence of aliphatic moieties in NOM and for larger aggregates with the presence of AromC. Such behavior is absent in nanopure water. Hydrophobic moieties influence strongly the aggregative behavior of AgNPs in salty water and depend on the groups involved in hydrophobicity (AliC and AromC). Non-polar aliphatic carbons have higher orientational and conformational degrees than aromatic and phenolic carbons. Presence of hydrophobic linear carbon could produce a volume restriction effect during aggregation, where the NOM adsorbed layer was compressed, resulting in steric hindrances or overlap repulsion (Grasso *et al.,* 2002). This explained the high proportion of aggregates less than 200 nm with SL4ILE and SL4OBE. As phenolic and aromatic carbons are forming more rigid structures, these groups can decrease overlap repulsion. Moreover, the presence of π-bonds can induce charge transfer complexes between electron rich moieties and electron deficient moieties (Gagné *et al.,* 2011), favoring attractive forces. This could explain the largest aggregates observed in presence of humic substances.

3.6 CONCLUSION

To our knowledge, it is the first study describing effects of NOM concentration and fraction on AgNPs aggregative behavior conducted at low AgNPs concentration, 10 µgAg.L^{-1}. Moreover, this study gives new knowledge on the effects of NOM concentration and chemical composition on silver aggregate size distribution. In presence of salt, the NOM concentration changed the aggregation of AgNPs and the particle size distribution of silver aggregates. At 2.5 mgNOM.L^{-1}, more than 90% of particles analyzed had a size smaller than 200 nm. At this concentration, the chemical composition of NOM had no effects on aggregates size. At 25 mgNOM.L^{-1}, the aggregative behavior and chemical composition of NOM affected the aggregate size distribution. This study highlights that the particle size distribution is strongly modulated by the proportion of non-polar aliphatic, aromatic and phenolic carbons, involving in hydrophobic effects, and by the NOM molecular weight. Non-

polar aliphatic carbons, flexible functional groups, promote steric or overlap repulsion resulting in the formation of smaller aggregates (0-200 nm). Otherwise rigid functional groups as aromatic and phenolic carbons produced aggregates larger than 200 nm.

These results are important to understand the behavior of AgNPs in the environment. For example, in river water, where NOM is generally between 20 and 50 mgNOM.L^{-1}, the NOM origin modulates the behavior. With allochthonous NOM, rich in aromatic carbon as humic substances, large aggregates could be formed. With autochthonous NOM, showing a high content of non-polar aliphatic carbon, aggregates smaller than 200 nm tends to be the majority. In seawater, as the NOM concentration is lower, near 2.5 mgNOM.L^{-1}, the NOM origin does not influence the particle size distribution. In these systems, NOM tends to form a high proportion of aggregates with size less than 200 nm.

3.7 ACKNOWLEDGMENTS

This work was supported by Strategic Project Grants of the National Sciences Engineering Research Council of Canada (Émilien Pelletier and Jean-Pierre Gagné), Discovery Project Grants of the National Sciences Engineering Research Council of Canada (Jean-Pierre Gagné) and Québec-Océan for its financial support. The authors are grateful to Isabelle Marcotte and Alexandre Arnold for the NMR facilities, Daniel Bourgault and Dany Dumont for the MATLAB programming and Floriane Le Bihan, Manon Albor, Mathieu Babin and Audrey Tiercin for their technical support.

CHAPITRE 4
COMPORTEMENT DES NANOPARTICULES D'ARGENT DANS DES MÉSOCOSMES ESTUARIENS STRATIFIÉS : DISTRIBUTION DE LA TAILLE DES PARTICULES ET RÔLE DE L'HALOCLINE

4.1 RÉSUMÉ

Cette étude décrit les résultats d'une expérience en mésocosme imitant un estuaire stratifié où une couche d'eau douce de surface est séparée d'une couche d'eau de mer de fond par une halocline bien définie. Cette expérience a été réalisée en ajoutant des nanoparticules d'argent (AgNPs) à 10 µgAg.L^{-1} dans la couche d'eau douce de surface contenant 10 mg.L^{-1} d'argile et 6 mg.L^{-1} de DOC. Une première étude menée sur 12 h montre une agrégation rapide des AgNPs dans chaque couche d'eau avec une taille finale des agrégats différente selon les propriétés physico-chimiques de la couche étudiée. Une étude à long terme, d'une durée de 35 jours, a été menée afin d'observer le devenir des AgNPs dans une colonne d'eau stratifiée. Les concentrations d'argent dissous et de particules (Ag_{dis} et Ag_{part}), définies par filtration à 0.45 µm, montrent une évolution selon la salinité des masses d'eau. La distribution de la taille des particules naturelles est polydisperse et multimodale sur toute la colonne d'eau. Deux populations de particules sont toujours observées entre 0-190 nm et entre 220-5 000 nm. La distribution naturelle des particules dans cette couche d'eau douce est fortement modifiée par l'addition d'AgNPs, montrant une plus grande proportion de petites particules (0-190 nm), contenant des AgNPs d'origine, des AgNPs transformées, des petits agrégats d'AgNPs et des particules naturelles. À l'halocline, les AgNPs s'agrègent avec la matière particulaire en suspension (SPM), la matière organique naturelle (NOM) et/ou les argiles

pour former des hétéroagrégats, ce qui induit une augmentation de l'Ag_{part} par rapport à l'Ag_{dis}. La très faible concentration d'argent mesurée dans la couche d'eau de mer de fond indique que l'halocline a agi comme une frontière de forte densité, limitant la sédimentation des AgNPs. Cette expérience montre que le comportement et le devenir des AgNPs sont des processus très dynamiques fortement influencés par la stratification estuarienne.

Ce quatrième article, intitulé « *Behavior of silver nanoparticles in stratified estuarine mesocosms: Particle size distribution and the role of the halocline* », fut corédigé par moi-même ainsi que par le professeur Émilien Pelletier et par le professeur Jean-Pierre Gagné. En tant que premier auteur, ma contribution à ce travail fut d'effectuer une recherche bibliographique poussée, l'échantillonnage, les analyses de laboratoire, le traitement des données et la rédaction de l'article. Les professeurs Émilien Pelletier et Jean-Pierre Gagné ont fourni l'idée originale et ont participé au traitement des données et à la rédaction de l'article. Une version abrégée de cet article a été présentée aux conférences *Québec-Océan* à Rivière-du-Loup (Québec) en automne 2013, *Gagilau* à Toulouse (France), *Ecobim* à Brest (France) et *Chapitre Saint-Laurent* au printemps 2014, *Society of Environmental Toxiciology and Chemistry (SETAC)* à Vancouver (Canada) en automne 2014, *Ecobim* à Québec (Québec) et *Association Canadienne-Française pour l'Avancement des Sciences (ACFAS)* à Rimouski (Québec) au printemps 2015.

BEHAVIOR OF SILVER NANOPARTICLES IN STRATIFIED ESTUARINE MESOCOSMS: PARTICLE SIZE DISTRIBUTION AND THE ROLE OF THE HALOCLINE

4.2 ABSTRACT

This study describes results of a flow-through mesocosm approach mimicking a stratified estuary where a surface freshwater layer was separated from a bottom seawater layer by a well-defined halocline. Mesocosm experiment was conducted by adding silver nanoparticles (AgNPs) at 10 µgAg.L^{-1} to the surface freshwater layer containing 10 mg.L^{-1} of fine clay particles and 6 mg.L^{-1} of DOC. A first 12 h study showed a fast aggregation of AgNPs, in each water layer, with final size of aggregates depending on physicochemical properties of the studied layer. A long-term study, over 35 days, was then conducted to observe the fate of AgNPs in a stratified water column. Dissolved and particulate silver concentrations (Ag_{dis} and Ag_{part}), defined by filtration at 0.45 µm, showed time evolution depending on salinity of water layers. Natural particle size distribution was polydisperse and multimodal on the whole water column. Two particle populations were always observed between 0-190 nm and between 220-5 000 nm. The natural distribution of particles in this freshwater layer was strongly modified by the addition of AgNPs, showing a higher proportion of small particles (0-190 nm) containing initial, transformed and small aggregates of AgNPs and natural particles. At the halocline, AgNPs aggregated with suspended particulate matter (SPM), natural organic matter (NOM), clay and microorganisms to form heteroaggregates and induced a rise of Ag_{part} compared to Ag_{dis}. Very low concentration of silver were found in the bottom seawater layer indicating that the halocline acted as a strong density frontier limiting the sedimentation of AgNPs. This experiment showed the behavior and fate of AgNPs as a very dynamic process strongly influenced by the estuarine stratification.

Keywords: Silver nanoparticles, aggregative behavior, stratified estuaries, particle size distribution

4.3 INTRODUCTION

A recent market survey showed that silver nanoparticles (AgNPs) have been incorporated in more than 440 consumer products up to now (Nanotechproject, 2017). Most of the applications are in food packaging, odor-resistant textiles, electronics and household appliances, cosmetics and medical devices (Kaegi *et al.,* 2010; Lem *et al.,* 2012; Nanotechproject, 2017; SCENIHR, 2014; Wijnhoven *et al.,* 2009; Yetisen *et al.,* 2016). Studies have shown that silver is released from nanotextiles during washing cycles (Benn and Westerhoff, 2008; Geranio *et al.,* 2009; Yetisen *et al.,* 2016). In 2009, US-EPA and European Commission included AgNPs to the list of contaminants of concern (SCENIHR, 2014; US-EPA, 2009). The use of probabilistic method predicted environmental concentrations of AgNPs between 1 and 10 $ngAg.L^{-1}$ in surface waters and in certain cases near 1 $\mu gAg.L^{-1}$ (Gottschalk *et al.,* 2013; Keller and Lazareva, 2014). However, these estimates may have to be revised as AgNPs are still in a strong phase of development and marketing susceptible to increase the demand, and their expected release in the aquatic environment. Moreover, it was recently observed that AgNPs can be found at high concentrations in the water surface microlayer with an enrichment factor up to 135 times the initial concentration in bulk water (Guo *et al.,* 2016).

The behavior of nanoparticles in the environment is generally controlled by their intrinsic properties and by the characteristics of the receiving environment (SCENIHR, 2014). Complex transformations of AgNPs in aquatic environment include: autoaggregation influenced by composition and concentration in dissolved salts (Baalousha *et al.,* 2013; Huynh and Chen, 2011; Millour *et al.,* 2015); heteroaggregation affected by natural organic matter (NOM) (Baalousha *et al.,* 2013; Millour *et al.,* 2013; Wang *et al.,* 2016) and clay

mineral (Zhou *et al.,* 2012); dissolution by oxidation (Liu and Hurt, 2010); oxysulfidation in oxic systems in presence of sulfur ions (Liu *et al.,* 2011); or sulfidation in anoxic systems (Levard *et al.,* 2012). Additional processes can affect these chemical changes such as the sorption of inorganic/organic compounds onto AgNP surface creating a new overlay. Sorption of NOM is known to modulate dissolution (Liu and Hurt, 2010) and autoaggregation, but can also promote heteroaggregation in presence of divalent cations (Baalousha *et al.,* 2013). A number of studies have been conducted at AgNP concentrations (1 to 100 $mgAg.L^{-1}$) not expected to be found in the natural environment, and could raise questions about the realness of processes found at high silver concentrations when compared to environmentally relevant AgNPs levels as low as 0.01 to 10 $\mu gAg.L^{-1}$.

In natural aquatic systems and particularly in coastal waters, some chemical alterations could deeply modify the fate, transport and toxicity of AgNPs (Fabrega *et al.,* 2011; Lowry *et al.,* 2012b). Direct observations of such phenomena in ocean water are mostly impossible due to field conditions and dilution process. However, large mesocosm setups are powerful experimental tools to elucidate the behavior of nanoparticles by mimicking the physicochemical changes occurring in the environment over time. Mesocosm assays using nanomaterials studied processes such as aggregation, sedimentation, transformation and bioaccumulation in freshwater (Bone *et al.,* 2012; Lowry *et al.,* 2012a; Unrine *et al.,* 2012), salt marshes (Buffet *et al.,* 2014; Cleveland *et al.,* 2012), and estuarine sediments (Bradford *et al.,* 2009; Mühling *et al.,* 2009). Also some biological effects have been observed on pelagic marine microbial communities (Doiron *et al.,* 2012). To our knowledge, no study has yet been conducted to elucidate the behavior and fate of AgNPs at low concentration during their transition through a stratified and dynamic estuarine system. Estuaries are land/ocean transition zones where early developmental stages of many species occur. Embryos, larvae and juveniles of fish, and invertebrates are known to be very sensitive to contaminants (Byrne, 2012; Magesky *et al.,* 2016). Considering that 60% of the world population is living

along coastlines (Bianchi, 2007), the risks of accidental or chronic discharges of AgNPs and other engineered nanoparticles to rivers and estuaries are increasing.

The aim of this study was to investigate the aggregation and dissolution behavior of AgNPs (10 $\mu gAg.L^{-1}$) into a stratified and dynamic estuarine system generated in large mesocosms receiving a continuous flow of freshwater and seawater. Specific objectives were: (1) to determine the natural particle size distribution in the water masses of estuarine mesocosms before adding AgNPs; (2) to study the short-term aggregation kinetics of AgNPs by assessing changes in particle size distribution following the addition of AgNPs during 12 h; (3) to study the long-term behavior of added AgNPs to the particle size distribution over 35 days in estuarine mesocosms, and (4) to examine the role of the halocline layer on the fate of AgNPs.

4.4 MATERIALS AND METHODS

4.4.1 MESOCOSM DESIGN TO MIMIC A STRATIFIED ESTUARINE SYSTEM

The experiments were conducted during 35 days from July 8 to August 11, 2013, at the ISMER-UQAR marine station (Rimouski, Canada) continuously supplied with filtered and dechlorinated drinking water and seawater from St.-Lawrence Estuary. A series of four large mesocosms were used (Figure 19, Table 13 in Annexe III p161).

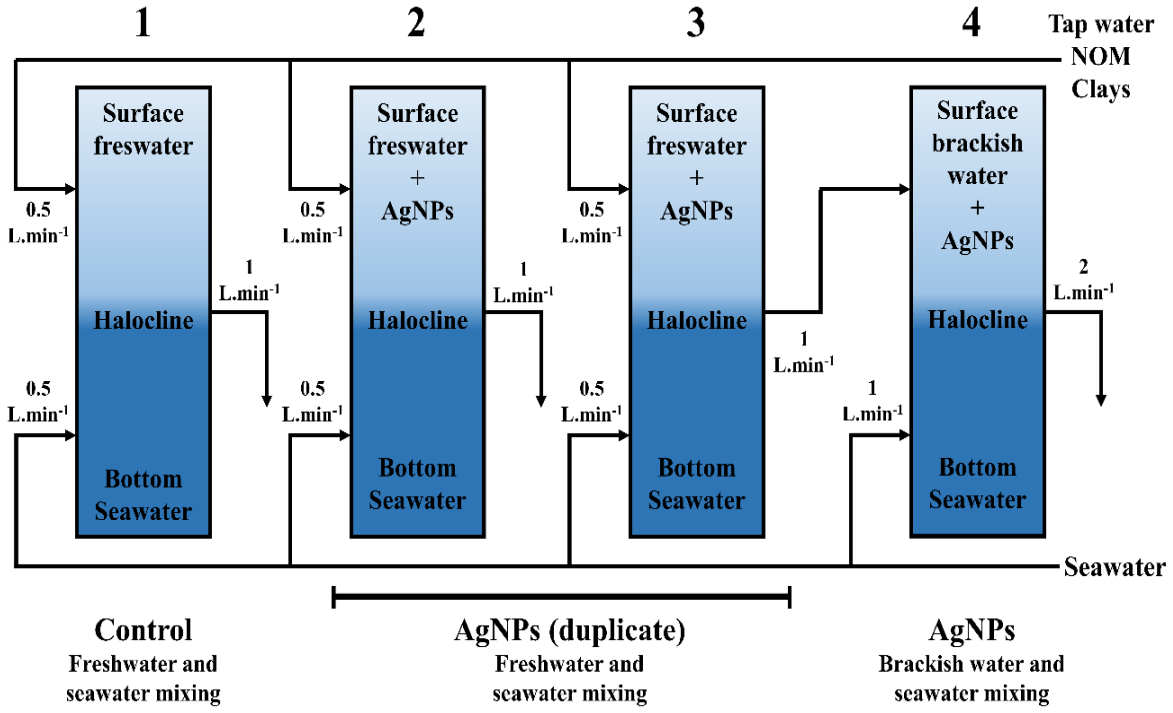

Figure 19: Mesocosms (diameter: 1.45 m; height: 2.1 m; volume: 3.4 m^3) setup using a continuous flow system mimicking interactions between freshwater and seawater for mesocosms 1, 2 and 3 and between brackish water from mesocosm 3 and seawater for mesocosm 4. Mesocosm 1 was the control unit without silver nanoparticles added. Silver nanoparticles (20 nm) were continuously added to the surface of mesocosms 2 and 3, and in mesocosm 4 by the halocline transfer from mesocosm 3. Silver nanoparticles were added at a nominal concentration of 10 µgAg.L^{-1}

In mesocosms 1, 2 and 3, inflow freshwater was introduced at the surface at a rate of 0.5 L.min^{-1}, as well as the seawater at the bottom of mesocosms at the same rate. The outflow pipe was located on the opposite side wall at about 80 cm below the water surface in each mesocosm (outflow rate: 1.0 L.min^{-1}). An air bubbler, supplied by an air pump with a porous stone, was located in the middle of each mesocosm at about 70 cm below the surface and air bubbling was adjusted to provide mixing energy to generate a constant mixing layer of about 10-12 cm thick. This setup produced stratification between surface freshwater layer and

bottom seawater layer separated by a well-defined halocline. Mesocosm 1 was used as the control (without silver addition), and AgNPs were added in mesocosms 2 and 3 which were used as replicates. The salinity profiles observed in mesocosms 1 to 3 were typical of salinity values observed in an estuary mostly influenced by rivers. The brackish water (14-16 PSU) outflow of the mesocosm 3 was transferred to the surface of mesocosm 4 at 1.0 $L.min^{-1}$ and seawater was added at the bottom at the same rate to mimic the mixing of brackish water with bottom seawater which was representative of coastal surface waters with intermediate salinity.

4.4.2 FRESHWATER AND SEAWATER INFLOWS

To obtain a representative natural riverine water with constant properties, municipal drinking water distribution system was used. Tap water was first forced through a dechlorinating system to remove chlorine and organic traces. Then natural dissolved organic matter and fine suspended particulate matter were added. To do so, 50 $mL.min^{-1}$ of natural river water collected near Rimouski with high dissolved organic carbon (DOC) concentration (60±10 $mgDOC.L^{-1}$) were added to tap water inflow (450 $mL.min^{-1}$) leading to a final concentration of 6±1 $mgDOC.L^{-1}$. A stock solution of clay minerals (Swy-2 Na-Montmorillonite, Clay Mineral Society, Colorado) was prepared at a concentration of 10 $g.L^{-1}$ in dechlorinated tap water. This stock solution was mixed continuously to prevent sedimentation. Clay suspension was added to surface layer of mesocosms 1, 2 and 3 at a rate of 0.5 $mL.min^{-1}$. The resulting concentration of clay in the surface freshwater layer was 10 $mg.L^{-1}$ corresponding to 7.7 x 10^6 $particles.mL^{-1}$.

Seawater was pumped continuously at a depth of 12 m in the St.-Lawrence Estuary near the biology station. Seawater was passed through a strainer and sand filtered to remove the particles larger than 50 µm. The salinity was stable between 28 and 30 PSU during the course of the experiment.

4.4.3 ADDITION OF SILVER NANOPARTICLES

Silver nanoparticles were prepared by reducing silver nitrate with citrate, as described in supporting information (Annexe III p161). The hydrodynamic diameter (D_h) of AgNPs, measured by dynamic light scattering (DLS, Zetasizer Nano ZS, Malvern), was observed at an average size of 20±6 nm. This diameter was estimated from volume size distribution (see supporting information Figure 30 to Figure 32, Annexe III p161). This size distribution is less sensitive to the presence of large particles (Anderson *et al.,* 2013). These AgNPs had zeta potential at -34.4±0.5 mV, a surface plasmon resonance peak wavelength at 420 nm and a spheroid shape (Figure 29, Annexe III p161). A stock solution of AgNPs was prepared at 10 mgAg.L^{-1} by diluting the purified solution in nanopure water. This solution, stable for months in dark, was added to the inflow surface freshwater of mesocosms 2 and 3 at a rate of 0.5 mL.min^{-1}. Using a freshwater inflow rate of 0.5 L.min^{-1}, the nominal concentration of AgNPs added to the surface freshwater layer was calculated at 10 µgAg.L^{-1}, corresponding to 2.3 x 10^8 particles.mL^{-1}. The choice of a nominal concentration of 10 µgAg.L^{-1} was motivated by the need to work close to environmental concentrations and the capability of DLS to measure size distribution of AgNPs at low concentrations (Figure 30 and Figure 31).

4.4.4 ANALYSIS OF DISSOLVED AND PARTICULATE SILVER

Silver was analyzed by Inductively Coupled Plasma-Mass Spectrometry (ICP-MS, Agilent 7500C™). Surface water, halocline and bottom seawater layers from each mesocosm were sampled every three days during the 35-day experiment. Water samples, 60 mL, were filtered on 0.45 µm membrane (MF-Millipore® membrane) to obtain particulate silver (Ag_{part}) and dissolved silver (Ag_{dis}) fractions. Particulate silver corresponded to any particles or aggregates with a size larger than 0.45 µm. The dissolved fraction was defined as silver ions, colloidal silver and silver aggregates with a size less than 450 nm. Filtrates were subsampled, 2 mL, for ICP-MS analysis. Samples (filtrates and filters) were digested with 1 mL of HNO_3 (≥ 69%, TraceSELECT, Fluka) and 0.5 mL of H_2O_2 at 30% (TraceSELECT,

Fluka). Then, 1.0 mL of the digestion solution was diluted in 5.0 mL of nanopure water (18.2 MΩ·cm resistivity, NANOpure Infinity, Barnstead) and analyzed by ICP-MS using argon plasma at 7 000 K and with a standard analytical protocol. Calibration curve was obtained from the analysis of nine concentrations, between 0.75 and 200 µgAg.L^{-1}. Detection limit (DL) was determined at 0.015 µgAg.L^{-1} and variation coefficient on 6 replicates was better than 1%.

4.4.5 MEASUREMENT OF HYDRODYNAMIC DIAMETER AND PARTICLE SIZE DISTRIBUTION

Mesocosms were sampled daily at three different depths: 10 cm below the surface; 80 cm in the halocline zone, and 175 cm, in the bottom seawater layer. Before DLS analysis, samples were equilibrated at room temperature, then gently shaken and filtered on 5 µm polycarbonate membrane (GE Osmonics). This step removed large particles such as plankton cells and debris with size larger than the measuring capability of particle size by DLS (0.6 nm to 6 µm, for the Zetasizer Nano ZS). Particle size distribution (PSD) and hydrodynamic diameter (D_h) were measured by DLS in volume size distribution (see supporting information, Annexe III p161), at 25 °C with 120 s of temperature equilibration time and applying backscatter detection at 173°. Due to the presence of different types of particles (AgNPs, clays, NOM, natural particles, natural colloids, microorganisms…), the refractive index used to convert intensity size distribution to volume size distribution was 1.59 (default value in Malvern software), respectively. Effects of refractive index on PSD was investigated with values of AgNPs, clays and default value in Malvern software. According to value of refractive index, weak evolution was observed, but were not significantly different (Tukey test, $p>0.05$). Analysis was performed with 6 measurements with a delay of 5 s between each measurement. One measurement corresponded to 6 scans of 15 s each. PSD of clay and NOM in dechlorinated water was performed at 10 mg.L^{-1} and 6 mgDOC.L^{-1}, respectively to know the size of particles or colloids added in mesocosms. Due to different scattered light

intensities by samples, the laser power was adjusted within acceptable limits. Correction for the count number was done when necessary (high counts number in Figure 30).

In this study, a multimodal PSD was observed and is presented in supporting information (Figure 32 to Figure 34, Annexe III p161). Following these results, a population of small particles was observed for particle sizes between 0 and 190 nm and was called $P_{0\text{-}200}$. Another particle population with sizes mainly between 220 and 1 280 nm was measured in samples and was termed $P_{200\text{-}5\,000}$. For each population, the PSD allowed to calculate an average hydrodynamic diameter called $D_{h0\text{-}200}$ or $D_{h200\text{-}5\,000}$. These averaged diameters were used to study the evolution and fate of nanoparticles and suspended particles in estuarine mesocosms.

4.4.6 SHORT-TERM AGGREGATION KINETICS OF SILVER NANOPARTICLES

Short-term aggregation kinetics of AgNPs added to different water samples were analyzed in time resolved dynamic light scattering (TR-DLS). Three samples were taken from mesocosm 1 at depths mentioned above. A volume of 3 mL of each sample was filtered through 5 µm polycarbonate filter (GE Osmonics). Before the TR-DLS analysis, the samples were stabilized at 25 °C during 240 s. Samples were then analyzed by DLS to determine the size of naturally occurring particles in filtered water. Afterwards, AgNPs were rapidly introduced into the sample cell to obtain a final concentration of 10 $\mu gAg.L^{-1}$. Parameters used for the TR-DLS were one measure each 10 min at an angle of 173°, during 12 h. Each measure was obtained with 10 scans of 15 s. To compare the size of clay and AgNP aggregates, average hydrodynamic diameters and PSD, in volume size distribution, were calculated between 420 and 720 min, corresponding to a time interval where the sizes of aggregates were stable.

4.5 RESULTS AND DISCUSSION

4.5.1 ESTUARINE MESOCOSMS

In this work, an estuarine environment was mimicked with three water masses showing important physicochemical differences in each mesocosm. Figure 20a shows a typical salinity profile obtained in mesocosms 1, 2 and 3 during the course of the experiment. The surface layer (0 to 70 cm depth) showed a very low salinity increasing slightly from 0.6 to 1 PSU, with an average temperature at 15.7±0.7 °C. Between 70 and 80 cm, salinity showed a strong gradient from 1 to 28 PSU. This transition between surface freshwater and bottom seawater represented the halocline layer of the system. Under 80 cm depth, the salinity varied between 28 and 30 PSU due to small variations in seawater supply. In this layer temperature was at 11.6±0.8 °C. In mesocosm 4, the surface water salinity was near 14 PSU (Figure 35, Annexe III p161) and temperature at 14.6±0.5 °C.

This salinity corresponds to brackish water transferred from the mixing layer of mesocosm 3. The salinity profiles observed in this experiment are characteristic of well-stratified estuaries and fjords (Bianchi, 2007). To reproduce at best marine conditions typical of suspended particulate matter (SPM) and DOC concentrations observed in the St.-Lawrence Estuary (D'Anglejan and Ingram, 1976; Hélie and Hillaire-Marcel, 2006; Kranck, 1979; Simons *et al.,* 2010; Tremblay and Gagné, 2009), fine clay particles were added to surface freshwater layer at a concentration of 10 $mg.L^{-1}$ and NOM was measured at 6 $mgDOC.L^{-1}$.

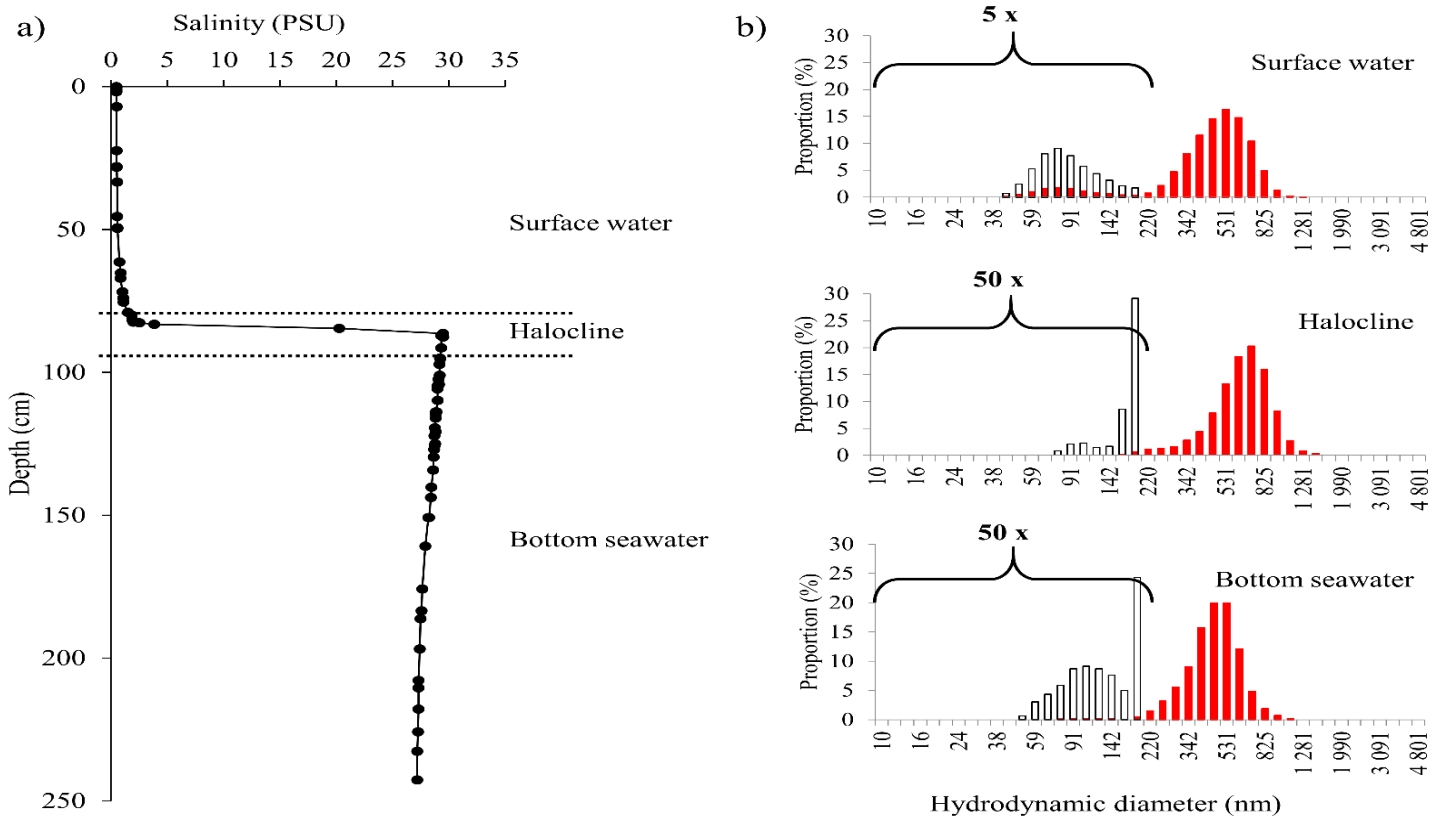

Figure 20: Salinity profile and natural particle size distributions in mesocosm 1. a) Salinity profile b) Particle size distributions obtained over 35 days between 0 and 5 000 nm (red) in freshwater, halocline and bottom seawater layers. The particle size distribution between 0 and 200 nm (black empty) have been magnified to show the presence of small particle populations

4.5.2 DISSOLVED AND PARTICULATE SILVER IN WATER LAYERS

Silver concentrations measured in mesocosms are summarized in Table 6. The control mesocosm 1 contained low levels of Ag_{dis} with concentrations below the detection limit (<0.015 µgAg.L^{-1}), and Ag_{part} were also low, at 0.1 µgAg.L^{-1}. These values correspond to the silver geochemical background specific to St.-Lawrence estuarine waters introduced into mesocosms (Gobeil, 1999; Gobeil *et al.,* 2005). Because mesocosms 2 and 3 were replicated and showed very similar Ag data, only concentrations obtained in mesocosms 3 and 4 are discussed in more details.

In mesocosm 3, Ag_{dis} in surface, halocline and bottom layers were at 3.1, 0.4 µgAg.L^{-1} and below DL, respectively. For Ag_{part}, concentrations reached 1.9 µgAg.L^{-1} in surface and halocline, and 0.1 µgAg.L^{-1} in bottom layer. In the mesocosm 4, Ag_{dis} and Ag_{part} levels were both at 1.0 µgAg.L^{-1} in surface brackish layer. In the halocline, Ag_{dis} and Ag_{part} reached 0.2 µgAg.L^{-1} and 0.7 µgAg.L^{-1}, respectively. The deeper marine layer showed the background silver level of the St.-Lawrence Estuary (Gobeil, 1999; Gobeil *et al.,* 2005). This suggests that the saline stratification, with a density gradient, was effective to limit the transfer of silver from the surface water layer to the deeper marine water layer by acting as a frontier retaining Ag_{dis} and Ag_{part} in surface and haloclines layers. Hydrodynamic processes present in estuarine mesocosms may have played in favor of an exportation of particulate silver before settling even if the renewal time of the freshwater layer was about 40 h which should have left enough time to silver aggregates to settle down and be observed in the seawater layer.

Table 6: Mean concentrations (n=12 by layer for each mesocosm) of dissolved and particulate silver in mesocosms over 35 days

	Mesocosm 1			Mesocosm 2			Mesocosm 3			Mesocosm 4		
	Ag_{dis} µgAg.L^{-1}	Ag_{part} µgAg.L^{-1}	Ag_{part} /Ag_{dis}	Ag_{dis} µgAg.L^{-1}	Ag_{part} µgAg.L^{-1}	Ag_{part} /Ag_{dis}	Ag_{dis} µgAg.L^{-1}	Ag_{part} µgAg.L^{-1}	Ag_{part} /Ag_{dis}	Ag_{dis} µgAg.L^{-1}	Ag_{part} µgAg.L^{-1}	Ag_{part} /Ag_{dis}
Surface water layer	<DL	0.1±0.1	NC	3.5±1.6	2.3±1.2	0.7	3.1±2.1	1.9±0.8	0.6	1.0±0.3	1.0±0.5	1
Halocline layer	<DL	0.1±0.1	NC	0.4±0.3	2.1±0.6	5.2	0.4±0.3	1.9±0.4	4.8	0.2±0.1	0.7±0.4	3.5
Bottom seawater layer	<DL	0.1±0.2	NC	<DL	0.1±0.1	NC	<DL	0.1±0.1	NC	<DL	0.1±0.2	NC

Ag_{dis}: dissolved silver obtained by filtration through 0.45 µm; Ag_{part}: Particulate silver retained by filtration at 0.45 µm; <DL: near-detection limit (0.015 µgAg.L^{-1}); NC: not calculated

Although only 20 nm nanoparticles have been used in mesocosms, it is well known that AgNPs can aggregate when ionic strength is increasing (Baalousha *et al.,* 2013; Huynh and Chen, 2011). AgNPs can also form heteroaggregates of different sizes in presence of SPM, clays or NOM (Lowry *et al.,* 2012b; Unrine *et al.,* 2012; Wang *et al.,* 2015) and sorbed on microorganisms (Bae *et al.,* 2010; Zouzelka *et al.,* 2016). In this case, as Ag_{dis} was defined by the passage through a 450 nm membrane filter, this fraction corresponded to truly dissolved silver (Ag^+ or silver chlorocomplex ($AgCl_n^{(n-1)-}$)) (Lanceleur *et al.,* 2013) and small particles such as original 20 nm AgNPs, transformed AgNPs (Unrine *et al.,* 2012) or small AgNPs aggregates (less than 450 nm). On the opposite, the Ag_{part} fraction corresponded to any form of silver with a size larger than 450 nm which could include: (1) large AgNPs autoaggregates (Unrine *et al.,* 2012); (2) AgNPs heteroaggregated with SPM, clay and/or NOM (Lowry *et al.,* 2012b; Unrine *et al.,* 2012; Wang *et al.,* 2015); and (3) silver ions and silver chlorocomplex in interaction with SPM (Lanceleur *et al.,* 2013), NOM, clay particles and microorganisms.

Calculating Ag_{part}/Ag_{dis} ratios makes it easier to compare fractions in different layers and figure out the aggregation process occurring in mesocosms (Table 6). Mesocosms 2 and 3 showed a very similar behavior as ratios varied from 0.6 to 0.7 in surface layers and from 4.8 to 5.2 in the halocline (Table 6). Small Ag_{part}/Ag_{dis} ratio observed in surface freshwater layer indicated that a large proportion of particles smaller than 450 nm (from 62 to 70%) persisted in this layer for hours (renewal time estimated to 40 h). In the halocline layer, the ratio Ag_{part}/Ag_{dis}, around 5, clearly indicated an enrichment in particles larger than 450 nm (83%). In regard to low Ag_{dis} in halocline (Table 6), the high salt concentration in this layer is promoting the aggregation of small particles (<450 nm) to larger one. The larger particles could result from interactions between many small AgNPs to form large autoaggregates (Millour *et al.,* 2015; Unrine *et al.,* 2012), but also from interactions with large size SPM, NOM clay particles and microorganisms to form heteroaggregates (Lowry *et al.,* 2012b; Unrine *et al.,* 2012; Wang *et al.,* 2015). Moreover, settling (Sempéré and Cauwet, 1995) of

Ag_{part} from the surface layer to the halocline is also contributing to a higher ratio in the halocline.

As the brackish water surface layer of mesocosm 4 was coming from the halocline of mesocosom 3, it was expected that the Ag_{part}/Ag_{dis} ratio should be preserved around 4.8, but that was not the case. The decrease of Ag_{part}/Ag_{dis} to about 1 indicated some change in the dynamic of particulate silver and seems to be the result of an increase of Ag_{dis} combined to a decrease of Ag_{part} (Table 6). The residence time of water in that surface brackish layer was about 20 h which allowed the settling of larger aggregates (reducing Ag_{part}) toward the halocline where Ag_{part}/Ag_{dis} was again relatively high at 3.5. The observed rise of Ag_{dis} could result from (1) a dissolution of Ag_{part} followed by the formation of silver chlorocomplexes under high chloride conditions; (2) a release of silver as Ag^{+} or $AgCl_n^{(n-1)-}$ (Lanceleur *et al.,* 2013) or AgNPs from SPM, NOM, clay and microorganisms. In the Gironde Estuary, a silver release from Ag_{part} to Ag_{dis} was reported when salinity was equal or higher than 15 PSU (Lanceleur *et al.,* 2013). Moreover, the disaggregation (Metreveli *et al.,* 2015) of large AgNPs aggregates to smaller aggregates (<450 nm) could also produce small particles and increase Ag_{dis}.

4.5.3 DISTRIBUTION OF NATURAL PARTICLES IN WATER MASSES BEFORE ADDING AGNPS

In natural systems, the presence of indigenous particles affect the fate of nanoparticles (Klaine *et al.,* 2008; Lowry *et al.,* 2012b). Before adding AgNPs in mesocosms, PSD of natural particles was characterized as their sizes could be in the same range as AgNPs. Furthermore, their characteristics could evolve rapidly with a possible masking effect on the AgNPs behavior. In the control mesocosm 1, the PSD of natural particles changed with salinity (Figure 20b). In the surface freshwater layer, two populations were observed; a first one between 40 and 190 nm and a second one between 220 and 1 280 nm (see supporting information Figure 32 and Figure 33, Annexe III p161). Population $P_{0\text{-}200}$ contributed for

10% of total particles with a $D_{h0\text{-}200}$ of 100 nm (Table 14, Annexe III p161). The second population $P_{200\text{-}5\ 000}$ showed a $D_{h200\text{-}5\ 000}$ at 522 nm accounting for 90% of total particles.

In freshwater and estuarine environments, humic substances (HS) may represent 15 to 80% of dissolved organic matter and 60 to 100% of suspended or particulate organic matter (Thurman, 1985; Tremblay and Gagné, 2009, 2007). According to the proportion of HS in aquatic system and the lack of knowledge about NOM, HS were used as a proxy to describe NOM behavior in this study. Studies have determined that humic acids (HA) and fulvic acids (FA) have hydrodynamic diameters between 1 nm and 5 µm depending on the salt valence and concentration, and the pH of the medium (Baalousha *et al.,* 2006; Esfahani *et al.,* 2015; Hosse and Wilkinson, 2001). At 10 mM NaCl (0.6 PSU), Baalousha *et al.* (2006) using DLS reported HA particle size between 10 and 120 nm. Esfahani *et al.* (2015), for their part, have observed three populations of particles formed from HA or FA with D_h in the ranges of 48-96 nm, 154-636 nm and 4 300-5 400 nm when measured in volume-based distribution. Considering the PSD observed in the surface freshwater layer of the control mesocosm, the particle population $P_{0\text{-}200}$ could correspond to a soluble or colloidal suspension of natural HA and/or FA, but other macromolecular substances or small colloids could also be present. The second population $P_{200\text{-}5\ 000}$ could be referred as FA and HA aggregates (Esfahani *et al.,* 2015). However, SPM particles made from inorganic matter as clay and/or organic matter (Buffle and Leppard, 1995; Esfahani *et al.,* 2015; Tremblay and Gagné, 2009) and small living or dead organisms can also be present. Due to their large sizes, SPM could be transferred to halocline by settling (Sempéré and Cauwet, 1995).

In the halocline layer, the PSD was multimodal as in surface water, but relative proportion of populations was changed (Figure 20b and Table 14). The population $P_{0\text{-}200}$ corresponded to 1% of particles with $D_{h0\text{-}200}$ at 145 nm whereas the second population $P_{200\text{-}5\ 000}$ represented 99% of total measured particles. This population had a range between 220 and 1 280 nm with $D_{h200\text{-}5\ 000}$ at 672 nm. Changes in proportion, size range and D_h of these

two particle populations are suspected of coming from the aggregation of colloidal particles such as HS, clay, HS with clay or from aggregates of various biological tissues and presence of microorganisms (Baalousha *et al.,* 2006; Buffle and Leppard, 1995; Sutton and Sposito, 2006; Tombácz and Szekeres, 2004). HS are considered as molecular aggregates (Piccolo, 2001; Sutton and Sposito, 2005) with hydrophilic (carboxylic and phenolic moieties) and hydrophobic properties (Stevenson, 1994). During this work, the pH in each layer varied between 7.5 and 8.1 which means that carboxylic and phenolic moieties were ionized (Sutton *et al.,* 2005) and could interact with cations (e.g. Na^{+}, Ca^{2+} or Mg^{2+}) (Mantoura *et al.,* 1978). Interactions of HS with cations could decrease electrostatic repulsion promoting the aggregation of HS (Baalousha *et al.,* 2006; Brigante *et al.,* 2007). Baalousha *et al.* (2006) and Esfahani *et al.* (2015), observed many HA and FA aggregates larger than 200 nm. Formation of large HS aggregates could explain the increased contribution of $P_{200\text{-}5\ 000}$. The presence of small HS aggregates could also explain the persistence of $P_{0\text{-}200}$. Furthermore, aggregation of clay could also change the PSD. At mesocosm pH, hydroxyl groups of clay (as Al-OH and Si-OH) were ionized (Tombácz and Szekeres, 2004). Two attraction processes can be involved in the aggregation of clay (Tombácz and Szekeres, 2004). At low salt concentrations, around 50 mM NaCl (2.9 PSU), aggregation of clay minerals are controlled by edge-to-face attraction (Tombácz and Szekeres, 2004). When salt concentration increases, as in the halocline, the aggregation process can change to face-to-face attraction (Tombácz and Szekeres, 2004). The aggregation of clay may also be altered by the presence of HS which interacts strongly with clay (Kretzschmar *et al.,* 1997; Sutton and Sposito, 2006). If aggregation of clay and/or NOM occur, aggregates could settle down (D'Anglejan and Ingram, 1976).

In bottom seawater layer, the multimodal PSD was different from those measured in the halocline layer. Near 2% of particles was observed between 50 and 190 nm with an average $D_{h0\text{-}200}$ at 140 nm. The remaining 98% of particles (220-1 100 nm) had average $D_{h200\text{-}5\ 000}$ at 474 nm. The evolution of PSD observed between the halocline and the bottom

seawater layer could be due to (1) a substitution of cations bonded to HS (Ca^{2+} to Na^{+}) changing the HS conformation and size (Baalousha *et al.,* 2006) by decreasing HS bridging due to Ca^{2+} (Brigante *et al.,* 2007); (2) the compaction of HS aggregates due to high ionic strength (Baalousha *et al.,* 2006; Ghosh and Schnitzer, 1980); (3) evolution of HS solubility depending on the dominant cation of water masses; (4) a change of clay aggregates size due to evolution of the attraction from edge-to-face attraction to face-to-face attraction (Tombácz and Szekeres, 2004); and (5) the presence of natural particles in seawater as HS, natural clay minerals or small living or death organisms.

4.5.4 SHORT-TERM AGGREGATIVE BEHAVIOR OF SILVER PARTICLES IN WATER MASSES

To understand changes in short-term dynamic of AgNPs added in natural water masses, aggregation kinetics were studied over 12 h. Samples from each layer were filtered on 5 µm filter. Then, PSD of samples was measured on aliquots before and after the addition of AgNPs at 10 $\mu Ag.L^{-1}$. After the addition of AgNPs, particle size evolution was measured over 12 h. Before the addition of AgNPs, the average D_h measured in water masses was between 400 and 700 nm (Figure 21). Clay, HS and SPM and other natural colloids can explain these sizes. After the addition of AgNPs, a strong evidence of the presence of small particles at 20 nm was observed (Figure 21), which is a D_h corresponding to the size of AgNPs added to nanopure water (Figure 30 in annexe IIII). The D_h increased faster (≈ 50 min) in halocline and bottom seawater layers (Figure 21b and 3c) compared to surface freshwater layer (≈ 100 min, Figure 21a). After this rapid evolution phase, the D_h reached a plateau (420 to 720 min) and was constant in all layers. The plateau observed after 420 min suggested that aggregation reached a steady state equilibrium. The average D_h estimated during this steady phase were 329±104 nm, 919±160 nm, and 343±79 nm in surface freshwater, halocline and bottom seawater layers, respectively. These results showed that aggregation rate and the final size of aggregates differed depending on the composition and properties of water masses.

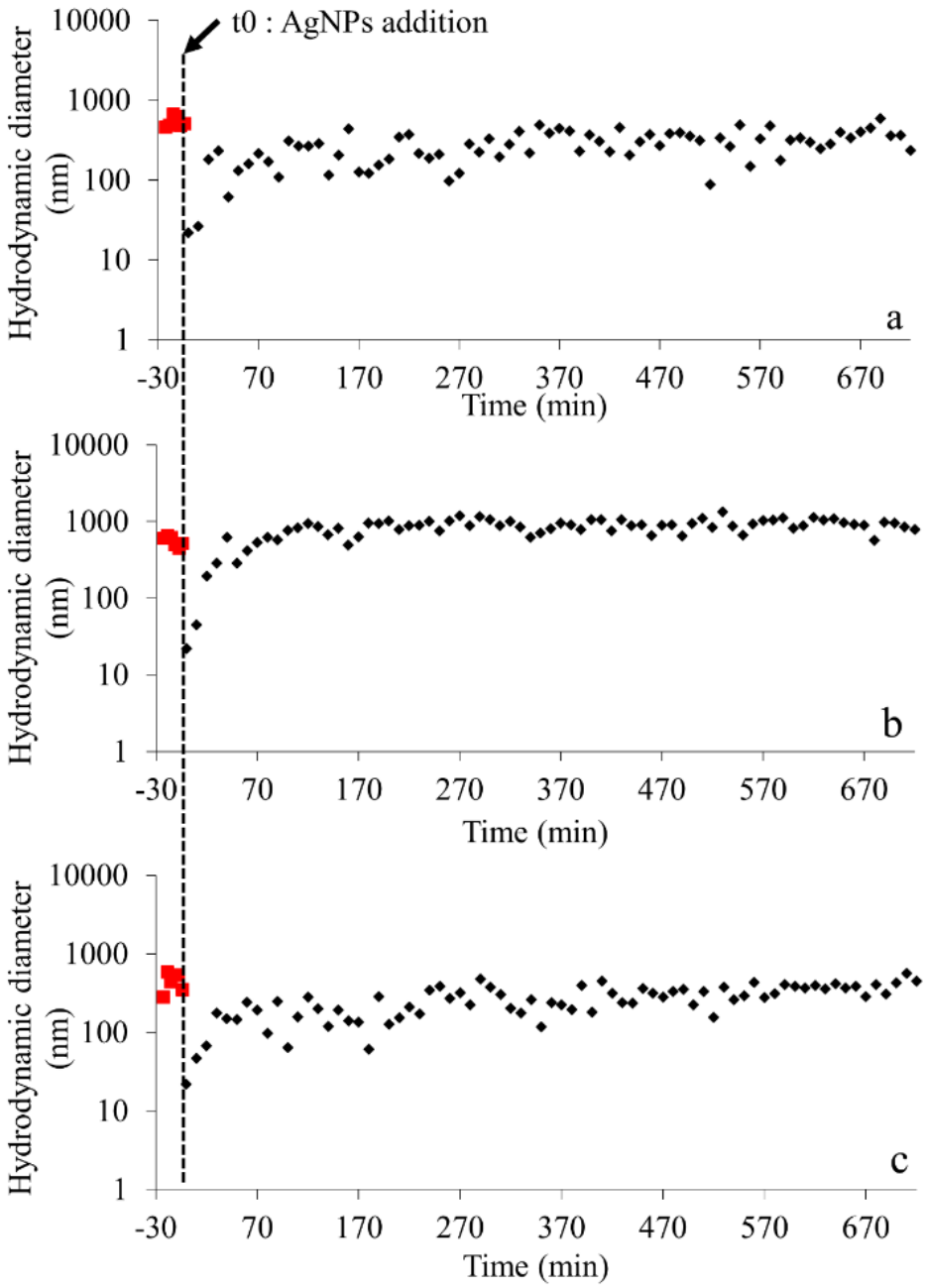

Figure 21: Aggregation kinetics over 12 h for AgNPs spiked at 10 µgAg.L^{-1}. a) surface water, b) halocline and c) bottom seawater layers in control mesocosm 1. Data in red correspond to hydrodynamic diameter before addition of AgNPs, and in black in presence of AgNPs

According to the Derjaguin, Landau, Verwey and Overbeek (DLVO) (Derjaguin and Landau, 1941; Verwey and Overbeek, 1948) and extended-DLVO (Grasso *et al.,* 2002) theories, the aggregation of nanoparticles is controlled by attractive and repulsive forces. When repulsive forces are more important than attractive ones, the aggregation is slow or reaction limited. But, when repulsive forces become equal or less than attractive ones, the aggregation is considered fast or diffusion limited. The transition between these two steps is determined by the critical coagulation concentration (CCC) of counterions (Petosa *et al.,* 2010). The collision between two AgNPs resulting in autoaggregation is not fully efficient when the salt concentration is below the CCC, and fully efficient when salt concentration is equal or above the CCC. The increase in salinity from the surface to bottom seawater layers in mesocosms increased the ionic strength. An increase of ionic strength induced a decrease of the electrical double layer thickness (Elimelech *et al.,* 1998) favoring the close encounter of AgNPs. The aggregate size distribution could also affect the charge at the surface of AgNPs. Under conditions used in mesocosms (pH 7.5-8.1), the carboxylic moieties of citrate were negatively charged and interacted with cations (counterions). Interactions between citrate and cations reduced negative surface charges of AgNPs and decreased the electrostatic repulsion between nanoparticles hence promoting aggregation. For AgNPs with citrate coating, CCC were determined at 48 mM of NaCl and near 2 mM of $CaCl_2$ and $MgCl_2$ (Huynh and Chen, 2011).

Other phenomena can also affect the fate of AgNPs. Sorption of NOM or HS to AgNPs surface or precipitation of silver salts as AgCl at the surface of AgNPs could occur (Baalousha *et al.,* 2013; Huynh and Chen, 2011; Topuz *et al.,* 2014). This new overlay could affect the stability and CCC of AgNPs by adding steric interaction, electrostatic repulsion, hydrogen bonding, hydrophobic interaction or by facilitating bridging flocculation (Philippe and Schaumann, 2014). In presence of HS, Huynh and Chen (2011) observed a modification of the CCC to 72 mM for NaCl and near 9 mM for $CaCl_2$. Moreover, in natural waters where a mixture of ions is present, the aggregation of AgNPs is driven by additive or synergistic

effects of each salt and controlled by the dominant salt (Baalousha *et al.,* 2013). The average concentration of major cations in world rivers are Na^+ (0.23 mM), Ca^{2+} (0.33 mM), and Mg^{2+} (0.15 mM). In seawater, major cations are Na^+ (468 mM), Ca^{2+} (10.2 mM), and Mg^{2+} (53.2 mM) (Bianchi, 2007). For salinity found in the halocline of mesocosms, near 15 PSU, concentrations are estimated as following: Na^+ (97 mM), Ca^{2+} (4.5 mM), and Mg^{2+} (22 mM), assuming the law of constant proportion of seawater (Libes, 2009). According to these cation concentrations, salt concentrations in surface freshwater layer were below the CCC of AgNPs with NOM. In this water mass, collisions were not fully efficient and a longer time is requested to observe the aggregation of AgNPs. In halocline and seawater layers, salt concentrations were higher than CCC of citrate AgNPs with NOM. In these cases, collisions were efficient promoting diffusion limited aggregation.

In addition, HS and clay could also be affected by the presence of salts and could have aggregated (Baalousha *et al.,* 2006; Brigante *et al.,* 2007; Tombácz and Szekeres, 2004) modifying the PSD. It has been shown that HA begun to aggregate when concentrations of NaCl or $CaCl_2$ are between 1 and 10 mM (Baalousha *et al.,* 2006). For clay, autoaggregation can be observed in brackish water at 60 mM NaCl or at higher concentrations depending on the pH (Tombácz and Szekeres, 2004). However, HS and clay could also aggregate with AgNPs (Baalousha *et al.,* 2013; Delay *et al.,* 2011; Huynh and Chen, 2011; Liu *et al.,* 2015; Zhou *et al.,* 2012) to form heteroaggregates.

4.5.5 LONG-TERM DISTRIBUTION OF PARTICLES IN WATER MASSES WITH ADDITION OF AGNPS

AgNPs were continuously added in surface layers of mesocosms 2 and 3 during 35 days and were exported to mesocosm 4 by the transfer of halocline water from mesocosm 3. Figure 22 shows the average PSD in mesocosms 2, 3 and 4, obtained by averaging the PSD measured over 35 days. PSD were characterized by a persistent multimodal distribution. In the surface layer of mesocosms 2 and 3, two particle populations were observed between 20 and 190 nm

and between 220 and 1 280 nm (Table 14, Figure 34). In these mesocosms (Figure 22a and 4b), the population $P_{0\text{-}200}$ represented 36% of particles with an average $D_{h0\text{-}200}$ at 70 nm. The population $P_{200\text{-}5\ 000}$ had $D_{h200\text{-}5\ 000}$ at 520 nm and represented 64% of particles (Table 14). In halocline layer, population $P_{0\text{-}200}$ represented only 1% of particles, with $D_{h0\text{-}200}$ at 120 nm, and the remaining 99% of particles had an average $D_{h200\text{-}5\ 000}$ at 700 nm. In bottom seawater layer, fewer than 3% of particles had $D_{h0\text{-}200}$ at 120 nm and the population $P_{200\text{-}5\ 000}$ ($\geq$ 97% of particles) had an average $D_{h200\text{-}5\ 000}$ at 520 nm.

In the brackish water (surface layer) of mesocosm 4 (Figure 22c and Table 14), the population $P_{0\text{-}200}$ representing 2% of particles had $D_{h0\text{-}200}$ at 126 nm, and 98% of particles had average $D_{h200\text{-}5\ 000}$ at 616 nm. In halocline, a very few 0.1% of particles composed $P_{0\text{-}200}$ with $D_{h0\text{-}200}$ at 139 nm, and the population $P_{200\text{-}5\ 000}$ (99.9%) had $D_{h200\text{-}5\ 000}$ 593 nm. In bottom seawater layer, populations $P_{0\text{-}200}$ and $P_{200\text{-}5\ 000}$ had a similar distribution (Table 14) to particles analyzed in seawater layers of the other mesocosms.

The PSD of $P_{0\text{-}200}$ in the surface freshwater layer of control mesocosm 1 (Figure 20b) was significantly different (Tukey test, $p<0.05$) from those observed in the surface freshwater layers of mesocosms 2 and 3 (Figure 22a and 4b). The deeper layers (halocline and bottom layers) of mesocosms 2 and 3 showed similar PSD to those layers in mesocosm 1.

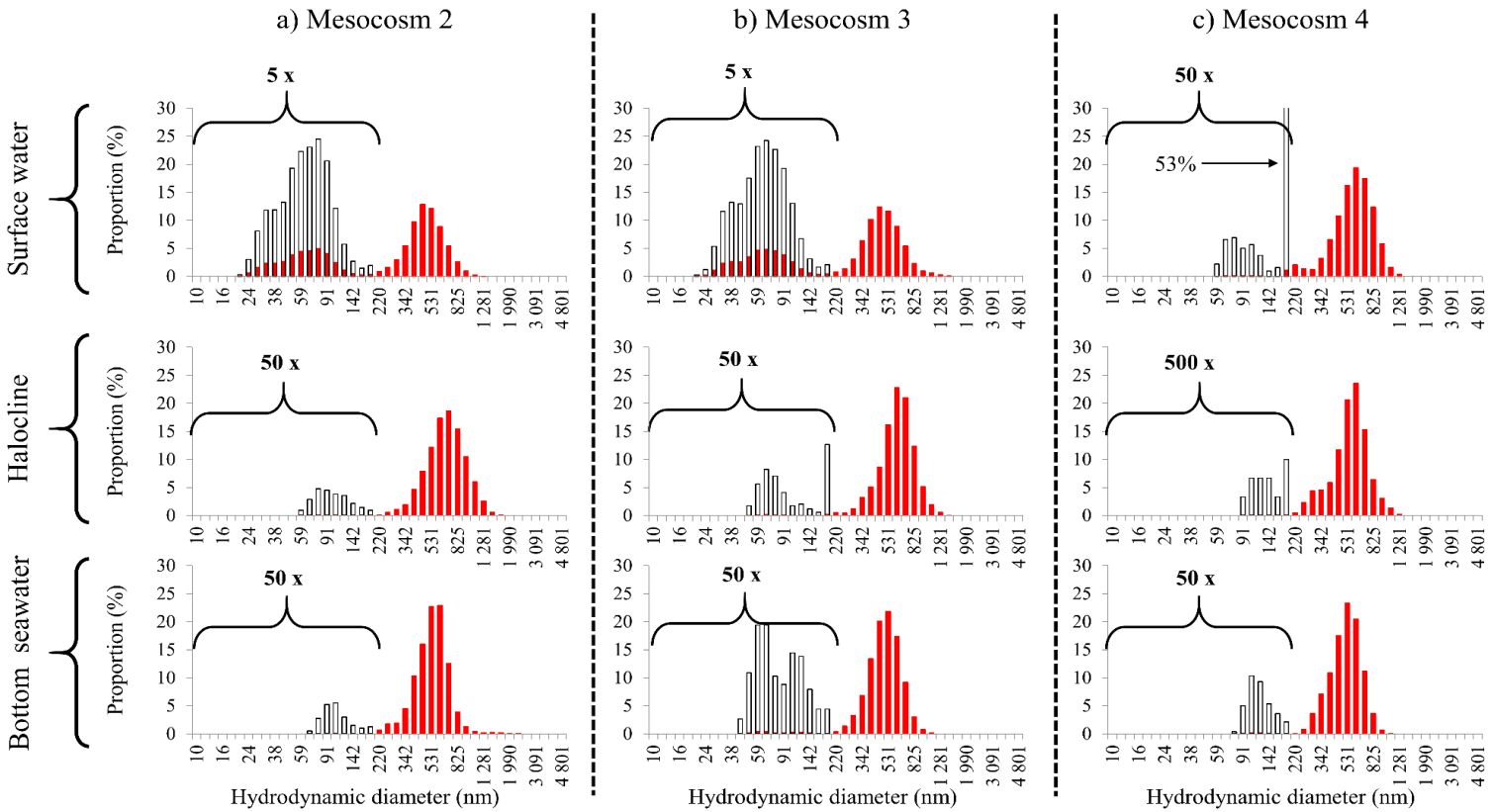

Figure 22: Average particle size distributions obtained over 35 days between 0 and 5 000 nm (red) in surface water, halocline and bottom seawater layers for a) mesocosm 2, b) mesocosm 3, and c) mesocosm 4. The particle size distribution between 0 and 200 nm (black empty) have been magnified to show the presence of small particle populations. Particle size distributions were obtained by averaging the PSD measured each day during this 35 days experiment

To assess if differences in PSD can be really attributed to the addition of AgNPs, it was important to investigate the role of clay and NOM in observed distributions. The PSD for clay at 10 mg.L^{-1} in dechlorinated water is a monomodal distribution of particles between 615 and 1 100 nm with an average $D_{h200\text{-}5\,000}$ at 997 nm (Figure 23a). Tombácz and Szekeres (2004) observed a similar PSD for the same clay. PSD of NOM was also determined at 6 mgDOC.L^{-1} in dechlorinated water (Figure 23b). NOM presented a complex PSD with three populations detected between 70-142 nm, 164-295 nm, and 342-825 nm. The first population had an average D_h at 110 nm, the second at 210 nm and the third at 500 nm. Considering the PSD observed and average diameters found for clay or NOM in water, these matrices cannot explain the proportion increase of $P_{0\text{-}200}$ detected in surface layers of mesocosms 2 and 3 with a continous addition of AgNPs.

To understand the evolution of $P_{0\text{-}200}$ in presence of AgNPs, PSD measured between 420 and 720 min from aggregation kinetic study in freshwater layer (data from Figure 21a) is illustrated in Figure 23c. Three particle populations are observed in the size ranges of 10-44 nm, 50-142 nm and 255-1 280 nm. The PSD observed between 10 and 44 nm has an average D_h at 25 nm, a size very close to the original D_h of AgNPs added. This suggest that a given proportion of initial AgNPs could persist for hours after their introduction to a complex aqueous media. Unrine *et al.* (2012) have also observed the persistence of initial silver nanoparticles 24 h after AgNP addition into a freshwater microcosm. The second particle population, observed between 50 and 142 nm, has a D_h near 70 nm. This population could be formed by the contribution of natural particles (HS and other colloidal particles see discussion about Figure 20b), by silver aggregates formed by few initial AgNPs or by the formation of new AgNPs from interactions of silver ions with HS (Akaighe *et al.,* 2011). The third population is composed of particles larger than 220 nm. The average D_h of this population was near 640 nm. This particle population agrees well with natural particles as clay and NOM (Figure 23a and b), but also with large silver heteroaggregates, as previously described (Table 6 and Figure 21b).

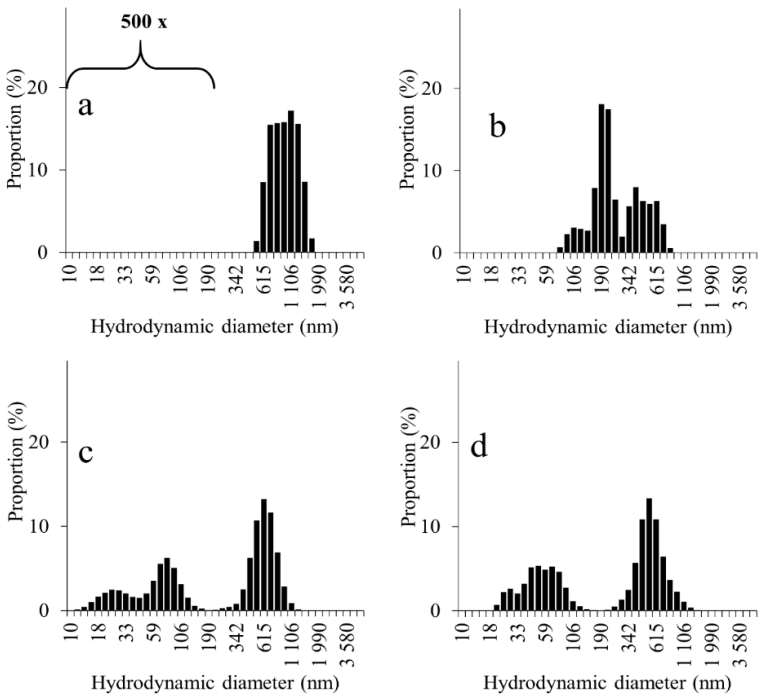

Figure 23: Distribution of different particle populations added to the surface freshwater of mesocosms. a) clay at 10 mg.L^{-1} in dechlorinated water and filtered at 5 µm, b) natural organic matter at 6 mgDOC.L^{-1} of NOM in dechlorinated water and filtered at 5 µm, c) particle distribution calculate between 420 and 720 min from aggregation kinetics over 12 h of silver nanoparticles spiked in freshwater samples filtered at 5 µm and d) means of surface freshwater layer particle distribution in mesocosms 2 and 3 during the first week

PSD of colloidal clay suspension without and with AgNPs were compared in an attempt to discriminate the presence of AgNPs from a clay suspension background (Figure 36 in Annexe III p161). In the absence of AgNPs, the PSD of clay was monomodal (Figure 23a) while it became polymodal in presence of AgNPs. Particles with size smaller than 200 nm appeared. The addition of AgNPs at 10 µgAg.L^{-1} contributed to producing a detectable population $P_{0\text{-}200}$ (Figure 36). These data suggest that it is possible to detect the presence of a low level of AgNPs in presence of clay. It is important to remember that silver nanoparticles

added correspond to 2.3 x 10^8 particles.mL^{-1} for AgNPs and to 7.7 x 10^6 particles.mL^{-1} for clay, even if the mass concentrations were at 10 µgAg.L^{-1} and 10 mgclay.L^{-1}.

Although these data suggests that it was possible to observe the presence of AgNPs on a short time period of 12 h (Figure 23 a-c and S7), the long-term behavior was still uncertain. Figure 23d presents the average PSD obtained for the first week of the experiment for surface freshwater layers of mesocosms 2 and 3. Three populations were observed between 20-33 nm ($D_h \approx 25$ nm), 38-142 nm ($D_h \approx 60$ nm), and 255-1 280 nm ($D_h \approx 600$ nm). This PSD appeared quite similar to PSD obtained from the 12 h kinetics study (Figure 23c). However, as shown in Figure 22, the two populations observed with particle sizes less than 200 nm tend to form one population over a 35-day period. Observations on the presence and persistence (Figure 22, Figure 23 and Table 6) of small particles in aqueous media in presence of AgNPs were in agreement with measurements of Ag_{dis} in surface freshwater layer of mesocosms. Moreover, two days after the AgNPs addition was stopped, the PSD measured in surface freshwater layers of mesocosm 1, 2 and 3 were similar (data not shown). The addition of AgNPs at low concentration in estuarine waters could leave a measurable trace in water masses.

4.6 CONCLUSION

In model estuarine mesocosms described in the present work, the addition of 20 nm AgNPs in surface freshwater induced the formation of silver compounds with size smaller and larger than 450 nm. A close examination of PSD in water layers showed the existence of at least two populations of particles: (1) a first population (0-200 nm) could contain original AgNPs added to water and/or newly formed AgNPs aggregates; (2) a second population (200-5 000 nm) could be composed by large aggregates of AgNPs and different silver forms in interaction with SPM, clay, NOM and microorganisms.

We also observed that the halocline represented a strong density barrier to slow down the sedimentation and the transfer of silver materials to deep seawater layer. The mesocosms used in this study were not affected by tides and currents contrary to natural estuaries. Tidal intrusions in estuaries cause turbulence and mixing capable of breaking the halocline retaining particles in the surface water layer. Moreover, small size silver particles ($P_{0\text{-}200}$) in surface water will be exported to coastal or ocean systems due to the short residence time of estuarine surface waters.

Salinity had a strong effect on AgNPs added to mesocosms. Salinity changed the speciation (dissolved or particulate) and the size of nanoparticles. When salinity increased, as simulated in the halocline, the aggregation of small silver particles rose to produce larger aggregates found in SPM. This resulted in a diminution of Ag_{dis} and a relative increase in Ag_{part}. Moreover, a possible release of silver from SPM fraction ($\geq$ 450 nm) to dissolved fraction (<450 nm) can occur at higher salinity (brackish water of mesocosm 4).

Toxic effects of AgNPs on pelagic and benthic organisms could be influenced by the dynamic of the estuary. In a stratified estuary as modeled here, silver particles tend to persist hours and probably for days in surface and halocline layers. Presence of silver in these layers could have direct effects on pelagic organisms. In well-mixed estuarine systems, Ag_{dis} could affect organisms in the whole water column, but Ag_{part} would settle and exert effects on benthic organisms.

4.7 ACKNOWLEDGMENTS

This work was supported by Strategic Project Grants of the National Sciences Engineering Research Council of Canada (E. Pelletier and J.-P. Gagné), Discovery Project Grants of the National Sciences Engineering Research Council of Canada (Jean-Pierre Gagné) and network Québec-Océan. The authors are grateful to Dr Claude Rouleau for the

experimental design, and Mickael Barthe, Thomas Conte--Chenuc, Isabelle Desbiens, Kevin Osterheld and Alexandre Palardy for their technical support.

CONCLUSION GÉNÉRALE

L'objectif principal de cette thèse était de déterminer le comportement et le devenir des nanoparticules d'argent, à très faible concentration (10 µgAg.L^{-1}) durant une transition estuarienne. Afin de répondre à cet objectif, plusieurs questions importantes ont été posées : quelle est la principale transformation des AgNPs dans les systèmes aquatiques ? Peut-on caractériser leurs comportements à 10 µgAg.L^{-1} ? Comment les propriétés physico-chimiques du milieu, telles que la salinité et la matière organique naturelle, modifient-elles l'agrégation des AgNPs ? Quel est le devenir des AgNPs dans un estuaire stratifié ?

Une fois relarguées dans un système aquatique, les AgNPs peuvent subir plusieurs transformations. Cependant, certaines transformations peuvent être lentes (dissolution) ou bien limitées (oxysulfidation et sulfidation). L'agrégation étant le processus principal en milieu aquatique, la présence de sel, de NOM et de particules naturelles peut le moduler. L'agrégation des AgNPs est un mécanisme très étudié par la communauté scientifique. Mais beaucoup de ces études ont été réalisées à des concentrations irréalistes en AgNPs, en général de l'ordre du mgAg.L^{-1}, par rapport aux concentrations estimées dans les milieux naturels. Comme un des buts de ce projet était de travailler dans des conditions expérimentales proches des conditions environnementales, il a fallu adapter certaines techniques analytiques, essentiellement la DLS, afin de mesurer l'évolution de la taille des AgNPs dans le temps à très faible concentration (10 µgAg.L^{-1}). Pour cela, des suspensions d'AgNPs à différentes concentrations ont été analysées par DLS ce qui nous a permis de déterminer que la DLS pouvait être utilisée à 10 µgAg.L^{-1} malgré l'avis de nombreux auteurs ayant critiqué ou rejeté cette approche. L'ensemble des études menées sur le comportement agrégatif des AgNPs ont été effectuées afin de caractériser la phase d'augmentation rapide de la taille dans le temps.

Très peu de données existent sur la distribution de la taille des agrégats formés. À ma connaissance, les résultats obtenus dans cette thèse sont les premiers à avoir été réalisés à 10 $\mu gAg.L^{-1}$, et qui ont caractérisé la distribution de la taille des agrégats formés durant l'agrégation. Dans la littérature, la plus faible concentration utilisée en AgNPs pour étudier leurs agrégations par DLS était de 1 $mgAg.L^{-1}$. La plus faible concentration utilisée pour décrire l'évolution de la distribution de taille des agrégats était de 125 $\mu Ag.L^{-1}$. Dans cette étude, la stabilité des AgNPs été analysée en fonction de la salinité, mais aussi dans des solutions plus complexes (sel et NOM), où plusieurs paramètres peuvent influencer le devenir et le comportement des AgNPs durant une transition estuarienne.

Effets des sels

Les effets de la concentration et de la valence des sels sur le comportement agrégatif ont été étudiés pendant 2 h, 12 h et 17 h. Dans un premier temps, les AgNPs ont été ajoutées dans de l'eau nanopure. Les cinétiques réalisées ont montré que la taille des AgNPs n'évolue pas dans le temps. Elles gardent leurs tailles d'origine. Selon la théorie DLVO, cette stabilité est due à des forces répulsives plus importantes que les forces attractives. Pour les AgNPs avec un revêtement organique au citrate, la stabilité est essentiellement causée par des forces électrostatiques répulsives. Dans ces expériences, le pH du milieu a été maintenu à 7.00±0.05. À ce pH, les groupements carboxyliques du citrate sont ionisés (pKa_1 3.13 ; pKa_2 4.76 ; pKa_3 6.40), ce qui produit des charges négatives à la surface des AgNPs (Pζ entre -34 et -35 mV). L'ajout de sel dans le milieu induit une augmentation rapide de la taille des AgNPs dans le temps qui, ensuite, se stabilise indiquant un état d'équilibre. La présence de sel dans le milieu augmente la force ionique ce qui induit une compression de la double couche électrique des AgNPs. De plus, les cations (contre-ions) peuvent aussi interagir avec les charges négatives des AgNPs. La présence de sel dans le milieu tend à diminuer les forces répulsives, ce qui favorise le rapprochement et l'autoagrégation des AgNPs. Ces données ont montré que la vitesse d'agrégation, caractérisée durant la phase d'évolution rapide de la taille,

augmente en fonction de la concentration en NaCl jusqu'à une valeur maximale. Selon la DLVO, les conditions du milieu peuvent être favorables ou non à l'agrégation. Tant que la vitesse d'agrégation des AgNPs augmente en fonction de la concentration en NaCl, les conditions sont considérées comme non favorables à l'agrégation. Cela indique que la force ionique n'est pas assez élevée pour compresser efficacement la double couche électrique et que la quantité en Na^+ n'est pas suffisante pour neutraliser les charges négatives des AgNPs. Au-dessus d'une certaine concentration en NaCl, la vitesse d'agrégation n'évolue plus. Toutes les collisions sont efficaces. Dans ces conditions, l'agrégation des AgNPs est dépendante de leurs coefficients de diffusion. Les effets de la valence des sels sur les AgNPs ont été étudiés à 93 $\mu gAg.L^{-1}$. Ces données ainsi que les données de plusieurs études montrent que la vitesse d'agrégation est fortement influencée par la valence des contre-ions. L'agrégation est plus rapide en présence de cations divalents qu'en présence de cations monovalents. Lorsque l'état d'équilibre est atteint, la taille n'évoluant plus dans le temps, les agrégats formés ont une taille très semblable, proche de 500 nm, quelle que soit la valence des ions. Dans la littérature, les cinétiques sont généralement effectuées durant minutes, en général moins de 30 min. La caractérisation du comportement agrégatif durant plusieurs heures a permis de démontrer que même si la valence et la concentration en sel modifient la vitesse d'agrégation, la taille des agrégats formés semble être peu affectée par la nature et la concentration des cations.

Effets de la concentration en nanoparticules d'argent

L'agrégation a aussi été étudiée à différentes concentrations en AgNPs. Ces données montrent que la vitesse d'agrégation est fortement influencée par la concentration en AgNPs. Ces données montrent l'importance d'utiliser des concentrations plus faibles, car les forts taux d'agrégation présentés dans la littérature sont issus d'expériences effectuées à fortes concentrations en AgNPs. La distribution de la taille des agrégats est aussi fortement dépendante de la concentration initiale en AgNPs. À ma connaissance, c'est la première étude

décrivant l'évolution de la distribution de taille des agrégats selon la concentration en AgNPs et à différentes concentrations en sel. À forte concentration (10 et 1 mgAg.L^{-1}), plus de 70% des particules analysées ont une taille supérieure à 200 nm. À faible concentration (100 et 10 µgAg.L^{-1}), la distribution est différente puisqu'entre 50 et 90% des particules formées ont une taille inférieure à 200 nm. Les distributions de taille obtenues permettent une meilleure compréhension du type d'agrégats formés, ce que ne permettent pas les données de la littérature qui ne présentent que des vitesses d'agrégation et des CCC. Les données présentées dans cette thèse démontrent clairement que plus la concentration initiale en AgNPs est faible, plus les agrégats formés seront de petite taille. De plus ces données ont permis d'établir le rôle de la quantité de particules (particules.mL^{-1}) sur la formation des autoagrégats, Figure 24.

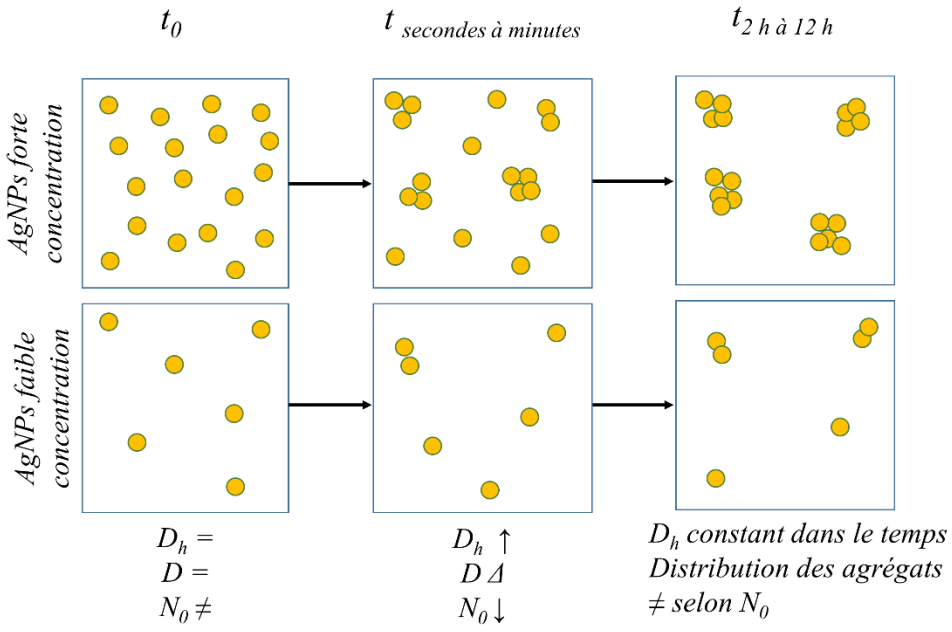

D_h : diamètre hydrodynamique, D : coefficient de diffusion, N_0 : concentration initiale en particule

Figure 24 : Mécanisme de formation des agrégats selon la concentration en nanoparticules d'argent

À t_0, au moment de l'ajout des AgNPs, la quantité de particules diffère selon la concentration en AgNPs (concentration massique) ajoutée. Les AgNPs se déplacent rapidement, car, plus les particules sont petites, plus le coefficient de diffusion est important (relation de Stoke-Einstein). Durant les premières secondes de l'agrégation, deux AgNPs originales entrent en collision et forment un agrégat. Après quelques minutes, ces petits agrégats peuvent interagir à la fois avec des AgNPs originales et avec d'autres agrégats. Plus le temps augmente, plus la quantité de particules diminue. L'augmentation de la taille dans le temps diminue le coefficient de diffusion des particules. Au bout d'un certain temps, la quantité de particules dans le milieu, environ 10^6 particules.mL^{-1}, est insuffisante pour qu'il se produise une agrégation et un état d'équilibre est atteint. Selon la quantité de particules initialement ajoutées, l'appauvrissement du milieu en particules diffère, ce qui explique les différences observées dans la distribution de la taille des particules.

Effets de la matière organique naturelle

Les effets de la matière organique naturelle sur le comportement agrégatif des AgNPs ont été étudiés. Ces données montrent que la présence de NOM module les vitesses d'agrégation et la distribution de la taille des agrégats, alors que dans la littérature les effets de la NOM ne sont étudiés que pour déterminer le rôle de la NOM sur les CCC et donc la stabilité des AgNPs. À ma connaissance, c'est la première étude décrivant le rôle de la concentration et de la composition chimique de la NOM sur la distribution de la taille des agrégats à très faible concentration en AgNPs.

Ces effets ont été étudiés à différentes concentrations en NaCl et en présence de 2.5 et 25 mgNOM.L^{-1}. Dans cette étude, la NOM provenant de 50 m^3 d'eau de l'estuaire du Saint-Laurent a été obtenue avec un tandem de résines chromatographiques (DAX-8 et XAD-4). Quatre fractions ont été obtenues selon leur affinité pour une des deux résines : les acides humiques, les acides fulviques, une fraction hydrophile et une fraction hydrophobe. Chaque fraction a été caractérisée afin d'estimer le poids moléculaire, la composition élémentaire et

la composition en groupements fonctionnels. Ces données ont permis d'évaluer les effets de la concentration et de la composition chimique de la NOM sur l'agrégation des AgNPs (Figure 25).

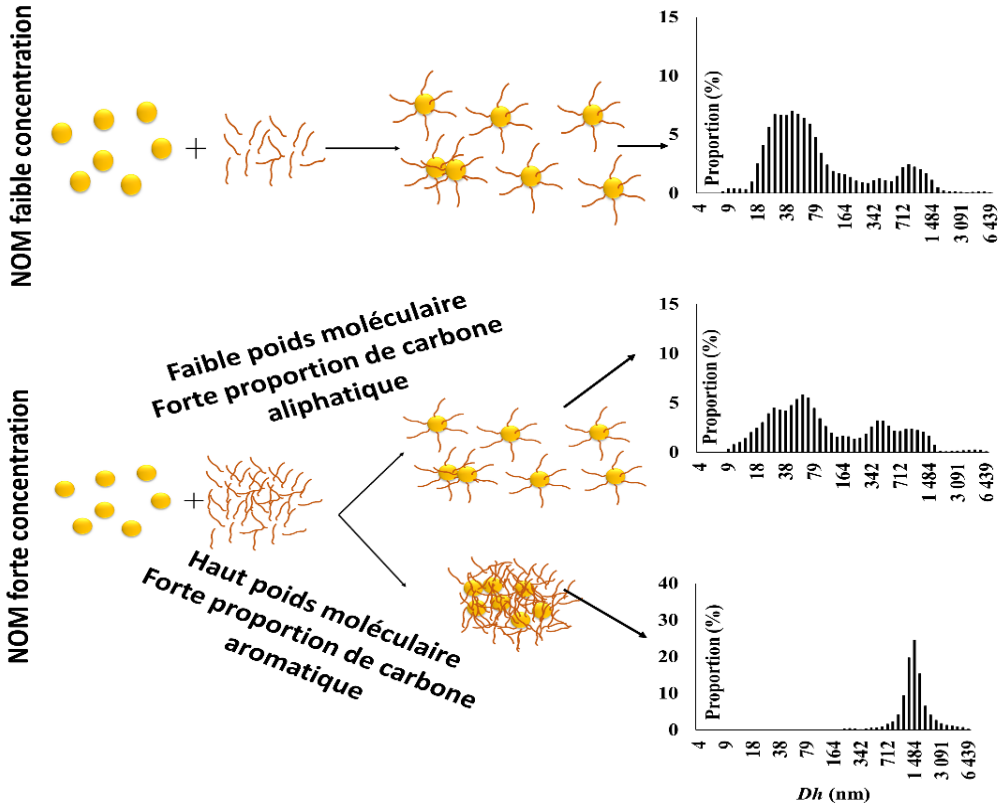

Figure 25 : Distribution de la taille des particules selon la concentration et la composition chimique de la NOM

En absence de sels, la présence de NOM induit une légère augmentation de la taille. Cette augmentation est due à des phénomènes de sorption de la NOM sur les surfaces des AgNPs. Toutefois, cette augmentation diffère en fonction de la concentration et de la fraction de la NOM utilisée. À 2.5 mgNOM.L^{-1} et en présence de sel, la taille des agrégats formés est similaire à la taille des agrégats formés en absence de NOM. Quelle que soit la fraction

utilisée, plus de 90% des particules analysées ont une taille inférieure à 200 nm. À cette concentration, la composition chimique de la NOM ne modifie pas la PSD. À faible concentration (Figure 25), la NOM qui a interagi à la surface des AgNPs a ajouté des effets stériques, des interactions de van der Waals, des interactions hydrophobes, des interactions électrostatiques et des liaisons hydrogène, ce qui stabilise les agrégats à des tailles plus petites. Ce mécanisme est cohérent avec la DLVO-étendue, car cette théorie considère le rôle des liaisons hydrogène, des interactions hydrophobes, des interactions stériques, des pressions d'hydratation, la polarisabilité des surfaces et des interactions acide-base de Lewis dans l'agrégation.

À 25 mgNOM.L^{-1}, la PSD des hétéroagrégats est fortement modulée par la composition chimique de la NOM. Cette étude montre que ces différences sont causées par la nature des groupements responsables des interactions hydrophobes ainsi que par leur poids moléculaire. La présence de NOM possédant une grande proportion de groupements aliphatiques non-polaires favorise la formation d'agrégats ayant une taille inférieure à 200 nm, alors qu'un effet inverse est observé avec de la NOM riche en groupements aromatiques. Ce comportement est relié à la conformation et à l'orientation de ces groupements hydrophobes pouvant ajouter des obstacles stériques et/ou des répulsions de chevauchement. La présence des liaisons π dans les groupements aromatiques favorise la formation de complexes de transfert de charge, ce qui peut favoriser l'agrégation de la NOM. Le soufre, présent en faible proportion dans la NOM, semble aussi intervenir dans l'agrégation des nanoparticules d'argent. La NOM peut aussi permettre le développement d'interactions de van der Waals, de liaisons hydrogène et des effets électrostatiques.

Ces résultats sont importants pour comprendre le comportement des AgNPs dans l'environnement. Dans les eaux douces, où la concentration en NOM est généralement entre 5 et 50 mgNOM.L^{-1}, la composition chimique de la NOM modulera la taille des agrégats. Dans le cas d'une NOM allochtone, généralement riche en carbones aromatiques comme les

substances humiques, de gros agrégats seront formés. En présence de NOM autochtone ayant une teneur élevée en carbones aliphatiques non-polaires, des agrégats de moins de 200 nm seront formés. En eau de mer, la concentration de NOM est plus faible, près de 2.5 mgNOM.L^{-1}, et l'origine de la NOM influence peu la PSD. Dans ces systèmes, la présence de NOM tend à former une forte proportion d'agrégats de taille inférieure à 200 nm.

Comportement et devenir en milieu estuarien

Afin de comprendre le comportement et le devenir des AgNPs en milieu estuarien, une expérience en mésocosme a été effectuée. Ces mésocosmes ont été conçus pour imiter un estuaire stratifié où une couche d'eau douce de surface était séparée de la couche d'eau de mer de fond par une halocline bien définie. Durant cette expérience, le comportement des AgNPs a été caractérisé pendant 12 h et 35 jours. Les données obtenues ont permis d'observer que les AgNPs s'agrègent dans chaque masse d'eau (eau de surface, halocline et eau de fond). Les vitesses d'agrégation diffèrent selon les paramètres physico-chimiques de la masse d'eau étudiée, car elles sont modulées par la concentration et la valence des ions ainsi que par la concentration et composition chimique de la NOM. Dans les mésocosmes, les tailles des agrégats formés diffèrent selon la masse d'eau. La composition complexe des masses d'eau des mésocosmes, présence de plusieurs types d'ions (Na^+, Ca^{2+}, Mg^{2+}, Cl^-, HCO_3^- …), d'argile et de NOM, a aussi pu favoriser la formation d'hétéroagrégats, ce qui explique les différences de taille des agrégats observées.

La distribution de la taille des agrégats a été caractérisée dans les mésocosmes en présence ou en absence d'AgNPs. La présence de deux populations a aussi été observée dans tous les mésocosmes et dans chaque masse d'eau. Les données montrent que la présence d'AgNPs, dans les eaux douces, modifie cette distribution et tend à augmenter la proportion des particules ayant une taille inférieure à 200 nm, 10% des particules analysées en absence d'AgNPs et 36% des particules en présence d'AgNPs. Cette distribution reste très semblable dans le temps (12 h à 35 jours). L'analyse par DLS ne permettant pas de déterminer le type

de particules présentes (AgNPs, particules naturelles, colloïdes, argiles ou NOM), l'utilisation des données obtenues dans les autres chapitres a permis de valider la formation d'agrégats ayant des tailles inférieures et supérieures à 200 nm. De plus, la distribution de la taille de la NOM, des argiles et des argiles en présence d'AgNPs a été caractérisée, ce qui a permis de discriminer le signal des AgNPs des autres particules et de démontrer la présence d'AgNPs non agrégées. Ceci confirme qu'une certaine proportion d'AgNPs originales peut persister pendant des heures après leur introduction dans un milieu aqueux complexe.

En plus d'avoir été caractérisées par DLS, les différentes masses d'eau ont été échantillonnées pour des analyses en ICP-MS. Les échantillons ont été filtrés avec des filtres de porosité 0.45 µm, afin d'obtenir l'argent dissous (analyse du filtrat) et l'argent particulaire (analyse du filtre). Dans cette étude, l'argent dissous (Ag_{dis}) correspond à toute forme de l'argent ayant une taille inférieure à 450 nm : les ions argent (Ag^+ ou les chlorocomplexes d'argent ($AgCl_n^{(n-1)-}$)), les AgNPs à 20 nm et des petits agrégats d'argent (inférieure à 450 nm). L'argent particulaire (Ag_{part}) comprend des autoagrégats d'argent, des hétéroagrégats d'argent avec de la matière particulaire en suspension (SPM) et des ions argent (Ag^+ ou les chlorocomplexes d'argent ($AgCl_n^{(n-1)-}$)) en interaction avec la SPM. Dans le mésocosme 1 (le contrôle), les niveaux d'Ag_{dis} et d'Ag_{part} sont similaires à ceux observés dans l'estuaire du Saint-Laurent. Dans les mésocosmes 2 à 4 (ajout d'AgNPs), les niveaux d'Ag_{dis} et d'Ag_{part} diffèrent selon les masses d'eau étudiées. Ces données ont permis de (1) valider les données de distribution de la taille obtenue par DLS (2 populations de particules contenant de l'argent) ; (2) montrer que les paramètres physico-chimiques à l'halocline favorisent la formation d'agrégats de taille supérieure à 200 nm ; et (3) observer un relargage de l'argent de la fraction Ag_{part} vers la fraction Ag_{dis} à des salinités égales ou supérieures à 15 PSU. De plus, les données montrent que les niveaux d'argent dans les masses d'eau salée (fond) des mésocosmes 2 à 4 étaient similaires à ceux observés dans le mésocosme 1. Ces données indiquent que l'halocline peut agir comme une frontière de forte densité limitant la

sédimentation des AgNPs. Les données présentées dans cette thèse ont permis de mieux comprendre le devenir des AgNPs dans un estuaire, tel que présenté à la Figure 26.

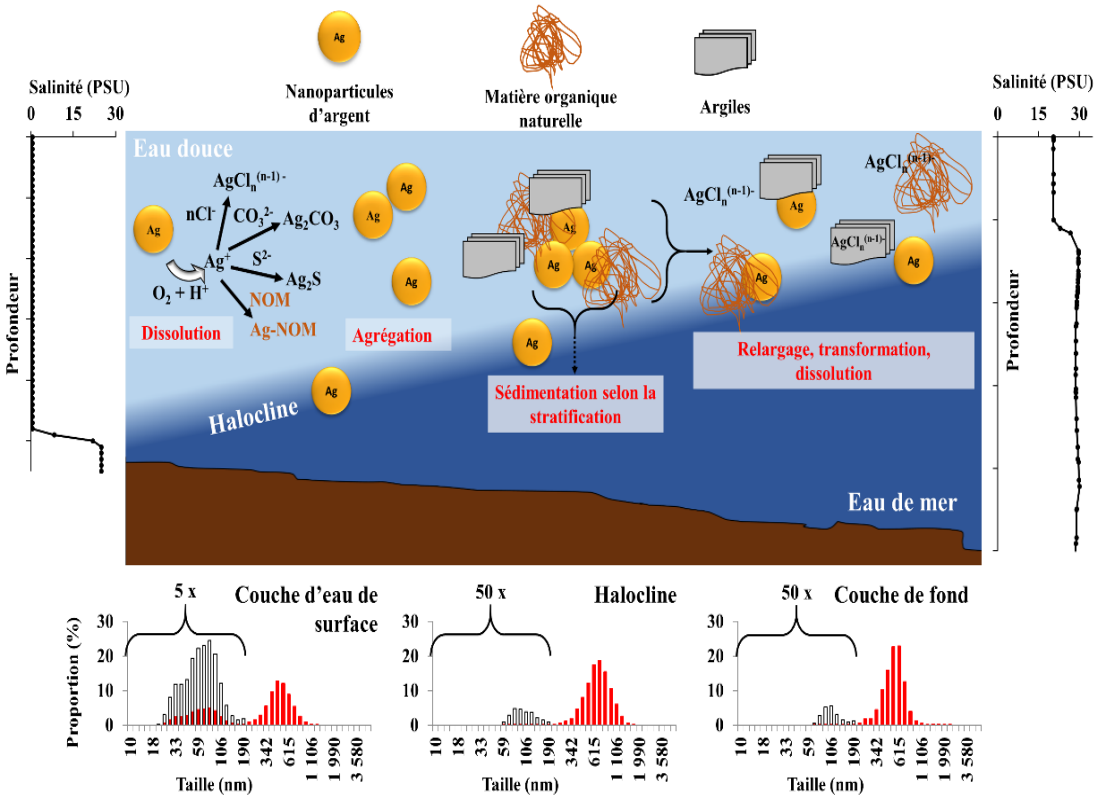

Figure 26 : Devenir des nanoparticules d'argent dans un estuaire modèle

En milieu aquatique, on s'attend à ce que les AgNPs soient principalement rejetées dans des systèmes d'eau douce puis exportées vers les estuaires et les océans. Dans ces systèmes, la présence de sel, de NOM et de SPM favorisera l'agrégation des AgNPs. L'agrégation produira deux populations de particules, dont les proportions diffèrent selon les paramètres physico-chimiques du milieu, comme la force ionique (concentration et composition en sel), la NOM (concentration et composition chimique) et la présence de SPM. Dans la partie fluviale de l'estuaire, une grande proportion des agrégats formés auront une taille inférieure à 200 nm. Par la suite, ces agrégats pourront être transportés vers la zone de

turbidité maximale des estuaires, présentant une très forte variation de la salinité et des niveaux élevés en NOM et SPM. Dans cette zone, les paramètres physico-chimiques favoriseront la formation d'agrégats ayant une taille supérieure à 200 nm. Selon le cycle des marées, les agrégats formés dans la zone de turbidité maximale pourront être exportés dans la partie maritime des estuaires. À une salinité égale ou supérieure à 15 PSU, une partie de l'argent (AgNPs, agrégats d'AgNPs, Ag^+ ou les chlorocomplexes d'argent ($AgCl_n^{(n-1)-}$)) en interaction avec la SPM (Ag_{part}) sera relargué vers la fraction dissoute (inférieur à 450 nm). Dans un estuaire stratifié, les AgNPs persisteront dans les eaux de surface ce qui pourrait favoriser leur exportation vers les océans selon la dynamique du milieu et la force des courants. Dans un estuaire bien mélangé, l'exportation vers les océans et/ou vers le fond sera influencée par la taille des agrégats. Les agrégats inférieurs à 200 nm auront tendance à persister dans les eaux de surface, car leur vitesse de sédimentation sera relativement faible. Les agrégats supérieurs à 200 nm, ayant une vitesse de sédimentation plus élevée, seront exportés vers le fond des estuaires et pourront se concentrer dans les sédiments. Ce travail illustre le fait que l'halocline doit être considérée comme une frontière de densité qui module fortement le devenir des AgNPs et très probablement d'autres nanoparticules dans les estuaires. Les changements climatiques peuvent aussi moduler le devenir des AgNPs durant une transition estuarienne. Il est connu que ces changements induisent une augmentation des précipitations au Québec ainsi qu'un réchauffement des eaux de surface. L'augmentation du débit des rivières risque de favoriser l'exportation des AgNPs et des agrégats d'argent vers les estuaires et les zones côtières. Une augmentation de la température des eaux de surface pourrait augmenter la stratification des certaines zones estuariennes et côtières, augmentant ainsi le temps de résidence des agrégats d'argent dans ces masses d'eaux.

Afin de mieux comprendre le devenir des ENMs dans l'environnement, les travaux effectués dans cette thèse pourraient être repris avec des AgNPs ayant une taille différente ou un autre recouvrement organique, comme du polyvinylpyrrolidone. De plus, d'autres ENMs, comme les oxydes de silice et de titane (SiO_2 et TiO_2) ou les nanomatériaux à base

de carbone, peuvent aussi se retrouver dans l'environnement. Comme pour les AgNPs, le comportement et le devenir de ces ENMs dans les systèmes aquatiques sont peu connus. Des études menées sur le rôle de la taille et du revêtement ainsi que sur la nature des ENMs pourraient permettre de mieux comprendre leur agrégation ainsi que la distribution de la taille des agrégats formés. Dans cette thèse, nous avons peu étudié l'impact des cations multivalents sur la distribution de la taille des particules. Il est connu que les cations divalents, comme Ca^{2+}, peuvent favoriser les pontages interparticules. De futurs travaux avec des solutions de $CaCl_2$ à différentes concentrations avec ou sans NOM pourraient permettre de mieux caractériser le rôle de la valence des sels dans la distribution de la taille des agrégats. L'effet de la température sur l'agrégation et la distribution de la taille des agrégats devrait aussi être étudié. Certaines études ont démontré qu'une augmentation de la température induit une diminution des CCC et une augmentation de la taille des agrégats pour des NMs à base d'oxydes métalliques. L'étude des effets de la température sur le comportement et le devenir des AgNPs en milieu estuarien est important, et plus particulièrement pour les milieux présentant une forte variation saisonnière la température des eaux de surface, comme l'estuaire du Saint-Laurent. De plus, dans ce projet, le rôle de la matière particulaire en suspension sur l'agrégation n'a pas permis de comprendre finement les interactions AgNPs-SPM. Des travaux effectués à différentes concentrations en argile, en sel et en présence ou en absence de NOM permettraient d'améliorer les connaissances sur les interactions entre les AgNPs et la SPM, ainsi que sur la distribution de la taille des agrégats. Quelques études ont démontré que des phénomènes de désagrégation pouvaient se produire, un sujet qui mériterait plus d'attention.

Cette thèse apporte des données de référence ainsi qu'une meilleure compréhension du comportement et du devenir des AgNPs en milieu estuarien. Cette étude fournit aussi des informations importantes pour les études écotoxicologiques et environnementales à faibles concentrations en AgNPs. Ce projet montre qu'il est important d'utiliser des AgNPs vieillies pour des essais toxicologiques, car, quelle que soit la concentration d'AgNPs utilisées, les

organismes seront exposés à la même quantité de particules (10^6 particules.mL^{-1}), mais pas aux mêmes tailles d'agrégats. Actuellement, il existe très peu de données sur les concentrations en AgNPs retrouvées dans les systèmes aquatiques naturels. Seules des estimations obtenues par modélisation sont disponibles. Les résultats obtenus dans cette thèse permettront d'améliorer les modèles, mais aussi contribuer à valider les estimations avec des échantillons naturels, car cette thèse permet de cibler des populations de particules pouvant contenir des AgNPs. Les résultats apportés seront aussi utiles aux organismes fédéraux et provinciaux pour la régulation et la législation des AgNPs et des autres ENMs dans l'environnement, car ils montrent la présence de deux populations de particules pouvant contenir des AgNPs. Ces données pourraient permettre une meilleure estimation des effets des AgNPs sur les services écosystémiques en prenant en compte le rôle de la taille des agrégats sur l'internalisation par les microorganismes, la bioaccumulation par les macroorganismes et donc la toxicité des AgNPs.

ANNEXE I

SUPPORTING INFORMATION FOR EFFECTS OF SILVER NANOPARTICLES CONCENTRATION ON THEIR AGGREGATIVE BEHAVIOR AND SIZE DISTRIBUTION OF AGGREGATES

Synthesis of Silver Nanoparticle

The solution of colloidal silver nanoparticles was prepared following the procedure of Turkevich.(Turkevich *et al.,* 1951) Ten milliliters (10 mL) of a solution of $AgNO_3$ (>99%, Sigma-Aldrich), at 58.9 mM, were added to 185 mL of nanopure water under reflux. At the recovery of boiling, 5 mL of a solution of sodium citrate (>99%, Sigma-Aldrich) at 0.25% was added dropwise. After 3 h of reaction, the system was cooled down at room temperature. The solution was filtered on 0.2 µm polycarbonate filter (Whatman). The filtrate was centrifuged at 6 000 g for 15 min. The pellet was resuspended with 8 mL of nanopure water and centrifuged at 6 000 g during 15 min. This procedure was repeated three times to remove the excess of silver ions and citrate.

After the synthesis and the purification process, the concentration of AgNPs was determined by inductively coupled plasma mass spectrometry (ICP-MS, Agilent 7500C^{TM}) using an argon plasma at 7 000 K and with a standard analytical protocol. Calibration curve was obtained from the analysis of nine concentrations, between 0.75 and 200 µg$Ag.L^{-1}$. The concentration of total silver and silver ions was determined. For silver ions concentration, a 500 µL of the solution was centrifugated at 6 000 g during 15 min in centrifugal filter units (Ultracel-10K, Millipore). After this process, 100 µL of the filtrate was digested with 1 mL of HNO_3 (TraceSELECT, Fluka) and 250 µL of H_2O_2 (TraceSELECT, Fluka). For the total

silver content, 100 µL of the colloidal solution was digested with 2 mL of HNO_3 (TraceSELECT, Fluka) and 500 µL of H_2O_2 (TraceSELECT, Fluka). By subtracting the silver ions content to the total silver content we obtained the AgNPs concentration. Silver ions concentration was below the detection limit and AgNPs at 585±13 $mgAg.L^{-1}$. Detection limit (DL) was at 0.015 $\mu gAg.L^{-1}$ and variation coefficient on 6 replicates was better than 1%.

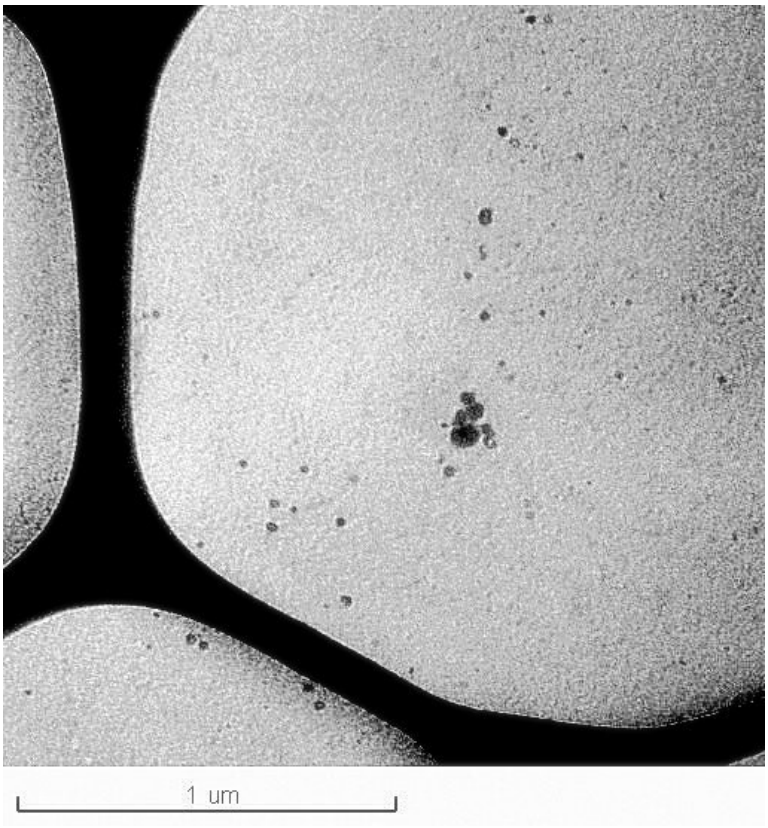

Figure 27: Transmission electron microscopy image of silver nanoparticles

Modified Thompson Tau test

The Modified Thompson Tau test is a method for deciding to keep or discard suspected outliers in a sample of a single variable (Cimbala, 2011). To determine the presence of an outlier in the data set, this procedure was used:

1. Determination of the sample mean $\bar{x}$ and standard deviation (S)

2. Determination of the absolute value of the deviation for each data point as

$$\delta_i = |d_i| = |x_i - \bar{x}|$$

The outlier is suspected when the data point has the maximum value of δ_i.

3. The value of the Modified Thompson Tau (τ) is calculated from the critical value of the student's *t* ($t_{\alpha/2}$) and is a function of the number of data points (n=480) in the sample, according to:

$$\tau = \frac{t_{\alpha/2} * (n-1)}{\sqrt{n} * \sqrt{n - 2 + t_{\alpha/2}^2}}$$

In this study, $t_{\alpha/2}$, the critical value of the student's *t*, is based on α=0.05, and τ was at 1.9572

4. To determine the outlier

If $\delta_i > \tau S$: data point is an outlier

If $\delta_i < \tau S$: data point is not an outlier

Table 7: Effects of AgNPs concentration on distance (l), interaction surface (πl^2) and time taken for interactions between nanoparticles for AgNPs at 10 $mgAg.L^{-1}$, 1 $mgAg.L^{-1}$, 100 $\mu gAg.L^{-1}$ and 10 $\mu gAg.L^{-1}$

	10 $mgAg.L^{-1}$ (92.7 µM)	**1 $mgAg.L^{-1}$ (9.27 µM)**	**100 $\mu gAg.L^{-1}$ (0.927 µM)**	**10 $\mu gAg.L^{-1}$ (0.0927 µM)**
Distance l (µm)	1.6	3.5	7.6	16.3
Interaction surface πl^2 (μm^2)	8.4	39	180	837
Time (s) in 0 mM NaCl solution	0.34	1.59	7.36	34.2
Time (s) in 500 mM NaCl solution	0.36	1.67	7.77	36.1

Table 8: Hydrodynamic diameter of aggregates calculated between 5 400 and 7 200 s (last 30 min) for kinetics of 2 h at 10 $mgAg.L^{-1}$, 1 $mgAg.L^{-1}$, 100 $\mu gAg.L^{-1}$ and 10 $\mu gAg.L^{-1}$ at 0, 10, 20, 30, 40, 50, 100, 200, 400 and 500 mM of NaCl

NaCl	10 $mgAg.L^{-1}$ (92.7 µM)	1 $mgAg.L^{-1}$ (9.27 µM)	100 $\mu gAg.L^{-1}$ (0.927 µM)	10 $\mu gAg.L^{-1}$ (0.0927 µM)
0 mM	17±3	19±5	18±3	18±5
10 mM	809±88	264±30	49±14	47±24
20 mM	720±62	273±36	79±24	53±21
30 mM	873±85	310±38	88±28	45±21
40 mM	814±115	321±31	73±18	52±20
50 mM	751±77	300±32	97±25	51±16
100 mM	810±94	326±31	100±28	63±23
200 mM	783±106	318±39	101±34	46±11
400 mM	885±95	298±23	142±38	66±29
500 mM	898±104	229±27	101±28	97±47
Average 10-500 mM	816±57	293±30	92±24	58±15

Table 9: Hydrodynamic diameter and proportions distribution of particle population less than 200 nm ($P_{0\text{-}200}$) and higher than 200 nm ($P_{200\text{-}10\ 000}$) observed between 5 400 and 7 200 s (last 30 min) for kinetics of 2 h at 10 mgAg.L^{-1}, 1 mgAg.L^{-1}, 100 µgAg.L^{-1} and 10 µgAg.L^{-1} at 0, 10, 20, 30, 40, 50, 100, 200, 400 and 500 mM of NaCl

		10 mgAg.L^{-1} (92.7 µM)		1 mgAg.L^{-1} (9.27 µM)		100 µgAg.L^{-1} (0.927 µM)		10 µgAg.L^{-1} (0.0927 µM)	
		$P_{0\text{-}200}$	$P_{200\text{-}10\ 000}$	$P_{0\text{-}200}$	$P_{200\text{-}10\ 000}$	$P_{0\text{-}200}$	$P_{200\text{-}10\ 000}$	$P_{0\text{-}200}$	$P_{200\text{-}10\ 000}$
0mM	***Dh* (nm)**	**16±1**	**451±241**	**16±1**	**344±92**	**17±1**	**384±92**	**18±2**	**288±47**
	Proportion (%)	99.9±0.1	0.1±0.1	99.8±0.1	0.1±0.1	99.7±0.1	0.2±0.1	99.9±0.1	0.1±0.1
10 mM	***Dh* (nm)**	**155±26**	**813±26**	**134±15**	**333±35**	**47±4**	**276±40**	**37±5**	**328±45**
	Proportion (%)	0.2±0.2	99.8±0.2	31.6±6.0	68.5±6.0	99.0±0.5	1.0±0.5	96.8±1.9	3.2±1.9
20 mM	***Dh* (nm)**	**152±37**	**724±17**	**152±14**	**316±16**	**67±5**	**277±48**	**41±4**	**286±46**
	Proportion (%)	0.2±0.2	99.8±0.2	21.9±4.5	78.1±4.5	94.7±2.2	5.3±2.2	96.2±1.7	3.8±1.7
30 mM	***Dh* (nm)**	**174±17**	**876±40**	**140±16**	**356±28**	**66±5**	**356±42**	**38±6**	**310±63**
	Proportion (%)	0.1±0.1	99.9±0.1	15.0±5.3	85.0±5.3	91.7±1.8	8.3±1.8	97.9±1.3	2.1±1.2
40 mM	***Dh* (nm)**	**146±24**	**816±34**	**139±22**	**346±9**	**60±5**	**315±37**	**46±9**	**247±21**
	Proportion (%)	0.2±0.2	99.8±0.2	10.7±4.1	89.3±4.1	95.0±1.1	5.0±1.1	97.0±1.8	3.0±1.8
50 mM	***Dh* (nm)**	**144±23**	**750±23**	**142±17**	**340±12**	**72±7**	**336±41**	**44±6**	**277±50**
	Proportion (%)	0.2±0.2	99.8±0.2	17.3±4.9	82.7±4.9	90.7±3.1	9.3±3.1	97.6±1.4	2.4±1.4
100 mM	***Dh* (nm)**	**148±25**	**809±28**	**147±21**	**353±10**	**69±4**	**379±68**	**51±9**	**274±41**
	Proportion (%)	0.1±0.1	99.9±0.1	10.7±3.4	90.0±4.3	90.2±1.8	9.8±1.8	95.1±3.3	4.9±3.3
200 mM	***Dh* (nm)**	**164±17**	**783±35**	**143±18**	**348±15**	**72±6**	**318±43**	**40±5**	**274±41**
	Proportion (%)	0.3±0.2	99.7±0.2	13.8±3.5	86.2±3.5	89.7±2.4	10.3±2.4	97.8±1.6	2.2±1.6
400 mM	***Dh* (nm)**	**159±22**	**886±50**	**147±16**	**328±10**	**87±6**	**344±67**	**45±10**	**299±53**
	Proportion (%)	0.2±0.2	99.8±0.2	14.0±2.7	86.0±2.7	80.7±4.0	19.3±4.0	91.7±6.2	8.3±6.2
500 mM	***Dh* (nm)**	**164±18**	**904±39**	**136±23**	**324±12**	**78±9**	**290±36**	**65±16**	**298±73**
	Proportion (%)	0.1±0.1	99.9±0.1	11.4±4.3	88.6±4.3	89.7±3.0	10.3±3.0	84.4±9.6	15.6±9.6
Average	***Dh* (nm)**	**156±9**	**818±58**	**142±5**	**338±13**	**69±11**	**321±34**	**45±8**	**288±22**
10-500 mM	Proportion (%)	0.2±0.1	99.8±0.1	16.3±6.4	83.8±6.4	91.3±4.8	8.8±4.8	94.9±4.1	5.1±4.1

ANNEXE II

SUPPORTING INFORMATION FOR EFFECTS OF CONCENTRATION AND CHEMICAL COMPOSITION OF NATURAL ORGANIC MATTER ON AGGREGATIVE BEHAVIOR OF SILVER NANOPARTICLES

Figure 28 present the linear regression between the slope ratio (SR) and the zeta potential of AgNPs in presence NOM. At 2.5 mgNOM.L^{-1} (Figure 28a) no correlation was observed between SR and the zeta potential ($p>0.005$). At 25 mgNOM.L^{-1} (Figure 28b) zeta potential was correlated with SR ($p<0.005$). Zeta potential was more negative with NOM having a lower SR. SR was inversely correlated to the average molecular weight of NOM. At 25 mgNOM.L^{-1}, the correlation indicates that the zeta potential was more negative in presence of NOM having a higher average molecular weight. NOM models described these compound as supramolecular aggregate containing different chemical functional groups. The correlation could be explained by the presence of chemical functional groups adding negative charges to the AgNPs. These functional groups could be carboxylic groups and some phenolic and alcohol functions ionized at pH 7.

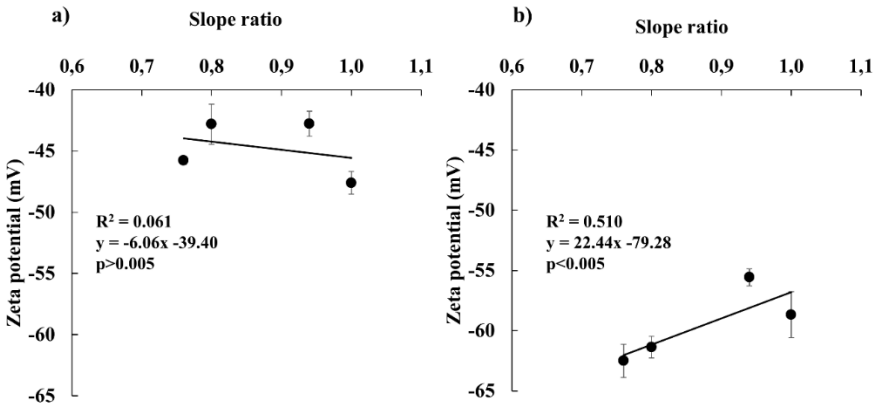

Figure 28: Linear regression between slope ratio and zeta potential (mV) at a) 2.5 mgNOM.L^{-1} in nanopure water and b) 25 mgNOM.L^{-1} in nanopure water

Table 10: Hydrodynamic diameter and proportions distribution of particle populations less than 200 nm ($P_{0\text{-}200}$) and higher than 200 nm ($P_{200\text{-}10\ 000}$) observed between 5 400 and 7 200 s (last 30 min) for kinetics of 2 h at 2.5 mgNOM.L^{-1}, of SLFA, SLHA, SL4ILE and SL4OBE at different NaCl concentration 0, 10, 20, 30, 40, 50, 100, 200, 400 and 500 mM

		SLFA		SLHA		SL4ILE		SL4IOBE	
		$P_{0\text{-}200}$	$P_{200\text{-}10\ 000}$	$P_{0\text{-}200}$	$P_{200\text{-}10\ 000}$	$P_{0\text{-}200}$	$P_{200\text{-}10\ 000}$	$P_{0\text{-}200}$	$P_{200\text{-}10\ 000}$
0 mM	**D_h (nm)**	**29±4**	**443±94**	**31±5**	**369±63**	**22±3**	**334±78**	**24±3**	**352±61**
	Proportion (%)	98±2	2±2	98±1	2±1	99±0.3	1±0.3	99±1	1±1
10 mM	**D_h (nm)**	**48±11**	**449±120**	**49±11**	**440±106**	**51±5**	**332±44**	**48±11**	**437±261**
	Proportion (%)	87±8	13±8	86±8	14±8	89±3	11±3	89±5	11±5
20 mM	**D_h (nm)**	**54±9**	**504±101**	**52±8**	**404±80**	**43±6**	**273±27**	**51±10**	**426±115**
	Proportion (%)	86±8	14±8	85±7	15±7	93±3	7±3	93±3	7±3
30 mM	**D_h (nm)**	**51±7**	**827±342**	**68±31**	**358±79**	**48±9**	**361±74**	**58±6**	**429±52**
	Proportion (%)	87±6	13±6	76±17	24±17	89±4	10±4	85±4	15±4
40 mM	**D_h (nm)**	**57±7**	**697±175**	**63±12**	**468±135**	**49±6**	**411±84**	**61±7**	**381±87**
	Proportion (%)	87±6	13±6	71±8	29±8	87±3	13±3	86±4	14±4
50 mM	**D_h (nm)**	**62±7**	**681±166**	**52±7**	**487±78**	**49±5**	**361±96**	**54±6**	**353±67**
	Proportion (%)	85±7	15±7	81±7	19±7	90±6	10±6	86±6	13±6
100 mM	**D_h (nm)**	**52±8**	**683±217**	**64±13**	**479±119**	**48±8**	**376±66**	**54±7**	**414±79**
	Proportion (%)	84±8	16±8	72±10	28±10	89±5	11±5	82±6	17±6
200 mM	**D_h (nm)**	**55±9**	**493±127**	**55±9**	**461±83**	**56±8**	**500±170**	**58±8**	**371±85**
	Proportion (%)	90±5	10±5	79±8	21±8	79±5	21±5	84±7	16±7
400 mM	**D_h (nm)**	**60±9**	**761±159**	**59±12**	**540±127**	**48±7**	**518±132**	**57±8**	**442±80**
	Proportion (%)	83±7	17±7	81±10	19±10	80±9	20±9	78±5	22±5
500 mM	**D_h (nm)**	**62±9**	**651±216**	**65±17**	**485±274**	**51±10**	**423±75**	**57±7**	**304±42**
	Proportion (%)	78±11	22±11	74±18	2618	79±8	21±8	84±5	16±5
Average 10-500 mM	**D_h (nm)**	**56±4**	**638±122**	**58±6**	**458±49**	**49±4**	**395±74**	**55±4**	**395±44**
	Proportion (%)	85±3	15±3	78±5	22±5	86±5	14±5	85±4	15±4

Table 11: Hydrodynamic diameter and proportions distribution of particle populations less than 200 nm ($P_{0\text{-}200}$) and higher than 200 nm ($P_{200\text{-}10\ 000}$) observed between 5 400 and 7 200 s (last 30 min) for kinetics of 2 h at 25 mgNOM.L^{-1}, of SLFA, SLHA, SL4ILE and SL4OBE at different NaCl concentration 0, 10, 20, 30, 40, 50, 100, 200, 400 and 500 mM

		SLFA		SLHA		SL4ILE		SL4IOBE	
		$P_{0\text{-}200}$	$P_{200\text{-}10\ 000}$	$P_{0\text{-}200}$	$P_{200\text{-}10\ 000}$	$P_{0\text{-}200}$	$P_{200\text{-}10\ 000}$	$P_{0\text{-}200}$	$P_{200\text{-}10\ 000}$
0 mM	**D_h (nm)**	**42±6**	**476±188**	**48±5**	**385±64**	**31±4**	**321±46**	**30±5**	**342±46**
	Proportion (%)	96±2	4±2	97±1	3±1	97±1	2±1	98±2	2±2
10 mM	**D_h (nm)**	**105±25**	**710±130**	**142±34**	**1070±119**	**50±8**	**519±96**	**36±5**	**304±60**
	Proportion (%)	17±7	83±7	0.6±0.5	99±0.5	79±6	21±6	97±1	3±1
20 mM	**D_h (nm)**	**118±27**	**813±102**	**184±9**	**1663±130**	**54±10**	**453±92**	**42±7**	**375±70**
	Proportion (%)	3±3	96±4	0.02±0.04	99.98±0.05	68±12	32±12	93±5	7±5
30 mM	**D_h (nm)**	**144±39**	**851±73**	**165±23**	**1524±173**	**52±15**	**459±95**	**48±6**	**385±67**
	Proportion (%)	2±3	98±3	0.2±0.2	99.8±0.2	78±10	22±10	90±5	10±5
40 mM	**D_h (nm)**	**141±50**	**983±92**	**175±8**	**1611±135**	**47±10**	**306±37**	**45±9**	**322±46**
	Proportion (%)	0.8±1.3	99.2±1.3	0.03±0.05	99.97±0.05	90±4	10±4	95±3	5±3
50 mM	**D_h (nm)**	**155±28**	**950±88**	**182±4**	**1780±236**	**42±11**	**266±36**	**45±6**	**357±46**
	Proportion (%)	0.4±0.4	99.6±0.4	0.1±0.2	99.9±0.2	96±3	4±3	91±5	9±5
100 mM	**D_h (nm)**	**117±25**	**1109±144**	**183±4**	**2022±173**	**53±10**	**431±80**	**61±14**	**573±161**
	Proportion (%)	1±0.8	99±0.8	0.1±0.1	99.9±0.1	80±9	20±9	78±13	22±13
200 mM	**D_h (nm)**	**150±17**	**984±107**	**163±17**	**1561±159**	**55±13**	**396±98**	**60±9**	**505±58**
	Proportion (%)	0.5±0.7	99.4±0.7	0.1±0.1	99.9±0.1	87±8	13±8	72±8	28±8
400 mM	**D_h (nm)**	**157±23**	**754±54**	**172±20**	**1669±176**	**72±13**	**428±171**	**77±16**	**723±170**
	Proportion (%)	2±3	97±3	0.1±0.1	99.9±0.1	83±7	16±7	60±13	40±13
500 mM	**D_h (nm)**	**109±24**	**808±108**	**174±18**	**1624±141**	**58±12**	**440±148**	**80±12**	**645±143**
	Proportion (%)	1±0.8	98±0.8	0.1±0.1	99.9±0.1	84±7	16±7	49±11	51±11
Average 10-500 mM	**D_h (nm)**	**113±19**	**885±122**	**171±12**	**1614±237**	**54±8**	**411±74**	**55±15**	**446±143**
	Proportion (%)	3±5	97±5	0.1±0.2	99.9±0.2	83±7	17±7	81±16	19±16

Table 12: Correlation between the principal components 1 and 2 (PC1 and PC2) and the variables

	Nanopure water		**500 mM NaCl**	
	PC1	PC2	PC1	PC2
$P_{0\text{-}200}$	0.114	0.106	0.558	-0.349
$P_{200\text{-}10\ 000}$	-0.115	-0.105	-0.558	0.349
$D_{h0\text{-}200}$	-0.306	0.172	-0.593	0.609
$D_{h200\text{-}10\ 000}$	-0.138	-0.116	-0.477	0.605
C	0.284	0.83	0.206	0.712
O	-0.567	-0.741	-0.472	-0.727
H	0.98	0.119	0.951	0.298
N	0.939	0.328	0.836	0.543
S	-0.503	0.863	-0.637	0.683
AliC	0.733	-0.637	0.859	-0.482
N-Alkyl/OCH_3	0.934	-0.306	0.928	-0.027
HOCH	-0.935	-0.199	-0.823	-0.477
O-C-O/O-CH-O	0.916	0.388	0.829	0.549
AromC	-0.638	0.597	-0.808	0.533
PhenolC	-0.401	0.909	-0.564	0.773
CAE	-0.847	-0.395	-0.693	-0.658
Ald/Ket	-0.904	0.013	-0.811	-0.306

ANNEXE III

SUPPORTING INFORMATION FOR BEHAVIOR OF SILVER NANOPARTICLES IN STRATIFIED ESTUARINE MESOCOSMS: PARTICLE SIZE DISTRIBUTION AND THE ROLE OF THE HALOCLINE

Table 13: Flow rates and salinities of water masses in the mesocosms

Layer	Mesocosms 1, 2, 3	Mesocosm 4*
Surface freshwater	Thickness = 75 cm Inflow = 0.5 $L.min^{-1}$ Salinity = 0-1 PSU	Thickness = 75 cm Inflow = 1.0 $L.min^{-1}$ Salinity = 14 PSU
Halocline	Thickness = 10 cm Outflow = 1 $L.min^{-1}$ Salinity = 1-28 PSU	Thickness = 10 cm Outflow = 2.0 $L.min^{-1}$ Salinity = 14-28 PSU
Bottom seawater	Thickness = 170 cm Inflow = 0.5 $L.min^{-1}$ Salinity = 28-30 PSU	Thickness = 170 cm Inflow = 1 $L.min^{-1}$ Salinity = 28-30 PSU

* Salinity of mesocosm 3 outflow water transferred to mesocosm 4 was 14±2 PSU.

Table 14: Size range, mean hydrodynamic diameter and proportion of particle populations $P_{0\text{-}200}$ and $P_{200\text{-}5\,000}$ in each mesocosm and water mass obtained over 35 days of experiment

		Mesocosm 1		**Mesocosm 2**		**Mesocosm 3**		**Mesocosm 4**	
		$P_{0\text{-}200}$	$P_{200\text{-}5\,000}$	$P_{0\text{-}200}$	$P_{200\text{-}5\,000}$	$P_{0\text{-}200}$	$P_{200\text{-}5\,000}$	$P_{0\text{-}200}$	$P_{200\text{-}5\,000}$
Surface water layer	Range (nm)	40-190	220-1 280	20-190	220-1 280	20-190	220-1 280	60-190	220-1 280
	D_h (nm)	100±19	522±76	71±14	521±106	68±13	517±98	126±43	616±92
	Proportion (%)	10±6	90±6	36±14	64±14	37±10	63±10	2±2	98±2
Halocline layer	Range (nm)	70-190	220-1 280	60-190	220-1 280	50-190	220-1 280	90-190	220-1 280
	D_h (nm)	145±39	672±101	130±38	727±150	108±43	671±117	139±27	593±76
	Proportion (%)	1±2	99±2	1±3	99±3	1±3	99±3	0.1±0.2	99.9±0.3
Bottom seawater layer	Range (nm)	50-190	220-1 100	60-190	220-1 100	40-190	220-1 100	80-190	220-1 100
	D_h (nm)	140±37	474±58	114±28	540±68	122±35	501±52	136±27	507±59
	Proportion (%)	2±2	98±2	0.3±0.6	100±0.6	3±5	97±5	1±1	99±1

Silver Nanoparticles Synthesis

Ten (10) mL of a solution of $AgNO_3$ (> 99%, Sigma-Aldrich) at 58.9 mM were added to 185 mL of nanopure water under reflux. At the recovery of boiling, 5 mL of a solution of sodium citrate (> 99%, Sigma-Aldrich) at 0.25% was added dropwise. After 3 h of reaction, the system was cooled down at room temperature. The yellow-dark solution was filtered on 0.2 µm polycarbonate filter (Whatman). The filtrate was centrifuged at 6 000 *g* for 15 min. The pellet was resuspended with 8 mL of nanopure water and centrifuged at 6 000 *g* during 15 min. This procedure was repeated three times to remove the excess of silver ions and citrate. After the purification process, the concentration of AgNPs and silver ions were determined by ICP-MS (Agilent 7500C^{TM}). Silver ion concentration was below the detection limit (0.015 µgAg.L^{-1}).

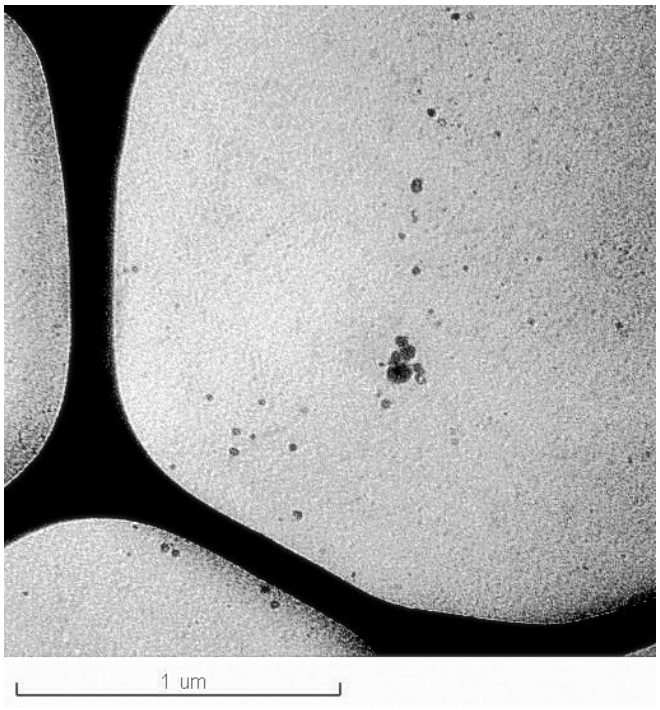

Figure 29: Transmission electron microscopy image of silver nanoparticles

Effects of AgNPs concentrations on dynamic light scattering analysis

Dynamic light scattering (DLS) is a mature and accepted technique that is used to determine the particle size distribution (PSD) profile and the aggregation stage of nanoparticles colloidal suspensions. Most of DLS measurements of nanoparticles are done at nanomaterials concentrations higher than 100 $\mu g.L^{-1}$. The measurement at low nanoparticles concentrations could be a difficult task for many reasons. As described by Xu (2015), for extremely dilute suspensions, if the number of particles is so small that the number fluctuation produces a scattering intensity fluctuation larger than that produced by Brownian motion, normal DLS experiment cannot be performed. At some low concentrations, the sample would not produce enough signal to detect the scattering from the nanoparticles beyond the random noise from the solvent. At low concentration, the sample is highly sensitive to large particles like dusts or other impurities in the solution because they produce intense scattering. In this last case, the intensity from larger particles overshadows the signal from smaller ones. Considering the important constraints presented, it was determined by a series of preliminary measurements that the best approach was to make a study of the DLS intensity at various AgNP concentrations to determine the lowest concentration amenable to DLS and to find the range of concentrations for which the size of AgNPs would be independent of concentrations.

Figure 30 shows the variation of the DLS signal (kilocounts per second, kcps, normalized for 100% of light intensity) for different AgNP concentrations (from 10 to 10 000 $\mu gAg.L^{-1}$) in filtered nanopure water. In absence of AgNPs, the solvent produced a "blank" count rate of 20 kcps. The presence of AgNPs increased the signal to 280 kcps at 10 $\mu gAg.L^{-1}$ and 170 000 kcps at 10 000 $\mu gAg.L^{-1}$. At 10 $\mu gAg.L^{-1}$, the signal/noise ratio was 14/1, higher than the ratio of 10 suggested by Hassan *et al.* (2015) for DLS and much more than the usual ratio 3/1 used to determine the limit of detection in analytical chemistry. Figure 30 also shows the volume averaged hydrodynamic diameter measured at each AgNP

concentration. Whatever was the AgNP concentration, the hydrodynamic diameter was at 20 nm (Tukey test, $p>0.05$). Moreover, the intercept of autocorrelograms was always comprised between 0.7 and 1 (data not shown). These data indicate that the light scattered by AgNPs at 10 µgAg.L^{-1} gave a sufficient signal to allow D_h measurements at low AgNPs levels.

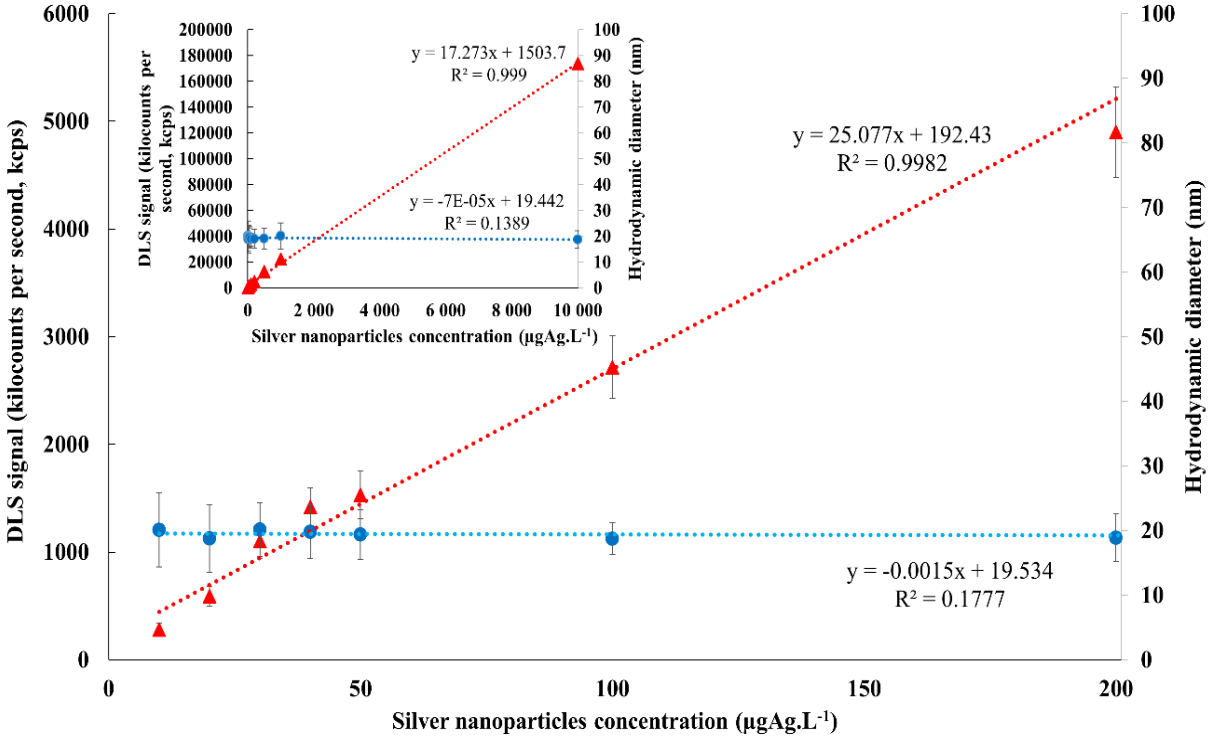

Figure 30: DLS signal (red triangle) and average hydrodynamic diameter (blue circle) at various AgNPs concentrations

The feasibility to detect AgNPs at 10 µgAg.L^{-1} in brackish water have been tested. Figure 31 shows the particle size distribution, in volume size distribution, and the cumulative frequency measured just after the addition of AgNPs at 10 µgAg.L^{-1} in saline solution at 10, 50 and 400 mM NaCl. These NaCl concentrations corresponded to salinity at 0.6, 2.9 and 23 PSU typical of estuarine waters. Before the addition of AgNPs in salty solutions, the count rate was near 20 kcps. The addition of AgNPs in these solutions increased the count rate to 300 kcps. This value was similar to the DLS signal measured when AgNPs was added at 10 µgAg.L^{-1} in nanopure water (Figure 30). In aggregate size distribution, two populations of particles were observed. First one was formed by small particles mostly between 8 and 164 nm and the second one was formed by particles with sizes mainly between 220 and 1 280 nm. The contribution of small particles was 95% at 10 mM, and 93% at 400 mM. The average diameter of the small particles were 34, 39 and 41 nm at 10, 50 and 400 mM NaCl, respectively. These higher hydrodynamic diameters, compared to zero salinity, were indicative of aggregation of AgNPs in salty water. For the second population of large particles, the average diameter was near 370 nm independently of NaCl concentration. The larger sizes corresponded to large autoaggregates of AgNPs. These data suggest that a continuous addition of AgNPs at 10 µgAg.L^{-1} in brackish water could give a persistent PSD fingerprint where small particles can be detected by DLS.

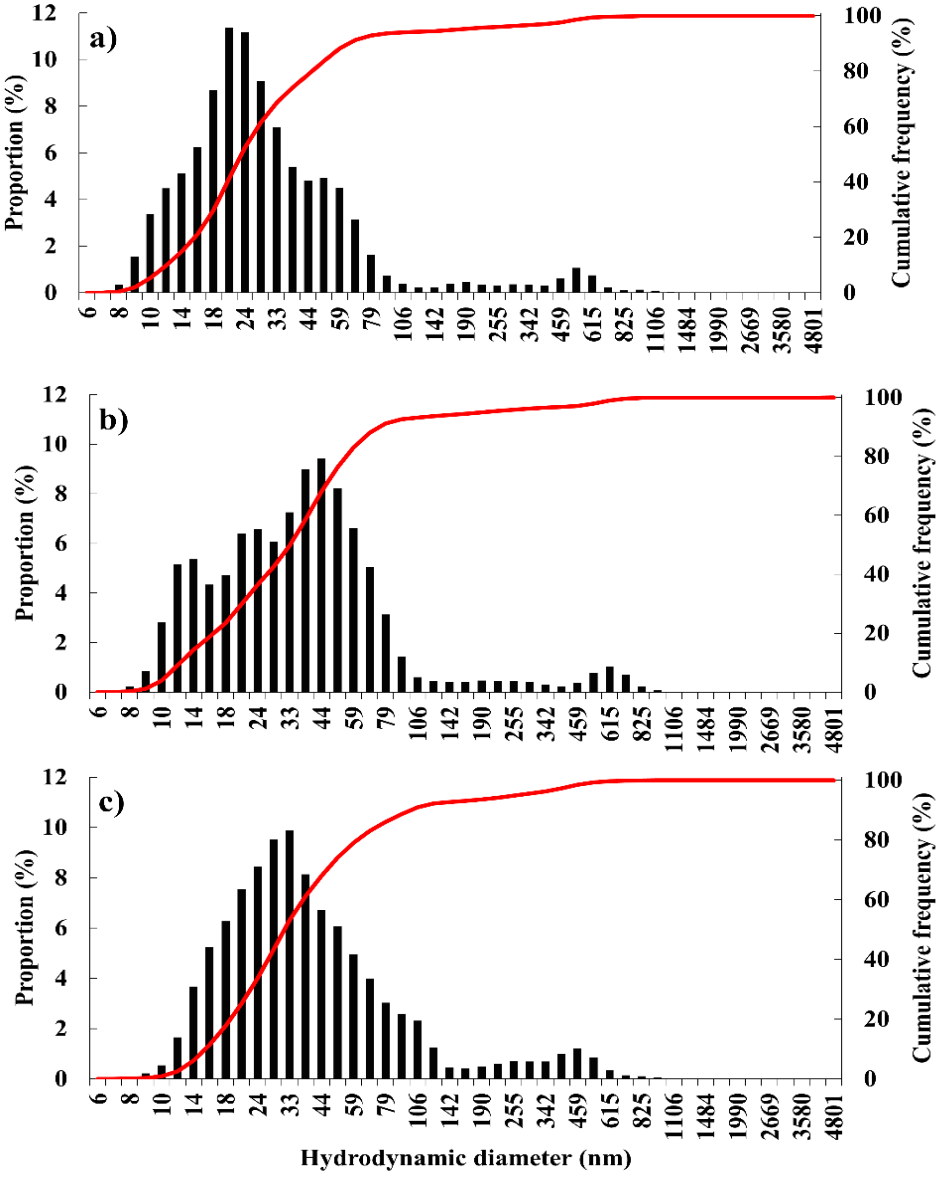

Figure 31: Particle size distributions (black lines) and cumulative frequency plots (red curve) of 10 µAg.L^{-1} of AgNPs in a) 10 mM NaCl; b) 50 mM NaCl and c) 400 mM NaCl. These NaCl concentrations corresponded to salinity at 0.6, 2.9 and 23 PSU. Measurement of particle size distribution of AgNPs was performed directly after the addition of AgNPs

Particle size distribution observed in different water masses in mesocosms

The selection of the appropriate way to express DLS results revealed to be a difficult task. The DLS technique measures the fluctuation of the light intensity scattered by particles in a colloidal suspension over time. Depending on the composition of the suspension and the data fitting algorithm used, few important features are obtained for monodispersed and polydispersed samples. In the simplest, but rare case of perfectly monodisperse samples, the use of cumulant method provides the Z-average size of the sample and polydispersity index (PDI). Z-average size is a unique mean value for every sample and PDI is an estimation of the width of the PSD in samples (Bhattacharjee, 2016; Malvern, 2013a). When available for monodispersed samples, these parameters should be used as recommended by the International Organization for Standardization in ISO 13321 (ISO13321:1996(E), 1996). For heterogeneous and polydispersed samples, it is not possible to use cumulant method (Hassan *et al.,* 2015; Xu, 2001b) and other mathematical treatments must be used to extract PSD from DLS signals. Methods like non-negatively constrained least-square (NNLS), exponential sampling and CONTIN allow to estimate PSD of samples (Hassan *et al.,* 2015; Xu, 2001b). The use of an appropriate method transforms the DLS signals into PSD linked primarily to intensity weighted distributions (Hassan *et al.,* 2015). This intensity distribution describes how much light is scattered by the particles in relation to the different size classes (bins) selected by the analyst to describe the polydispersity. Intensity distribution can be converted in volume distribution or in number distribution to estimate the total volume of particles or the number of particles in the different size classes. The PSD obtained are very useful and can be used as a guide to infer the nature of polydispersity in samples and help to determine the appropriate range of particle sizes in each peak of the multimodal distribution (Hassan *et al.,* 2015).

The DLS is based on the measure of the intensity of scattered light and not upon particles counting. Hence, intensity based PSD is very representative of the raw signal and

should be used for monodispersed samples. However, intensity based results are biased toward detecting larger particles within polydispersed suspensions (Anderson *et al.,* 2013). As a result, a small amount of large particles can mask the presence of numerous small particles. In the case of environmental samples where tiny to bulky particles coexist this is an important disadvantage. However, Tomaszewska *et al.* (2013) have detected the presence of small particles if the proportion of small/large particles is lower than 4%. A way to decrease the dependence of PSD to large particles is to express the results in volume distribution. In that case, the PSD is related to the size of the particle to the third power instead to the sixth power in the case of intensity (Malvern, 2009). Even if the effect of large particles can be minimized by using volume based PSD, the analysis should always be limited by restricted resolution of the DLS. DLS technique cannot discriminate particles with diameters differing by less than 3 folds (Anderson *et al.,* 2013; Baalousha and Lead, 2012). In environmental samples, many particles differ by more than 3 folds. For instance, iron oxide like ferrihydrite occurs in oxygenated aqueous solution in a narrow size distribution of 2-7 nm or clay-sized fraction defined as particles smaller than 2 μm (Montano *et al.,* 2014). In this study, the DLS analysis cannot discriminate AgNPs particles between 20 and 60 nm. However, the particles between 20-60 nm are clearly discriminated from particles with hydrodynamic diameters larger than 200 nm.

In this study, the DLS results are given in volume size distribution. Figure 32 shows PSD obtained during the first week of the long-term experiment for control mesocosm 1. Two particle populations were observed. A first population was detected between 10 and 164 nm and the second one between 220 and 1 280 nm. In Figure 33, the cumulative frequency of particle distribution from Figure 32 is presented. We observed an increase of cumulative frequency for small particles that reached a plateau for sizes smaller than 200 nm. For bigger particles, a sharp increase in cumulative frequency is observed that also reached a plateau. The same scheme on average cumulative frequency is obtained over 35 days of AgNP addition for each water masses of each mesocosm as shown in Figure 34. These data

validate the presence of two particle populations with PSD between 20 and 190 nm for the first population and between 220 and 5 000 nm for the second one. These distributions are called $P_{0\text{-}200}$ and $P_{200\text{-}5\,000}$. The value of 200 nm was chosen as a limit between the two populations because we have rarely observed particles between 190 and 220 nm. Absence of particles with D_h superior to 5 000 nm is explained by filtration at 5 µm. The average hydrodynamic diameter for these two particle populations, identified as $D_{h0\text{-}200}$ and $D_{h200\text{-}5\,000}$, were calculated by a weighted arithmetic mean between 0 and 190 nm for $P_{0\text{-}200}$ and between 220 and 5 000 nm for $P_{200\text{-}5\,000}$.

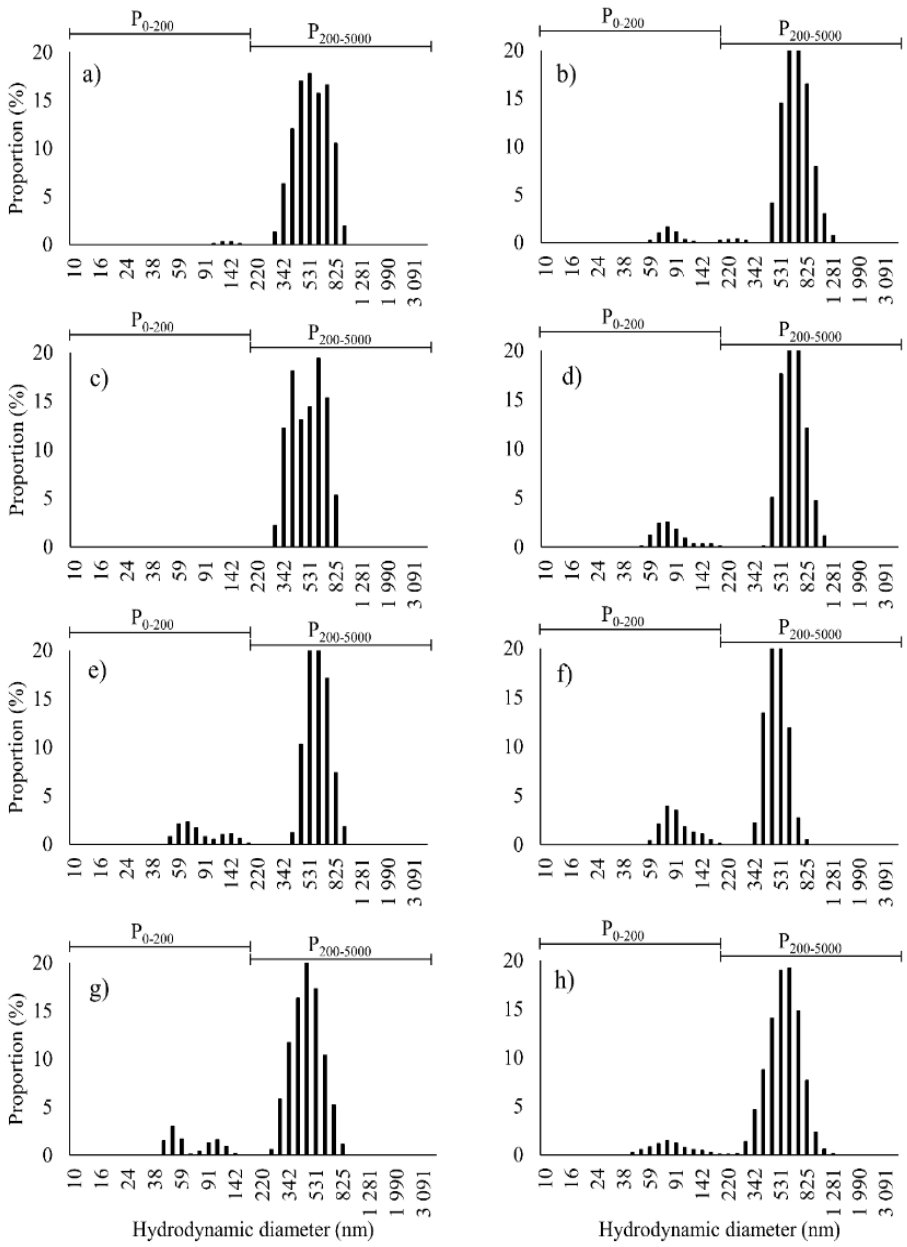

Figure 32: Particle size distributions observed in surface freshwater layer of mesocosm 1, during one week a) July 9, b) July 10, c) July 11, d) July 12, e) July 13, f) July 15, g) July 16 and h) the results averaged for the week

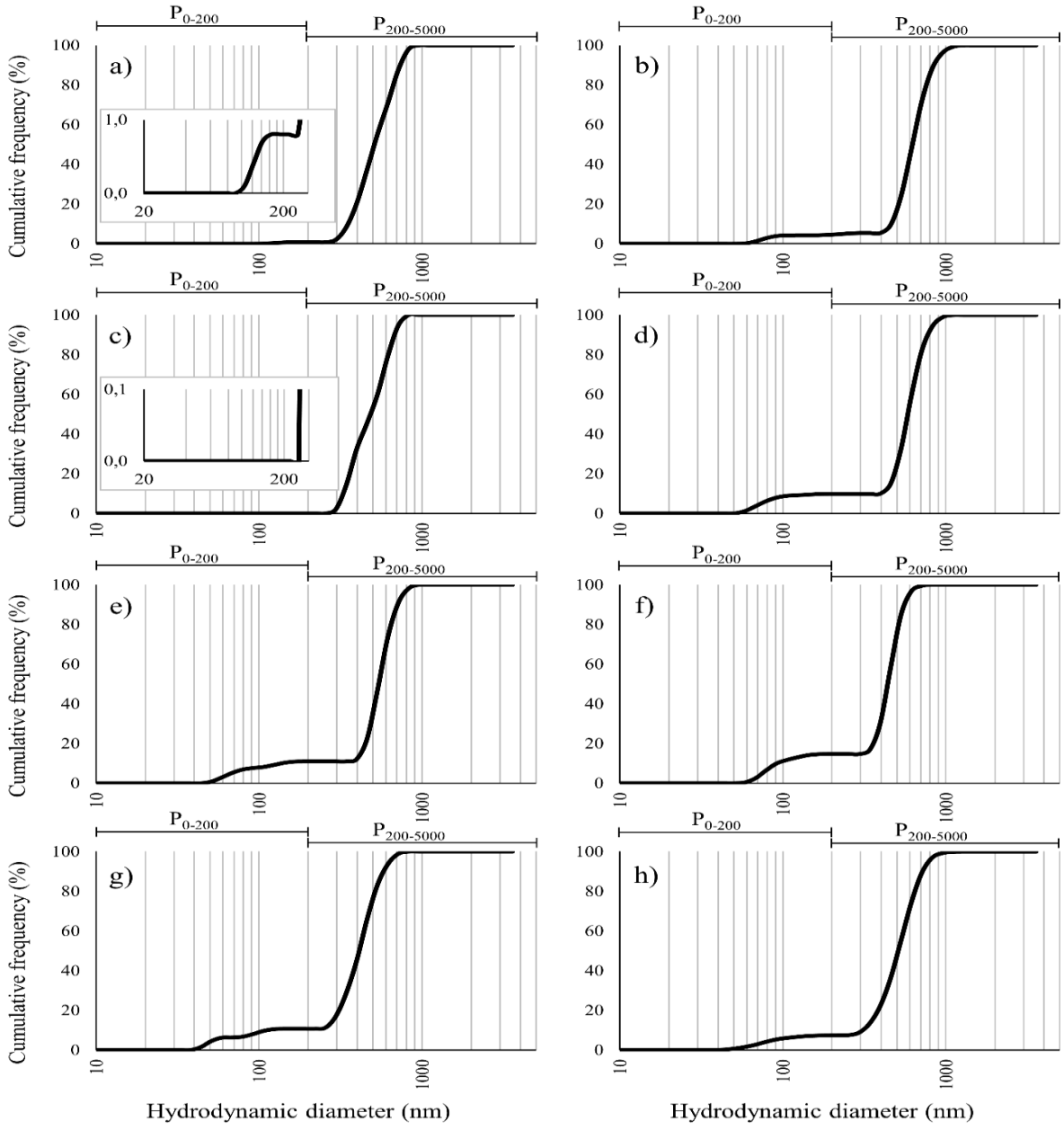

Figure 33: Cumulative frequency plots of particle size distributions observed in surface freshwater layer of mesocosm 1, during one week a) July 9, b) July 10, c) July 11, d) July 12, e) July 13, f) July 15, g) July 16 and h) the results averaged for the week. Some cumulative frequencies between 20 and 200 nm have been magnified to show the presence of small particles

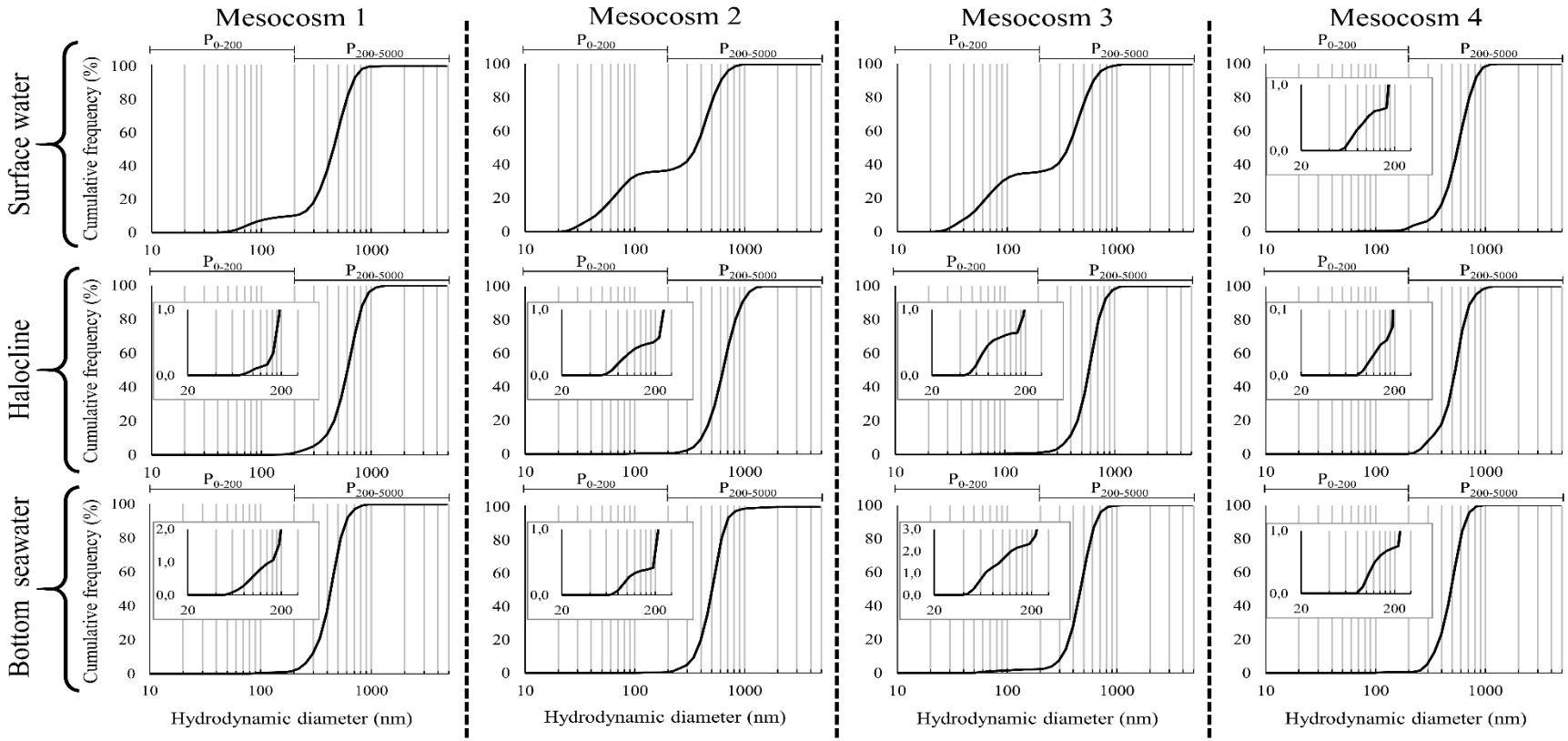

Figure 34: Average cumulative frequency plots of particle size distributions, obtained over 35 days of experiment, observed in mesocosms 1, 2, 3 and 4 in surface water, halocline and bottom seawater. Some cumulative frequencies between 20 and 200 nm have been magnified to show the presence of small particles

Salinity profile in mesocosm 4

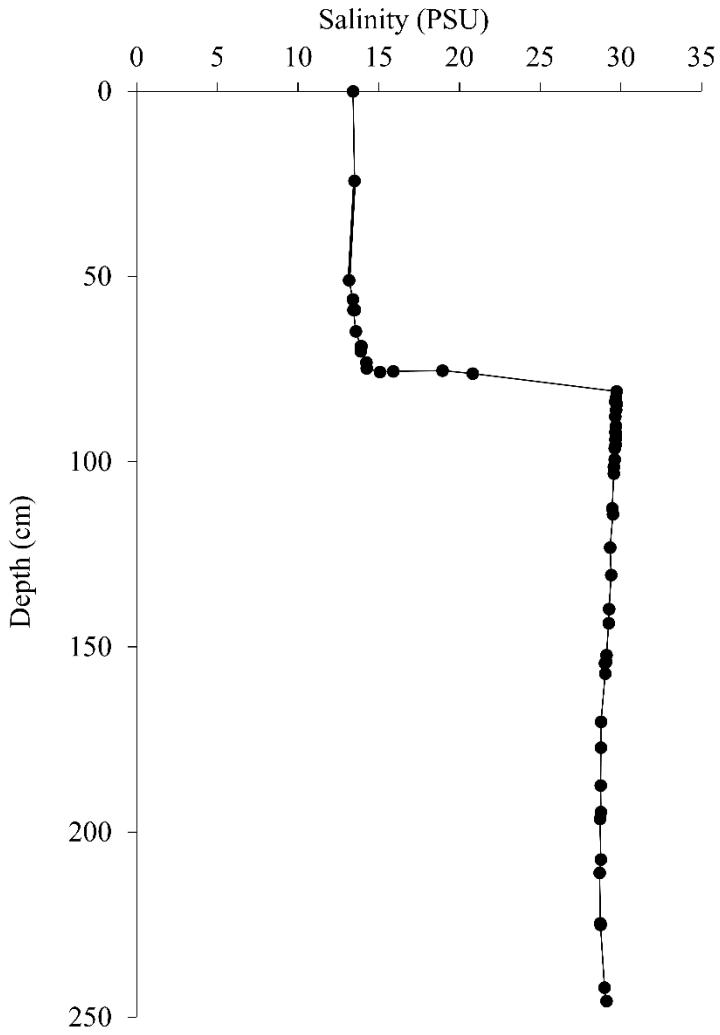

Figure 35: Salinity profile in mesocosm 4

Detection of silver nanoparticles in aqueous sample in presence of clay

Figure 36 shows the proportion and the PSD of clay suspension at 10 mgclay.L^{-1} in absence and in presence of AgNPs added at 10 µgAg.L^{-1}. In absence of AgNPs, the clay suspension shown a monomodal PSD with clay particles distributed between 615 and 1 100 nm. The average D_h was at 997 nm. According to this D_h, the concentration and a density of 2.5 g.cm^{-3}, the particle concentration was estimated at 7.7 x 10^6 particles.mL^{-1}. The addition of AgNPs induced a modification in PSD where multimodal distribution is observed. A first peak in particle distribution was between 13 and 33 nm, a second peak was in the range 38 to 190 nm and a third peak is seen between 615 and 1 100 nm. The averages D_h of these three populations were 25, 72 and 1 000 nm. The addition of AgNPs induced the presence of particles between 0 and 200 nm. The third peak had particle sizes in the same range as clay without AgNPs. This experiment shows that DLS measures the presence of clay and AgNPs and allows them to be discriminated. In this test, 10 µgAg.L^{-1} of AgNPs with a D_h at 20 nm and a density of 10.5 g.cm^{-3} results in the presence of 2.3 x 10^8 particles.mL^{-1}. Thus, this experiment has been done with 29 folds more AgNPs than clay. With this proportion of different particles, it has been possible to detect the presence of AgNPs.

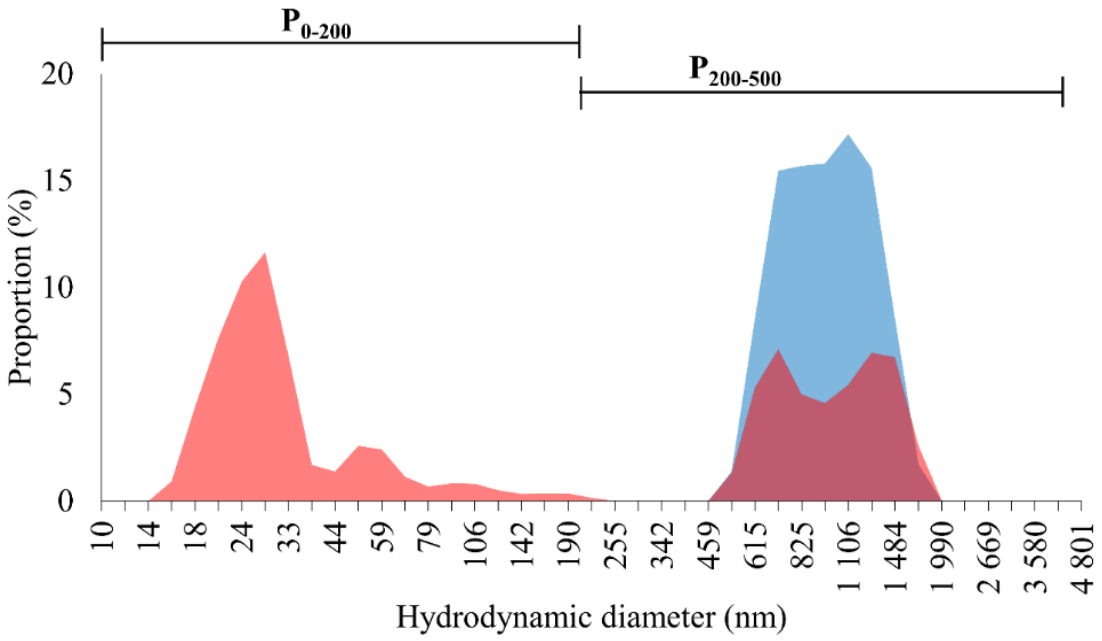

Figure 36: Particle size distributions of clay in absence (blue) and in presence (red) of 10 µAg.L^{-1} of AgNPs in dechlorinated water. Analysis of particle size distributions of clay with AgNPs was performed directly after the addition of AgNPs

RÉFÉRENCES BIBLIOGRAPHIQUES

Adegboyegs, N.F., Sharma, V.K., Siskova, K., Zboril, R., Sohn, M., Schultz, B.J., Banerjee, S., 2013. Interactions of aqueous Ag^+ with fulvic acids : Mechanisms of silver nanoparticle formation and investigation of stability. *Environmental Science & Technology* 47(2), 757–764. DOI: 10.1021/es302305f

Aiken, G.R., Thurman, E.M., Malcolm, R.L., Walton, H.F., 1979. Comparison of XAD macroporous resins for the concentration of fulvic acid from aqueous solution. *Analytical Chemistry* 51(11), 1799–1803. DOI: 10.1021/ac50047a044

Akaighe, N., Depner, S.W., Banerjee, S., Sharma, V.K., Sohn, M., 2012. The effects of monovalent and divalent cations on the stability of silver nanoparticles formed from direct reduction of silver ions by Suwannee River humic acid/natural organic matter. *Science of the Total Environment* 441, 277–289. DOI: 10.1016/j.scitotenv.2012.09.055

Akaighe, N., Maccuspie, R.I., Navarro, D.A., Aga, D.S., Banerjee, S., Sohn, M., Sharma, V.K., 2011. Humic acid-induced silver nanoparticle formation under environmentally relevant conditions. *Environmental Science & Technology* 45(9), 3895–3901. DOI: 10.1021/es103946g

Al-Sid-Cheikh, M., Pelletier, É., Rouleau, C., 2011. Synthesis and characterization of [^{110m}Ag]-nanoparticles with application to whole-body autoradiography of aquatic organisms. *Applied Radiation and Isotopes* 69(10), 1415–1421. DOI: 10.1016/j.apradiso.2011.06.017

Alexander, J.W., 2009. History of the medical use of silver. *Surgical Infections* 10(3), 289–292. DOI: 10.1089/sur.2008.9941

Aluwihare, L.I., Repeta, D.J., Chen, R.F., 2002. Chemical composition and cycling of dissolved organic matter in the Mid-Atlantic Bight. *Deep-Sea Research Part II: Topical Studies in Oceanography* 49(20), 4421–4437. DOI: 10.1016/S0967-0645(02)00124-8

Alvarez-Puebla, R.A., Valenzuela-Calahorro, C., Garrido, J.J., 2006. Theoretical study on fulvic acid structure, conformation and aggregation. A molecular modelling approach. *Science of the Total Environment* 358(1–3), 243–254. DOI: 10.1016/j.scitotenv.2004.11.026

Amini, R., Brar, S.K., Cledon, M., Surampalli, R.Y., 2016. Intertechnique comparisons for nanoparticle size measurements and shape distribution. *Journal of Hazardous, Toxic, and Radioactive Waste* 20(1), 1–8. DOI: 10.1061/(ASCE)HZ.2153-5515.0000286.

Anderson, W., Kozak, D., Coleman, V.A., Jämting, Å.K., Trau, M., 2013. A comparative study of submicron particle sizing platforms: Accuracy, precision and resolution analysis of polydisperse particle size distributions. *Journal of Colloid and Interface Science* 405, 322–330. DOI: 10.1016/j.jcis.2013.02.030

Baalousha, M., Arkill, K.P., Romer, I., Palmer, R.E., Lead, J.R., 2015. Transformations of citrate and Tween coated silver nanoparticles reacted with Na_2S. *Science of the total environment* 502, 344–353. DOI: 10.1016/j.scitotenv.2014.09.035

Baalousha, M., Lead, J.R., 2012. Rationalizing nanomaterial sizes measured by atomic force microscopy, flow field-flow fractionation, and dynamic light scattering: Sample preparation, polydispersity and particle structure. *Environmental Science & Technology* 46(11), 6134–6142. DOI: 10.1021/es301167x

Baalousha, M., Motelica-Heino, M., Coustumer, P.L., 2006. Conformation and size of humic

substances: Effects of major cation concentration and type, pH, salinity, and residence time. *Colloids and Surfaces A: Physicochemical and Engineering Aspects* 272(1–2), 48–55. DOI: 10.1016/j.colsurfa.2005.07.010

Baalousha, M., Nur, Y., Römer, I., Tejamaya, M., Lead, J.R., 2013. Effect of monovalent and divalent cations, anions and fulvic acid on aggregation of citrate-coated silver nanoparticles. *Science of the Total Environment* 454–455, 119–131. DOI: 10.1016/j.scitotenv.2013.02.093

Baalousha, M., Sikder, M., Prasad, A., Lead, J., Merrifield, R., Chandler, G.T., 2016. The concentration-dependent behaviour of nanoparticles. *Environmental Chemistry* 13(1), 1–3. DOI: 10.1071/EN15142

Bae, E., Park, H.J., Yoon, J., Kim, Y., Choi, K., Yi, J., 2010. Bacterial uptake of silver nanoparticles in the presence of humic acid and $AgNO_3$. *Korean Journal of Chemical Engineering* 28(1), 267–271. DOI: 10.1007/s11814-010-0351-z

Balnois, E., Wilkinson, K.J., Lead, J.R., Buffle, J., 1999. Atomic force microscopy of humic substances: Effects of pH and ionic strength. *Environmental Science & Technology* 33(21), 3911–3917. DOI: 10.1021/es990365n

Barnes, W.L., Dereux, A., Ebbesen, T.W., 2003. Surface plasmon subwavelength optics. *Nature* 424(6950), 824–30. DOI: 10.1038/nature01937

Beaudoin, G.J., Chavanne, M., Jullien, A., Flamand, E., 1987. Analyse qualitative par voie chimique, in: Modulo (Ed.), *Chimie Organique Expérimentale*. pp. 461–503.

Benn, T.M., Westerhoff, P., 2008. Nanoparticle silver released into water from commercially available sock fabrics. *Environmental Science & Technology* 42(11), 4133–4139. DOI: 10.1021/es7032718

Bhatt, I., Tripathi, B.N., 2011. Interaction of engineered nanoparticles with various components of the environment and possible strategies for their risk assessment. *Chemosphere* 82(3), 308–317. DOI: 10.1016/j.chemosphere.2010.10.011

Bhattacharjee, S., 2016. DLS and zeta potential - What they are and what they are not? *Journal of Controlled Release* 235, 337–351. DOI: 10.1016/j.jconrel.2016.06.017

Bianchi, T.S., 2007. *Biogeochemistry of Estuaries*. Oxford University Press, New York pp.687.

Blaser, S.A., Scheringer, M., MacLeod, M., Hungerbühler, K., 2008. Estimation of cumulative aquatic exposure and risk due to silver: Contribution of nano-functionalized plastics and textiles. *Science of the Total Environment* 390(2–3), 396–409. DOI: 10.1016/j.scitotenv.2007.10.010

Boerschke, R.C., Gallie, E.A., Belzile, N., Gedye, R.N., Morris, J.R., Lake, R., 1996. Quantitative elemental and structural analysis of dissolved organic carbon fractions from lakes near Sudbury, Ontario. *Canadian Journal of Chemistry* 74, 2460–2470. DOI: 10.1139/v96-275

Bone, A.J., Colman, B.P., Gondikas, A.P., Newton, K.M., Harrold, K.H., Cory, R.M., Unrine, J.M., Klaine, S.J., Matson, C.W., Di Giulio, R.T., 2012. Biotic and abiotic interactions in aquatic microcosms determine fate and toxicity of Ag nanoparticles: Part 2-toxicity and Ag speciation. *Environmental Science & Technology* 46(13), 6925–6933. DOI: 10.1021/es204683m

Bradford, A., Handy, R.D., Readman, J.W., Atfield, A., Mühling, M., 2009. Impact of silver nanoparticle contamination on the genetic diversity of natural bacterial assemblages in estuarine sediments. *Environmental Science & Technology* 43(12), 4530–4536. DOI: 10.1021/es9001949

Brar, S.K., Verma, M., Tyagi, R.D., Surampalli, R.Y., 2010. Engineered nanoparticles in wastewater and wastewater sludge - evidence and impacts. *Waste Management* 30(3), 504–520. DOI: 10.1016/j.wasman.2009.10.012

Brigante, M., Zanini, G., Avena, M., 2007. On the dissolution kinetics of humic acid particles: Effects of pH, temperature and Ca^{2+} concentration. *Colloids and Surfaces A: Physicochemical and Engineering Aspects* 294(1–3), 64–70. DOI: 10.1016/j.colsurfa.2006.07.045

Buffet, P.-E.P.E., Zalouk-Vergnoux, A., Châtel, A., Berthet, B., Métais, I., Perrein-Ettajani, H., Poirier, L., Luna-Acosta, A., Thomas-Guyon, H., Risso-de Faverney, C., Guibbolini, M., Gilliland, D., Valsami-Jones, E., Mouneyrac, C., 2014. A marine mesocosm study on the environmental fate of silver nanoparticles and toxicity effects on two endobenthic species: The ragworm *Hediste diversicolor* and the bivalve mollusc *Scrobicularia plana*. *Science of the Total Environment* 470–471, 1151–1159. DOI: 10.1016/j.scitotenv.2013.10.114

Buffle, J., 1977. Les substances humiques et leurs interactions avec les ions mineraux, in: *Conférence Proceedings de La Commission d'Hydrologie Appliquée de A.G.H.T.M.* Université d'Orsay, Paris, pp. 3–10.

Buffle, J., Leppard, G.G., 1995. Characterization of aquatic colloids and macromolecules. 1. Structure and behavior of colloidal material. *Environmental Science & Technology* 29(9), 2169–2175. DOI: 10.1021/es00009a004

Buffle, J., Wilkinson, K.J., Stoll, S., Filella, M., Zhang, J., 1998. A generalized description of aquatic colloidal interactions: The three-colloidal component approach. *Environmental Science and Technology* 32(19), 2887–2899. DOI: 10.1021/es980217h

Byrne, M., 2012. Global change ecotoxicology: Identification of early life history bottlenecks

in marine invertebrates, variable species responses and variable experimental approaches. *Marine Environmental Research* 76, 3–15. DOI: 10.1016/j.marenvres.2011.10.004

Cascio, C., Gilliland, D., Rossi, F., Calzolai, L., Contado, C., 2014. Critical experimental evaluation of key methods to detect, size and quantify nanoparticulate silver. *Analytical Chemistry* 86(24), 12143–12151. DOI: 10.1021/ac503307r

Cauwet, G., 2002. DOM in the coastal zone, in: Hansell, D.A., Carlson, C.A. (Eds.), *Biogeochemistry of Marine Dissolved Organic Matter*. Academic Press, San Diego, pp. 579–609.

Chambers, B.A., Afrooz, A.R.M.N., Bae, S., Aich, N., Katz, L., Saleh, N.B., Kirisits, M.J., 2014. Effects of chloride and ionic strength on physical morphology, dissolution, and bacterial toxicity of silver nanoparticles. *Environmental Science and Technology* 48(1), 761–769. DOI: 10.1021/es403969x

Chang, R., Goldsby, K.A., 2014. *Chimie des solutions*, 4th ed. McGraw-Hill Companies pp.476.

Chen, K.L., Elimelech, M., 2006. Aggregation and deposition kinetics of fullerene (C_{60}) nanoparticles. *Langmuir* 22(26), 10994–1001. DOI: 10.1021/la062072v

Chen, S.-F., Zhang, H., 2012. Aggregation kinetics of nanosilver in different water conditions. *Advances in Natural Sciences: Nanoscience and Nanotechnology* 3(3), 035006. DOI: 10.1088/2043-6262/3/3/035006

Chen, Y., Huang, Y., Li, K., 2012. Temperature effect on the aggregation kinetics of CeO_2 nanoparticles in monovalent and divalent electrolytes. *Environmental and Analytical Toxicology* 2(7), 1–5. DOI: 10.4172/2161-0525.1000158

Chen, Y., Schnitzer, M., 1976. Scanning electron microscopy of a humic acid and of a fulvic acid and its metal and clay complexes. *Soil Science Society of America Journal* 40(5), 682–686. DOI: 10.2136/sssaj1976.03615995004000050024x

Cimbala, J.M., 2011. Outliers pp.1-5.

Cleveland, D., Long, S.E., Pennington, P.L., Cooper, E., Fulton, M.H., Scott, G.I., Brewer, T., Davis, J., Petersen, E.J., Wood, L., 2012. Pilot estuarine mesocosm study on the environmental fate of silver nanomaterials leached from consumer products. *Science of the Total Environment* 421–422, 267–272. DOI: 10.1016/j.scitotenv.2012.01.025

Coll, C., Notter, D., Gottschalk, F., Sun, T., Som, C., Nowack, B., 2016. Probabilistic environmental risk assessment of five nanomaterials (nano-TiO_2, nano-Ag, nano-ZnO, CNT, and fullerenes). *Nanotoxicology* 10(4), 436–444. DOI: 10.3109/17435390.2015.1073812

Colman, B.P., Arnaout, C.L., Anciaux, S., Gunsch, C.K., Hochella, M.F., Kim, B., Lowry, G.V., McGill, B.M., Reinsch, B.C., Richardson, C.., Unrine, J.M., Wright, J.P., Yin, L., Bernhardt, E.S., 2013. Low concentrations of silver nanoparticles in biosolids cause adverse ecosystem responses under realistic field scenario. *PloS ONE* 8(2), e57189. DOI: 10.1371/journal.pone.0057189

Colombo, C., Palumbo, G., Angelico, R., Cho, H.G., Francioso, O., Ertani, A., Nardi, S., 2015. Spontaneous aggregation of humic acid observed with AFM at different pH. *Chemosphere* 138, 821–828. DOI: 10.1016/j.chemosphere.2015.08.010

Conte, P., Piccolo, A., 1999. Conformational arrangement of dissolved humic substances. Influence of solution composition on association of humic molecules. *Environmental Science & Technology* 33(10), 1682–1690. DOI: 10.1021/es9808604

D'Anglejan, B., Ingram, R.G., 1976. Time-depth variations in tidal flux of suspended matter

in the Saint Lawrence estuary. *Estuarine and Coastal Marine Science* 4, 401–416. DOI: 10.1016/0302-3524(76)90015-3

Dale, A.L., Lowry, G.V., Casman, E.A., 2013. Modeling nanosilver transformations in freshwater sediments. *Environmental Science & Technology* 47(22), 12920–12928. DOI: 10.1021/es402341t

Das, P., Williams, C.J., Fulthorpe, R.R., Hoque, M.E., Metcalfe, C.D., Xenopoulos, M.A., 2012a. Changes in bacterial community structure after exposure to silver nanoparticles in natural waters. *Environmental Science & Technology* 46(16), 9120–9128. DOI: 10.1021/es3019918

Das, P., Xenopoulos, M.A., Williams, C.J., Hoque, M.E., Metcalfe, C.D., 2012b. Effects of silver nanoparticles on bacterial activity in natural waters. *Environmental Toxicology and Chemistry* 31(1), 122–130. DOI: 10.1002/etc.716

Davies, G., Ghabbour, E.A., Khairy, K.A., 2014. *Humic Substances Structures, Properties and Uses*, 2nd ed, Royal Society of Chemistry. Royal Society of Chemistry, Cornwall pp.255. DOI: 10.1016/B978-0-444-53354-8.00012-8

Delay, M., Dolt, T., Woellhaf, A., Sembritzki, R., Frimmel, F.H., 2011. Interactions and stability of silver nanoparticles in the aqueous phase: Influence of natural organic matter (NOM) and ionic strength. *Journal of Chromatography. A* 1218(27), 4206–4212. DOI: 10.1016/j.chroma.2011.02.074

Delay, M., Frimmel, F.H., 2012. Nanoparticles in aquatic systems. *Analytical and Bioanalytical Chemistry* 402(2), 583–592. DOI: 10.1007/s00216-011-5443-z

Deonarine, A., Lau, B.L.T., Aiken, G.R., Ryan, J.N., Hsu-Kim, H., 2011. Effects of humic substances on precipitation and aggregation of zinc sulfide nanoparticles. *Environmental Science and Technology* 45(8), 3217–3223. DOI: 10.1021/es1029798

Derjaguin, B.V., Landau, L., 1941. Theory of the stability of strongly charged lyophobic sols and of the adhesion of strongly charged particles in solutions of electrolytes. *Acta Physica Chimica URSS* 14, 633–662.

Diegoli, S., Manciulea, A.L., Begum, S., Jones, I.P., Lead, J.R., Preece, J.A., 2008. Interaction between manufactured gold nanoparticles and naturally occurring organic macromolecules. *Science of the Total Environment* 402(1), 51–61. DOI: 10.1016/j.scitotenv.2008.04.023

Doane, T.L., Chuang, C.-H., Hill, R.J., Burda, C., 2012. Nanoparticle ζ-potentials. *Accounts of Chemical Research* 45(3), 317–326. DOI: 10.1021/ar200113c

Dobias, J., Bernier-Latmani, R., 2013. Silver release from silver nanoparticles in natural waters. *Environmental Science & Technology* 47(9), 4140–4146. DOI: 10.1021/es304023p

Doiron, K., Millour, M., Gagné, J.-P., Lemarchand, K., 2014. Combined effects of silver nanoparticles and humic and fulvic acids on *Vibrio splendidus* growth. *Journal of Xenobiotics* 4(4893), 59–61. DOI: 10.4081/xeno.2014.4893

Doiron, K., Pelletier, E., Lemarchand, K., 2012. Impact of polymer-coated silver nanoparticles on marine microbial communities: A microcosm study. *Aquatic Toxicology* 124–125, 22–27. DOI: 10.1016/j.aquatox.2012.07.004

Duval, J.F.L., Wilkinson, K.J., Van Leeuwen, H.P., Buffle, J., 2005. Humic substances are soft and permeable: Evidence from their electrophoretic mobilities. *Environmental Science & Technology* 39(17), 6435–6445. DOI: 10.1021/es050082x

Dwivedi, A.D., Dubey, S.P., Sillanpää, M., Kwon, Y.N., Lee, C., Varma, R.S., 2015. Fate of engineered nanoparticles: Implications in the environment. *Coordination Chemistry Reviews* 287, 64–78. DOI: 10.1016/j.ccr.2014.12.014

Eggersdorfer, M.L., Kadau, D., Herrmann, H.J., Pratsinis, S.E., 2011. Aggregate morphology evolution by sintering: Number and diameter of primary particles. *Journal of Aerosol Science* 46, 7–19. DOI: 10.1016/j.jaerosci.2011.11.005

Eglinton, T.I., Repeta, D.J., 2003. Organic matter in the contemporary ocean. *Treatise on Geochemistry* 6, 145–180. DOI: 10.1016/B0-08-043751-6/06155-7

El Badawy, A.M., Luxton, T.P., Silva, R.G., Scheckel, K.G., Suidan, M.T., Tolaymat, T.M., 2010. Impact of environmental conditions (pH, ionic strength, and electrolyte type) on the surface charge and aggregation of silver nanoparticles suspensions. *Environmental Science & Technology* 44(4), 1260–1266. DOI: 10.1021/es902240k

El Badawy, A.M., Scheckel, K.G., Suidan, M., Tolaymat, T.M., 2012. The impact of stabilization mechanism on the aggregation kinetics of silver nanoparticles. *Science of the Total Environment* 429, 325–331. DOI: 10.1016/j.scitotenv.2012.03.041

Elimelech, M., Gregory, J., Jia, X., Williams, R.A., 1998. *Particle deposition & aggregation measurement, modelling and simulation*. Butterworth-Heinemann pp.441.

Emerson, S.R., Hedges, J.I., 2008. *Chemical Oceanography and the Marine Carbon Cycle*. Cambridge University Press, Cambridge pp.453.

ENRHES, 2009. Engineered nanoparticles: Review of health and environmental safety. Edinburg pp.426p. DOI: 10.1002/pfi.4180130307

Esfahani, M.R., Stretz, H.A., Wells, M.J.M., 2015. Abiotic reversible self-assembly of fulvic and humic acid aggregates in low electrolytic conductivity solutions by dynamic light scattering and zeta potential investigation. *Science of the Total Environment* 537, 81–92. DOI: 10.1016/j.scitotenv.2015.08.001

Everett, D.H., 1992. *Basic Principles of Colloid Science*, RSC Paperbacks. The Royal

Society of Chemistry, London pp.243.

Fabrega, J., Fawcett, S.R., Renshaw, J.C., Lead, J.R., 2009. Silver nanoparticle impact on bacterial growth: Effect of pH, concentration, and organic matter. *Environmental Science & Technology* 43(19), 7285–7290. DOI: 10.1021/es803259g

Fabrega, J., Luoma, S.N., Tyler, C.R., Galloway, T.S., Lead, J.R., 2011. Silver nanoparticles: Behaviour and effects in the aquatic environment. *Environment International* 37(2), 517–531. DOI: 10.1016/j.envint.2010.10.012

Furman, O., Usenko, S., Lau, B.L.T., 2013. Relative importance of the humic and fulvic fractions of natural organic matter in the aggregation and deposition of silver nanoparticles. *Environmental Science & Technology*. DOI: 10.1021/es303275g

Gagné, J.-P., Gouteux, B., Soubaneh, Y.D., Brindle, J.R., 2011. Sorption of pesticides on natural geosorbents, in: Stoytcheva, M. (Ed.), *Pesticides - Formulations, Effects, Fate*. Intech, Rijeka, pp. 785–802.

Gao, J., Powers, K., Wang, Y., Zhou, H., Roberts, S.M., Moudgil, B.M., Koopman, B., Barber, D.S., 2012. Influence of Suwannee River humic acid on particle properties and toxicity of silver nanoparticles. *Chemosphere* 89(1), 96–101. DOI: 10.1016/j.chemosphere.2012.04.024

Geranio, L., Heuberger, M., Nowack, B., 2009. The behavior of silver nanotextiles during washing. *Environmental Science & Technology* 43(21), 8113–8. DOI: 10.1021/es9018332

Ghosh, K., Schnitzer, M., 1980. Macromolecular structure of humic substances. *Soil Science* 129(5), 266–276.

Gjessing, E.T., 1976. *Physical and Chemical Characteristics of Aquatic Humus*. Ann Arbor

Science Publishers, Ann Arbor pp.120.

Gobeil, C., 1999. Silver in sediments from the St. Lawrence River and Estuary and the Saguenay Fjord. *Environmental Science & Technology* 33(17), 2953–2957. DOI: 10.1021/es981322u

Gobeil, C., Rondeau, B., Beaudin, L., 2005. Contribution of municipal effluents to metal fluxes in the St. Lawrence River. *Environmental Science & Technology* 39(2), 456–464. DOI: 10.1021/es049335x

Goldberg, R.N., Kishore, N., Lennen, R.M., 2002. Thermodynamic quantities for the ionization reactions of buffers. *Journal of Physical and Chemical Reference Data* 31(2), 231–370. DOI: 10.1063/1.1416902

Gorham, J.M., Wnuk, J.D., Shin, M., Fairbrother, H., 2007. Adsorption of natural organic matter onto carbonaceous surfaces: Atomic force microscopy study. *Enviromental Science & Technology* 41(4), 1238–1244. DOI: 10.1021/es061793d

Gottschalk, F., Sonderer, T., 2009. Modeled environmental concentrations of engineered nanomaterials (TiO_2, ZnO, Ag, CNT, fullerenes) for different regions. *Environmental Science & Technology* 43(24), 9216–9222. DOI: 10.1021/es9015553

Gottschalk, F., Sun, T., Nowack, B., 2013. Environmental concentrations of engineered nanomaterials: Review of modeling and analytical studies. *Environmental Pollution* 181, 287–300. DOI: 10.1016/j.envpol.2013.06.003

Graham, R.P., Cragg, L.H., 1956. Suspensions and colloidal dispersions, in: Graham, R.P., Cragg, L.H. (Eds.), *The Essentials of Chemistry*. Clarke, Irwin & Company Limited, Toronto, pp. 490–502.

Grasso, D., Subramaniam, K., Butkus, M., Strevett, K., Bergendahl, J., 2002. A review of

non-DLVO interactions in environmental colloidal systems. *Reviews in Environmental Science and Biotechnology* 1(1), 17–38. DOI: 10.1023/A:1015146710500

Gunsolus, I.L., Mousavi, M.P.S., Hussein, K., Bühlmann, P., Haynes, C.L., 2015. Effects of humic and fulvic acids on silver nanoparticle stability, dissolution, and toxicity. *Environmental Science & Technology* 49(13), 8078–8086. DOI: 10.1021/acs.est.5b01496

Guo, X., Yin, Y., Tan, Z., Zhang, Z., Chen, Y., Liu, J., 2016. Significant enrichment of engineered nanoparticles in water surface microlayer. *Environmental Science & Technology Letters* 3(10), 381–385. DOI: 10.1021/acs.estlett.6b00271

Hassan, P.A., Rana, S., Verma, G., 2015. Making sense of brownian motion: Colloid characterization by dynamic light scattering. *Langmuir* 31(1), 3–12. DOI: 10.1021/la501789z

Hayes, M.H.B., Clapp, C.E., 2001. Humic substances: Considerations of compositions, aspects of structure, and environmental influences. *Soil Science* 166(11), 723–737. DOI: 10.1097/00010694-200111000-00002

Hélie, J.-F., Hillaire-Marcel, C., 2006. Sources of particulate and dissolved organic carbon in the St Lawrence River: Isotopic approach. *Hydrological Processes* 20(9), 1945–1959. DOI: 10.1002/hyp.5962

Helms, J.R., Stubbins, A., Ritchie, J.D., Minor, E.C., Kieber, D.J., Mopper, K., 2008. Absorption spectral slopes and slope ratios as indicators of molecular weight, source, and photobleaching of chromophoric dissolved organic matter. *Limnology and Oceanography* 53(3), 955–969.

Ho, C.-M., Yau, S.K.-W., Lok, C.-N., So, M.H., Che, C.-M., 2010. Oxidative dissolution of silver nanoparticles by biologically relevant oxidants: A kinetic and mechanistic study.

Chemistry An Asian Journal 5(2), 285–293.

Holden, P.A., Klaessig, F., Turco, R.F., Priester, J.H., Rico, C.M., Avila-Arias, H., Mortimer, M., Pacpaco, K., Gardea-Torresdey, J.L., 2014. Evaluation of exposure concentrations used in assessing manufactured nanomaterial environmental hazards: Are they relevant? *Environmental Science and Technology* 48(18), 10541–10551. DOI: 10.1021/es502440s

Holthoff, H., Schmitt, A., Fernandez-Barbero, A., Borkovec, M., Cabrerizo-Vilchez, M.A., Schurtenberger, P., Hidalgo-Alvarez, R., 1997. Measurement of absolute coagulation rate constants for colloidal particles: Comparison of single and multiparticle light scattering techniques. *Journal of Colloid and Interface Science* 192(2), 463–470. DOI: 10.1006/jcis.1997.5022

Hosse, M., Wilkinson, K.J., 2001. Determination of electrophoretic mobilities and hydrodynamic radii of three humic substances as a function of pH and ionic strength. *Environmental Science & Technology* 35(21), 4301–4306. DOI: 10.1021/es010038r

Hu, X., Chen, Q., Jiang, L., Yu, Z., Jiang, D., Yin, D., 2011. Combined effects of titanium dioxide and humic acid on the bioaccumulation of cadmium in Zebrafish. *Environmental Pollution* 159(5), 1151–1158. DOI: 10.1016/j.envpol.2011.02.011

Huynh, K.A., Chen, K.L., 2011. Aggregation kinetics of citrate and polyvinylpyrrolidone coated silver nanoparticles in monovalent and divalent electrolyte solutions. *Environmental Science & Technology* 45(13), 5564–5571. DOI: 10.1021/es200157h

IHSS, 2017. *April 2017. http://humic-substances.org/* [WWW Document]. *http://humic-substances.org/*.

ISO/TS27687:2008, 2008. Nanotechnologies -- Terminology and definitions for nano-objects -- Nanoparticle, nanofibre and nanoplate.

ISO/TS80004-2:2015, 2015. Nanotechnologies — Vocabulary — Part 2: Nano-objects.

ISO13321:1996(E), 1996. Particle size analysis - Photon correlation spectroscopy.

Jin, X., Li, M., Wang, J., Marambio-Jones, C., Peng, F., Huang, X., Damoiseaux, R., Hoek, E.M.V., 2010. High-throughput screening of silver nanoparticle stability and bacterial inactivation in aquatic media: Influence of specific ions. *Environmental Science & Technology* 44(19), 7321–7328. DOI: 10.1021/es100854g

Ju-Nam, Y., Lead, J.R., 2008. Manufactured nanoparticles: An overview of their chemistry, interactions and potential environmental implications. *Science of the Total Environment* 400(1–3), 396–414. DOI: 10.1016/j.scitotenv.2008.06.042

Kaegi, R., Sinnet, B., Zuleeg, S., Hagendorfer, H., Mueller, E., Vonbank, R., Boller, M., Burkhardt, M., 2010. Release of silver nanoparticles from outdoor facades. *Environmental Pollution* 158(9), 2900–2905. DOI: 10.1016/j.envpol.2010.06.009

Kaegi, R., Voegelin, A., Sinnet, B., Zuleeg, S., Hagendorfer, H., Burkhardt, M., Siegrist, H., 2011. Behavior of metallic silver nanoparticles in a pilot wastewater treatment plant. *Environmental Science & Technology* 45(9), 3902–8. DOI: 10.1021/es1041892

Keller, A.A., Lazareva, A., 2014. Predicted releases of engineered nanomaterials: From global to regional to local. *Environmental Science and Technology Letters* 1(1), 65–70. DOI: 10.1021/ez400106t

Kim, S., Ryu, D.-Y., 2013. Silver nanoparticle-induced oxidative stress, genotoxicity and apoptosis in cultured cells and animal tissues. *Journal of Applied Toxicology* 33(2), 78–89. DOI: 10.1002/jat.2792

Klaine, S.J., Alvarez, P.J.. J., Batley, G.E., Fernandes, T.F., Handy, R.D., Lyon, D.Y., Mahendra, S., McLaughlin, M.J., Lead, J.R., 2008. Nanomaterials in the environment:

Behavior, fate, bioavailability, and effects. *Environmental Toxicology and Chemistry* 27(9), 1825–1851. DOI: 10.1897/08-090.1

Kranck, K., 1979. Dynamics and distribution of suspended particulate matter in the St Lawrence estuary. *Naturaliste Canadien* 106(1), 163–173.

Kretzschmar, R., Hesterberg, D., Sticher, H., 1997. Effects of adsorbed humic acid on surface charge and flocculation of kaolinite. *Soil Science Society of America Journal* 61(1), 101–108. DOI: 10.2136/sssaj1997.03615995006100010016x

Kühn, M., Ivleva, N.P., Klitzke, S., Niessner, R., Baumann, T., 2015. Investigation of coatings of natural organic matter on silver nanoparticles under environmentally relevant conditions by surface-enhanced Raman scattering. *Science of The Total Environment* 535, 122–130. DOI: http://dx.doi.org/10.1016/j.scitotenv.2014.12.026

Labille, J., Brant, J., 2010. Stability of nanoparticles in water. *Nanomedicine* 5(6), 985–998.

Lanceleur, L., Schäfer, J., Blanc, G., Coynel, A., Bossy, C., Baudrimont, M., Glé, C., Larrose, A., Renault, S., Strady, E., 2013. Silver behaviour along the salinity gradient of the Gironde Estuary. *Environmental Science and Pollution Research International* 20(3), 1352–1366. DOI: 10.1007/s11356-012-1045-3

Lapresta-Fernández, A., Fernández, A., Blasco, J., 2011. Nanoecotoxicity effects of engineered silver and gold nanoparticles in aquatic organisms. *Trends in Analytical Chemistry* 32, 40–59. DOI: 10.1016/j.trac.2011.09.007

Lawler, D.F., Youn, S., Zhu, T., Kim, I., Lau, B.L.T., 2015. Comprehensive understanding of nano-sized particle separation processes using nanoparticle tracking analysis. *Water Science and Technology* 72(12), 2318–2324. DOI: 10.2166/wst.2015.459

Lea, M.C., 1889. Allotropic forms of silver. *American Journal of Science* s3-37(222), 476–

491. DOI: 10.2475/ajs.s3-37.222.476

Lead, J.R., Wilkinson, K.J., 2006. Aquatic colloids and nanoparticles: Current knowledge and future trends. *Environmental Chemistry* 3(3), 159–171. DOI: 10.1071/EN06025

Leenheer, J.A., 2009. Systematic approaches to comprehensive analyses of natural organic matter. *Annals of Environmental Science* 3(1), 1–130.

Lem, K.W., Choudhury, A., Lakhani, A.A., Kuyate, P., Haw, J.R., Lee, D.S., Iqbal, Z., Brumlik, C.J., 2012. Use of nanosilver in consumer products. *Recent Patents on Nanotechnology* 6(1), 60–72. DOI: 10.2174/187221012798109318

Levard, C., Hotze, E.M., Lowry, G.V., Brown, G.E., 2012. Environmental transformations of silver nanoparticles: Impact on stability and toxicity. *Environmental Science & Technology* 46(13), 6900–6914. DOI: 10.1021/es2037405

Levard, C., Mitra, S., Yang, T., Jew, A.D., Badireddy, A.R., Lowry, G.V., Brown, G.E., 2013. Effect of chloride on the dissolution rate of silver nanoparticles and toxicity to *E. coli*. *Environmental Science & Technology* 47(11), 5738–5745. DOI: 10.1021/es400396f

Levard, C., Reinsch, B.C., Michel, F.M., Oumahi, C., Lowry, G.V., Brown, G.E., 2011. Sulfidation processes of PVP-coated silver nanoparticles in aqueous solution: Impact on dissolution rate. *Environmental Science & Technology* 45(12), 5260–5266. DOI: 10.1021/es2007758

Li, X., Lenhart, J.J., Walker, H.W., 2012. Aggregation kinetics and dissolution of coated silver nanoparticles. *Langmuir* 28(2), 1095–1104. DOI: 10.1021/la202328n

Li, X., Lenhart, J.J., Walker, H.W., 2010. Dissolution-accompanied aggregation kinetics of silver nanoparticles. *Langmuir* 26(21), 16690–16698. DOI: 10.1021/la101768n

Libes, S.M., 2009. Seasalt is more than NaCl, in: Libes, S.M. (Ed.), *Introduction to Marine Biogeochemistry*. Elsevier Academic Press, San Diego, pp. 41–64.

Lin, D., Ma, S., Zhou, K., Wu, F., Yang, K., 2015. The effect of water chemistry on homoaggregations of various nanoparticles: Specific role of Cl^- ions. *Journal of Colloid and Interface Science* 450, 272–278. DOI: 10.1016/j.jcis.2015.03.027

Lin, S., Cheng, Y., Liu, J., Wiesner, M., 2012. Polymeric coatings on silver nanoparticles hinder auto-aggregation but enhance attachment to uncoated surfaces. *Langmuir* 28(9), 4178–4186. DOI: 10.1021/la202884f

Liu, J.-F., Yu, S.-J., Yin, Y.-G., Chao, J.-B., 2012. Methods for separation, identification, characterization and quantification of silver nanoparticles. *Trends in Analytical Chemistry* 33, 95–106. DOI: 10.1016/j.trac.2011.10.010

Liu, J., Hurt, R.H., 2010. Ion release kinetics and particle persistence in aqueous nano-silver colloids. *Environmental Science & Technology* 44(6), 2169–2175. DOI: 10.1021/es9035557

Liu, J., Hwang, Y.S., Lenhart, J.J., 2015. Heteroaggregation of bare silver nanoparticles with clay minerals. *Environmental Science: Nano* 2(5), 528–540. DOI: 10.1039/C5EN00130G

Liu, J., Pennell, K.G., Hurt, R.H., 2011. Kinetics and mechanisms of nanosilver oxysulfidation. *Environmental Science & Technology* 45(17), 7345–7353. DOI: 10.1021/es201539s

Lok, C.-N., Ho, C.-M., Chen, R., He, Q.-Y., Yu, W.-Y., Sun, H., Tam, P.K.-H., Chiu, J.-F., Che, C.-M., 2007. Silver nanoparticles: Partial oxidation and antibacterial activities. *Journal of Biological Inorganic Chemistry* 12(4), 527–534. DOI: 10.1007/s00775-007-0208-z

Louie, S.M., Spielman-Sun, E.R., Small, M.J., Tilton, R.D., Lowry, G.V., 2015. Correlation of the physicochemical properties of natural organic matter samples from different sources to their effects on gold nanoparticle aggregation in monovalent electrolyte. *Environmental Science & Technology* 49(4), 2188–2198. DOI: 10.1021/es505003d

Louie, S.M., Tilton, R.D., Lowry, G.V., 2016. Critical review: Impacts of macromolecular coatings on critical physicochemical processes controlling environmental fate of nanomaterials. *Environmental Science: Nano* 3(2), 283–310. DOI: 10.1039/C5EN00104H

Lourenco, C., Teixeira, M., Simões, S., Rogério, G., 1996. Steric stabilization of nanoparticles: Size and surface properties. *International Journal of Pharmaceutics* 138(1), 1–12. DOI: 10.1016/0378-5173(96)04486-9

Lowry, G.V., Espinasse, B.P., Badireddy, A.R., Richardson, C.J., Reinsch, B.C., Bryant, L.D., Bone, A.J., Deonarine, A., Chae, S., Therezien, M., Colman, B.P., Hsu-Kim, H., Bernhardt, E.S., Matson, C.W., Wiesner, M.R., 2012a. Long-term transformation and fate of manufactured Ag nanoparticles in a simulated large scale freshwater emergent wetland. *Environmental Science & Technology* 46(13), 7027–7036. DOI: 10.1021/es204608d

Lowry, G.V., Gregory, K.B., Apte, S.C., Lead, J.R., 2012b. Transformations of nanomaterials in the environment. *Environmental Science & Technology* 46(13), 6893–6899. DOI: 10.1021/es300839e

MacCarthy, P., 2001. The principles of humic substances. *Soil Science* 166(11), 738–751. DOI: 10.1097/00010694-200111000-00003

Magesky, A., Ribeiro, C.A.O., Pelletier, É., 2016. Physiological effects and cellular responses of metamorphic larvae and juveniles of sea urchin exposed to ionic and

nanoparticulate silver. *Aquatic Toxicology* 174, 208–227. DOI: 10.1016/j.aquatox.2016.02.018

Malcolm, R.L., MacCarthy, P., 1992. Quantitative evaluation of XAD-8 and XAD-4 resins used in tandem for removing organic solutes from water. *Environment International* 18(6), 597–607. DOI: 10.1016/0160-4120(92)90027-2

Malvern, 2013a. *Zetasizer Nano Series User Manual*, MAN0485 Is. ed, Malvern Instruments Ltd. Malvern pp.250. DOI: 10.1016/S0294-3506(99)80105-7

Malvern, 2013b. Zeta potential theory, in: *Zetasizer Nano Series User Manual*. Malvern Instruments Ltd, Malvern, pp. 229–240.

Malvern, 2010a. *What is a correlogram ? FAQ : frequently asked question*.

Malvern, 2010b. *What is the Z-Average ? FAQ : frequently asked question*.

Malvern, 2010c. *How accurate is the DLS volume distribution ? FAQ : frequently asked question*, FAQ : frequently asked question.

Malvern, 2010d. *Evaluating DLS Data Quality. FAQ : frequently asked question*.

Malvern, 2009. Intensity – Volume – Number : Which Size is Correct? Technical note MRK1357-01. Malvern pp.1-3.

Mantoura, R.F.C., Dickson, A., Riley, J.P., 1978. The complexation of metals with humic materials in natural waters. *Estuarine and Coastal Marine Science* 6(4), 387–408. DOI: 10.1016/0302-3524(78)90130-5

Mao, J., Cao, X., Olk, D.C., Chu, W., Schmidt-Rohr, K., 2017. Advanced solid-state NMR spectroscopy of natural organic matter. *Progress in Nuclear Magnetic Resonance Spectroscopy* 100, 17–51. DOI: 10.1016/j.pnmrs.2016.11.003

Mao, J., Tremblay, L., Gagné, J.-P., 2011. Structural changes of humic acids from sinking organic matter and surface sediments investigated by advanced solid-state NMR: Insights into sources, preservation and molecularly uncharacterized components. *Geochimica et Cosmochimica Acta* 75(24), 7864–7880. DOI: 10.1016/j.gca.2011.09.044

Mao, J., Tremblay, L., Gagné, J.-P., Kohl, S., Rice, J., Schmidt-Rohr, K., 2007. Humic acids from particulate organic matter in the Saguenay Fjord and the St. Lawrence Estuary investigated by advanced solid-state NMR. *Geochimica et Cosmochimica Acta* 71(22), 5483–5499. DOI: 10.1016/j.gca.2007.09.022

Marambio-Jones, C., Hoek, E.M.V., 2010. A review of the antibacterial effects of silver nanomaterials and potential implications for human health and the environment. *Journal of Nanoparticle Research* 12(5), 1531–1551. DOI: 10.1007/s11051-010-9900-y

Markus, A.A., Parsons, J.R., Roex, E.W.M., de Voogt, P., Laane, R.W.P.M., 2017. Modelling the release, transport and fate of engineered nanoparticles in the aquatic environment – A review, in: *Reviews of Environmental Contamination and Toxicology*. pp. 77. DOI: 10.1007/398_2016_17

Martin-Mousset, B., Croue, J.-P., Lefebvre, E., Legube, E., 1997. Distribution and characterization of dissolved organic matter of surface waters. *Water Research* 31(3), 541–553. DOI: 10.1016/S0043-1354(96)00259-X

McGillicuddy, E., Murray, I., Kavanagh, S., Morrison, L., Fogarty, A., Cormican, M., Dockery, P., Prendergast, M., Rowan, N., Morris, D., 2017. Silver nanoparticles in the environment: Sources, detection and ecotoxicology. *Science of the Total Environment* 575, 231–246. DOI: 10.1016/j.scitotenv.2016.10.041

McNaught, A.D., Wilkinson, A., 2014. *Compendium of Chemical Terminology (the "Gold*

Book"), 2nd ed, IUPAC. Blackwell Scientific Publications pp.1670. DOI: http://dx.doi.org/10.1351/goldbook.I03352

Metreveli, G., Philippe, A., Schaumann, G.E., 2015. Disaggregation of silver nanoparticle homoaggregates in a river water matrix. *Science of The Total Environment* 535, 35–44. DOI: 10.1016/j.scitotenv.2014.11.058

Millour, M., Doiron, K., Lemarchand, K., Gagné, J.-P., 2015. Does the bacterial media culture chemistry affect the stability of nanoparticles in nanotoxicity assays? *Journal of Xenobiotics* 5(2), 34–36. DOI: 10.4081/xeno.2015.5772

Millour, M., Pelletier, É., Gagné, J.-P., 2013. Interactions between silver nanoparticles and dissolved organic matter under estuarine conditions, in: Xu, J., Wu, J., He, Y. (Eds.), *Functions of Natural Organic Matter in Changing Environment*. Springer Netherlands, Dordrecht, pp. 805–809. DOI: 10.1007/978-94-007-5634-2

Milne, C.J., Lapworth, D.J., Gooddy, D.C., Elgy, C.N., Valsami-Jones, É., 2017. Role of humic acid in the stability of Ag nanoparticles in suboxic conditions. *Environmental Science & Technology* 51(11), 6063–6070. DOI: 10.1021/acs.est.6b06054

Montano, M.D., Ranville, J., Lowry, G.V., Blue, J., Hiremath, N., Koenig, S., Tuccillo, M.E., 2014. Detection and characterization of engineered nanomaterials in the environment : Current state-of-the-art and future directions (No. EPA/600/R-14/244, 2014). Washington, DC, USA pp.186.

Mühling, M., Bradford, A., Readman, J.W., Somerfield, P.J., Handy, R.D., 2009. An investigation into the effects of silver nanoparticles on antibiotic resistance of naturally occurring bacteria in an estuarine sediment. *Marine Environmental Research* 68(5), 278–283. DOI: 10.1016/j.marenvres.2009.07.001

Nanotechproject, 2017. *April 2017. Project on Emerging Nanotechnologies.*

http://www.nanotechproject.org [WWW Document]. URL http://www.nanotechproject.org/

Nason, J.A., McDowell, S.A., Callahan, T.W., 2012. Effects of natural organic matter type and concentration on the aggregation of citrate-stabilized gold nanoparticles. *Journal of Environmental Monitoring* 14(7), 1885–1892. DOI: 10.1039/C2EM00005A

Navarro, E., Baun, A., Behra, R., Hartmann, N.B., Filser, J., Miao, A.-J., Quigg, A., Santschi, P.H., Sigg, L., 2008a. Environmental behavior and ecotoxicity of engineered nanoparticles to algae, plants, and fungi. *Ecotoxicology* 17(5), 372–386. DOI: 10.1007/s10646-008-0214-0

Navarro, E., Piccapietra, F., Wagner, B., Marconi, F., Kaegi, R., Odzak, N., Sigg, L., Behra, R., 2008b. Toxicity of silver nanoparticles to *Chlamydomonas reinhardtii*. *Environmental Science & Technology* 42(23), 8959–8964. DOI: 10.1021/es801785m

Neihof, R.A., Loeb, G.I., 1974. Dissolved organic matter in seawater and the electric charge of immersed surfaces. *Journal of Marine Research* 32(1), 5–12.

Neihof, R.A., Loeb, G.I., 1972. The surface charge of particulate matter in seawater. *Limnology and Oceanography* 17(1), 7–16. DOI: 10.4319/lo.1972.17.1.0007

Nel, A.E., Mädler, L., Velegol, D., Xia, T., Hoek, E.M.V., Somasundaran, P., Klaessig, F., Castranova, V., Thompson, M., 2009. Understanding biophysicochemical interactions at the nano-bio interface. *Nature materials* 8(7), 543–557. DOI: 10.1038/nmat2442

Nowack, B., Krug, H.F., Height, M., 2011. 120 Years of nanosilver history: Implications for policy makers. *Environmental Science & Technology* 45(4), 1177–1183. DOI: 10.1021/es103316q

Nwanya, A.C., Ugwuoke, P.E., Ezekoye, B.A., Osuji, R.U., Ezema, F.I., 2013. Structural and

optical properties of chemical bath deposited silver oxide thin films : Role of deposition time. *Advances inMaterials Science and Engineering* ID 450820, 8.

OECD, 2011. *Fostering Nanotechnology to Address Global Challenges: Water* pp.76.

Osterheld, K., Millour, M., Pelletier, É., Magesky, A., Doiron, K., Lemarchand, K., Gagné, J.P., 2018. Nanotoxicity of silver nanoparticles: from environmental spill to effects on organisms, in: Kumar, V., Dasgupta, N., Ranjan, V. (Eds.), *Environmental Toxicity of Nanomaterials*. CRC Press Taylor & Francis Group, Boca Raton, pp. 537.

Perdue, E.M., Ritchie, J.D., 2005. Dissolved organic matter in freshwaters, in: Drever, J.I. (Ed.), *Surface and Ground Water, Weathering, and Soils: Treatise on Geochemistry*. Elsevier Science, pp. 273–311.

Peretyazhko, T.S., 2014. Size-controlled dissolution of silver nanoparticles at neutral and acidic pH conditions: Kinetics and size changes. *Environmental Science & Technology* 48, 11954–11961. DOI: 10.1021/es5023202

Petosa, A.R., Jaisi, D.P., Quevedo, I.R., Elimelech, M., Tufenkji, N., 2010. Aggregation and deposition of engineered nanomaterials in aquatic environments: Role of physicochemical interactions. *Environmental Science & Technology* 44(17), 6532–6549. DOI: 10.1021/es100598h

Philippe, A., Schaumann, G.E., 2014. Interactions of dissolved organic matter with natural and engineered inorganic colloids: A review. *Environmental Science & Technology* 48(16), 8946–8962. DOI: 10.1021/es502342r

Piccapietra, F., Sigg, L., Behra, R., 2012. Colloidal stability of carbonate-coated silver nanoparticles in synthetic and natural freshwater. *Environmental Science & Technology* 46(2), 818–825. DOI: 10.1021/es202843h

Piccolo, A., 2001. The supramolecular structure of humic substances. *Soil Science* 166(11), 810. DOI: 10.1097/00010694-200111000-00007

Pillai, Z.S., 2004. What factors control the size and shape of silver nanoparticles in the citrate ion reduction method? *The Journal of Physical Chemistry B* 108(3), 945–951. DOI: 10.1021/jp037018r

Powell, M.C., Griffin, M.P.A., Tai, S., 2008. Bottom-up risk regulation? How nanotechnology risk knowledge gaps challenge federal and state environmental agencies. *Environmental Management* 42(3), 426–443. DOI: 10.1007/s00267-008-9129-z

Quik, J.T.K., Velzeboer, I., Wouterse, M., Koelmans, A.A., van de Meent, D., 2014. Heteroaggregation and sedimentation rates for nanomaterials in natural waters. *Water Research* 48(1), 269–279. DOI: 10.1016/j.watres.2013.09.036

Ratte, H.T., 1999. Bioaccumulation and toxicity of silver compounds: A review. *Environmental Toxicology and Chemistry* 18(1), 89–108. DOI: 10.1002/etc.5620180112

Sánchez-Cortés, S., Francioso, O., Ciavatta, C., García-Ramos, J.V., Gessa, C., 1998. pH-dependent adsorption of fractionated peat ĥumic substances on different silver colloids studied by surface-enhanced raman spectroscopy. *Journal of Colloid and Interface Science* 198(2), 308–318. DOI: 10.1006/jcis.1997.5293

Sani-Kast, N., Labille, J., Ollivier, P., Slomberg, D., Hungerbühler, K., Scheringer, M., 2017. A network perspective reveals decreasing material diversity in studies on nanoparticle interactions with dissolved organic matter. *Proceedings of the National Academy of Sciences* 114(10), E1756–E1765. DOI: 10.1073/pnas.1608106114

Sayes, C.M., Aquino, G.V., 2017. Nano-exposure science: How does exposure to engineered

nanomaterials happen?, in: Mansfield, E., Kaiser, D.L., Fujita, D., Van de Voorde, M. (Eds.), Metrology and Standardization of Nanotechnology. Wiley-VCH Verlag GmbH & Co. KGaA, Weinheim, Germany, pp. 343–362. DOI: 10.1002/9783527800308.ch22

SCENIHR, 2014. *Nanosilver: Safety, health and environmental effects and role in antimicrobial resistance*. Luxembourg pp.103.

Seitz, F., Rosenfeldt, R.R., Storm, K., Metreveli, G., Schaumann, G.E., Schulz, R., Bundschuh, M., 2015. Effects of silver nanoparticle properties, media pH and dissolved organic matter on toxicity to *Daphnia magna*. *Ecotoxicology and Environmental Safety* 111, 263–270. DOI: 10.1016/j.ecoenv.2014.09.031

Sempéré, R., Cauwet, G., 1995. Occurrence of organic colloids in the stratified estuary of the Krka River (Croatia). *Estuarine, Coastal and Shelf Science* 40(1), 105–114. DOI: 10.1016/0272-7714(95)90016-0

Senesi, N., 1999. Aggregation patterns and macromolecular morphology of humic substances: A fractal approach. *Soil Science* 164(11), 841–856. DOI: 10.1097/00010694-199911000-00009

Senesi, N., Xing, B., Huang, P.M., 2009. *Biophysico-Chemical Processes Involving Natural Nonliving Organic Matter in Environmental Systems*. John Wiley & Sons, Inc., Hoboken, NJ, USA pp.876. DOI: 10.1002/9780470494950

Shlens, J., 2014. A Tutorial on Principal Component Analysis. DOI: 10.1.1.115.3503

Sholkovitz, E.R., 1976. Flocculation of dissolved organic and inorganic matter during the mixing of river water and seawater. *Geochimica et Cosmochimica Acta* 40(7), 831–845. DOI: 10.1016/0016-7037(76)90035-1

Simons, R.D., Monismith, S.G., Saucier, F.J., Johnson, L.E., Winkler, G., 2010. Modelling

stratification and baroclinic flow in the estuarine transition zone of the St. Lawrence estuary. *Atmosphere-Ocean* 48(2), 132–146. DOI: 10.3137/OC316.2010

Somorjai, G.A., 1994. *Introduction of surface chemistry and catalysis*. Wiley Interscience, New-York pp.643.

Song, J.E., Phenrat, T., Marinakos, S., Xiao, Y., Liu, J., Wiesner, M.R., Tilton, R.D., Lowry, G.V., 2011. Hydrophobic interactions increase attachment of gum Arabic- and PVP-coated Ag nanoparticles to hydrophobic surfaces. *Environmental Science & Technology* 45(14), 5988–5995. DOI: 10.1021/es200547c

Sotiriou, G.A., Meyer, A., Knijnenburg, J.T.., Panke, S., Pratsinis, S.E., 2012. Quantifying the origin of released Ag^+ ions from nanosilver. *Langmuir* 28(45), 15929–15936. DOI: 10.1021/la303370d

Stevenson, F.J., 1994. *Humus Chemistry : Genesis, Composition, Reactions*, 2nd ed. Wiley, New York. NY pp.512. DOI: 10.1021/ed072pA93.6

Sun, T.Y., Gottschalk, F., Hungerbühler, K., Nowack, B., 2014. Comprehensive probabilistic modelling of environmental emissions of engineered nanomaterials. *Environmental Pollution* 185, 69–76. DOI: 10.1016/j.envpol.2013.10.004

Sutton, R., Sposito, G., 2006. Molecular simulation of humic substance–Ca-montmorillonite complexes. *Geochimica et Cosmochimica Acta* 70(14), 3566–3581. DOI: 10.1016/j.gca.2006.04.032

Sutton, R., Sposito, G., 2005. Molecular structure in soil humic substances: The new view. *Environmental Science & Technology* 39(23), 9009–9015. DOI: 10.1021/es050778q

Sutton, R., Sposito, G., Diallo, M.S., Schulten, H.-R., 2005. Molecular simulation of a model of dissolved organic matter. *Environmental Toxicology and Chemistry* 24(8), 1902–

1911. DOI: 10.1897/04-567R.1

Swift, R.S., 1989. Molecular weight, size, shape and charge characteristics of humic substances: Some basic considerations, in: Hayes, M.H.B., MacCarthy, P., Malcolm, R.L., Swift, R.S. (Eds.), Humic Substances II. In Search of Structure. Wiley, New York, pp. 449–466.

Tejamaya, M., Römer, I., Merrifield, R.C., Lead, J.R., 2012. Stability of citrate, PVP, and PEG coated silver nanoparticles in ecotoxicology media. *Environmental Science & Technology* 46(13), 7011–7017. DOI: 10.1021/es2038596

Thurman, E.M., 1985. Amount of organic carbon in natural waters, in: Thurman, E.M. (Ed.), *Organic Geochemistry of Natural Waters*. Kluwer Academic Publishers, Hingham, pp. 7–65.

Thurman, E.M., Malcolm, R.L., 1981. Preparative isolation of aquatic humic substances. *Environmental Science & Technology* 15(4), 463–466. DOI: 10.1021/es00086a012

Thurman, E.M., Malcolm, R.L., Aiken, G.R., 1978. Prediction of capacity factors for aqueous organic solutes adsorbed on a porous acrylic resin. *Analytical Chemistry* 50(6), 775–779. DOI: 10.1021/ac50027a028

Tilton, L.W., Plyler, E.K., Stephens, R.E., 1950. Refractive index of silver chloride for visible and infra-red radiant energy. *Journal of the Optical Society of America* 40(8), 540. DOI: 10.1364/JOSA.40.000540

Tolaymat, T.M., El Badawy, A.M., Genaidy, A., Scheckel, K.G., Luxton, T.P., Suidan, M., 2010. An evidence-based environmental perspective of manufactured silver nanoparticle in syntheses and applications: A systematic review and critical appraisal of peer-reviewed scientific papers. *Science of the Total Environment* 408(5), 999–1006. DOI: 10.1016/j.scitotenv.2009.11.003

Tomaszewska, E., Soliwoda, K., Kadziola, K., Tkacz-Szczesna, B., Celichowski, G., Cichomski, M., Szmaja, W., Grobelny, J., 2013. Detection limits of DLS and UV-Vis spectroscopy in characterization of polydisperse nanoparticles colloids. *Journal of Nanomaterials* ID 313081, 10. DOI: 10.1155/2013/313081

Tombácz, E., Szekeres, M., 2004. Colloidal behavior of aqueous montmorillonite suspensions: The specific role of pH in the presence of indifferent electrolytes. *Applied Clay Science* 27(1–2), 75–94. DOI: 10.1016/j.clay.2004.01.001

Topuz, E., Sigg, L., Talinli, I., 2014. A systematic evaluation of agglomeration of Ag and TiO_2 nanoparticles under freshwater relevant conditions. *Environmental Pollution* 193, 37–44. DOI: 10.1016/j.envpol.2014.05.029

Tourbin, M., Frances, C., 2008. Experimental characterization and population balance modelling of the dense silica suspensions aggregation process. *Chemical Engineering Science* 63(21), 5239–5251. DOI: 10.1016/j.ces.2008.06.028

Tremblay, L., Gagné, J.-P., 2009. Organic matter distribution and reactivity in the waters of a large estuarine system. *Marine Chemistry* 116(1–4), 1–12. DOI: 10.1016/j.marchem.2009.09.006

Tremblay, L., Gagné, J.-P., 2007. Distribution and biogeochemistry of sedimentary humic substances in the St.-Lawrence Estuary and the Saguenay Fjord, Québec. *Organic Geochemistry* 38(4), 682–699. DOI: 10.1016/j.orggeochem.2006.11.003

Turkevich, J., Stevenson, P.C., Hillier, J., 1951. A study of the nucleation and growth processes in the synthesis of colloidal gold. *Discussions of the Faraday Society* 11, 55–75. DOI: 10.1039/DF9511100055

Unrine, J.M., Colman, B.P., Bone, A.J., Gondikas, A.P., Matson, C.W., 2012. Biotic and abiotic interactions in aquatic microcosms determine fate and toxicity of Ag

nanoparticles. Part 1. Aggregation and dissolution. *Environmental Science & Technology* 46(13), 6915–6924. DOI: 10.1021/es204682q

US-EPA, 2014. *Technical Fact sheet - Nanomaterials; EPA 505-F-14-002*. Washington, DC, USA pp.1-9. DOI: 10.1016/B978-0-12-374849-2.00004-6

US-EPA, 2009. *Emerging Contaminants—Nanomaterials. Solid Waste and Emergency Response (5106P); 505-F-09-011* (No. EPA 505-F-09-011). Washington, DC, USA pp.1-7.

Vance, M.E., Kuiken, T., Vejerano, E.P., McGinnis, S.P., Hochella, M.F., Hull, D.R., 2015. Nanotechnology in the real world: Redeveloping the nanomaterial consumer products inventory. *Beilstein Journal of Nanotechnology* 6(1), 1769–1780. DOI: 10.3762/bjnano.6.181

Verwey, E.J.W., Overbeek, J.T.G., 1948. *Theory of the stability of lyophobic colloids*. Elsevier, Amsterdam pp.108.

Wakeham, S.G., Lee, C., Hedges, J.I., Hernes, P.J., 1997. Molecular indicators of diagenetic status in marine organic matter. *Geochimica et Cosmochimica Acta* 61(24), 5363–5369. DOI: 10.1016/S0016-7037(97)00312-8

Wang, H., Adeleye, A.S., Huang, Y., Li, F., Keller, A.A., 2015. Heteroaggregation of nanoparticles with biocolloids and geocolloids. *Advances in Colloid and Interface Science* 226, 24–36. DOI: 10.1016/j.cis.2015.07.002

Wang, Z., Zhang, L., Zhao, J., Xing, B., 2016. Environmental processes and toxicity of metallic nanoparticles in aquatic systems as affected by natural organic matter. *Environmental Science: Nano* 3(2), 240–255. DOI: 10.1039/C5EN00230C

Wasmuth, C., Rüdel, H., Düring, R.A., Klawonn, T., 2016. Assessing the suitability of the

OECD 29 guidance document to investigate the transformation and dissolution of silver nanoparticles in aqueous media. *Chemosphere* 144(2016), 2018–2023. DOI: 10.1016/j.chemosphere.2015.10.101

Wershaw, R.L., 1986. A new model for humic materials and their interactions with hydrophobic organic chemicals in soil-water or sediment-water systems. *Journal of Contaminant Hydrology* 1(1–2), 29–45. DOI: 10.1016/0169-7722(86)90005-7

Wijnhoven, S.W.P., Peijnenburg, W.J.G.M., Herberts, C.A., Hagens, W.I., Oomen, A.G., Heugens, E.H.W., Roszek, B., Bisschops, J., Gosens, I., Van De Meent, D., Dekkers, S., De Jong, W.H., van Zijverden, M., Sips, A.J.A.M., Geertsma, R.E., 2009. Nano-silver – a review of available data and knowledge gaps in human and environmental risk assessment. *Nanotoxicology* 3(2), 109–138. DOI: 10.1080/17435390902725914

Wiley, B., Sun, Y., Mayers, B., Xia, Y., 2005. Shape-controlled synthesis of metal nanostructures: The case of silver. *Chemistry - A European Journal* 11(2), 454–463. DOI: 10.1002/chem.200400927

Wu, L., Ortiz, C.P., Jerolmack, D.J., 2017. Aggregation of elongated colloids in water. *Langmuir* 33(2), 622–629. DOI: 10.1021/acs.langmuir.6b03962

Xu, R., 2015. Light scattering: A review of particle characterization applications. *Particuology* 18, 11–21. DOI: 10.1016/j.partic.2014.05.002

Xu, R., 2001a. Electrophoretic light scattering, in: Xu, R. (Ed.), *Particle Characterization: Light Scattering Methods*. Kluwer Academic Publishers, Dordrecht, pp. 289–343.

Xu, R., 2001b. Photon correlation spectroscopy, in: Xu, R. (Ed.), *Particle Characterization: Light Scattering Methods*. Kluwer Academic Publishers, Dordrecht, pp. 223–288.

Yetisen, A.K., Qu, H., Manbachi, A., Butt, H., Dokmeci, M.R., Hinestroza, J.P.,

Skorobogatiy, M., Khademhosseini, A., Yun, S.H., 2016. Nanotechnology in textiles. *ACS Nano* 10(3), 3042–3068. DOI: 10.1021/acsnano.5b08176

Yu, W.L., Borkovec, M., 2002. Distinguishing heteroaggregation from homoaggregation in mixed binary particle suspensions by multiangle static and dynamic light scattering. *Journal of Physical Chemistry B* 106(51), 13106–13110. DOI: 10.1021/jp021792h

Yung, M.M.N., Kwok, K.W.H., Djurišić, A.B., Giesy, J.P., Leung, K.M.Y., 2017. Influences of temperature and salinity on physicochemical properties and toxicity of zinc oxide nanoparticles to the marine diatom *Thalassiosira pseudonana*. *Scientific Reports* 7(1), 3662. DOI: 10.1038/s41598-017-03889-1

Zhang, C., Hu, Z., Deng, B., 2016. Silver nanoparticles in aquatic environments: Physiochemical behavior and antimicrobial mechanisms. *Water Research* 88, 403–427. DOI: 10.1016/j.watres.2015.10.025

Zhang, H., Smith, J.A., Oyanedel-Craver, V., 2012. The effect of natural water conditions on the anti-bacterial performance and stability of silver nanoparticles capped with different polymers. *Water Research* 46(3), 691–699. DOI: 10.1016/j.watres.2011.11.037

Zhang, T., Lu, D., Zeng, L., Yin, Y., He, Y., Liu, Q., Jiang, G., 2017. Role of secondary particle formation in the persistence of silver nanoparticles in humic acid containing water under light irradiation. *Environmental Science & Technology* 51(24), 14164–14172. DOI: 10.1021/acs.est.7b04115

Zhang, Y., Chen, Y., Westerhoff, P., Crittenden, J., 2009. Impact of natural organic matter and divalent cations on the stability of aqueous nanoparticles. *Water Research* 43(17), 4249–4257. DOI: 10.1016/j.watres.2009.06.005

Zhou, D., Abdel-Fattah, A.I., Keller, A.A., 2012. Clay particles destabilize engineered nanoparticles in aqueous environments. *Environmental Science & Technology* 46(14),

7520–7526. DOI: 10.1021/es3004427

Zouzelka, R., Cihakova, P., Rihova Ambrozova, J., Rathousky, J., 2016. Combined biocidal action of silver nanoparticles and ions against Chlorococcales (*Scenedesmus quadricauda*, *Chlorella vulgaris*) and filamentous algae (*Klebsormidium sp.*). *Environmental Science and Pollution Research* 23(9), 8317–8326. DOI: 10.1007/s11356-016-6361-6

Zumdahl, S.S., 1998. Propriétés des solutions, in: Zumdahl, S.S. (Ed.), *Chimie Des Solutions*. pp. 55–97.